Yukon

Yukon University

YGS Miscellaneous Report MR-22

Greater Whitehorse area permafrost characterization

L.-P. Roy, F. Calmels, C. Laurent and N. Vogt Yukon University

P.S. Lipovsky and J. Humphries Yukon Geological Survey

Published under the authority of the Department of Energy, Mines and Resources, Government of Yukon yukon.ca.

Printed in Whitehorse, Yukon, 2021.

Publié avec l'autorisation du Ministères de l'Énergie, des Mines et des Ressources du gouvernement du Yukon, yukon.ca.

Imprimé à Whitehorse (Yukon) en 2021.

This, and other Yukon Geological Survey publications, may be obtained from:
Yukon Geological Survey
102-300 Main Street
Box 2703 (K-102)
Whitehorse, Yukon, Canada Y1A 2C6
email geology@gov.yk.ca

Yukon Geological Survey website https://yukon.ca/en/science-and-natural-resources/geology.

In referring to this publication, please use the following citation:

Roy, L.-P., Lipovsky, P.S., Calmels, F., Laurent, C., Humphries, J. and Vogt, N., 2021. Greater Whitehorse area permafrost characterization. Yukon Geological Survey, Miscellaneous Report MR-22, 185 p. including appendices.

Cover: Aerial view of Ibex Valley thermokarst terrain, looking north, with Alaska Highway in the background (P. Lipovsky photo).

ACKNOWLEDGEMENTS

We gratefully acknowledge that this project took place on lands within the traditional territories of Kwanlin Dün First Nation, Ta'an Kwäch'än Council and Champagne Aishihik First Nations.

We appreciate the support of all participants and partners who have contributed to this project, including: YG Department of Energy Mines and Resources (Land Planning and Agriculture Branches; YG Department of Highways and Public Works (Transportation Engineering Branch); YG Department of Environment (Water Resources Branch); YG Department of Community Services; Kwanlin Dün First Nation; and City of Whitehorse (Engineering and Planning Departments).

We extend sincere thanks to all the community residents who provided invaluable information and access to their properties, including: Bill and Barbara Drury; Dev Hurlbert; Dave Andrews; and Larry and Monique Carlyle.

Many thanks to the numerous field assistants who made this work possible, including: Emilie Stewart-Jones, Moya Painter, Justin Emberley, Daniel Jolkowski, and Pamela Godin.

Funding for this project was provided by Crown-Indigenous Relations and Northern Affairs Canada (CIRNAC) Climate Change Preparedness in the North (CCPN) program, and was administered by Yukon Environment's Climate Change Secretariat. In-kind contributions were also made by Yukon Geological Survey, Yukon University Research Centre and Yukon Government partners listed above.

Contents

FORWARD

This document comprises a compilation of technical reports for field investigations completed by Yukon University Research Centre (YRC) at seven case study sites that represent common permafrost environments in the greater Whitehorse area. This work was completed for Yukon Geological Survey (YGS) with core funding from Crown-Indigenous Relations and Northern Affairs Canada (CIRNAC) Climate Change Preparedness in the North (CCPN) program.

The primary purpose of the report is to document results of field investigations (*e.g.,* ERT geophysics, drilling and geotechnical laboratory analysis) completed by YRC at each site. Supporting background material (Chapter 2) and case study geological descriptions were prepared by YGS, along with general discussion relating to climate change and implications for development (Sections 10 and 11).

1 INTRODUCTION

Permafrost in the Greater Whitehorse Area (GWA) is found in sporadic isolated patches within specific geological and environmental contexts. The southern Yukon generally falls within the sporadic discontinuous permafrost zone (Heginbottom, 1995), and the presence of permafrost is largely influenced by the thickness of the surface organic layer and ground moisture content (Burn, 2004). While impacts of permafrost in Whitehorse are not as acute as other regions of the territory, several cases have reported the negatives effects of permafrost thaw on infrastructure in the GWA. Examples include the Hamilton Boulevard extension, the Alaska Highway, as well as homes in Takhini Valley, Mount Sima and Mendenhall subdivisions. Trails and agricultural land in the GWA have also been impacted. Increasing development pressure, high population density, and the economic value of infrastructure at risk substantiate the need for comprehensive investigations of permafrost in the region. However, there has been no comprehensive mapping or documentation of permafrost conditions for the area to date.

In 2017–2018, YGS retained YRC to conduct stakeholder consultation across various sectors to gather local information on potential permafrost sites within the GWA. Their findings were summarized in a report to the YGS. YGS also retained YRC from 2018–2021 to conduct detailed field investigations to characterize the range of permafrost environments in the GWA and disseminate this information to relevant stakeholders. The project objectives were to:

- Locate and characterize permafrost (ground temperature, soil texture, ground ice content) in the GWA using geophysics, drilling, instrumentation, and lab analyses at a minimum of seven sites;
- Develop a network of instrumented permafrost monitoring stations to track the long-term evolution of permafrost in the context of a growing Yukon population and climate change; and
- Share tailored information such as case study reports, maps, and GIS products with various stakeholders, including developers, consultants, and planners and decision-makers from First Nations governments, City of Whitehorse, and Yukon Government.

Seven case study sites were selected within the GWA based on the: (1) presence of permafrost, (2) presence of ongoing permafrost thaw issues likely to persist over a multi-year period, and (3) representativeness of the geomorphologic and environmental setting to other areas with similar conditions and issues (Fig. 1.1). Each of the sites selected will be presented as individual case studies. Detailed investigation methodologies are presented in Appendix E.

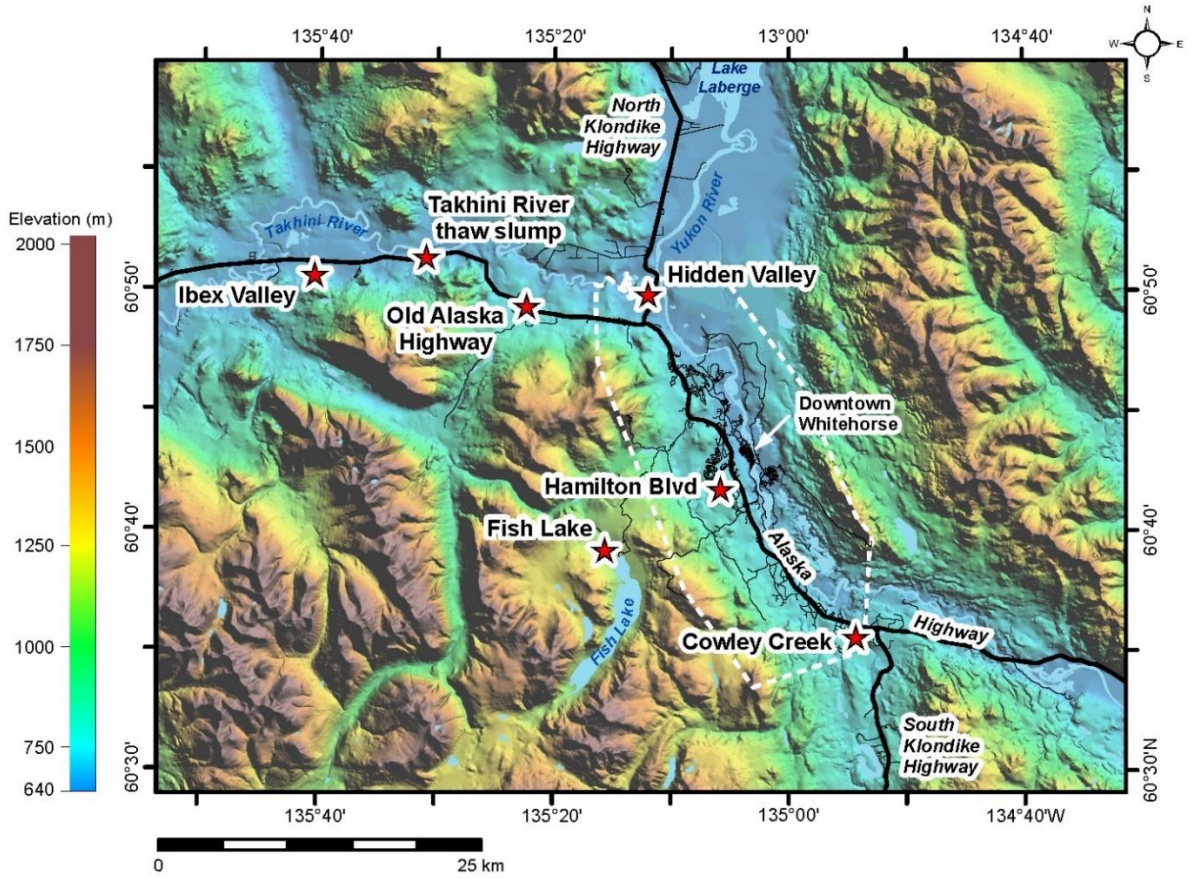

Figure 1.1 Locations of the seven case study sites in relation to Whitehorse City limits, marked by a white dashed line.

1.1 Report organization

The report is organized into 11 sections:

- Section 1 introduces the project and establishes the scope of the report.
- Section 2 provides general background on the geologic and climatic setting, along with an introduction to permafrost and its distribution in the GWA.
- Sections 3 through 9 present site-specific information on vegetation, surficial geology and permafrost conditions, together with the basic methodology and results from each of the seven case study sites: Cowley Creek, Hamilton Boulevard, Hidden Valley, Ibex Valley, Takhini River Thaw Slump, Old Alaska Highway, and Fish Lake.
- Section 10 provides a discussion on the results from fieldwork, explores climate change effects, and considerations for development.
- Section 11 summarizes key results and issues identified in the case studies.
- Detailed methodologies and raw data, such as geotechnical laboratory analysis results, borehole logs, and ground temperature data, are provided in the appendices.

1.2 Methodology

Note: Investigation methods are only briefly introduced in this section. Please refer to Appendix E for more detailed methodology descriptions.

Site selection

The identification of key field sites representing the full spectrum of local permafrost environments was informed through air photo and GIS analysis, and consultation with various stakeholders. Following site selection, local permafrost conditions were characterized using a combination of field observations, borehole logs, ground temperature monitoring, electrical resistivity tomography (ERT) and previous research where available.

Borehole drilling and geotechnical analysis

Borehole logs are a record of observations detailing the ground materials encountered during drilling of a borehole. Logs typically include descriptions of soil and ground ice at regular depths but can include more detailed information such as ice content and the distribution of grain size if a core is retrieved for laboratory analysis. Cores were retrieved, and detailed borehole logs were completed at six of the seven case study sites, with the Old Alaska Highway case study site being the exception.

The objective of the drilling program was to core and collect permafrost samples from predetermined study sites. The borehole drilling locations were selected in advance through interpretation of ERT surveys in combination with desktop interpretation of available maps, aerial photos, satellite images and consultation with various stakeholders (property owners, infrastructure and land managers, consultants, and industry). Commercial drill rigs were contracted to drill deep boreholes (>5 m), while shallow boreholes generally used a hand auger and a custom GÖLZ™ portable core-drill system. Boreholes were drilled along ERT survey lines in representative areas (*e.g.*, forested areas, open fields) or in an area belonging to a particular surficial geology unit. For each borehole, the same sampling and drilling procedures were followed. The site was described (*e.g.*, vegetation type and density, and topography), photographed, and locations were recorded using a handheld GPS. Frozen core samples were briefly described on site, after which they were packaged and transported to a storage facility for laboratory processing.

Laboratory analyses were carried out to measure geotechnical properties of active layer and permafrost samples. Soil and ice characteristics were evaluated by: (1) conducting a grain-size analysis on each sample, (2) describing the cryostructure (the structure of the frozen ground materials), and (3) quantifying volumetric ice content, gravimetric ice content and subsidence potential. Detailed methods are described in Appendix E.

Ground temperature monitoring

At the six sites where drilling was completed (*i.e.,* all except Old Alaska Highway), one or two of the boreholes were instrumented with ground temperature loggers to monitor ground temperature at various depths. For ground temperature monitoring installations, electrical-grade PVC conduit casings were inserted into the newly-drilled boreholes, and were filled with silicone oil. The holes were backfilled with earth extracted from the borehole or filter sand. The boreholes were instrumented with thermistor strings attached to external data loggers, either a HOBO (UX120-006M) four-channel external or LogR Systems (ULogC16-32). Ground temperature monitoring stations were visited regularly throughout the project to retrieve data. Data was averaged to create figures such as ground temperature profiles. Ground

temperature data were used with ERT profiles and geotechnical information to develop a better understanding of the permafrost and ground conditions at each site.

Electrical Resistivity Tomography (ERT) surveys

ERT is a geophysical method that is used to determine the electrical resistivity of the subsurface. Resistivity (measured in ohm·m) is the mathematical inverse of conductivity, and indicates a material's ability to conduct electrical current (*i.e.*, a flow of electrons). Electrical resistivity measures how difficult it is for electricity to flow through a material. ERT surveys involve sending electrical current through two steel current electrodes (C1 and C2 in Appendix E, Figure 2) electrodes driven into the ground surface. A resistivity meter then measures the resistivity distribution of the subsurface by measuring current with two potential electrodes (P1 and P2 in Appendix E, Figure 2). A line of electrodes are spaced at regular intervals to transmit electricity into the ground. The current is measured following a specific sequence to measure the resistivity distribution of the subsurface along a linear transect. The data are then used to create an ERT profile, which is a 2-D cross sectional plot of resistivity versus depth.

Frozen water in the solid phase has a significantly higher resistivity than unfrozen water. This allows permafrost distribution to be inferred from changes in resistivity between frozen and frozen ground and is why ERT is relevant for permafrost and hydrology research. In permafrost environments the resistivity of a sediment will increase concomitant with the decrease of temperature *i.e.*, decrease of liquid water content and increase of ice-content. Sediments containing massive ice will have higher resistivities than ice-rich sediments, followed by ice-poor sediments. However, in addition to the amount and type of ice present, resistivity of a material in a permafrost environment also varies with a number of other factors, including soil type (*e.g.*, grain size, porosity, permeability, mineralogy, clay content), temperature, unfrozen water content and electrolyte concentration (De Pascale *et al*., 2008; Hoekstra *et al*., 1974; Calmels *et al.,* 2018).

Interpretation of ERT data is nuanced due to the complexity of factors governing a material's resistivity and the magnitude by which resistivity can vary. General permafrost resistivity values range from as low as a few hundred ohm·m in 'warm' fine-grained sediment (Holloway, 2020; Way and Lewkowicz), up to tens of thousands ohm·m in massive ice bodies and bedrock (Wolfe *et al.,* 1997; Krautblatter and Hauck, 2007). For example, Holloway (2020), reported resistivity values between 85 and 1000 ohm·m for frozen silt at 'warm' temperatures of −0.5 to 0°C in the southern Northwest Territories. In contrast, De Pascale *et al.,* (2008) reported resistivities values between 6000 and 60 000 ohm·m for massive ice in the northern Mackenzie Delta region. Reported resistivity values by Holloway (2020) are much lower than what is typically used to delimit permafrost in ERT profiles. Ten out of eleven ERT studies conducted in Canada and Alaska used 300 to 1000 ohm·m as the boundary between frozen and unfrozen soils (Table 4.1 in Holloway, 2020). One study used a boundary value of 18 000 ohm·m; however, it was the only one to investigate massive ice. These results inform the range of potential resistivity values for permafrost in the GWA and suggest that a resistivity of 300 to 1000 ohm·m is a useful starting point to differentiate between frozen and unfrozen ground. However, it is important to note that because so many of the factors affecting resistivity commonly vary spatially both horizontally and vertically, it is difficult to select a single resistivity threshold that distinguishes permafrost from unfrozen ground across a single survey.

An ERT system consists of an automated imaging unit and a set of wires connected to a configuration (array) of electrodes. To conduct a survey, 81 electrodes are driven into the ground along a survey line and connected to the electrode cables. There are several common electrode arrays. In this study two types of arrays were used, the Wenner and dipole-dipole array. In general, the Wenner array is good at resolving vertical changes in resistivity (*i.e.*, horizontal structures), but relatively poor in detecting horizontal changes in resistivity (*i.e.*, narrow vertical structures), while the dipole-dipole array is very sensitive to horizontal

changes, but relatively insensitive to vertical changes. Further details about the system are presented in Appendix E. ERT profiles were interpreted in conjunction with the results of frost probing along the profiles, field descriptions of vegetation cover at the site, borehole and laboratory analyses undertaken by the research team, and surficial mapping.

1.3 Key findings

The key results from the field investigations at seven case study sites in the GWA are:

- Permafrost at all case study sites is warm (*i.e.*, >-1°C), suggesting permafrost throughout the GWA is in disequilibrium with its environment and is particularly vulnerable to thaw by disturbance or environmental change. The lowest average annual ground temperature encountered in permafrost was -0.13°C at 2 m depth at Cowley Creek. Permafrost temperatures as low as -0.39°C were encountered at 4.1 m depth at Fish Lake (averaged over a five month winter period, but expected to remain close to this value year round).
- The presence of permafrost was associated with specific geologic settings: (1) low-lying fine-grained or organic-rich terrain, particularly within abandoned meltwater channels; (2) fine-grained glaciolacustrine sediments; (3) north-facing slopes underlain by till; and (4) subalpine peat plateaus.
- Terrain features associated with the presence of permafrost included thermokarst lakes, ground subsidence, drunken forests, hummocky permafrost mounds, and slope creep.
- Estimates of active layer depth and base of permafrost varied depending on if they were defined using boreholes or ERT surveys, however active layer depth generally ranged from as shallow as 0.5 m to more than 4 m, and the permafrost base ranged from as little at 2 m to as deep as 25 m.
- Case study sites with the thinnest permafrost were Old Alaska Highway and Hamilton Boulevard (<1 m thick), while sites with thicker and more spatially extensive permafrost were Ibex Valley and Cowley Creek.
- The Ibex Valley case study site had the highest potential for ground subsidence with an average excess-ice content of 49% (IV_BH1) and an estimated permafrost thickness of 12.6 m, which would equate to a potential subsidence of 6.2 m following complete permafrost thaw.
- In several boreholes, ground ice was encountered during drilling, but subsequent monitoring indicated ground temperatures slightly above 0°C. This suggests that while permafrost was present prior to drilling, it subsequently thawed in the immediate vicinity of the borehole as a result of the drilling process. Warm ice-rich permafrost in undisturbed areas is generally only preserved due to the ice's high latent heat of fusion (melting) (*i.e.*, a large amount of heat is required to change ice from solid to liquid phase, during which no change in temperature occurs).

2 BACKGROUND

2.1 Surficial geology setting

The landforms and surficial materials within the Greater Whitehorse Area are largely a product of the most recent (McConnell) ice age, and subsequent modification by fluvial and colluvial activity throughout the Holocene (the last 11 000 years). This section presents some key highlights of a very complex local landscape history, which is discussed and illustrated in detail by Bond (2004) and Mougeot GeoAnalysis (1997).

The McConnell (Late Wisconsinan) Glaciation occurred between ~24 000 and 11 000 years ago (Bond, 2004). At the maximum extent of this glaciation ~18 000 years ago, the entire GWA was covered in ice at least 1350 m thick (Bond, 2004). At this time, ice flow was generally in a northwesterly direction, and was unobstructed by local topography. During deglaciation, the ice thinned and retreated to the southeast, punctuated by occasional standstills and topographically-controlled readvances (Bond, 2004; Bond *et al.,* 2005). Cosmogenic radionuclide (10Be) surface exposure dating of large glacially transported boulders (erratics) indicate that the top of Mount McIntyre was ice-free by about 15 500 years ago, while the Raven's Ridge subdivision area (north of the city center) was ice-free ~2000 years later (Menounos *et al.,* 2017).

During early deglaciation (Cassiar Readvance phase), a lobe of ice readvanced northward down the Yukon River valley to the north end of Lake Laberge, where it deposited a large recessional moraine (Bond, 2004). As the ice later retreated to the south, Glacial Lake Laberge was impounded between this moraine and the ice front. The lake outlet gradually eroded through the moraine, causing lake levels to drop from a maximum elevation of about 716 m ~12 000 years ago, to 650 m ~10 600 years ago, and continuing to drop throughout the Holocene to 634 m ~3000 years ago (Horton, 2007).

During the Cassiar Readvance, another lobe of ice advanced up Takhini River valley as far west as the village of Champagne (Bond, 2004) where a recessional moraine was deposited. This ice lobe dammed the Takhini River, while the St. Elias Lobe also dammed the Dezadeash River valley further to the west. These two dams impounded Glacial Lake Champagne which inundated much of the Kusawa Lake, Takhini River and Dezadeash River valleys. The lake rose to a maximum level of 854 m, with prominent stages at 765 m, and 725 m (Barnes, 1997; Gilbert and Desloges, 2005). The 746 m lake stage was controlled by an outlet draining northward through a divide located near Taye Lake which drains into the headwaters of Nordenskiold River (Bond *et al.*, 2005-8). It has been speculated that Lake Champagne existed sometime between 12 500 and 10 500 years ago for a relatively short period of a few hundred years (Barnes, 1997), although others have argued that the lake drained as late as 7200 years ago based on the lack of older archeological sites in the valley (Heffner, 2008). Smaller glacial lakes also formed in the Ibex and Fish Lake valleys during this phase.

Once ice fully retreated out of Takhini Valley, Glacial Lake Champagne drained into Glacial Lake Lebarge. A thick (often exceeding 50 m) sequence of fine-grained (fine sand, silt, and clay) glaciolacustrine sediment settled out at the bottom of these glacial lakes, filling much of the Takhini and Yukon River valleys. Thicknesses in excess of 100 m are often reported in water well records in Takhini Valley, and greater than 300 m were encountered in a well located near the Alaska Highway crossing of Takhini River (EBA, 2014). Ice-rich permafrost and thermokarst terrain is commonly associated with these fine-grained glaciolacustrine sediments. The sediments also constitute some of the most productive agricultural soil in the Whitehorse area. Throughout the Holocene, the Takhini and Yukon rivers and smaller tributaries cut down through the glaciolacustrine sediments, creating the steep bluffs that are now found in these valley bottoms, *e.g.,* the Whitehorse airport escarpment.

As Glacial Lake Laberge gradually shrunk to its modern size, its southern shoreline migrated northward, and a thick (up to 4 m) blanket of well-sorted deltaic sand was deposited on top of the glaciolacustrine sediment. As lake levels continued to drop, dry deltaic sediments were exposed to extensive wind-erosion, and a thin veneer of loess (wind-blown fine sand and silt) was deposited at the ground surface in many locations around Whitehorse. Extensive fields of sand dunes also formed north of the municipal sewage lagoons, and near the junction of Takhini Hot Springs Road and the North Klondike Highway.

Till (or moraine) is a very widespread surficial material generally found above 700 m elevation throughout the Whitehorse area. Till is sediment that has been transported directly by glacier ice, *i.e.,* beneath, within, or on top of the glacier. The nature and composition of till can vary widely, but basal or lodgement till is one of the most common forms, which typically comprises a dense poorly-drained, matrix-supported diamicton, with a silty sand matrix and a large proportion of pebbles, cobbles and boulders. Basal till is commonly fluted or streamlined indicating the direction of ice-flow. Thick blankets of till may be found in valley bottoms and lower slope positions. Middle to upper slope positions and ridge crests are generally mantled with thinner till veneers which are modified by colluvial activity (downslope gravitational movement). Till found in recessional, lateral and stagnation moraines is typically less dense and coarser-grained than basal till. During deglaciation, ice stagnation occurred several times, leaving behind a series of prominent recessional moraine ridges in Takhini Valley, *e.g.,* Stevens quarry.

Coarse-grained glaciofluvial sediments primarily comprising sand and gravel were deposited by glacial meltwater streams during deglaciation. Glaciofluvial plains, fans, terraces, and hummocky kame topography are particularly extensive near the subdivisions of Whitehorse Copper, Wolf Creek and Cowley Creek. The hummocky Chadburn and Long Lake ice-contact kame and kettle complexes were also deposited during a period of ice-stagnation as orphaned blocks of ice were buried and subsequently thawed. Glaciofluvial materials are generally coarse and well-drained, and therefore are not usually associated with ice-rich permafrost.

Lateral meltwater channels (*e.g.,* most notably along the lower east flanks of Mt. McIntyre, west and south of Grey Mountain, and in the Scout Lake area) are distinctive erosional features formed by glacial meltwater flowing along the margins of ice lobes. The channels typically support much smaller (underfit) contemporary streams and adjacent wetlands. Thick organic materials (fibric peaty material formed from decomposed vegetation fragments) generally accumulate in their floors. Organic veneers also commonly mantle north-facing slopes. These settings are commonly associated with permafrost due to the insulative capacity of the organic materials.

2.2 Vegetation

All seven case study sites are within the Southern Lakes Ecoregion, and all but the Fish Lake site are in the Southern Lakes Boreal Low Subzone (BOLsl), which generally comprises continuously forested areas at low to middle elevations, with mixed wood forests (lodgepole pine, white spruce and aspen) and wetlands also common (Flynn, 2017). The Fish Lake site is in the Boreal High bioclimate zone, which is found at higher elevation than the Boreal Low zone, with more open forests dominated by white spruce, lodgepole pine and subalpine fir (Flynn, 2017).

2.3 Climate

2.3.1 Contemporary climate

The subarctic continental climate of the Greater Whitehorse area is relatively dry, with long cold winters, short warm summers, and large seasonal temperature variations. Long term climate data (Figs. 2.1 and 2.2) are available from Environment and Climate Change Canada (ECCC) weather stations Whitehorse A, at Whitehorse airport (706 m asl, climate ID: 2101300 and 2101303), Whitehorse AUTO, 3 km north of Whitehorse airport (707 m asl, climate ID: 2101310), and Takhini River Ranch near Alaska Highway km 1460 (671 m asl, climate ID: 2101095) (ECCC, 2021a). Figure 2.1 shows monthly air temperature and precipitation normals at Whitehorse airport (ECCC Whitehorse A, climate ID: 2101300). The average annual air temperature for the 1981–2010 period was −0.1°C. Maximum monthly temperatures up to 14°C occur in July, while minimum monthly temperatures of −15° C occur in January. Extreme minimum and maximum temperatures recorded were −52°C and 34°C, respectively. For the 1981–2010 period, the average length of the frost-free period was 80 days (June 5–August 25). For the same period, average annual precipitation was 262 mm, with maximum monthly precipitation of 38 mm occurring in July. Snow cover is typically present from late-October to mid-April in valley floor settings (Smith *et al*., 2004), with greater than 5 cm of snow on the ground for 156 days per year. Average total monthly sunshine ranges from 27 hours in December to 267 hours in June (ECCC 1981–2010 Whitehorse A climate normals).

Air temperature typically decreases with altitude from April through October at a surface lapse rate of −6°C/km. In winter months, however, inversions commonly occur whereby air temperature increases with altitude at a rate of 3–5°C/km due to cold air pooling at lower elevations (Wahl, 2004; Wahl *et al*., 1987). Lewkowicz and Bonnaventure (2011) found that the annual surface lapse rate above treeline was −6°C/km in the Wolf Creek watershed, and that monthly lapse rates were consistently negative (*i.e.,* decreasing temperature with altitude) throughout the year. Below treeline, however, they found that monthly lapse rates were generally positive (*i.e.,* increasing with altitude) throughout most of the winter months.

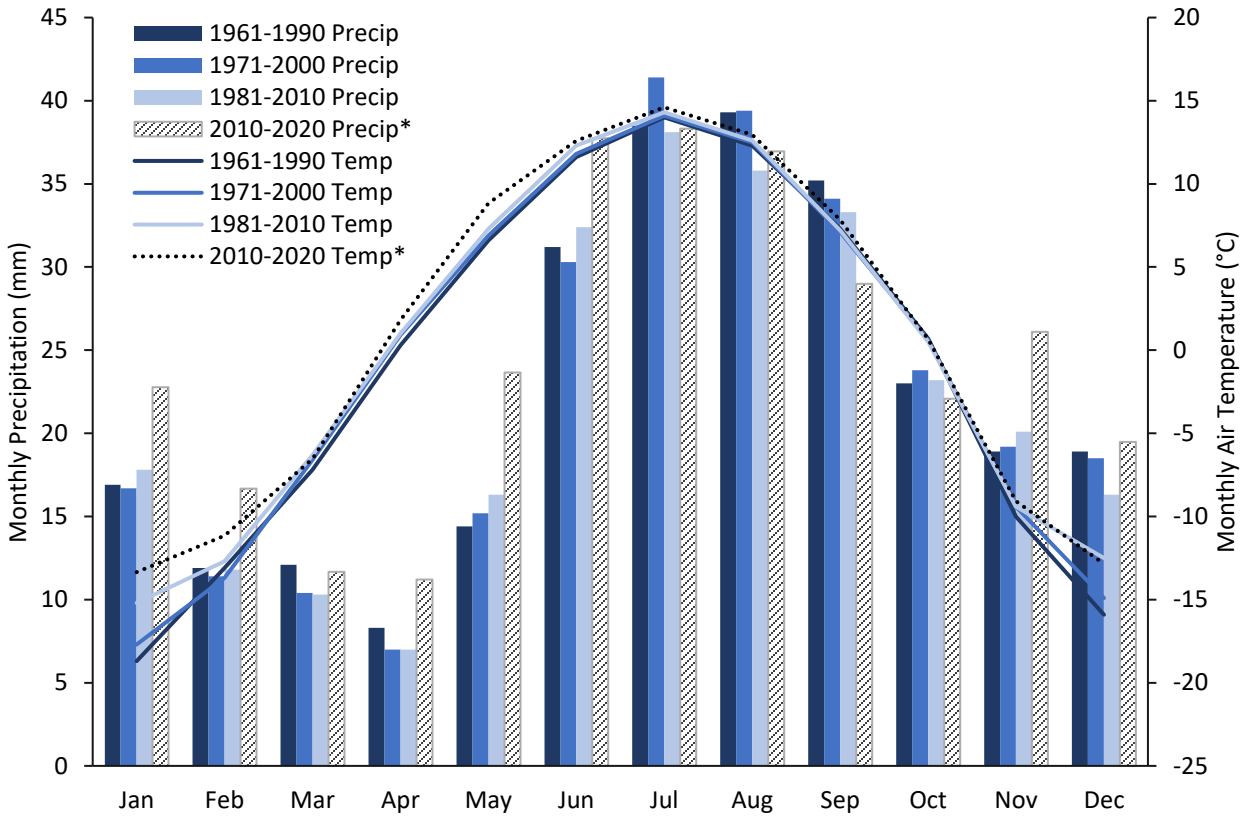

*Figure 2.1 Monthly air temperature and precipitation normals for Whitehorse airport (Whitehorse A), 1960–2010 (ECCC, 2021b). *Mean monthly air temperature and precipitation for 2010–2020 were calculated from Whitehorse AUTO (located 3 km north of airport) daily data (ECCC, 2021a).*

2.3.2 Historical climate trends

Figure 2.1 shows changes in the climate normals at Whitehorse airport covering the period 1961–2010 (ECCC Whitehorse A, climate ID: 2101300). Air temperature normals during this period increased slightly, most notably in the winter months of December through February. Changes in precipitation normals are more variable, with the most pronounced increases in the months of January, May, June and November, and the most pronounced decreases in the months of July, August, September, and December. More recent climate records from the nearby Whitehorse AUTO station (ECCC, climate ID: 2101310) for the 2010–2020 period show notably higher monthly precipitation levels than the three previous Whitehorse A station normals for the months of November through June.

Figure 2.2 shows annual mean air temperatures at Whitehorse airport from 1943 to 2020. An overall warming trend of 2.2°C/century is shown by the trendline. However, a notable period of cooling was observed from 1943 to 1974 at a rate of −6.4°C/century, followed by a period of warming that has occurred since 1974 at a rate of 3.8°C/century.

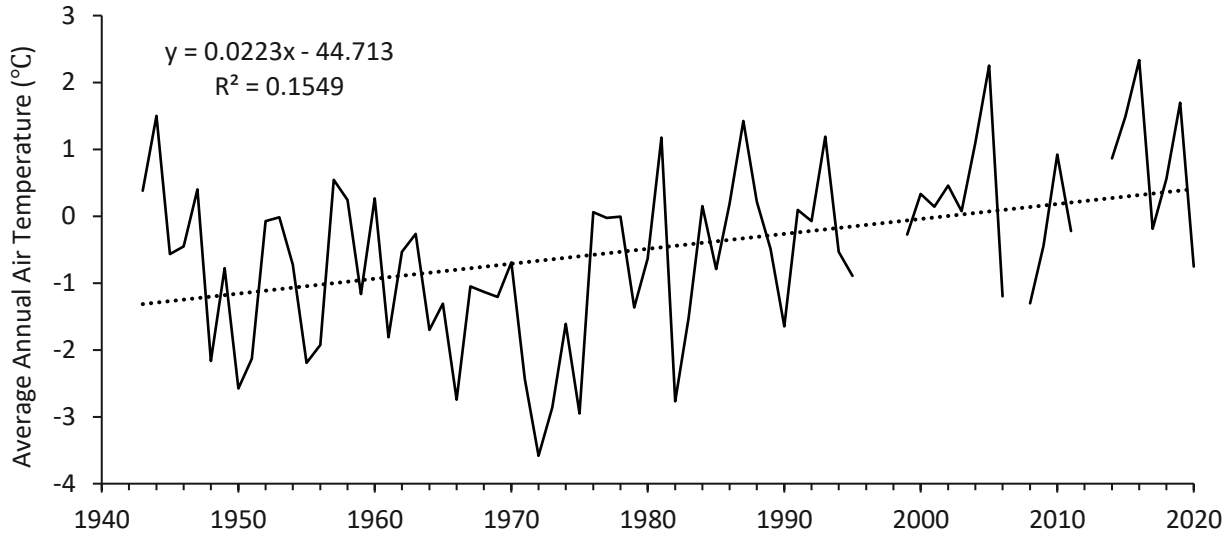

Figure 2.2 Annual mean air temperature at Whitehorse airport from 1943 to 2020, calculated from monthly averages at Whitehorse A (climate ID: 2101300) for 1942–2006, and daily averages at Whitehorse A (climate ID: 2101303) for 2008–2020 (ECCC, 2021a).

Former Yukon Weather Centre meteorologist, Michael Purves (2006, 2010) described several other historical climate change observations in his analysis of 1942–2010 climate records for Whitehorse. Some of his findings included:

Temperature

- Mean daily minimum winter (November through February) temperatures cooled at a steep rate of 16.9°C/century from 1943 to 1973, then warmed at a rate of 4.3°C/century from 1980 to 2009. Mean daily winter minimum temperatures rose 3.4°C/century for the whole period of record (1943–2009).
- Mean daily maximum summer (May through August) temperatures cooled at a rate of 5.5°C/century from 1954 to 1974, then warmed at a rate of 3.0°C/century from 1980 to 2009. Mean daily maximum summer temperatures rose 1.1°C/century for the whole period of record.
- The number of days per year below −40°C decreased at a rate of 5 days/century between 1942 and 2009 and decreased at a rate of 11 days/century between 1980 and 2009.
- The number of frost-free days per year decreased at a rate of 7 days/century for the 1942–2010 period. However, the number of frost-free days increased at a rate of 42 days/century for the 1981–2010 period.

Precipitation

- Total winter (November through February) precipitation decreased at a rate of 18% (14 mm)/century for the period 1942–2009. Total winter precipitation decreased at a rate of 38% (21 mm)/century from 1980 to 2009.
- Total summer (May through August) precipitation increased at a rate of 17% (20 mm)/century for the period 1942–2010. Total summer precipitation increased at a rate of 28% (33 mm)/century from 1981 to 2010.
- Total annual precipitation increased slightly from 1943 to 2009 at a rate of 4% (11 mm)/century. However, from 1980 to 2009, total annual precipitation increased at a rate of 20% (53 mm)/century.

- Total depth of snow on the ground on February 28 decreased by 39% (13 cm)/century for the years 1955–2010, although there was a noticeable increase in snow depths in the late 1960s and 1970s. From 1981 to 2010, snow depth at the end of February decreased at a rate of 105% (32 cm)/century.

Sunshine

- Winter sunshine increased 39 hours (~20%) over the 37-year record (1958–1995).
- Summer sunshine declined 44 hours (~4%) over the 39-year record (1957–1996).
- Total annual sunshine increased by about 30 hours (<2%) over the 38-year record (1957–1995).

2.3.3 Projected climate

Climate projection summaries are included for Whitehorse to better understand potential future changes in various climate scenarios. The graphs are intended for examining temporal trends, rather than prediction of precise values due to the variability associated with climate models and the natural climate system. Representative Concentration Pathways, or RCPs, represent future climate scenarios based on atmospheric greenhouse gas concentrations. The paths are based on a range of potential human behaviours extrapolated out to the year 2100. Figures 2.3 and 2.4 summarize climate change projections (under a mid-emissions scenario) by month for the Whitehorse area, produced by the University of Alaska Fairbanks Scenarios Network for Alaska and Arctic Planning (SNAP, 2021). These projections were regionally downscaled to 2 km resolution using PRISM as a historical baseline and were based on three future socioeconomic scenarios:

- RCP 4.5 – low scenario (emissions peak in 2040 and radiative forcing stabilizes after 2100);
- RCP 6.0 – medium scenario (emissions peak in 2080 and radiative forcing stabilizes after 2100);
- RCP 8.5 – high scenario (emissions increase through the 21st century).

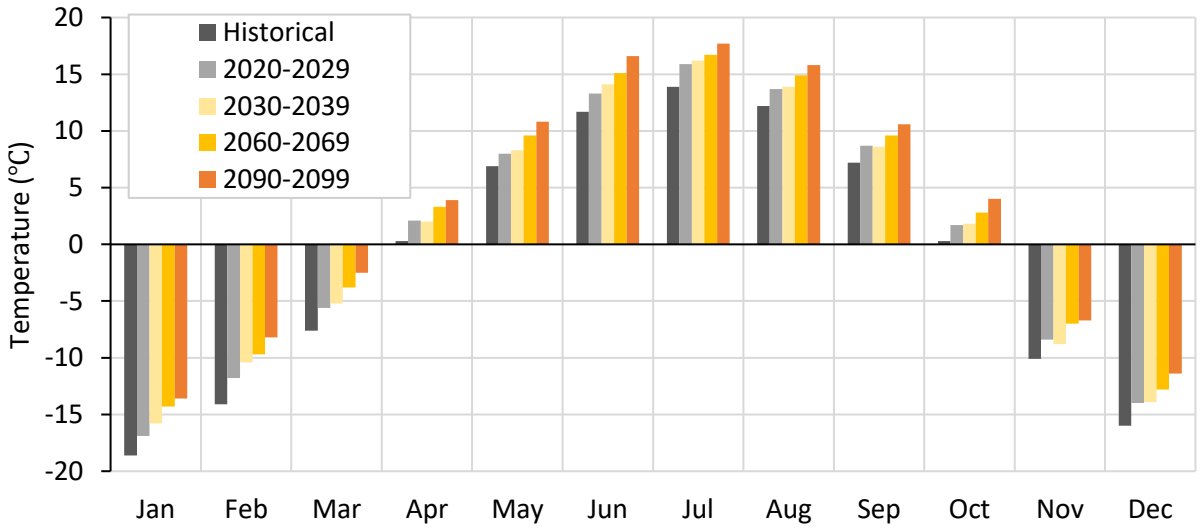

Figure 2.3. Mean monthly temperature for Whitehorse, YT, using historical (1961–1990) PRISM and 5-model projected average at 2-km resolution under a mid-emissions scenario (RCP 6.0) (SNAP, 2021).

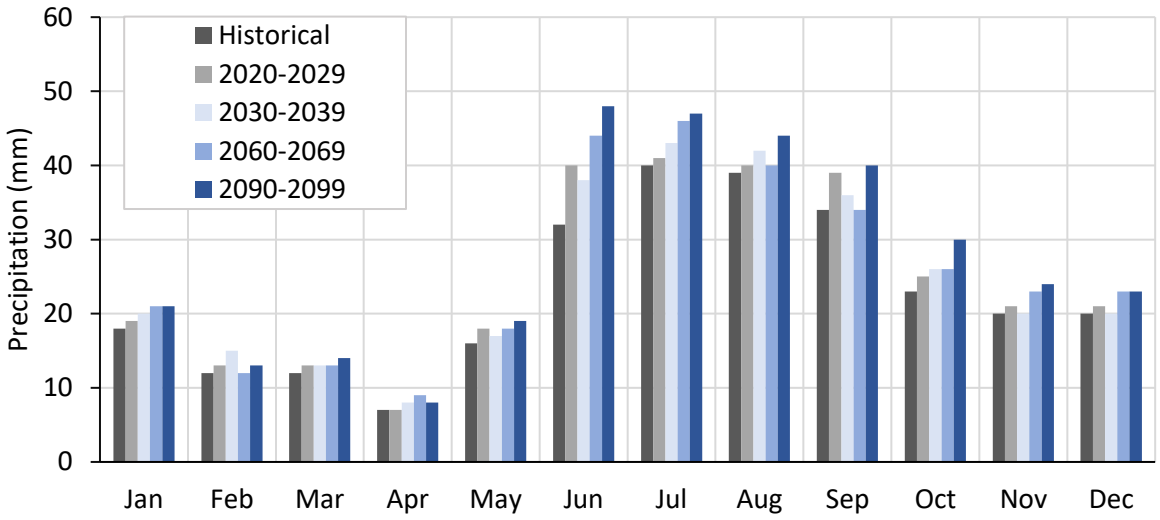

Figure 2.4 Mean monthly precipitation for Whitehorse, YT using historical (1961–1990) PRISM and 5-model projected average at a 2 km resolution under a mid-emissions scenario (RCP 6.0) (SNAP, 2021).

As shown in Table 2.1 and Figure 2.5a, b, all scenarios predict a steady increase in both mean January and July temperatures at rates ranging from 2.3 to 5.4°C/century. Projected mean monthly air temperature per decade suggest air temperatures between the 2020s and 2090s will increase 1.2–3.5°C in January, and 1.6–4.0°C in July (Fig. 2.5a, b and Table 2.1). Slight increases in mean monthly precipitation per decade are also projected (Fig. 2.4). From the 2020s to the 2090s, January precipitation is projected to increase between 0 and 2 mm (0–10.5%), while July precipitation is expected to increase between 2 and 6 mm (4.3–14.6%) (Table 2.2).

Table 2.1. Summary of SNAP (2021) projected mean January and July temperature for selected future decades under various RCP scenarios. Values in brackets indicate change in temperature between the current (2020–2029) and projected decade.

Temperature (°C)	Scenario	2020–2029	2030–2039	2060–2069	2090–2099
Mean January	RCP 4.5	−16.2	−16.3 (−0.1)	−14.9 (1.3)	−15 (1.2)
	RCP 6.0	−16.9	−15.8 (1.1)	−14.3 (2.6)	−13.6 (3.3)
	RCP 8.5	−15.4	−15.8 (−0.4)	−14.4 (1.0)	−11.9 (3.5)
Mean July	RCP 4.5	15.7	16.1 (0.4)	16.9 (1.2)	17.3 (1.6)
	RCP 6.0	15.9	16.2 (0.3)	16.7 (0.8)	17.7 (1.8)
	RCP 8.5	15.5	15.8 (0.3)	17.7 (2.2)	19.5 (4.0)

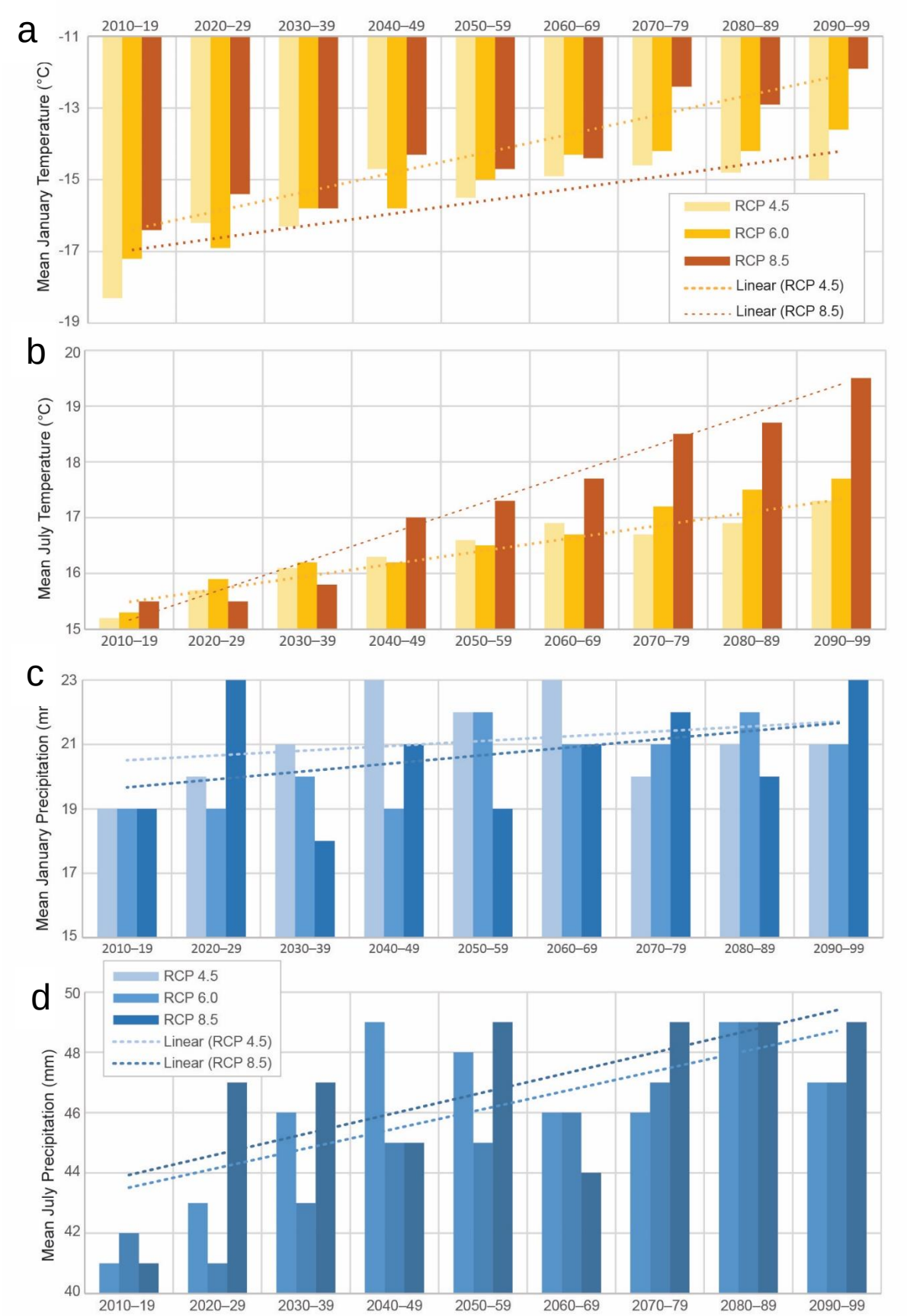

Figure 2.5 Projected mean (a) January air temperature, (b) July air temperature, (c) January precipitation, and (d) July precipitation–per decade under RCP scenarios 4.5, 6.0 and 8.5 (SNAP, 2021).

Table 2.2 Summary of SNAP (2021) projected mean January and July precipitation for selected future decades. Values in brackets indicate change in precipitation between the current (2020–2029) and projected decade.

Precipitation (mm)	Scenario	2020–2029	2030–2039	2060–2069	2090–2099
Mean January	RCP 4.5	20	21 (1)	23 (3)	21 (1)
	RCP 6.0	19	20 (1)	21 (2)	21 (2)
	RCP 8.5	23	18 (−5)	21 (−2)	23 (0)
Mean July	RCP 4.5	43	46 (3)	46 (3)	47 (4)
	RCP 6.0	41	43 (2)	46 (5)	47 (6)
	RCP 8.5	47	47 (0)	44 (−3)	49 (2)

2.4 Permafrost

2.4.1 Introduction

In some regions long cold winters and short summers lead to the development of a ground layer that remains perennially frozen. This frozen ground is called permafrost and is defined as ground (soil or rock) that remains at or below 0°C for a minimum of two years (French, 2007). Figure 2.6 shows a typical temperature versus depth profile in permafrost terrain. The profile consists of an active layer which freezes and thaws annually, overlying permafrost. The base of the active layer is generally at the top of permafrost, and the base of permafrost is found where ground temperatures rise above 0°C below the active layer.

Permafrost grows from a combination of freezing of its base downward, or upward from its top when new surface material is added. Depth to the base of permafrost depends on mean annual surface temperature, geothermal heat flux, and thermal conductivity of ground materials (Fig. 2.6) (French, 2007). The mean annual surface temperature, and the loss of heat from the ground surface depend on the surface energy balance, which is the sum of all energy fluxes at the surface over a given time interval (see Oke, 1987 for more information on the energy balance). So, while permafrost distribution generally varies with climate, considerable regional variation is introduced by factors which alter the surface energy balance, such as snow cover and vegetation (Smith and Riseborough, 2002).

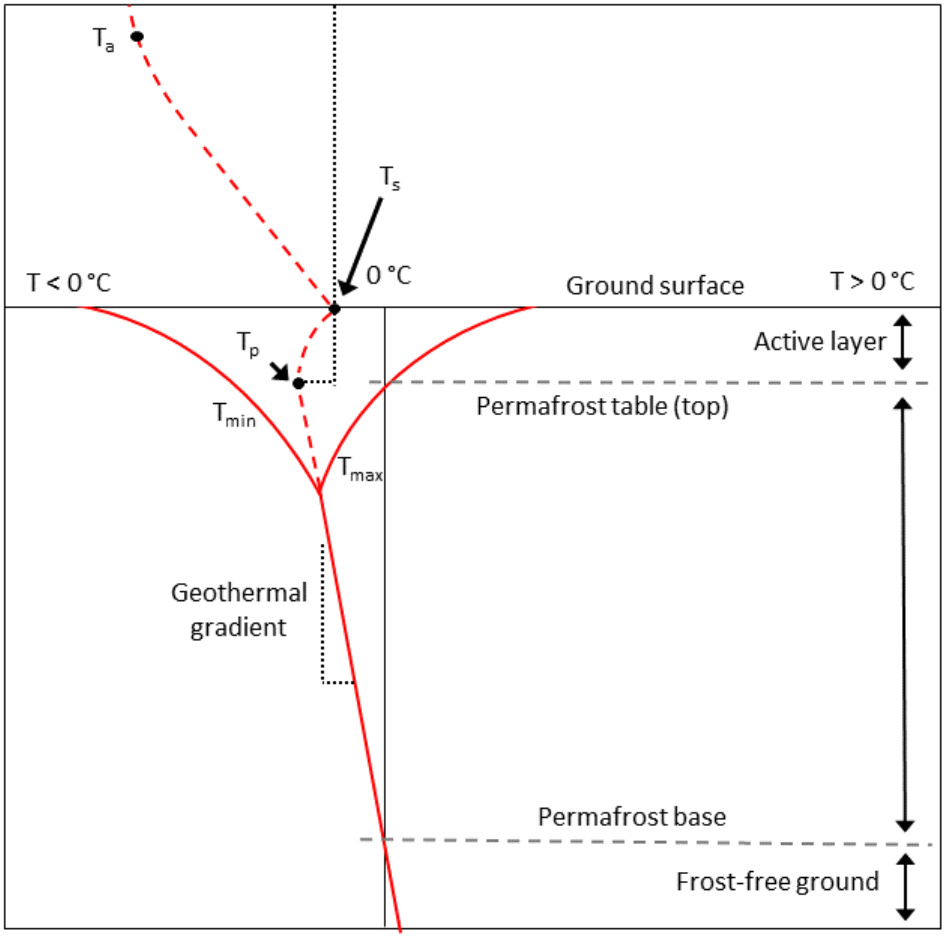

Figure 2.6. Ground thermal regime typical of a periglacial environment. After French (2007, Fig. 5) and Osterkamp and Burn (2003, Fig. 1, p. 1717). Where T_a, T_s, and T_p are the mean annual temperature of the air, ground surface, and top of permafrost, while T_{max} and T_{min} represent the maximum and minimum annual temperatures, respectively, and the dashed red line represents the mean annual temperature.

2.4.2 Distribution

Continental permafrost underlies over half of Canada. In general, permafrost regions are divided into broad zones based on the distribution and thickness of ground underlain by permafrost. One of the most widely used classifications was developed by Heginbottom (1995) and uses four distinct zones. In the northernmost regions where permafrost is practically ubiquitous (90–100%), the area is considered the continuous permafrost zone. The proportion of permafrost-free ground increases progressively towards the south. South of the continuous zone lies the extensive discontinuous zone (50–90%), sporadic discontinuous zone (10–50%), and isolated patches (0–10%). All seven case study sites and entirely of the Greater Whitehorse Area are within the sporadic discontinuous permafrost zone according to Heginbottom (1995).

Following the Alaska Highway, permafrost becomes less abundant south of Kluane Lake, and becomes patchy near Whitehorse (James *et al.,* 2013; Lewkowicz *et al.,* 2011), and is limited to localized areas where surface conditions favour its preservation. Geotechnical investigations along the Alaska Highway in the 1970s indicate permafrost thickness can exceed 45 m depth near the Alaska border, but is less than 20 m thick for most of the corridor (Foothills Pipeline, 1979). Ground temperatures investigation from 1966 to 1981 by Burgess *et al.* (1982) encountered permafrost at only two sites along the corridor south of Kluane

Lake. One site ~15 km northeast of Haines Junction had a permafrost thickness of 12 m, while the other site, southeast of Whitehorse had an observed permafrost thickness of 5 m.

Ground temperature investigations by James *et al.* (2013) examined the degradation of permafrost along the Alaska Highway from Whitehorse to Fort St John, BC, by duplicating the transect by Brown (1967). During original site selection Brown appeared to have preferentially chosen sites beneath poorly drained and stunted black spruce stands, likely to locate permafrost (James *et al.,* 2013). Between Whitehorse and Watson Lake, 18 sites were re-examined. Permafrost was present at ten of those sites in 1964, however by 2007–2008 only six encountered permafrost. Degradation has occurred across the entire transect, with nearly half of the sites that exhibited permafrost in 1964 no longer doing so in 2007–2008. Where permafrost had persisted it was patchy, less than 15 m thick, with mean ground temperatures ranging from −0.5°C to 0.0°C and was in peat or beneath a thick organic layer. Degradation of permafrost in the region is attributed to an increase in mean annual air temperature. The warm temperature suggests the remaining permafrost is sensitive to further climate warming or disturbance of the surface.

These results along with other ground temperature investigations (*e.g.,* Burgess *et al.,* 1982; Burn, 1998; Lewkowicz *et al.,* 2012) reinforce that permafrost found nearby along the northwestern Alaska Highway corridor is generally warm with temperatures above −3°C (Smith *et al.,* 2017). Applied to the GWA, these investigations suggest permafrost encountered in the area is expected to be scattered and discontinuous spatially, as well as relatively thin (<20 m), warm, and sensitive to degradation (Bonnaventure and Lewkowicz, 2013).

In recent years Bonnaventure *et al.* (2012) produced a high-resolution permafrost probability model for northern British Columbia and South-central Yukon, which was made available as an online map (Government of Yukon, 2019). The model combines seven local statistical models that were developed from basal snowpack temperature measurements and ground-truthing, with the main predictive variable being equivalent elevation. Broadly speaking, the model shows the permafrost probability for most of City of Whitehorse between 10 and 50%, with increasing probability at higher elevations.

In southern Yukon, the distinction between latitudinal and mountain permafrost is gradual, and there is no defined lower elevational limit (Lewkowicz *et al.,* 2011). Permafrost probability ranges from continuous on mountain plateaus (*e.g.,* Lewkowicz and Ednie, 2004; Bonnaventure and Lewkowicz, 2008) to low on most of the main valley floors. There have been several studies at Wolf Creek, an example of mountainous permafrost that sits near altitudinal treeline, southeast of Whitehorse *(e.g.,* Lewkowicz and Coultish, 2004; Lewkowicz and Ednie, 2004).

Permafrost is only found where surface conditions, aspect and vegetation favour the maintenance of frozen ground (Foothills Pipelines, 1979), and is generally localized to areas with poor drainage, low sun exposure, and thick organic layers (Foothills Pipelines, 1979; James *et al.,* 2013). Permafrost is commonly confined to fine-grained sediment and is estimated to underlie less than 25% of the region (Burn, 2001; Foothills Pipeline, 1979). The confinement of permafrost to fine-grained sediment is why it is typically found in glaciolacustrine deposits in the Takhini Valley (Rampton 1972; Klassen, 1979). Deposits of gravelly, glaciofluvial material are generally permafrost-free (Burn 1987). Other areas where permafrost occurs are creek bottoms with no standing water, and morainal deposits on the western side of the Yukon Valley covered by a thick layer of organic material (Mougeot Geoanalysis, 1979). Vegetation can be a good indicator of permafrost below treeline, with its presence suggested by stunted black spruce on north-facing slopes in poorly drained depressions or on raised plateaus (Brown, 1967).

The seven case study sites, shown in Figure 1.1, are located at lower elevations. Prior research has established that probability of permafrost lessens at lower elevations and is dependent on the surface conditions and thermal nature of the ground material favouring its preservation. In the GWA permafrost is expected to be spatially discontinuous, relatively thin, and warm. In addition, permafrost is more likely to be encountered in glaciolacustrine sediment, and occasionally morainal deposits, on north facing slopes, where drainage is poor, and organic material is thick.

3 COWLEY CREEK

3.1 Site setting

The Cowley Creek case study site is in the southeastern portion of the City of Whitehorse limits within the Cowley Creek subdivision (Fig. 3.1). The site is south of Salmon Trail and northeast of Cowley Creek, ~50 m east of the creek bank and 4 km upstream from its confluence with Yukon River (Fig. 3.1). The site lies at an elevation of 718 m on a low fluvial terrace (Fig. 3.2) with hummocky microtopography.

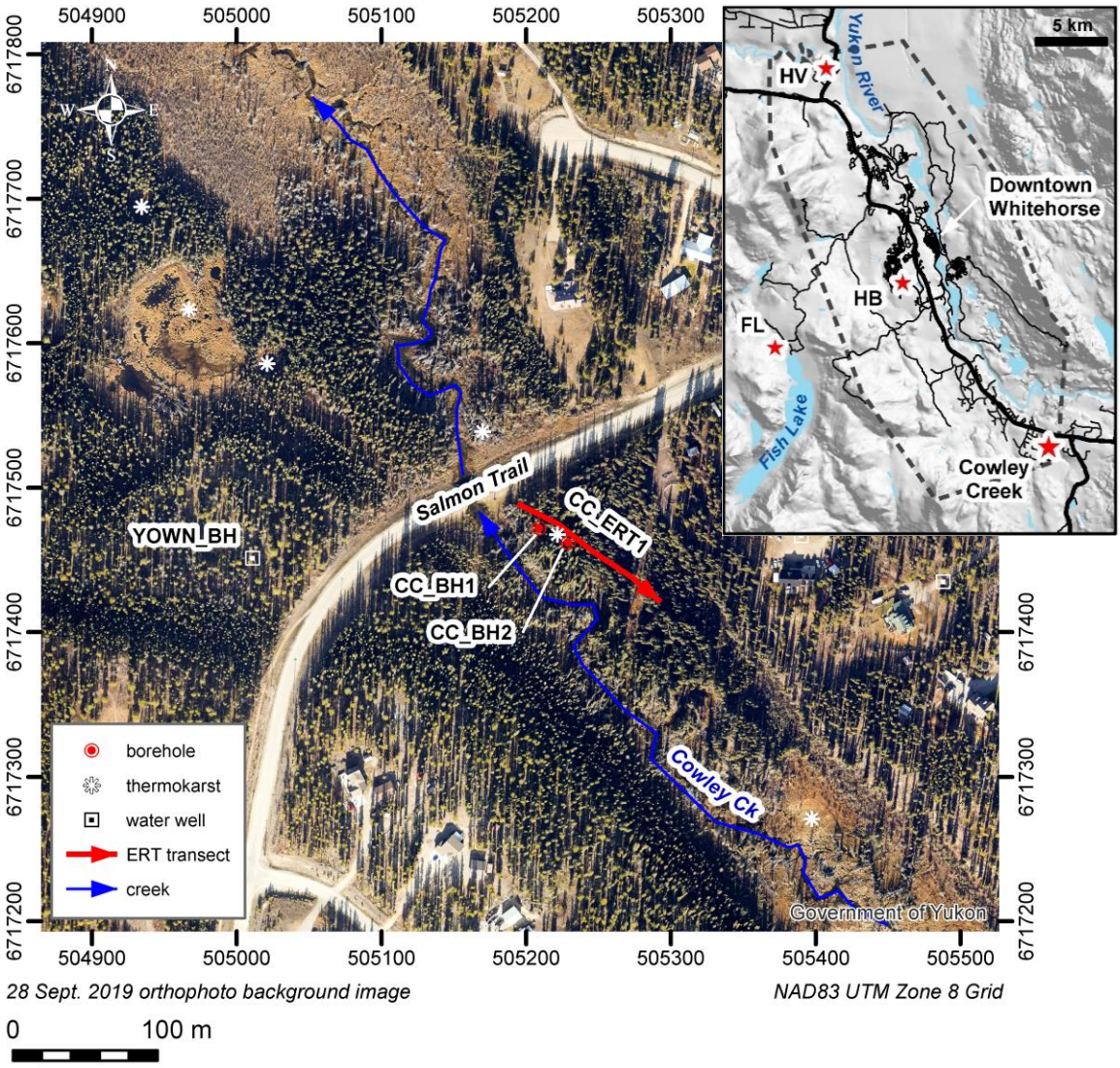

Figure 3.1 Location of Cowley Creek case study site in relation to Salmon Trail, with borehole and ERT survey locations. Inset map shows location relative to Whitehorse city limits (dashed line) and other nearby case study sites (FL = Fish Lake, HB = Hamilton Blvd, HV = Hidden Valley).

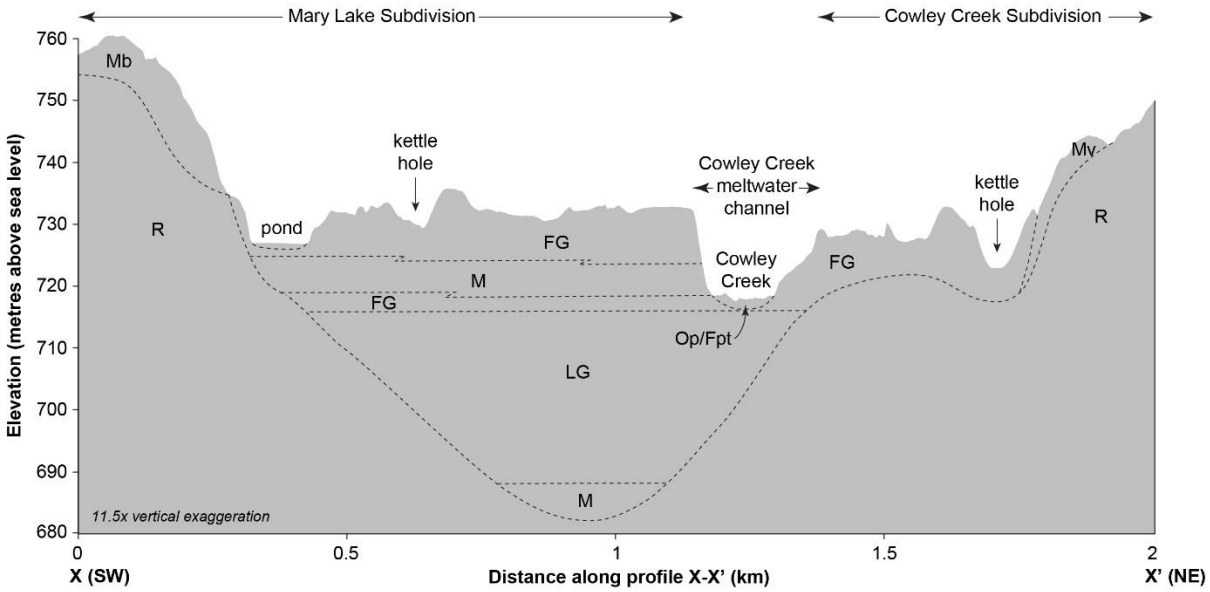

Figure 3.2 Generalized stratigraphic cross section from 2013 LiDAR DEM along transect X-X' (shown in Fig. 3.3).

3.1.1 Climate and vegetation

For 2009–2012, mean annual air temperature (MAAT) at a Cowley Creek borehole (CC_BH1) was reported as −2.0°C (Lipovsky, 2014). MAAT at Whitehorse airport was 0.02°C over the same four-year period (ECCC, Whitehorse A). Stable areas of the case study site are classified as BOLsl/01Z-Sw27s in the Yukon Bioclimate Ecosystem Classification System (McKenna, *et al.,* 2017). This classification is characterized by mesic to submesic soils, dominated by medium to dense white spruce (*Picea glauca*) stands, feathermoss, and sparse ground vegetation (McKenna, *et al.,* 2017). Common plant species include shrubs (*Vaccinium vitis-idaea*), forbs (*Geocaulon lividum, Orthilia secunda*), mosses (*Hylocomium, Pleurozium*), and lichens (*Cladonia spp., Peltigeria spp*.). Areas of the site where permafrost thaw is occurring are characterized by subhygric soils, willow (*Salix spp.*), sedges (*Carex spp*.) and horsetails (*Equisetum arvense*).

Vegetation and tree surveys identified intact permafrost areas as forested with large white spruce (Vogt, 2021, in prep). Transitional and degraded areas remain forested; however, forest density was lower by ~50%, which may be due to increased surface moisture and ground subsidence causing unfavourable conditions for tree growth (Vogt, 2021, in prep). Many fallen trees were observed along the transect.

3.1.2 Surficial geology

Figure 3.3 summarizes the local surficial geology of the study area. The case study site lies in the floor of a former glacial meltwater channel which is now occupied by the modern Cowley Creek, a slow-moving underfit stream. In the late stages of deglaciation, this meltwater channel was the outlet for Glacial Lake Watson, which inundated the major river valleys extending south towards Carcross (Bond, 2004). During the Holocene, the floor of the meltwater channel has gradually built up with fluvial sediment (largely silt and sand with pockets of gravel) and organic material. This is one of the primary geomorphological settings which has supported the local development of ice-rich permafrost in the Whitehorse area. The Cowley Creek valley bottom also is subject to periodic flooding due to beaver damming which temporarily increases local groundwater levels.

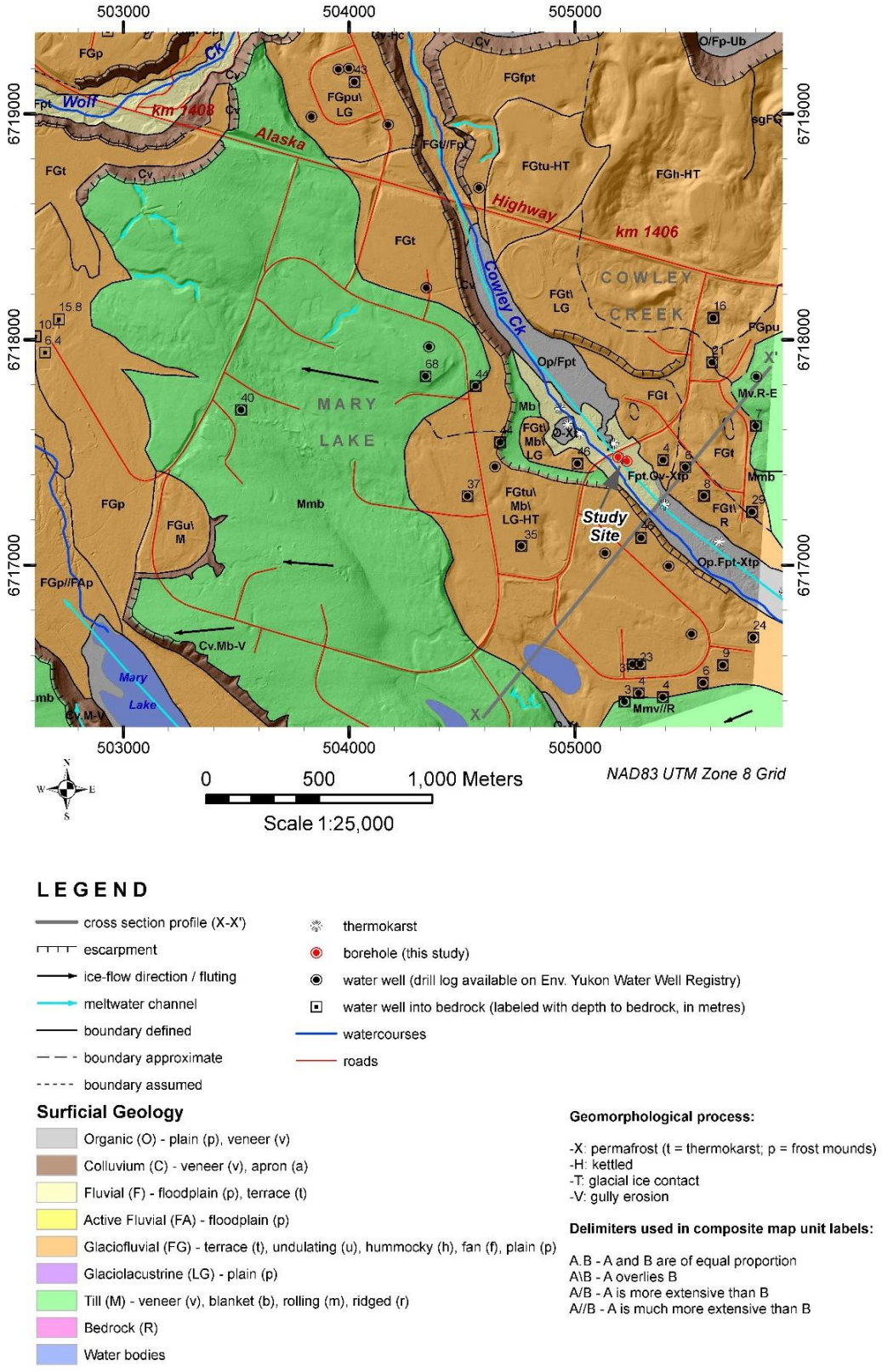

LEGEND

- cross section profile (X-X')
- escarpment
- ice-flow direction / fluting
- meltwater channel
- boundary defined
- boundary approximate
- boundary assumed
- thermokarst
- borehole (this study)
- water well (drill log available on Env. Yukon Water Well Registry)
- water well into bedrock (labeled with depth to bedrock, in metres)
- watercourses
- roads

Surficial Geology

- Organic (O) - plain (p), veneer (v)
- Colluvium (C) - veneer (v), apron (a)
- Fluvial (F) - floodplain (p), terrace (t)
- Active Fluvial (FA) - floodplain (p)
- Glaciofluvial (FG) - terrace (t), undulating (u), hummocky (h), fan (f), plain (p)
- Glaciolacustrine (LG) - plain (p)
- Till (M) - veneer (v), blanket (b), rolling (m), ridged (r)
- Bedrock (R)
- Water bodies

Geomorphological process:

-X: permafrost (t = thermokarst; p = frost mounds)
-H: kettled
-T: glacial ice contact
-V: gully erosion

Delimiters used in composite map unit labels:

A.B - A and B are of equal proportion
A\B - A overlies B
A/B - A is more extensive than B
A//B - A is much more extensive than B

Figure 3.3 Simplified surficial geology map showing major landscape units, landforms and boreholes drilled in the vicinity of Cowley Creek.

The dominant surface materials in the surrounding Cowley Creek subdivision area comprise thick packages of glaciofluvial sand and gravel that were deposited by meltwater draining the receding glaciers. In many locations in the Cowley Creek area, the glaciofluvial materials are underlain by a thick (20+ m) sequence of fine-grained (fine sand, silt and clay) glaciolacustrine materials. These glacial lake bottom sediments were deposited in Glacial Lake Laberge, which occupied the Yukon River valley up to 716 m elevation (see introduction for more background). Incision of these materials in the Yukon River valley has also caused a regional reduction in base level throughout the Holocene.

Much of the higher ground (above ~735 m elevation) is covered by till, which is locally streamlined or fluted in the Mary Lake subdivision (Fig. 3.3). The orientation of these flutings indicate that the dominant ice-flow direction was westerly in the immediate area during the latest (Cassiar) readvance phase.

Basal till in the vicinity typically comprises a dense, nearly impermeable, diamict with a sandy silt matrix and a wide range of coarse fragment characteristics (size, lithology, and rounding). Basal till on the order of 10–15 m thick was commonly encountered in nearby water wells (Fig. 3.3; Environment Yukon, 2021). Till veneers are also found where bedrock is located within 1 m of the surface.

The study area is underlain by the mid-Cretaceous (116 Ma) Whitehorse Pluton which largely comprises granodiorite (Yukon Geological Survey, 2021). Based on a handful of local water wells drilled in the vicinity (Environment Yukon, 2021), depth to bedrock immediately adjacent to Cowley Creek is relatively shallow (4–8 m) on the northeast side of the creek but is deeper (24–46 m) on the southwest side (Fig. 3.3).

3.1.3 Permafrost

Permafrost is present at the site, as verified by frost probing and boreholes. Thermokarst ponds and drunken forests along both sides of the creek in the vicinity indicate degrading ice-rich permafrost. Several large thermokarst ponds are discernible in aerial photographs within the 3-km long segment of the Cowley Creek valley bottom extending 2 km upstream and 1 km downstream of the study site (Fig. 3.3). Thermokarst ponds occupy a closed depression formed by settlement of the ground following thawing of ice-rich permafrost. They are usually shallow and may expand by active-layer failure. Lithalsas (a type of permafrost mound) are also observed at this site. The formation process of a lithalsa is similar to a palsa, but the growth of the segregated ice (producing the mound) is favored by the high thermal conductivity of fine mineral soil and not organic material.

3.2 Results

3.2.1 Borehole geotechnical data

The first borehole at this site, CC_BH1, was drilled and instrumented in 2007 by Kenji Yoshikawa (University of Alaska Fairbanks) and has since been maintained by the YGS (Lipovsky and Yoshikawa, 2009; Lipovsky, 2014). Borehole CC_BH1 was drilled to a depth of 4.95 m using a 2-inch auger stem and was instrumented with seven thermistors to measure ground temperature and one thermistor to measure air temperature (Table 3.1). The site had a surface organic layer 0.10 m thick, underlain by at least 5 m of silt and fine sand with lenses of wood fragments and organics. Permafrost is present below 2 m, and a layer of ice-rich, light grey clay was encountered between 4 and 5 m depth (Lipovsky and Yoshikawa, 2009). Due to the drilling method, no permafrost or geotechnical cores were collected. No visible ice was observed in the upper 4 m of silt and fine sand, however ice-rich clay was encountered from 4 to 5 m depth. A 120-m ERT survey was conducted on 22 May 2018 (Fig. 3.1 and Table 3.1), following the methods described in Appendix E.

Table 3.1 Location details of field surveys at the Cowley Creek study site, including two instrumented boreholes, and one ERT survey.

Site	Coordinates (NAD83 UTM Zone 8)	Depth (m)	Ground Temperature Sensor Depth (m)
CC_BH1	505209 6717472	4.95	AT, 0.0, 0.5, 1.0, 2.0, 3.0, 4.0, 4.95
CC_BH2	505229 6717462	5.11	0.0, 0.5, 1.0, 1.5, 2.0, 3.0, 4.0, 5.10
CC_ERT1	Dipole-dipole and Wenner	Length (m): 120	Electrode Spacing (m): 1.5
0 m	505194 6717489		
30 m	505222 6717475		
60 m	505246 6717456		
90 m	505273 6717438		
120 m	505293 6717421		

A second 5 m borehole, CC_BH2, was drilled and instrumented on 29 September 2018 on the top of a small permafrost mound. The borehole was cased with a sealed 1-inch PVC pipe, instrumented with two 4-channel Hobo loggers to record ground temperatures at eight depths (Table 3.1), and backfilled with earth to the surface (Fig. 3.4). CC_BH2 is ~20 m southeast of CC_BH1, and 42 m along the ERT survey (CC_ERT1). Vegetation at the site consists of mature white spruce forest up to about 20 m high, with a 0.05 m thick ground cover of moss and lichen. Bare mineral soil was also observed at the surface in the vicinity of the borehole (Fig. 3.4). Prior to drilling from the frost table, the unfrozen active layer was excavated by shovel to 0.80 m depth, then hand augered to the thaw front at 1.2 m depth. The unfrozen active layer primarily comprises fine-grained silty-sand.

The cryostratigraphical profile of CC_BH2 (see Figure A1), shows interbedded layers of microlenticular and lenticular gray fine sand and silt from 1.4 to 2.5 m, underlain by layers of silty sand from 2.5 to 4.8 m. Centimeter-scale ice lenses were visible throughout the profile in the silty material, and the thickness of ice lenses increases with depth below 2.8 m. The increase of ice lens thickness with depth may be explained by the epigenetic origin of the permafrost; *i.e.,* the permafrost formed after the ground material was deposited. During frost progression the temperature gradient decreases with depth. So, at lower depths more time is given for cryosuction to occur. Cryosuction is the process whereby (unfrozen) pore water is ‘sucked’ towards the zone where freezing is occurring (the freezing plane) because of a negative pressure that develops as pore water freezes. A greater amount of time for cryosuction allows the ice lenses to grow thicker while the freezing plane remains at a stable depth. The borehole ended at 5.1 m depth, where ice-poor gravelly sand prevented further drilling. Excess ice (*i.e.*, the volume of ice in excess of the total pore volume of the ground when unfrozen), ranged from 26 to 55% throughout the profile, with a mean of 42%. Assuming an active layer depth of 1.5 m (based on linear interpolation of the ground temperature envelope), and a permafrost base of 5.1 m (at the end of the borehole, however permafrost likely extends past this), the potential subsidence is 1.5 m.

Figure 3.4 Location of borehole CC_BH2 and surrounding vegetation cover.

A groundwater monitoring well (YOWN_BH in Fig. 3.1) was drilled for Environment Yukon Water Resources by Northern Sonic Drilling using a sonic rig which allowed recovery of intact 6-inch core. The 48-m-deep well was drilled on 30 and 31 December 2019 on a low glaciofluvial terrace located ~200 m west of the study site (Fig. 3.3). The terrace lies ~5 m higher than the elevation of the study site on the inactive terrace. Based on the core samples, stratigraphy at this site from top to bottom, comprises the following: 3.5 m of loose sand and gravel glaciofluvial material at the surface, 3.5 m of looser ablation (melt out) till, 3 m of dense basal till, 2 m of coarse sand and gravel glaciofluvial sediment, 28 m of fine-grained glaciolacustrine sediment, and 5 m of till overlying bedrock (46 m depth). No permafrost was encountered in the well, presumably due to the thick cover of coarse-grained sediment.

3.2.2 Ground temperatures

The ground temperature recorded since 2007 at CC_BH1 shows warm permafrost, with temperatures at 4.9 m depth sitting just below 0.0°C (Fig. 3.5), averaging −0.2°C from 2007–2020. Since 2012, a slight cooling of −0.1°C has been observed at 4.9 m depth (Fig. 3.5). Gaps in data collection prevent an analysis of more recent active layer depth trends, however the active layer was reported as 1.9 m for the 2009–2012 period (Lipovsky, 2014).

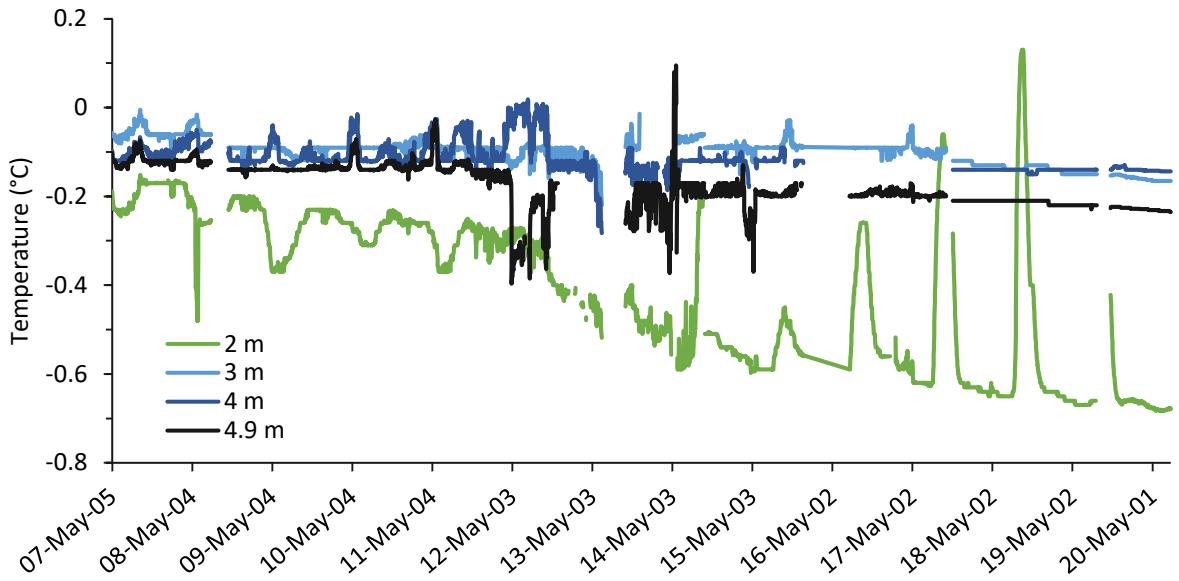

Figure 3.5 Cowley Creek daily mean ground temperatures at CC_BH1 for the period 5 May 2007 to 24 July 2020 from 2 to 5 m depth.

The rapid fluctuation of temperature in May 2014 at 4.9 m depth (Fig. 3.5) suggests a quick thaw episode in spring could have allowed ground water flow to produce a rapid ground temperature increase. In 2017, it was noted that the ground surface at CC_BH1 had subsided by 40 cm since installation in May 2007. Decreasing daily temperature and increasing intra-annual variation at 2 m depth (Fig. 3.5) may either be due to the subsidence experienced at the borehole, or an increase in active layer depth. Subsidence at the borehole would mean the distance between the thermistor at 2 m depth and the ground surface has gradually lessened.

Recording at borehole CC_BH2 began on 8 November 2018 and data was downloaded on 24 July 2020. Daily mean temperatures at CC_BH2 suggest the active layer is less than 2.0 m thick (Fig. 3.6b), as does the ground temperature envelope for the one-year period from 1 January to 31 December 2019 (Fig. 3.7). Ground temperature at the deepest point, 5.10 m, is stable at −0.08°C (Fig. 3.6b and Table 3.2). Stable ground temperatures are also seen in Table 3.2, where annual maximum, minimum and mean ground temperatures between 1.5 and 5.1 m depth remained below the freezing point and ranged from −0.01°C to −0.14°C. Ground temperatures at CC_BH2 are similar to those of CC_BH1.

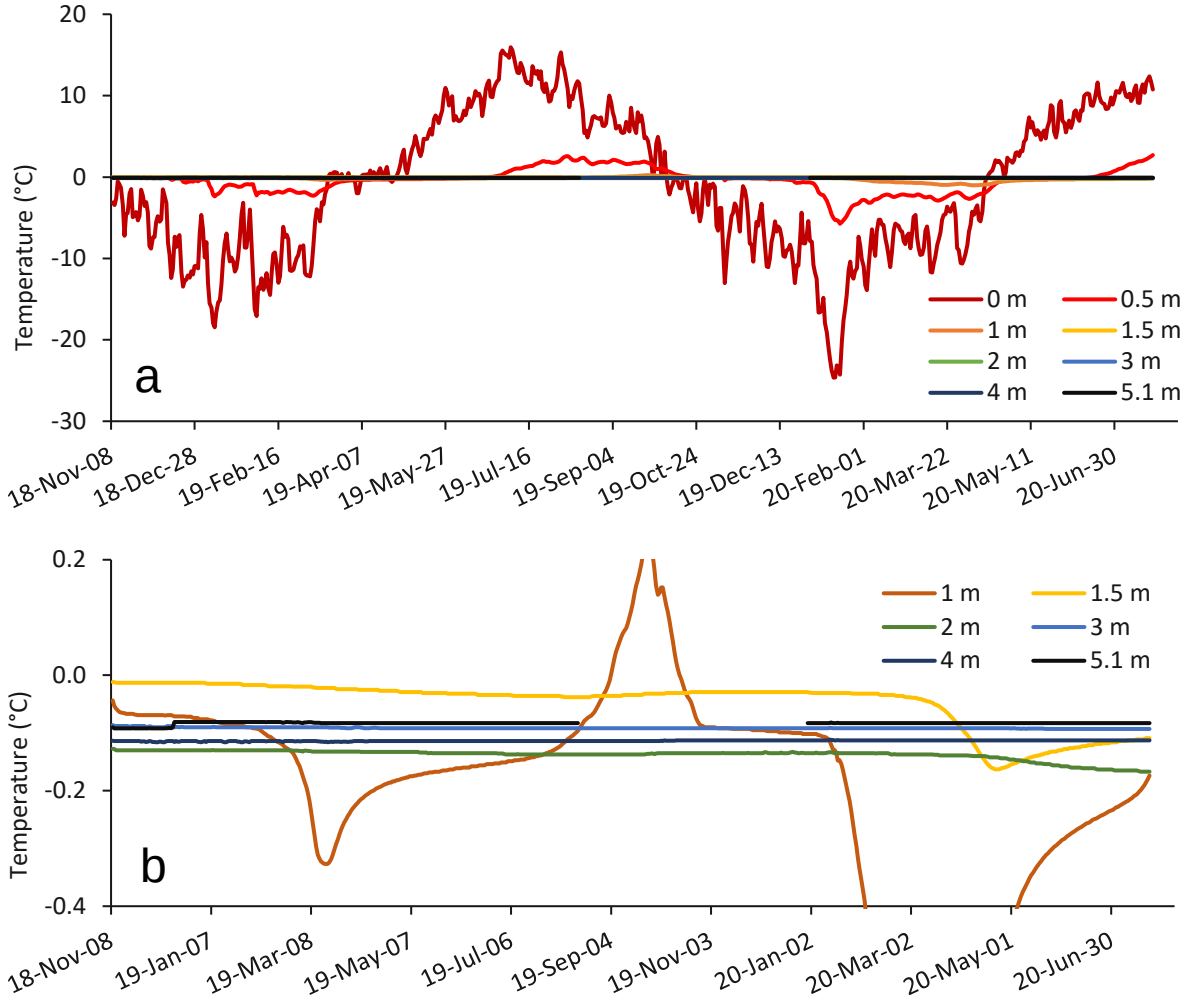

Figure 3.6 Cowley Creek daily mean ground temperatures at CC_BH2 for the period 8 November 2018 to 23 July 2020, from a) 0 to 5.1 m depth, and b) 1 to 5.1 m depth.

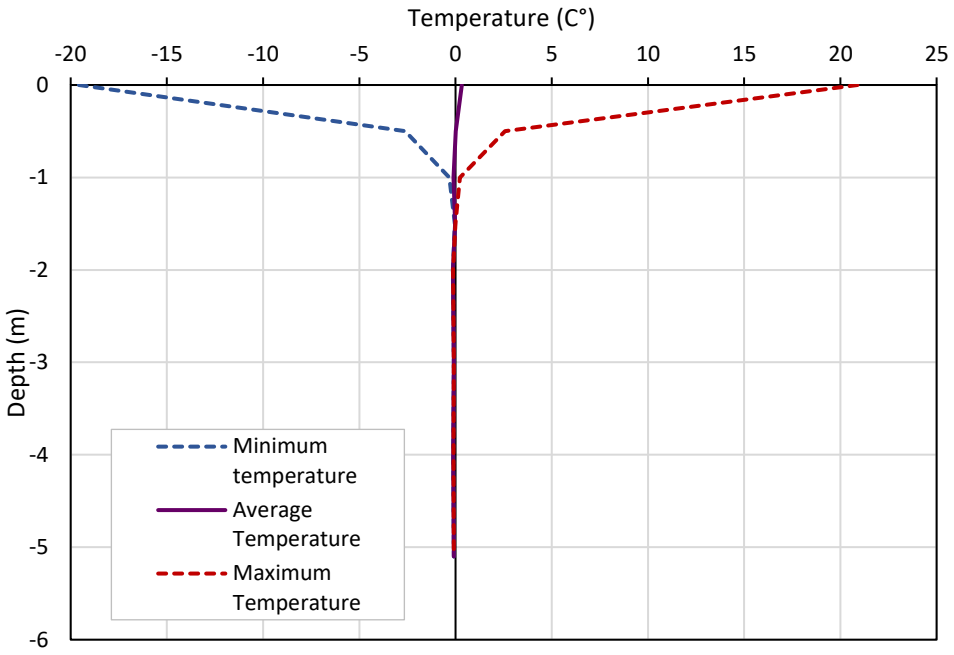

Figure 3.7 Cowley Creek ground temperature envelope at CC_BH2 for the period 1 January 2019 to 31 December 2019.

Table 3.2 Annual minimum, maximum and mean ground temperature (from daily mean values) at CC_BH2 for the period 1 January 2019 to 31 December 2019.

Depth (m)	0	0.5	1.0	1.5	2.0	3.0	4.0	5.1*
Annual min GT (°C)	−19.57	−2.61	−0.33	−0.04	−0.14	−0.09	−0.12	−0.08
Annual mean GT (°C)	0.33	0.01	−0.11	−0.03	−0.13	−0.09	−0.11	−0.08
Annual max GT (°C)	20.89	2.58	0.23	−0.01	−0.13	−0.09	−0.11	−0.08

* Ground temperature values at 5.1 m depth missing data for 17 August 2019–30 December 2019.

3.2.3 ERT

Figure 3.8 shows results from both the Wenner and dipole-dipole ERT surveys carried out on 22 May 2018. The results show a similar distribution of resistivity in the ground in both surveys; however, the dipole-dipole appears to show more detail for the low resistivity values.

In the Wenner array (Fig. 3.8b), high resistivity values, represented by darker blue shades, are mainly localized in the middle of the profile between 5 and 15 m in depth. The lowest resistivity values which suggest unfrozen ground and represented by red shades, are located across most of the profile from 0 to 5 m depth. This unfrozen area is consistent with active layer thicknesses measured in boreholes CC_BH1 and CC_BH2. There are additional low-resistivity areas on the eastern side of the profile surrounding small high resistivity bodies. These particular low resistivity areas could be due to groundwater movement.

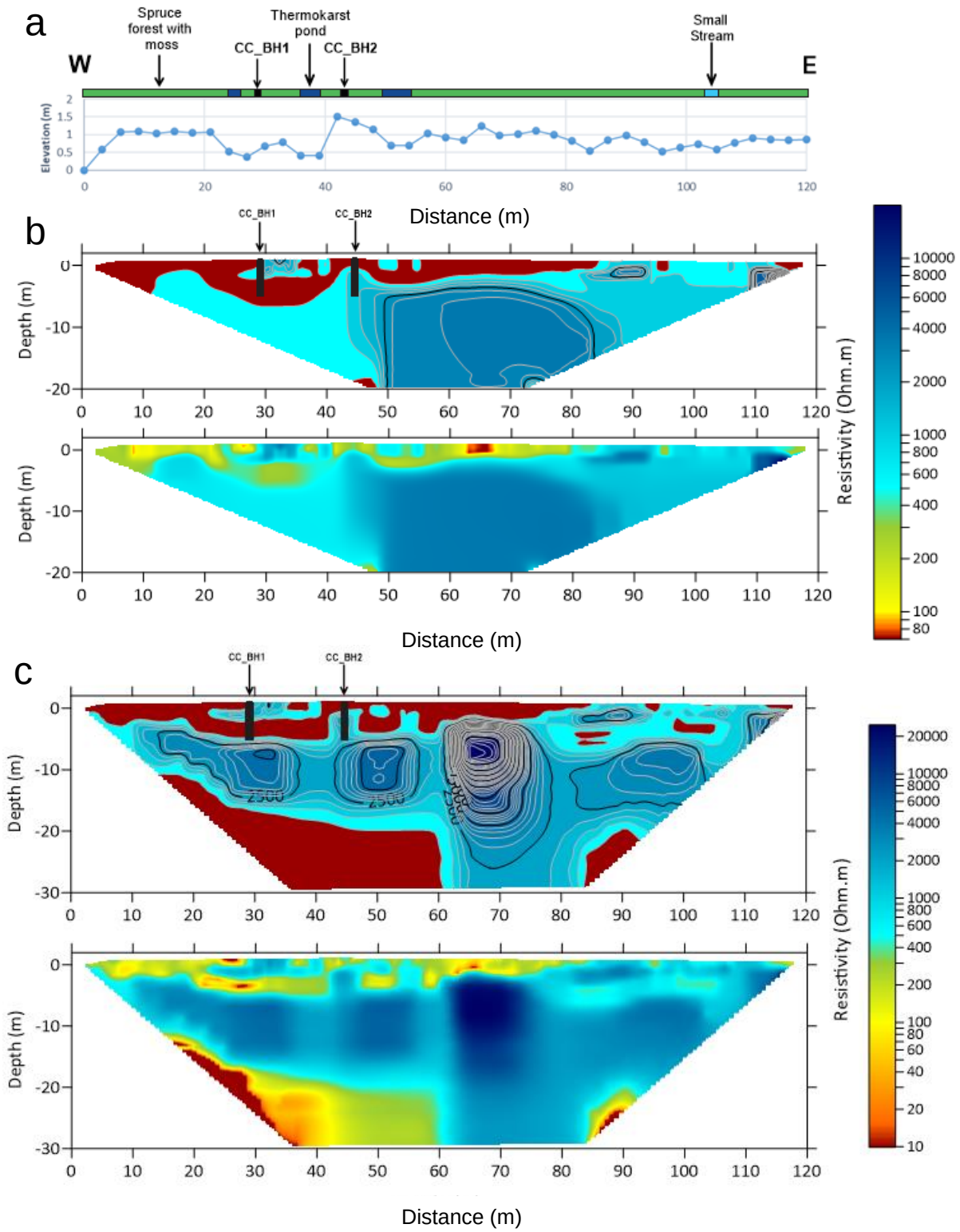

Figure 3.8 Cowley Creek ERT survey (CC_ERT1) showing the (a) topographic profile, (b) ERT profile using Wenner array, 6th iteration, RMS error= 3.96%, and (c) ERT profile using dipole-dipole array, 4th iteration, RMS error= 5.58%. The upper figure in each of (b) and (c) is homogenized to differentiate between ground material interpreted as frozen (blue) and unfrozen (red). Resistivities above the 2500 ohm·m isoline in the upper figure in (b) and (c) suggest a higher likelihood of ice-rich permafrost.

In the dipole-dipole array (Fig. 3.8c), high resistivity values are present along the entire profile between 2 and 20 m depths. The depths are variable, and the thickest high-resistivity layer is especially prominent at the middle of the profile, where it reaches 15–18 m (near electrode 65, at 96 m). Areas of low resistivity occur in the uppermost 5 m of the profile and are better defined than in the Wenner array. Some distinct low-resistivity bodies are apparent close to the water ponding area near to borehole CC_BH1.

Overall, the very high-resistivity areas are attributable to ice-rich fine-grained ground. High-resistivity areas decrease with depth, as permafrost becomes warmer and liquid water content increases, and as the soil might become coarser and ice-content decreases. Low resistivity values are attributable to ice-poor and/or unfrozen material. The lowest resistivity values may indicate the presence of liquid ground water passing near permafrost. Interpretation of the ERT geophysical data, and geotechnical knowledge suggests the base of permafrost at this site is between 15 and 20 m.

3.2.4 Synthesis

Borehole and ERT data are consistent with one another, and indicate the presence of fine-grained, ice-rich material from the surface to a depth between 10 and 15 m. Maximum permafrost depth is likely between 15 and 20 m. At depths greater than 10–15 m, the frozen ground appears to become coarser and ice-poor, leading to decreasing resistivity with depth (shown in the dipole-dipole array in Fig. 3.8c).

The permafrost at Cowley Creek is relatively warm with the temperature of permafrost sitting just below the freezing point. The lowest annual mean ground temperature was −0.13°C at 2 m depth. High ice contents close to the surface are currently preserving the permafrost, as a large amount of energy is required to melt the ice and release its latent heat. Complete permafrost thaw could cause subsidence on the order of 40% of the permafrost thickness, or more, if underground water movement leaches sediment. This corresponds to a potential subsidence of 1.6 m. Subsidence is the main hazard for this site and similar landscape units as no slope instability exists. As observed in the neighboring ponds and creek, the height of the water table is above the base of permafrost. Consequently, it is possible for groundwater to seep through permafrost at this site.

4 HAMILTON BOULEVARD

4.1 Site setting

The Hamilton Boulevard case study site is located near the Copper Ridge and Granger subdivisions in the central portion of the City of Whitehorse limits (Fig. 4.1). The site is 750 m southeast of Falcon Drive on the southwest side of Hamilton Boulevard. The area investigated is the triangular-shaped area bounded between Hamilton Boulevard to the northeast and a gravel road to the southwest (Fig. 4.2). The site lies at an elevation of ~750 m asl and slopes gently to the northeast at less than 5°. Drainage is poor as the site is located within a local depression with hummocky microtopography. The site is surrounded by linear disturbances including a paved road, cutline, power lines and a gravel road (Fig. 4.1).

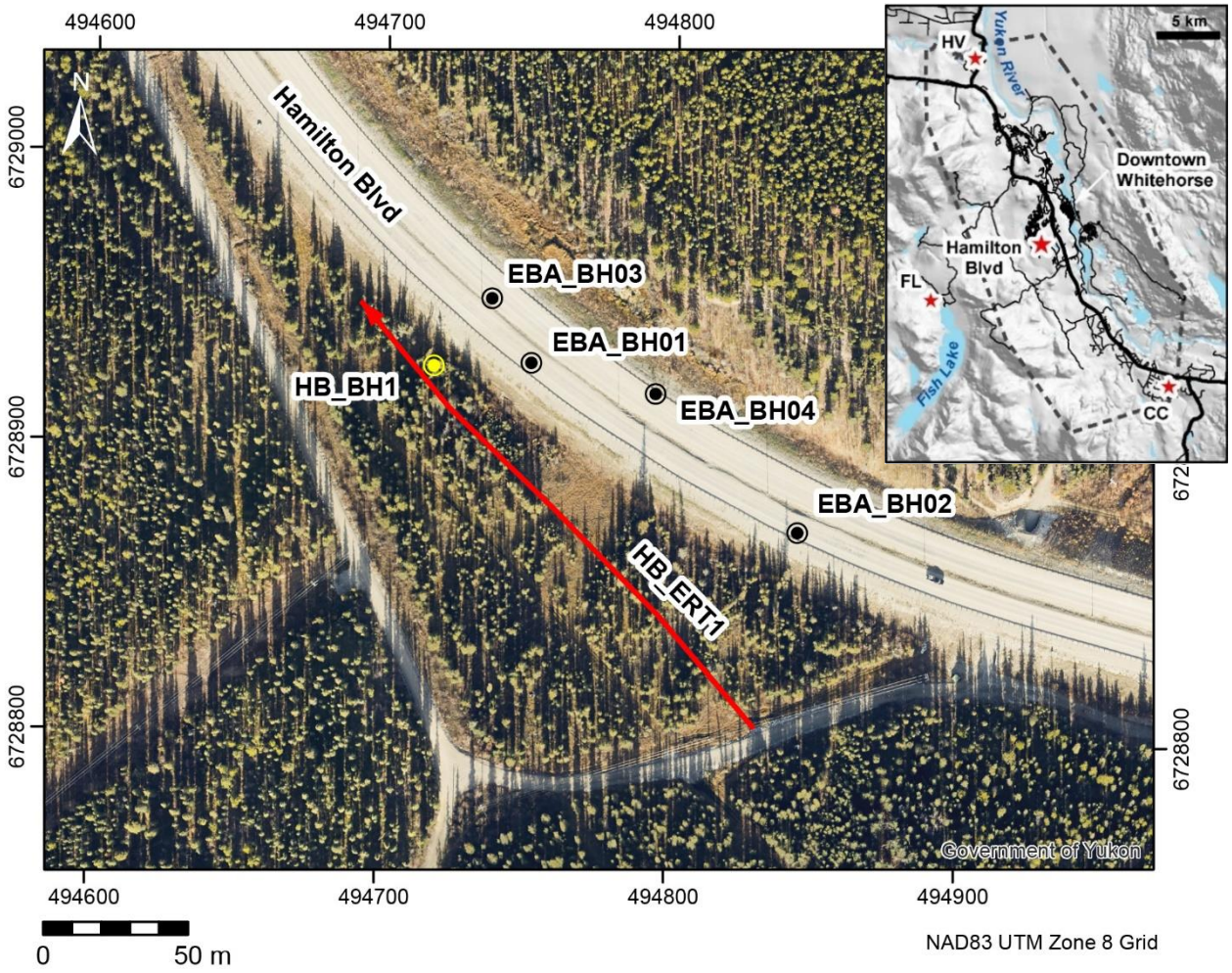

Figure 4.1 Location of Hamilton Boulevard case study site with borehole and ERT survey locations. Orthophoto background image (28 September 2019). Inset map shows location with respect to Whitehorse city limits (dashed line) and nearby case study sites (FL= Fish Lake, HV= Hidden Valley, and CC= Cowley Creek).

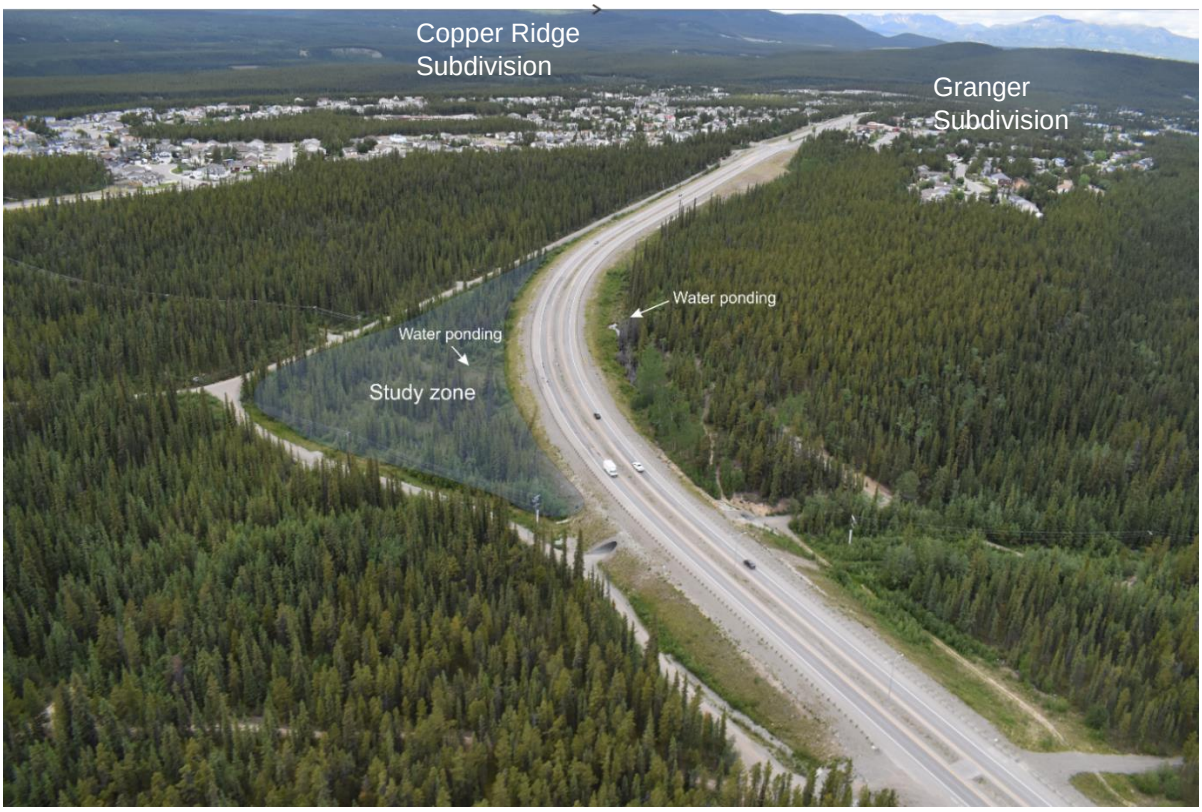

Figure 4.2 Oblique aerial view of study site, shaded blue, with Copper Ridge and Granger subdivisions visible to the north.

4.1.1 Climate and vegetation

Stable areas of the case study site are classified as BOLsl/33P-Sw39z in the Yukon Bioclimate Ecosystem Classification (YBEC) System (McKenna, *et al*., 2017). This classification is characterized by subhygric to hygric soils, dominated by an open to well-developed canopy of white spruce (*Picea glauca*), with willow as the dominant understory species. Characteristic vegetation includes common horsetail (*Equisetum arvense*), and mosses (*Aulacomium, Tomenthypnum, Hylocomium*) (Mckenna *et al.,* 2017). Other common species at this site are lowbush cranberry (*vaccinium vitis-idaea*), Bastard toadflax (*Geocaulon lividum),* and lichens (*cladonia spp., peltigaria spp.).* In degraded and transitioning open areas, sedges and grasses are more common (Mckenna *et al.,* 2017).

Results from a tree survey indicate intact and transitional permafrost areas are densely forested with white spruce (Vogt, 2021, in prep). Permafrost at this site is shallow and very little subsidence is observed. Subsequently, forest cover on transitional permafrost appears unaffected by thaw. The degraded area is unforested, however, the area surveyed has a large amount of disturbance, including a cut line. As no observations of fallen or dead trees are present in this area, it is likely trees were removed by human disturbance rather than lost due to permafrost thaw.

4.1.2 Surficial geology

The surficial geology and landscape features of the Hamilton Boulevard case study site area are summarized in Figures 4.3 and 4.4. The dominant surficial material in the vicinity of the case study site is basal till, which was deposited directly beneath glacier ice. The dominant ice-flow direction during the latest (Cassiar) glacial readvance phase was northwesterly, as indicated by fluted landforms and striae exposed on nearby streamlined bedrock (*e.g.,* 18PL121; located 1 km east of the study site).

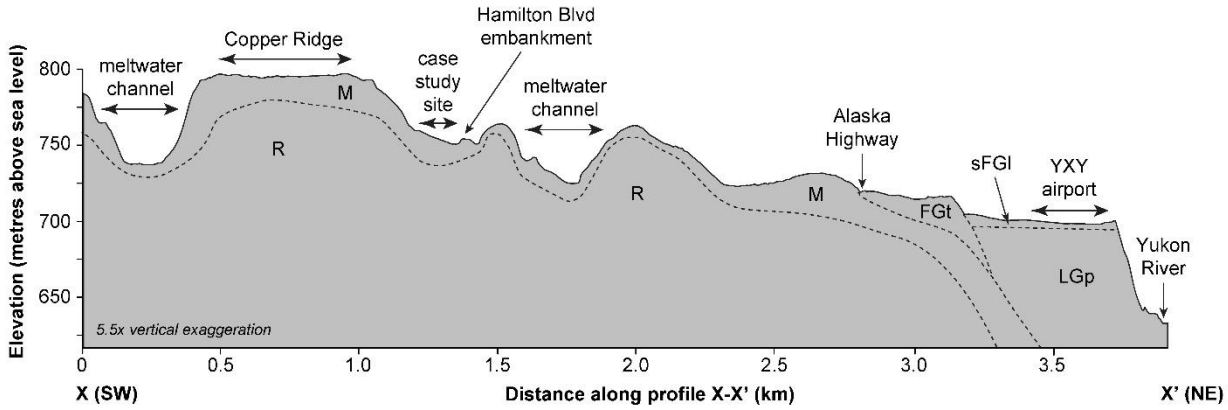

Figure 4.3 Generalized stratigraphic cross section from 2013 LiDAR DEM along transect X-X' (shown in Fig. 4.4).

Basal till in the vicinity typically comprises a dense, poorly-sorted diamict supported by a sandy silt matrix with a wide range of coarse fragment characteristics (size, lithology, and roundness). Till up to 10 m thick was encountered in water wells located near Lobird subdivision (Environment Yukon, 2021). Till veneers are found where bedrock is located within 1 m of the surface. Crevasse fillings are common landforms that overprint many basal till units in the area (Mbr on Fig. 4.4); these are small-scale, low-relief (<2 m) ridges, oriented transverse to the primary direction of ice-flow and comprise a diamict that is less dense than basal till.

During deglaciation, glacial meltwater carved numerous erosional landforms into the local landscape. These include small shallow meltwater channels in basal till, scoured bedrock and canyons in the vicinity of Yukon Gardens, and the large meltwater channel that flanks the west side of Copper Ridge. Thick terraces of glaciofluvial sand and gravel were deposited along the margins of the receding glaciers in the Hillcrest and South Access areas. A thick sequence of fine-grained glaciolacustrine sand, silt and clay was also deposited in the Yukon River valley bottom (up to 716 m elevation), due to the impoundment of Glacial Lake Laberge (see introduction for a more detailed background). After this lake drained, the exposed lake bottom sediments were subsequently reworked by wind which deposited a thin (<2 m) cap of silty eolian material across much of the local landscape.

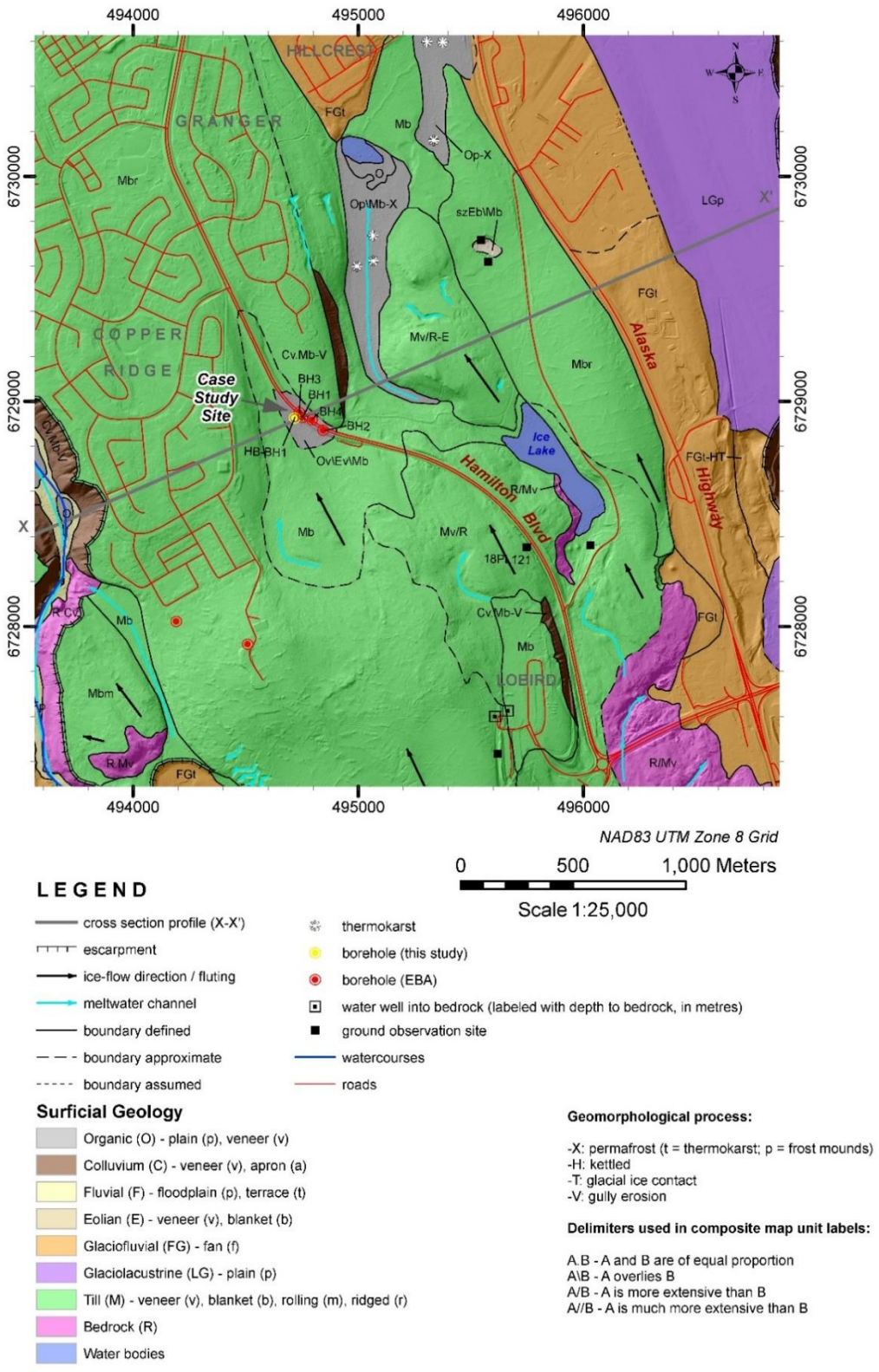

Figure 4.4 Simplified surficial geology map showing major landscape units, landforms and boreholes drilled in the vicinity of Hamilton Boulevard.

During the Holocene, moderate and steep slopes (*e.g.,* meltwater channel escarpments) have been subjected to colluvial processes through the action of gullying and surface sloughing. Partially decomposed plant or organic materials have accumulated in poorly-drained low-lying areas such as the floors of meltwater channels and where small depressions in the local bedrock topography occur. The latter example is the specific setting of the Hamilton Boulevard case study site, where the local stratigraphy comprises a mantle of organic material overlying silty eolian material (loess) deposited above till.

Several thermokarst ponds are present within 500 m of the case study site (Fig. 4.4) in low-lying organic-rich terrain, which is a common setting for ice- rich permafrost to develop in the Whitehorse area. Factors favouring the development of permafrost in these environments include a topographic position which promotes cold air drainage, high soil moisture, and the highly insulative capacity of the organic materials.

The entire case study area is underlain by the mid-Cretaceous (116 Ma) Whitehorse Pluton which largely comprises granodiorite (Yukon Geological Survey, 2021). Where it is exposed at the surface, the granodiorite commonly decomposes into a veneer of unconsolidated coarse sand to pebble-sized grus, *e.g.,* at the south end of Ice Lake. Bedrock is relatively shallow in the area, with up to 10 m of overburden encountered in water wells in the Lobird Subdivision area (Environment Yukon, 2021) and 2–4 m of overburden near the hilltop snow dump ~1 km south of the study site. Weathered bedrock was encountered at the study site at a depth of ~10 m below the road fill (EBA, 2013 – BH02). Bedrock outcrops are also common along Hamilton Boulevard road cuts west of Ice Lake, the southern shores of Ice Lake, the steep flanks of the Copper Ridge meltwater channel, and in the Yukon Gardens area.

4.1.3 Site history

The site history has been well summarized by EBA (2013): “The northern portion of Hamilton Boulevard was constructed to provide transportation, evacuation and utility corridors for residential, commercial, and recreational areas west of the city center. Continuing development has created a necessity for alternate access routes requiring the extension of Hamilton Boulevard south to the intersection of Robert Service Way and the Alaska Highway. Construction on the south section of Hamilton Boulevard began in 2008 and was completed in 2009. The embankment consists of about 3 m of quarry rock, from nearby rock cuts, placed over existing organics, fine-grained and granular materials. This area has since experienced significant settlements [on the order of 0.30–0.90 m from 2009 to 2013] that have affected trafficability”. EBA (2013) attribute the main cause of road settlement at the site to thawing of ice-rich silt and consolidation of peat beneath the quarry rock fill. They also note the cost of ongoing road maintenance (stripping and resurfacing) from 2010 to 2013 was ~$110 000 per year.

Government of Yukon Community Services Infrastructure Development Branch has been exploring different alternatives to attempt to stabilize sections STA 4+640 to 4+860 (*i.e.*, 4.64 to 4.86 km from the intersection of the Alaska Highway and Hamilton Boulevard, which corresponds to the section of road adjacent to the Hamilton Boulevard case study site). EBA Engineering Consultants Ltd. completed a geotechnical investigation of Hamilton Boulevard in 2013 to provide mitigation methods to stabilize the embankment (EBA, 2013).

The Hamilton Boulevard site is poorly-drained as it is in a local depression, and the road embankment appears to be intercepting surface water runoff from the northeast slope. No drainage paths have been constructed to manage surface water (EBA, 2013). Ponds have started to form on the south-western side of the road. It is unclear whether ponding is the result of impeded runoff or permafrost degradation.

4.1.4 Permafrost

Permafrost is present at the site, as verified by frost probing and boreholes. Differential settlement of the road embankment and guard rails (Fig. 4.5), as well as additional ponding on the northern side of the road embankment and a large wet muskeg area on the south side suggest the presence of degrading ice-rich permafrost. Drunken trees (*i.e*., trees tilted by ground movements) along both sides of the road provide further evidence of permafrost degradation.

Figure 4.5 Example of differential road settlement (4 October 2018).

Two small ponds (likely thermokarst ponds) are visible within tens of metres of EBA boreholes BH01, BH02 and BH03 in historical aerial photographs from 1946. However, in aerial photographs from 2007, captured just prior to road construction, only one pond was visible. Thermokarst ponds occupy a closed depression formed by settlement of the ground caused by the thaw of ice-rich permafrost. Lithalsas (permafrost mounds that form by ice segregation in fine mineral soil) are also observed at this site.

4.2 Results

4.2.1 Borehole geotechnical data

A shallow 2.2 m borehole HB_BH1 was drilled using a portable drill on 27 September 2018 by Louis-Philippe Roy and Fabrice Calmels of YRC (Table 4.1) to sample permafrost and install ground temperature monitoring instrumentation. Borehole HB_BH1 was cased with a 1-inch PVC pipe and instrumented with one 4-channel Hobo data logger to record temperatures at 0.0, 0.5, 1.0, and 2.2 m depths (Table 4.1). Borehole HB_BH1 is located on the southwestern side of Hamilton Boulevard at the foot of the embankment in a forested area (Figs. 4.1 and 4.6). The site of the borehole was selected due to the presence of an elevated frost heave mound, characteristic of shallow permafrost. A hole was dug using shovels and hand auger to the permafrost thaw front at 0.40 m depth, after which the portable drill was utilized. Prior to drilling, a 200-m ERT survey was conducted on 1 September 2017 (Fig. 4.1).

Four nearby boreholes (EBA_BH01 to EBA_BH04) were drilled into the Hamilton Boulevard shoulder by Midnight Sun Drilling Company Inc. under the supervision of EBA using a Sandvik M5 ODEX air rotary drill in June 2013 (Table 4.1) (EBA, 2013). They drilled in depressions along the shoulder of Hamilton Boulevard; two along the northbound lane (EBA_BH01 and EBA_BH02) and two along the southbound lane (EBA_BH03 and EBA_BH04, Fig. 4.1). One thermistor string was installed in EBA_BH03 to a depth of 10.5 m.

Table 4.1 Location details of field surveys at the Hamilton Boulevard study site, including five boreholes, two of which are instrumented, and one ERT survey.

Site	Date	Coordinates (NAD83 UTM Zone 8)	Depth (m)	Ground Temperature Sensor Depths (m)
HB_BH1	27/09/2018	494719 6728929	2.18	0.0, 0.5, 1.0, 2.2
EBA_BH01	17/06/2013	6728929 494751	15.7	
EBA_BH02	18/06/2013	6728872 494844	14.6	
EBA_BH03	20/06/2013	6728951 494737	11.6	0.0, 1.0, 1.5, 2.5, 3.0, 3.5, 4.0, 4.5, 5.5, 6.0, 6.5, 7.0, 8.5, 9.5, 10.5
EBA_BH04	20/06/2013	6728919 494794	10.1	
HB_ERT1	1/9/2017	Dipole-dipole and Wenner	Length (m): 200	Electrode Spacing (m): 2.5
0 m		494830 6728804		
50 m		494796 6728843		
100 m		494760 6728878		
150 m		494723 6728913		
200 m		494692 6728949		

Figure 4.6 Borehole HB_BH1 in surrounding forest.

The cryostratigraphical profile of HB_BH1 (see Figure A2) shows an initial layer of peat 0.66 m thick confirming drilling was within undisturbed ground. This was underlain by a cobble-rich layer from 0.66 to 1.23 m depth. Dense till with varying amounts of coarse fragments and fine-grained material were encountered from 1.23 to 2.18 m depth. The borehole ended at 2.18 m in ice-poor gravelly sediment. Crustal-ice coating gravel was observed in some of the samples, and the volumetric excess ice content ranged from 0 to 53% (Table 4.2). The cobble-rich horizon from 0.66 to 1.23 m depth decreased the average excess ice content. Overall, the borehole has a mean volumetric excess ice content of 36%, which represents a potential subsidence of 0.54 m if permafrost were to thaw entirely from 0.5 to 2 m depth.

Table 4.2 Grain-size distributions and excess ice content from borehole HB_BH1 at Hamilton Boulevard study site.

Depth (m)	Volumetric Excess Ice (%)	Organics (%)	Pebbles and Cobbles† (%)	Fine Gravel/ Granules† (%)	Sand (%)	Silt and Clay (%)
0.66	33	100	0	0	0	0
0.92	0	0	100	0	0	0
1.40	53	0	45	4	22	29
1.58	49	0	25	2	32	42
1.73	48	0	8	1	32	59
1.85	20	0	82	0	6	12
2.00	51	0	33	1	25	41
2.18	34	0	34	2	19	44

†Pebbles and cobbles were distinguished from gravel; grain size of pebbles and cobbles and grain size was from >4 to 256 mm, while fine gravel and granules was from 2 to 4 mm.

Table 4.3 summarizes the generalized stratigraphy encountered in the EBA (2013) boreholes. Boreholes consisted of up to 3 m of sand and gravel (fill) overlying up to 3 m of quarry rock, followed by varying thicknesses of organics, silt, sand, and till. Weathered bedrock was encountered in EBA_BH02 at a depth of 14.4 m below grade. EBA (2013) notes “Permafrost was encountered in three of the four boreholes advanced, within the underlying peat and silt. The thickness of permafrost varied from 0.8 m of frozen peat in Borehole BH01, 2.0 m of frozen silt in BH02, and 1.4 m of ice-rich permafrost and frozen silt in BH03. The peat in BH01 had a moisture content of 178% (by weight), the frozen silt in BH02 contained 27% moisture content (by weight), and the ice-rich permafrost and frozen silt in BH03 contained 60% moisture content (by weight). No permafrost was encountered in Borehole BH04.”

Table 4.3 Soil straigraphy from four boreholes drilled by EBA adjacent the Hamilton Boulevard study site on the road (EBA, 2013).

Soil Stratigraphy (m)	EBA_BH01	EBA_BH02	EBA_BH03	EBA_BH04
SAND and GRAVEL (fill)	0–1.3	0–3.1	0–0.5	0–3.4
Quarry Rock (Fill)	1.3–5.1	3.1–5.2	0.5–4.0	3.4–5.8
PEAT	5.1–6.9	5.2–5.9	4.0–5.5	5.8–7.6
SILT	6.9–7.5	5.9–8.7	5.5–6.7	7.6–9.5
SAND	-	-	6.7–8.5	-
ORGANICS	7.5–9.1	-	-	-
SAND and GRAVEL	-	8.7–12.6	-	-
SILT	9.1–10.7	-	-	-
TILL	10.7–15.7	12.6–14.4	8.5–11.6	9.5–10.1
Weathered Bedrock	-	14.4–14.6	-	-
End of Hole	15.7	14.6	11.6	10.1

4.2.2 Ground temperatures

Borehole HB_BH1 ground temperature measurements began at 16:00 on 30 November 2018. Data was last downloaded in February 2021 (Fig. 4.7 and Table 4.4). Annual mean ground temperature at the deepest point (2.2 m) is above 0°C, which indicates the base of permafrost lies above that depth. Daily mean temperatures shown in Figures 4.7 and 4.8, suggest the base of permafrost sits at 2 m depth, while the active layer extends to ~0.5 m below the ground surface.

Annual mean ground temperature in permafrost at HB_BH1 range from -0.03 to -0.28 (Table 4.4), suggesting that permafrost at this site is sensitive to air temperature fluctuations and prone to degradation. While it is not possible to accurately estimate when this site will be free of permafrost, the warm ground temperatures and thin permafrost imply that if degradation occurred it would happen rapidly.

The EBA_BH03 temperature profile from 23 July 2013 to 17 January 2014 (see Figure B1) showed similar ground temperatures very close to 0°C from 5.5 to 6.8 m depth. The active layer in EBA_BH03 is much thicker as it is under the road embankment. Temperatures did not remain below 0°C over the duration of the year despite ground ice in the borehole. This suggests the permafrost was in disequilibrium, and the high latent heat required to melt ice allowed for ground ice to be preserved for a short while. By 2015, ground temperature profiles for EBA BH03 (see Figure B2) suggest all permafrost had thawed (EBA, 2015). It was noted there was a possibility of other frozen areas near this location along the alignment and further settlement of the subsurface soils could be observed in the future.

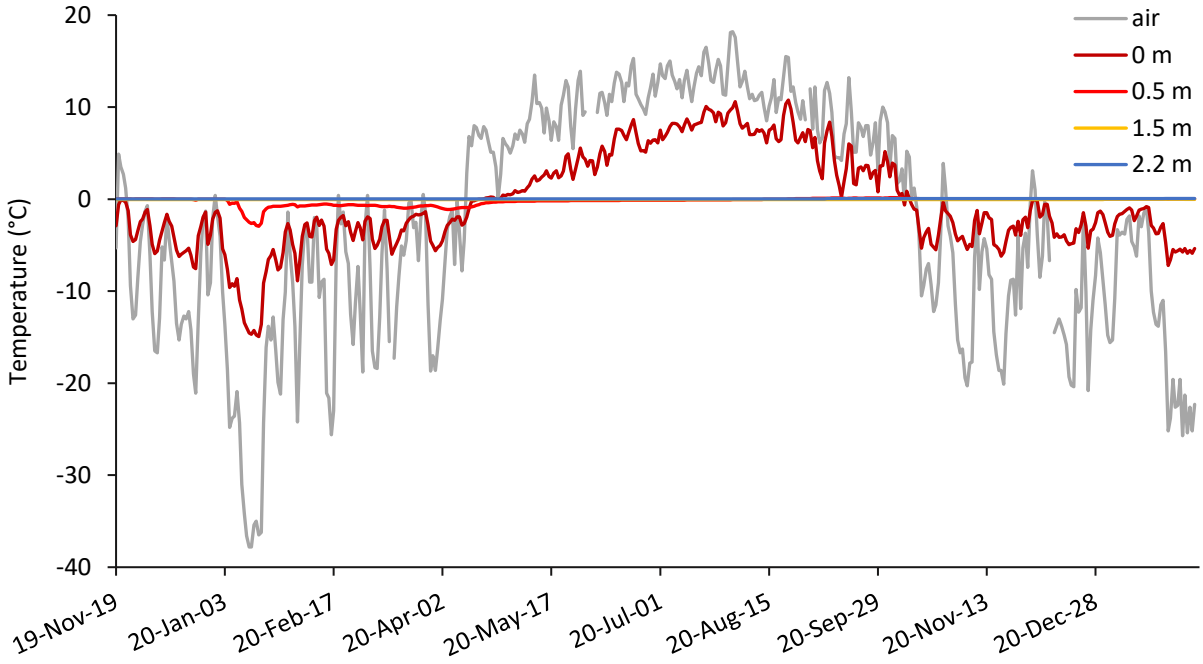

Figure 4.7 Hamilton Boulevard daily mean ground temperatures at HB_BH1 for the period 19 November 2019 to 7 February 2021. Daily mean air temperatures from Whitehorse airport (ECCC, Whitehorse AUTO).

Table 4.4 Annual minimum, maximum and mean ground temperatures (from daily mean values) at HB_BH1 for the period January 2020 to 31 December 2020. Air temperatures are from ECCC Whitehorse AUTO station, located approximately 4 km north.

Depth (m)	Air	0.0	0.5	1.5	2.2
Annual min GT (°C)	−37.80	−14.94	−2.95	−0.04	0.04
Annual mean GT (°C)	−0.75	0.35	−0.28	−0.03	0.05
Annual max GT (°C)	18.20	10.8	0.16	−0.03	0.07

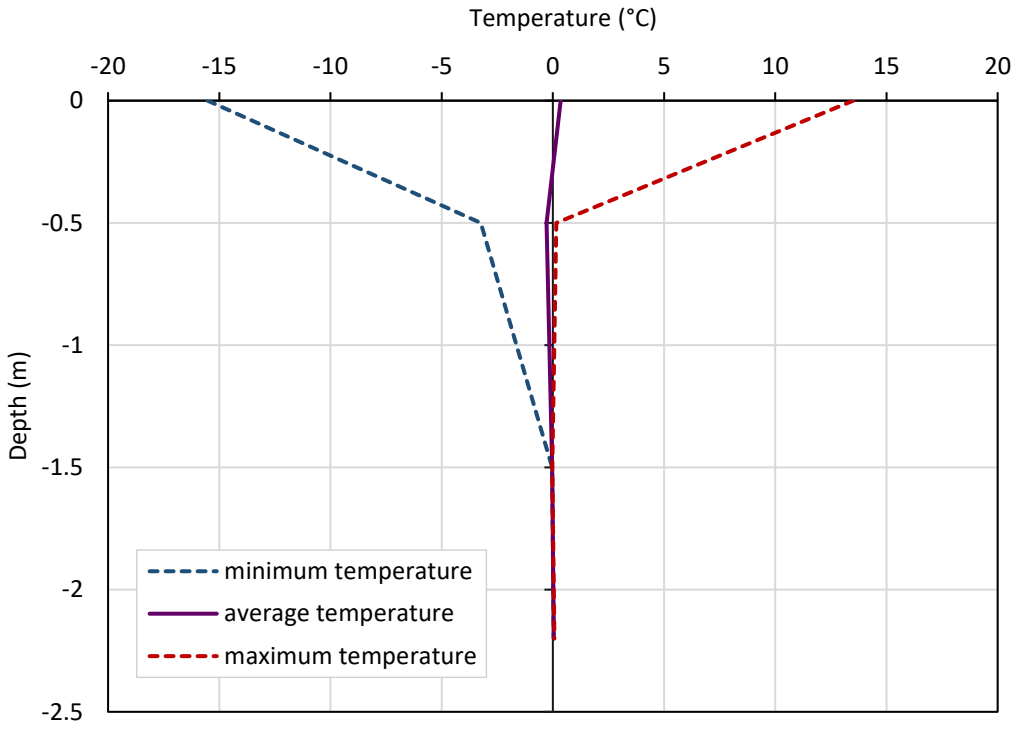

Figure 4.8 Hamilton Boulevard ground temperature envelope at HB_BH1 for the period 1 January 2020 to 31 December 2020.

4.2.3 ERT

Figures 4.8 and 4.9 show the Wenner and dipole-dipole array ERT survey results. The distribution of resistivity in the ground is similar between the two, however, the dipole-dipole results show more detail in low resistivity areas. Both surveys were completed on 1 September 2017.

Both the dipole-dipole and Wenner arrays show a high resistivity pocket, represented by blue shades, from 120 to 140 m distance along the survey. This high resistivity pocket also corresponds to the frost mound observed in the field and in the topographic profile (Fig. 4.8a). The ERT data also suggests a thin layer of permafrost is present along the entire length of the profile from 4 to 8 m depth (Fig. 4.8b, c). The area surrounding HB_BH01 (120–135 m along the profile) shows permafrost closer to the surface, from 40 m to 100 m. Towards the northernmost section of the profile, from 120 to 200 m, permafrost potentially extends down to 15 m depth. Some distinct high-resistivity bodies are close to the wet areas. In these areas, fine-grained sediment and groundwater movement have likely created favorable conditions for the formation of segregated ice.

Very low resistivities, represented by dark red shades, are present below 8 m depth along nearly the entire length of the profile (apart from the northernmost portion where they are present below 15 m). These very low resistivity areas indicate the presence of unfrozen ground and could be due to either groundwater movement, or the presence of till, or bedrock. Resistivities are typically lower where the soil is coarser-grained and ice-poor. Groundwater can also circulate more easily through coarser-grained soil (*i.e.*, gravel) because the pores between soil particles are larger. In finer-grained soil (*i.e.,* silt or clay), groundwater cannot circulate as easily. Overall, high-resistivity areas are generally attributable to ice-rich ground within fine-grained material while low-resistivity areas are generally attributable to ice-poor ground within coarse-grained material.

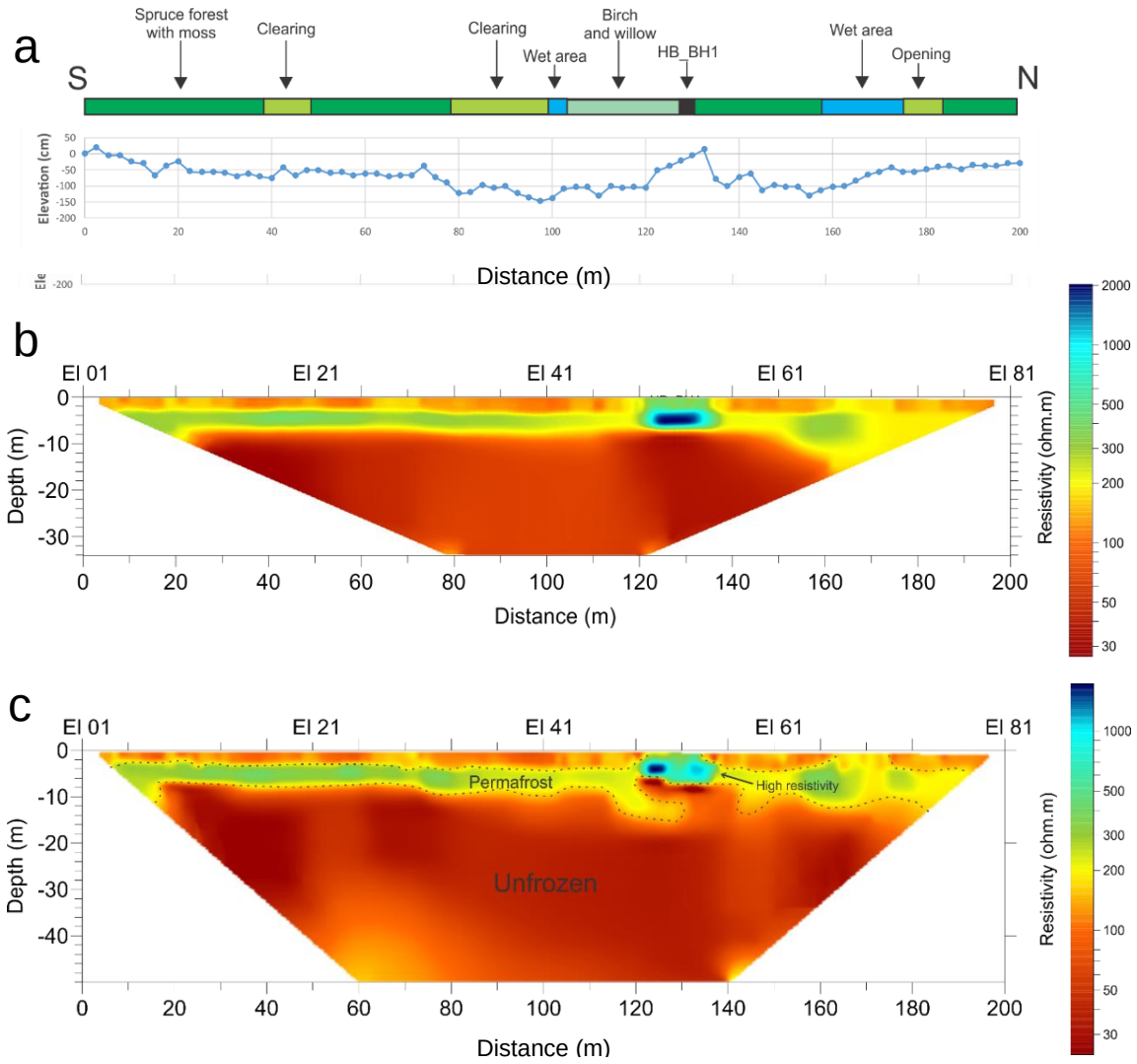

Figure 4.9 Hamilton Boulevard ERT survey (HB_ERT1) showing the (a) topographic profile, (b) ERT profile using Wenner array, 3rd iteration, RMS error = 3.26%, and (c) ERT profile using dipole-dipole array, 2nd iteration, RMS error =3.62%. Figure (c) is annotated to differentiate between ground material interpreted as permafrost (greenish yellow to blue) and unfrozen (red).

4.2.4 Synthesis

ERT data suggest the presence of permafrost from 1 m to a depth that could exceed 8 m throughout the transect. The northernmost section of the profile from 140 to 200 m along the survey line shows permafrost potentially extending down to 15 m depth. Here, fine-grained sediment and groundwater movement have likely created favorable conditions for the formation of segregated ice. Below 15 m depth, ground materials are likely coarser-grained and unfrozen.

Based on the 2013 and 2015 temperature data gathered by EBA (EBA, 2013; 2015), most of the permafrost under the road at EBA_BH03 has thawed, but it is possible that some permafrost remains along the road in nearby areas. Ice-rich permafrost may also persist in the less disturbed environments adjacent to the embankment. At borehole HB_BH1 ice-rich sediment is preserving the permafrost due to its latent heat.

Permafrost at the Hamilton Boulevard case study site is warm with temperatures ranging from −0.04 to −0.03°C at 1.5 m depth in natural ground. Assuming an active layer depth of ~0.5 m, a permafrost base of ~2.0 m from ground temperatures, and a volumetric excess ice content of 36%, the potential subsidence would be 0.5 m if permafrost thawed entirely.

Subsidence on the order of 36% of the permafrost thickness, or more if groundwater movement leaches sediment, is the main hazard for this site and similar landscape units. If similar permafrost and ground conditions (*i.e.,* ice-rich till) occurred on a hillslope, groundwater flow and thermokarst activity could potentially trigger landslides.

5 HIDDEN VALLEY

5.1 Site setting

The Hidden Valley case study site is located on private property in the Hidden Valley Subdivision ~16 km north of downtown Whitehorse, immediately west of the North Klondike Highway and south of the Takhini River (Fig. 5.1). The house and main driveway are off Soapberry Lane and lie on a cleared bench at 655 m elevation on the upper (southern) portion of the property. This bench is a remnant of the glacial lakebed that has been eroded away on all sides by a tortuously meandering channel of the former Takhini River. From the north side of the house (on the bench), elevation falls ~5 m over a steep (~25–30°) cleared escarpment (Fig. 5.2). This transitions to a gentle (~6–10°) north-facing forested slope which falls another 5 m in elevation on the northern half of the property (Fig. 5.2).

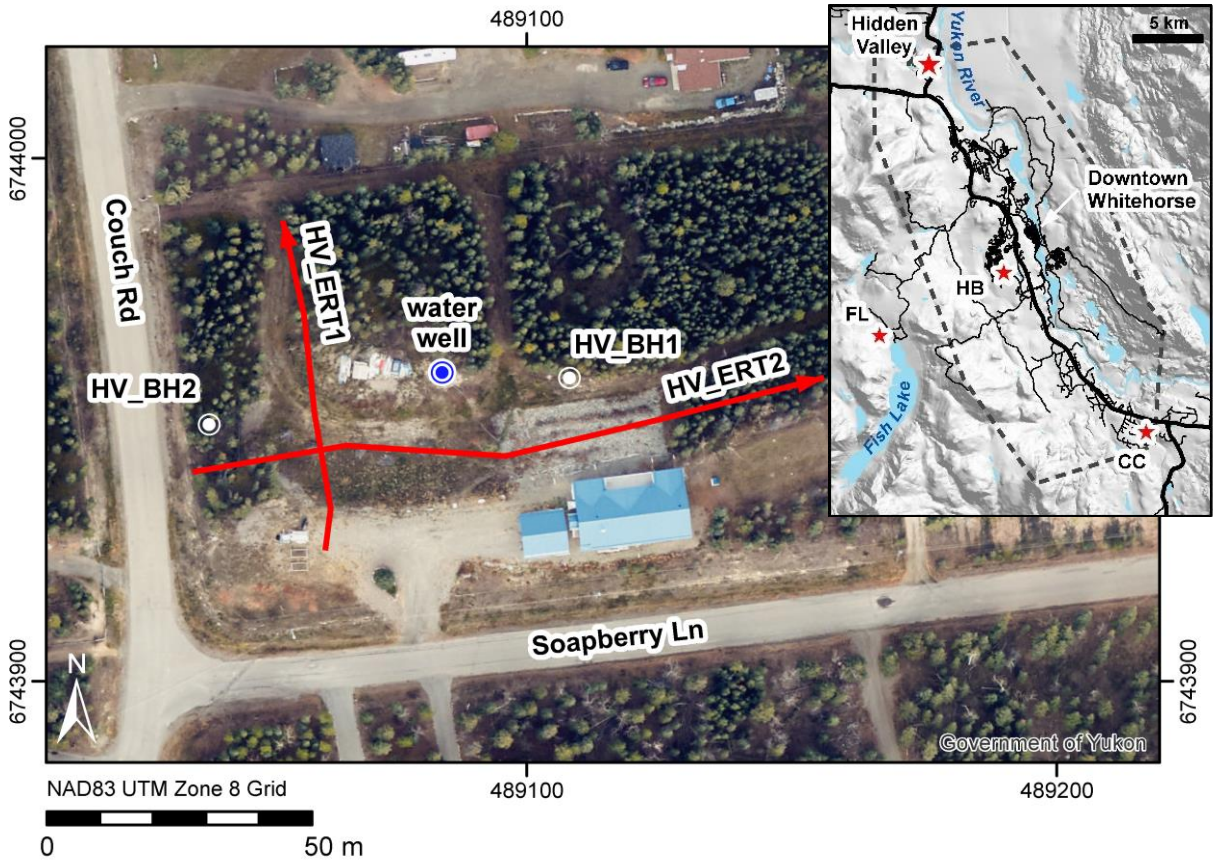

Figure 5.1 Location of Hidden Valley case study site with borehole and ERT survey locations. Orthophoto background image (28 September 2019). Inset map shows location with respect to Whitehorse city limits (dashed line) and nearby case study sites (FL = Fish Lake, HB = Hamilton Boulevard, and CC = Cowley Creek).

Figure 5.2 North-facing cleared escarpment at Hidden Valley case study site, showing (a) south end of HV_ERT1 transect running across the driveway and grass slope, and (b) west end of HV_ERT2 transect running along the bottom of the steep escarpment. Dashed lines show approximate locations of the ERT transects.

5.1.1 Vegetation

This area was likely part of the 1958 wildfire that burned most of Takhini Valley. Stable areas are classified as BOLsl/01-APSw25z in the Yukon Bioclimate Ecosystem Classification (YBEC) System (McKenna, *et al.,* 2017). This classification is characterized by mesic to submesic soils, with a mixed forest including white spruce (*Picea glauca*), lodgepole pine (*Pinus contorta*), and trembling aspen (*Populus tremuloides*) trees, and soapberry (*Shepherdia canadensis*) shrubs (McKenna, *et al.,* 2017).

On the north-facing slope, the understory is largely open with a feathermoss ground cover on the order of 5–10 cm thick, underlain by ~10 cm of partially decomposed peat. Other common plant species on the property include shrubs such as willow (*salix* spp.) and lowbush cranberry (*Vaccinium vitis-idaea)*, and forbs such as single delight (*Moneses uniflora)* and bastard toadflax (*Geocaulon lividum).*

5.1.2 Surficial geology

As outlined in the Section 2.1, Glacial Lake Laberge inundated much of the Yukon River and lower Takhini River valleys during deglaciation. A thick sequence of fine-grained (fine sand, silt and clay) sediment settled out at the bottom of this glacial lake, and these glaciolacustrine sediments comprise the dominant sediment in the study area.

As Glacial Lake Laberge gradually shrunk to its modern size, a blanket of deltaic sand was deposited above the glaciolacustrine sediments, and in many locations, these were reworked by wind to form a cap of loess and/or extensive dune fields. The Takhini and Yukon Rivers have subsequently cut down through this entire package of sediments, which is exposed in steep cutbanks along many sections of both rivers.

Fifty-one metres of glaciolacustrine sediments are exposed in a Takhini River cutbank about 1 km west of Hidden Valley (Fig. 5.3 - 19PL035), while water well drill logs record up to 65 m of glaciolacustrine sediment throughout Hidden Valley Subdivision (Environment Yukon, 2021). The glaciolacustrine sediment generally fines upward from sandier units at depth to more silt and clay-rich units near the surface, reflecting an increasingly distal sediment source as the ice-front retreated.

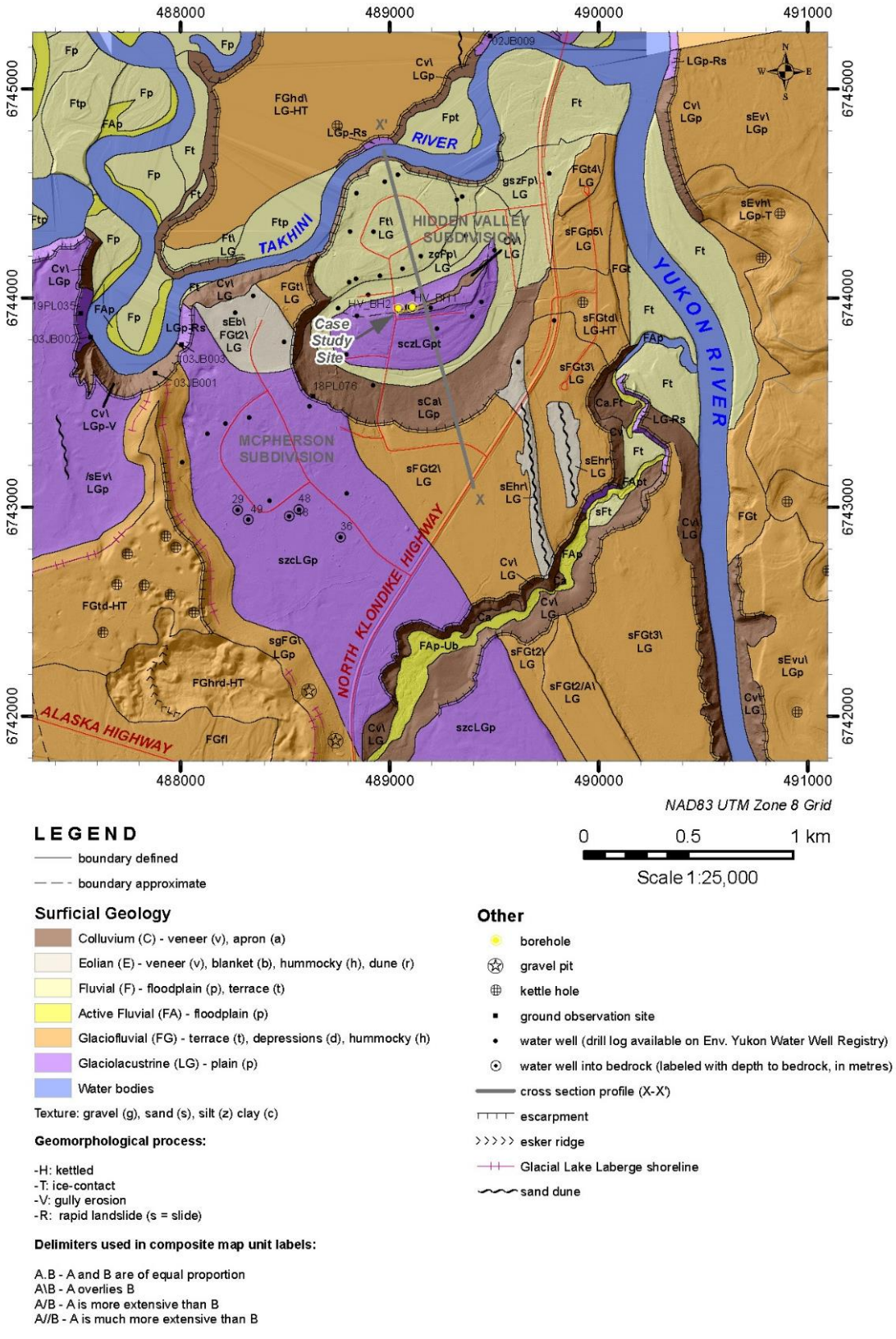

Figure 5.3 Simplified surficial geology map showing major landscape units, landforms and boreholes drilled in the vicinity of Hidden Valley and McPherson subdivisions.

The northern portion (lower bench) of Hidden Valley Subdivision sits on an abandoned meandering channel of the Takhini River, which eroded into the underlying glaciolacustrine sediment (Fig. 5.3). Thin layers of coarse-grained sand and gravel floodplain sediments commonly occur near the surface on this lower bench, underlain by fine-grained glaciolacustrine sediment. The Hidden Valley case study site itself lies on a remnant glaciolacustrine terrace which protrudes above an abandoned meander bend on this former floodplain.

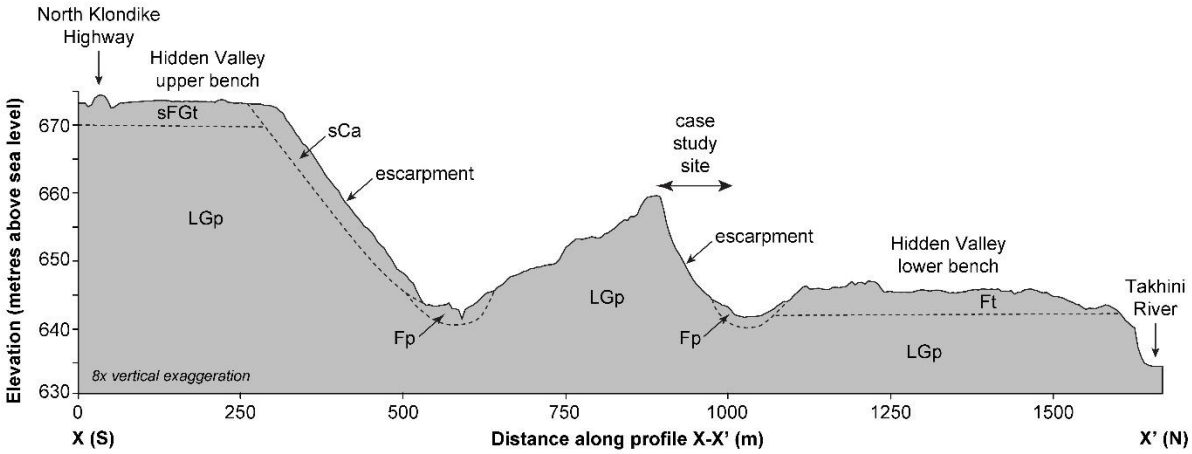

Figure 5.4 Generalized stratigraphic cross section from 2013 LiDAR DEM along transect X-X' (shown in Fig. 5.3).

The southern portion of Hidden Valley Subdivision, as well as McPherson Subdivision, sit on an upper bench of glaciolacustrine sediment, capped in some locations by sandy deltaic sediments. The escarpment that separates the upper and lower benches was carved by the abandoned channel of the Takhini River and is mantled by a sandy colluvial apron. As glacier ice retreated eastward out of Takhini River Valley, it stagnated a few kilometers southwest of Hidden Valley, depositing a large amount of sand and gravel in the proposed Stevens Quarry aggregate reserve area.

Bedrock was encountered from 29 to 48 m depth in at least 5 water wells in the McPherson Subdivision, located ~500 m to the southwest of Hidden Valley (Fig. 5.4; Environment Yukon, 2021). Bedrock within 5 km north and south of the study area consists of Upper Triassic (~200 Ma) Lewes River Group/Aksala Formation sedimentary lithologies. Mandanna Member green and maroon sandstone, mudstone and conglomerate are most extensive, with lesser amounts of Hancock Member limestone (Hart, 1997). Striations on exposed bedrock along the Alaska Highway just west of the study area also indicate that ice was moving in a northwesterly direction during the last glacial maximum.

5.1.3 Permafrost

The presence of ice-rich sediment was first identified in 2008 by the contractor who excavated the bench the house is built on. The property owner also reported encountering permafrost down to a depth of 6.7 m in his water well when it was drilled in 2004. The presence of permafrost was further verified by the project team in 2018 and 2019 in several locations on the property, using probing, borehole drilling and ground temperature monitoring.

Damage to man-made structures provides the primary indication of permafrost degradation. The house was built in 2008 and first showed evidence of settlement after the surrounding vegetation was cleared in 2009–2010. Foreseeing possible settlement issues due to permafrost thaw, 35 foundation jacks were installed during the construction of the house to relevel the house up to 5 cm/year (Fig. 5.5). The homeowner has reported up to 50 cm of total settlement occurred in the 11 years since the jacks were installed in 2008. Leaning trees and vegetation die-off suggests changing ground conditions and may be related to degrading permafrost and slope creep induced by clearing of vegetation on the escarpment.

Figure 5.5 (a) Foundation jack located under the house, where (b) a wrench is used to raise or lower the support beams.

5.2 Results

5.2.1 Borehole geotechnical data

The first borehole at this site, HV_BH1 (653 m asl), was drilled on 15 January 2019 by Midnight Sun Drilling Inc. under the supervision of Louis-Philippe Roy and Panya Lipovsky (Table 5.1). The location of the borehole was selected based on the ERT assessment (see Section 5.2.3). It is located on the northern side of the property at the edge of a forested area. Ideally, this borehole would have been located on the escarpment slope, along the west to east ERT transect HV_ERT2 (Fig. 5.1). In this area there was a high resistivity body about 10 m deep. However, the Midnight Sun drill rig was unable to access the ideal location due to angle of the escarpment slope. The borehole was therefore drilled at the base of the slope, just north of the lower access road, and offset about 11 m north of ERT transect HV_ERT2 at a horizontal distance of 74 m (Fig. 5.1).

Once drilling was completed, the borehole was cased with 1-inch PVC pipe, instrumented with eleven thermistors, and backfilled to the surface with filter sand. The cores were stored in a freezer, then photographed in the laboratory and sub-sampled every 1 m to collect a 50 cm sample for further geotechnical analysis (See Appendix E).

Table 5.1 Location details of field surveys at the Hidden Valley study site, including two boreholes, one of which was instrumented, and two ERT surveys.

Site	Date	Coordinates (UTM NAD83)	Depth (m)	Ground Temperature Sensor Depths (m)
HV_BH1	15/01/2019	489108 6743958	21	0.0, 0.25, 0.5, 1.0, 2.0, 3.0, 5.0, 8.0, 10.0, 15.0, 18.8
HV_BH2	4/10/2018	489040 6743949	3.5	
HV_ERT 1	17/05/2018	Dipole-dipole and Wenner	Length (m): 80	Electrode Spacing (m): 1
0 m		489062 6743925		
20 m		489063 6743933		
40 m		489060 6743951		
60 m		489058 6743970		
80 m		489054 6743988		
HV_ERT 2	24/05/2018	Dipole-dipole and Wenner	Length (m): 120	Electrode Spacing (m): 1.5
0 m		489037 6743940		
30 m		489066 6743945		
60 m		489096 6743943		
90 m		489125 6743950		
120 m		489156 6743958		

Figure 5.6 Midnight Sun Drilling at borehole HV_BH1 using a sonic drill.

A second 3.5 m borehole, HV_BH2 (649 m asl), was drilled using a hand auger on 4 October 2018. Borehole HV_BH2 was drilled to characterize the frost table in the forested area which appeared to be the least disturbed. The borehole was augered to a point of refusal without hitting permafrost. The hole was cased with a 1-inch PVC pipe to allow for future monitoring of the active layer if desired.

Grain size analysis and excess ice content geotechnical results for HV_BH1 are summarized in Table 5.2 and the borehole log is shown in Figure A3. The entire profile consists of fine-grained glaciolacustrine sediment that is primarily silt sized (69–83%) with 5–22% clay and 5–15% very fine sand by weight. The borehole log shows centimeter-scale layers of ice-rich gray sandy clayey silt alternating with very fine sandy lenses (Fig. 5.7) which likely represent turbidity current depositional events. The borehole ends at 21 m depth in clayey-silt sediment.

Lenticular and microlenticular cryostructures were identified throughout the profile and the volumetric excess ice content ranged from 23 to 48%. The interval from 14 to 15 m depth contained the highest excess ice content (41 and 49%). Overall, the borehole has a mean volumetric excess ice content of 36%, which represents a potential subsidence of 4.86 m should permafrost (extending from 7.5-21 m depth) thaw completely.

Table 5.2 Grain-size distributions and excess ice content from borehole HV_BH1 at Hidden Valley study site. Note that excess ice was observed throughout the core at the time of drilling on 15 January 2019, but ground temperatures in the borehole have not since recovered to below 0°C.

Depth (m)	Volumetric Excess Ice (%)	Gravel (%)	Sand (%)	Silt (%)	Clay (%)
1.0	28	0	7	79	14
2.0	29	0	15	79	6
3.0	28	0	15	69	16
4.0	34	0	12	72	16
5.0	24	0	15	80	5
6.0	32	0	12	72	16
7.0	28	0	13	72	14
8.0	24	0	7	79	14
9.0	27	0	9	74	18
10.0	35	0	15	76	10
11.0	34	0	15	69	16
12.0	30	0	10	76	14
13.0	28	0	9	79	13
14.0	41	0	12	84	5
15.0	49	0	12	80	8
16.0	23	0	12	74	14
17.0	33	0	9	69	22
18.0	36	0	5	74	21
19.0	33	0	7	74	19
20.0	37	0	11	71	17
21.0	33	0	9	77	14

Figure 5.7 Permafrost core containing gray sandy clayey silt alternating with very fine sandy lenses at HV_BH1.

5.2.2 Ground temperatures

Borehole HV_BH1 was instrumented with one 11-channel LogR Systems logger and thermistors to record ground temperatures (Table 5.1). The precision of these instruments is ±0.1°C. The recording started 9 April 2019 at 14:00 and was downloaded in August 2020, providing 17 months of ground temperature data (Fig. 5.8). The annual mean ground temperature at the deepest point (18.8 m) for the period August 2019 to August 2020 was 1.2°C (Table 5.3).

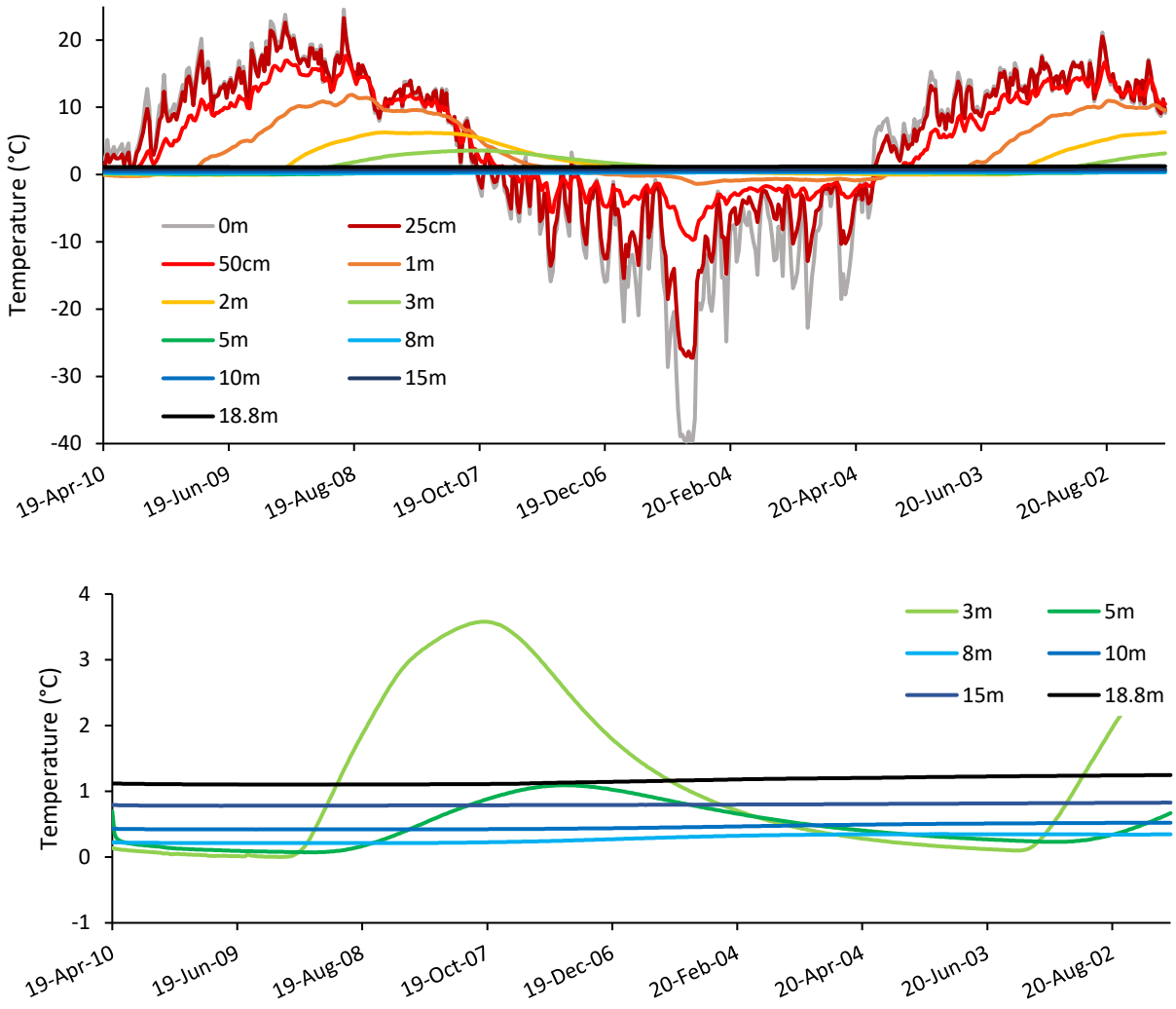

Figure 5.8 Hidden Valley daily mean ground temperatures at HV_BH1 for the period 10 April 2019 to 30 August 2021 from (a) 0.0 to 18.8 m depth, and (b) 3.0 to 18.8 m depth.

Table 5.3 Annual minimum, maximum and mean ground temperature (from daily mean values) at HV_BH1 for the period 31 August 2019 to 30 August 2020.

Depth (m)	0.0	0.25	0.5	1.0	2.0	3.0	5.0	8.0	10.0	15.0	18.8
Annual min GT (°C)	−39.73	−27.26	−9.74	−1.38	0.01	0.10	0.23	0.21	0.42	0.79	1.11
Annual mean GT (°C)	0.46	1.85	3.15	2.91	2.11	1.41	0.60	0.31	0.47	0.80	1.18
Annual max GT (°C)	21.15	20.56	16.71	11.00	6.29	3.58	1.09	0.35	0.52	0.83	1.25

All temperatures fluctuated above 0°C which suggest no permafrost is left at HV_BH1 (Fig. 5.8). However, high excess-ice content was encountered throughout the depth of the borehole (Table 5.2) during drilling, suggesting permafrost was recently present at the borehole site, and may still exist nearby where the ground has been less disturbed from drilling. The depth of zero annual amplitude (*i.e.,* the depth where annual temperature fluctuations are essentially 0°C) is ~8 m below the surface (Fig. 5.9). The large volume of water used during drilling could have caused the permafrost immediately surrounding the borehole to thaw, while the high excess-ice content could have dampened the warming effect and preserved permafrost at some distance from the borehole. A high ground ice content helps to temporarily preserve permafrost or delay its thaw, as ice has a very high latent heat of fusion (melting) (*i.e.,* a large amount of energy must be supplied for ice to melt, so energy supplied when melting ice does not cause a change in temperature; rather the energy is stored through the phase change of the water molecules).

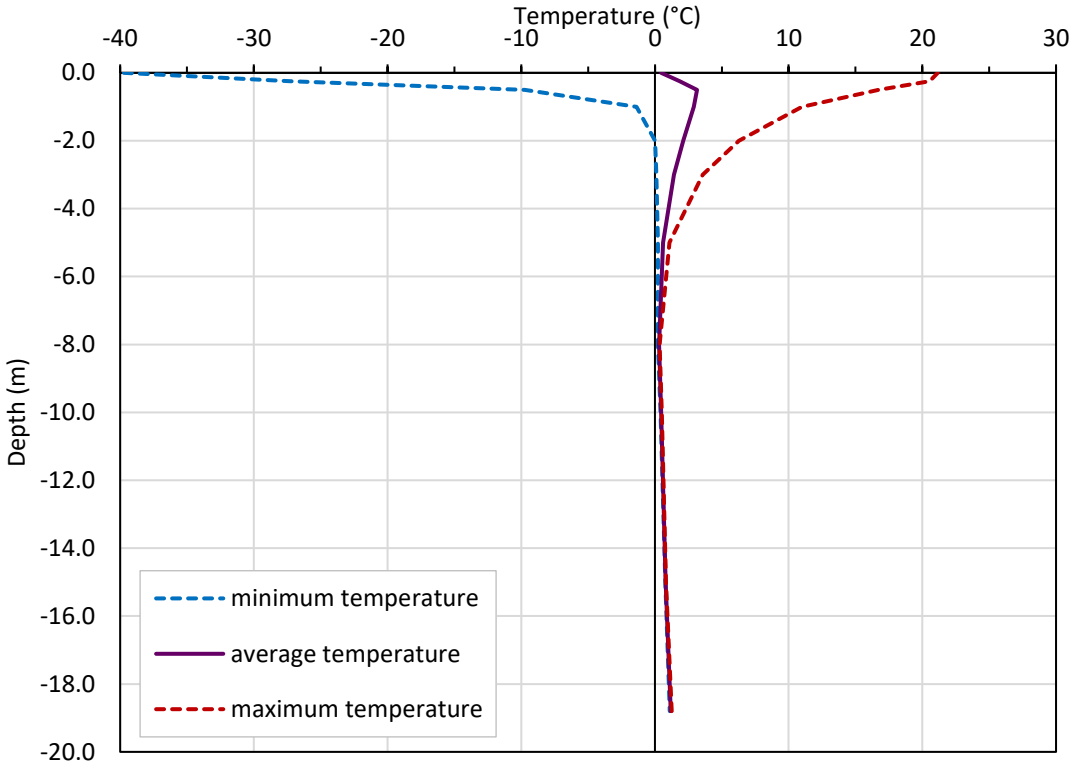

Figure 5.9 Hidden Valley ground temperature envelope at HV_BH1 for the period 31 August 2019 to 30 August 2020.

5.2.3 ERT

Two ERT surveys, HV_ERT1 and HV_ERT2, were conducted on 17 and 24 May 2018, respectively (Table 5.1). HV_ERT1 was oriented from south to north starting from the upper bench and running down the escarpment and gentle slope below (Fig. 5.1 and 5.2a). HV_ERT2 was oriented from west to east, extending along the base of the escarpment (Fig. 5.1 and 5.2b). For each of the two surveys both the Wenner and dipole-dipole array were measured. The results obtained with the Wenner and dipole-dipole arrays show a similar distribution of resistivity in the ground, however the dipole-dipole shows more detail in low resistivity areas. Very high-resistivity areas, shown in dark blue, are generally attributable to ice-rich fine-grained sediment, and/or colder permafrost at depth. Low resistivity values could be attributable to ice-

poor and/or unfrozen material. The lowest values may indicate the presence of liquid ground water, or the impact of organic cover loss after the construction of the house, *i.e.*, dry thawed ground.

HV_ERT1

The first ERT survey, HV_ERT1, ran from south to north, across a gravel driveway and down a slope (Fig. 5.2b and 5.10). High resistivity zones, represented as dark blue shades, were located on top of the slope towards the beginning of the profile and under a grassy mound at 53 m (Fig. 5.10b). The thicker organic cover on this mound likely contributes to the preservation of the underlying permafrost by insulating the ground. A higher resistivity pocket (A) can also be observed at 30 m at the intersection with HV_ERT2 (Fig. 5.10b) and may be evidence of what is left of the ice-rich soil excavated at the base of the slope in 2008. Below 5 m depth, it appears most of the profile is unfrozen (Fig. 5.10b).

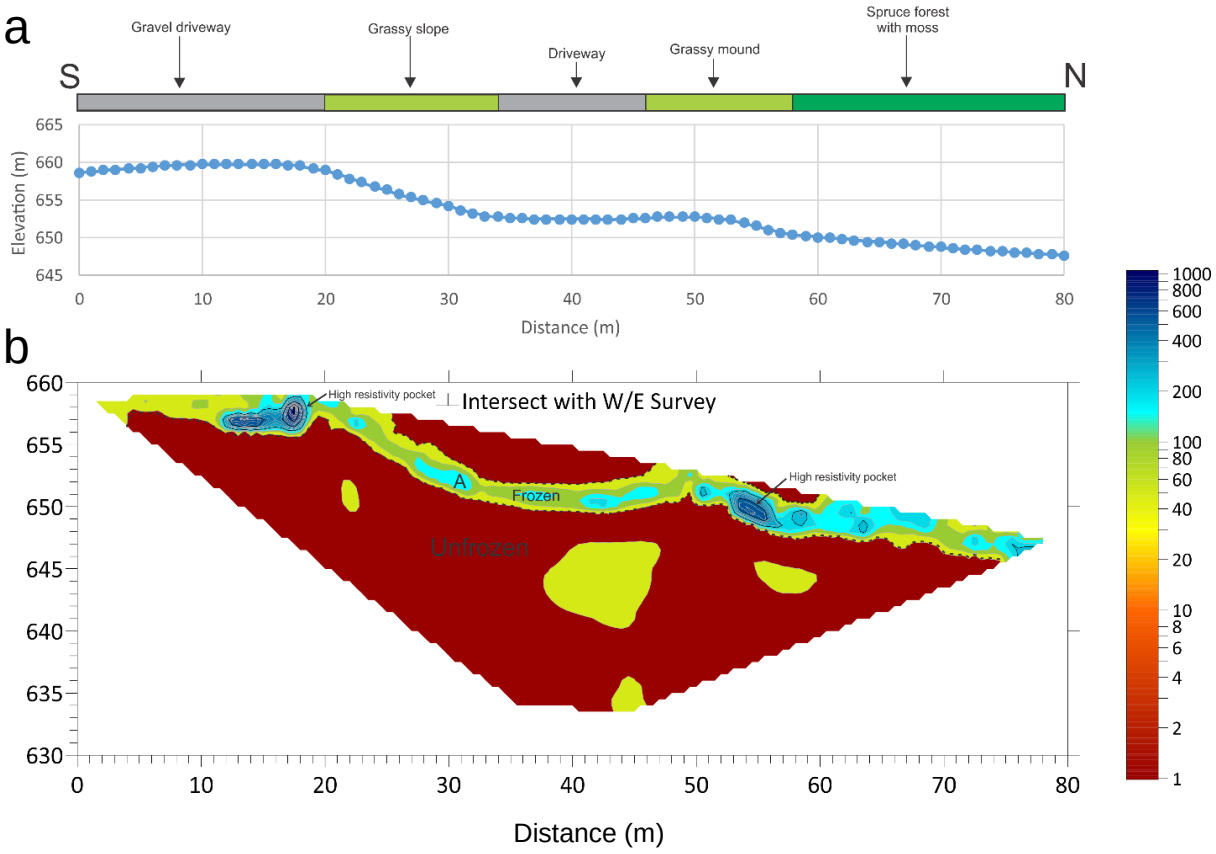

Figure 5.10 Hidden Valley S-N ERT survey (HV_ERT1) showing the (a) elevation profile and (b) ERT profile using dipole-dipole array, 5th iteration, RMS error = 4.0%. Figure (b) is annotated and homogenized to differentiate between ground material interpreted as frozen (greenish blue to dark blue) and unfrozen (red).

HV_ERT2

The second survey, HV_ERT2, ran along the lower escarpment slope from west to east (Fig. 5.2a and 5.11a) and intercepted HV_ERT1 at 21 m horizontal distance. High resistivity values are present along the entire profile from 0 to 25 m depth. The highest resistivity pocket was detected in the middle of the profile from 64 to 74 m distance, at a depth of 5 to 15 m. This very high resistivity zone is located below a low resistivity area covered with 4 x 4-inch wire mesh and cobble rip rap. The rip rap was placed on top of the mesh to slow movement on the slope extending below the house. This ice-rich permafrost is located directly downslope of the house and helps to explain the amount of settlement that occurs each year. Removal of vegetation and insulating organic cover on this portion of the slope during construction likely caused the ice-rich permafrost body to thaw, causing settlement of the soil above it. Towards the eastern end of the profile, below undisturbed forest with thick moss cover (90–120 m distance), the permafrost appears to be very close to the surface. Before construction of the house, shallow permafrost may have existed along the entire length of the profile, including where it is now unfrozen down to depths of up to 10 m.

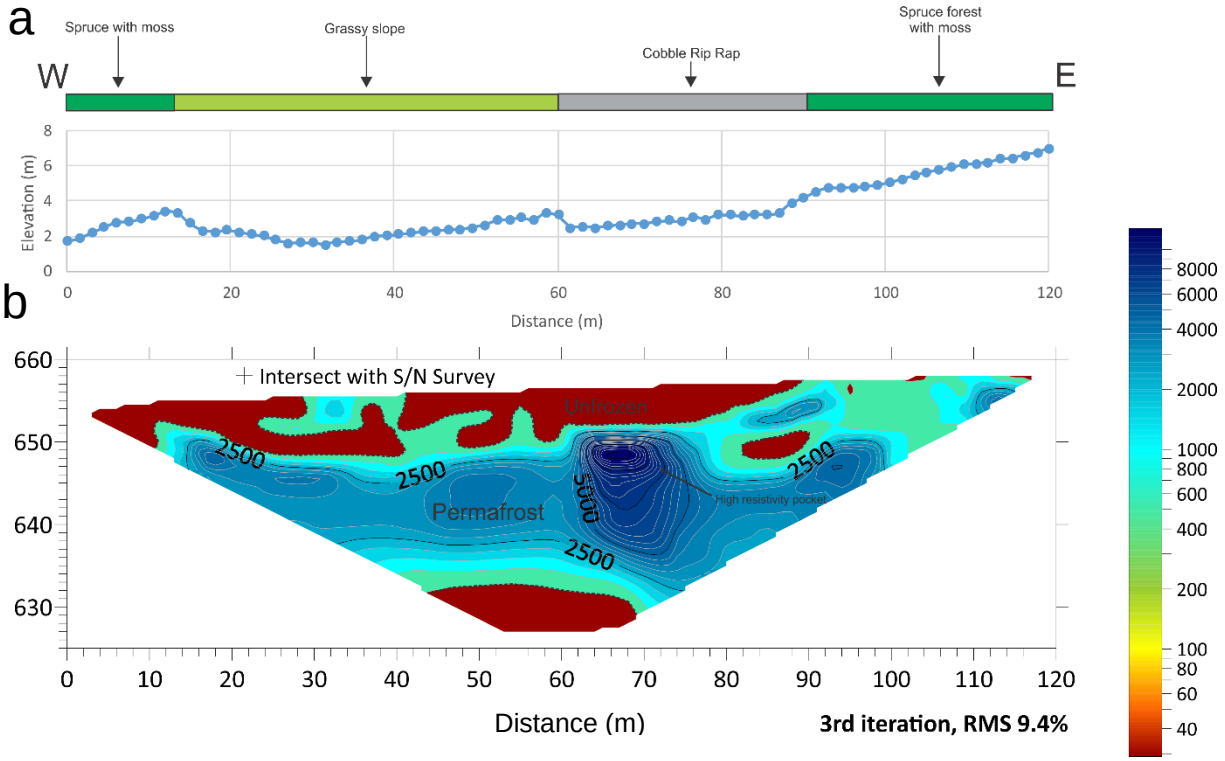

Figure 5.11 Hidden Valley W-E ERT survey (HV_ERT2) showing the (a) elevation profile, and (b) ERT profile using dipole-dipole array, 3rd iteration, RMS error = 9.4%. Figure (b) is annotated and homogenized to differentiate between ground material interpreted as permafrost (greenish blue to dark blue) and unfrozen (red). Resistivities above the 2500 ohm·m isoline in (b) suggest a higher likelihood of ice-rich permafrost. HV_BH1 was drilled 11 m downslope (north) of this profile at a distance of 74 m.

5.2.4 Synthesis

The frozen cores collected on site show the presence of fine-grained, frost-susceptible sediment down to 21 m depth. The steep slope prevented drilling and collection of core samples at the highest resistivity pocket shown in the ERT data (Fig. 5.11). The geophysical data suggests permafrost is still present on this site but is warm and vulnerable to thaw. A lack of insulating material at the ground surface below the footprint of the house has led to thawing of the underlying permafrost and continued settlement of the ground surface.

Ground temperatures at HV_BH1 did not remain below freezing all year long, and therefore the ground surrounding HV_BH1 cannot be considered permafrost. It is possible the drilling thawed the permafrost in a zone surrounding the casing. While permafrost is not present at HV_BH1, ERT data suggests there is still ice-rich frozen ground on the slope directly below the house. The high resistivity pocket shown in HV_ERT2 (Fig. 5.11) is inferred to be an ice-rich permafrost body that is currently being preserved due to the relatively large amount of energy required to melt ice. If this body were to thaw it could cause ground subsidence on the order of 36% of the permafrost thickness. Unlike at other case study sites, the ground temperature data at Hidden Valley cannot be used to estimate permafrost depth and potential subsidence as no permafrost currently remains at the borehole following drilling. Based on ERT surveys, permafrost is estimated to extend from 5 to 15 m depth for an approximate thickness of 10 m. Assuming a volumetric excess ice content of 36% (from geotechnical data), the potential subsidence would be 4 m if permafrost thawed entirely.

Subsidence is the main hazard for this site and similar landscape units where north-facing slopes are underlain by ice-rich glaciolacustrine sediment. This fine-grained material drains poorly once it thaws due to its low hydraulic conductivity. Additionally, fine-grained sediments commonly contain excess ice (*i.e.*, the volume of ice in excess of the total pore volume of the ground when unfrozen) and may form ice lenses by ice segregation. Slope aspect can also have a strong influence on ground temperature. In the northern hemisphere, north and east facing slopes are cooler than south and west facing slopes due to sun angle geometry and resultant shading effects. Slope instability could be an issue with time, although some slope stabilisation has been employed as a preventative measure.

6 IBEX VALLEY

6.1 Site setting

The Ibex Valley case study site (Fig. 6.1) is located about 40 km west of downtown Whitehorse along the Alaska Highway and sits between 680 and 690 m asl. The area is referred to as Ibex Valley by local residents, but is technically situated in the Takhini River valley (Fig. 1.1). In 1958, a series of wildfires swept through the area, burning most of the vegetation and the organic surface cover. In small patches of unburned spruce forest, the thickness of the organic cover was not affected, and permafrost remained in equilibrium (Burn, 1998). Thermokarst lakes are distinct on aerial imagery on either side of the Alaska Highway and in various parts of the valley, with most present before the fire (Burn, 1998).

Three sites were chosen to characterize these different environments: the “Forest” site, the “Burned” site and the recently established “Burned 2” site (Fig. 6.1). The first two were drilled and instrumented by Chris Burn in 1990 (Burn, 1998). The Forest site was untouched by the wildfire and the Burned site was selected to study the impact of wildfire on ground conditions. The Burned 2 (IV_BH1) site was drilled and instrumented under the supervision of the YRC and YGS to examine geotechnical ground conditions and ground temperatures in the area.

This portion of the Ibex Valley has been subject to extensive agricultural use for many years. Differential thaw settlement in recently cleared fields is common. Four large forested lots of ~63 ha were released in the new Murray Agricultural Subdivision in 2019; one of these was cleared the same year and would be interesting to monitor for future signs of thaw settlement. Many of the permafrost investigations conducted in the Ibex Valley site are located on a large grazing lease (disposition #GR AGR 577).

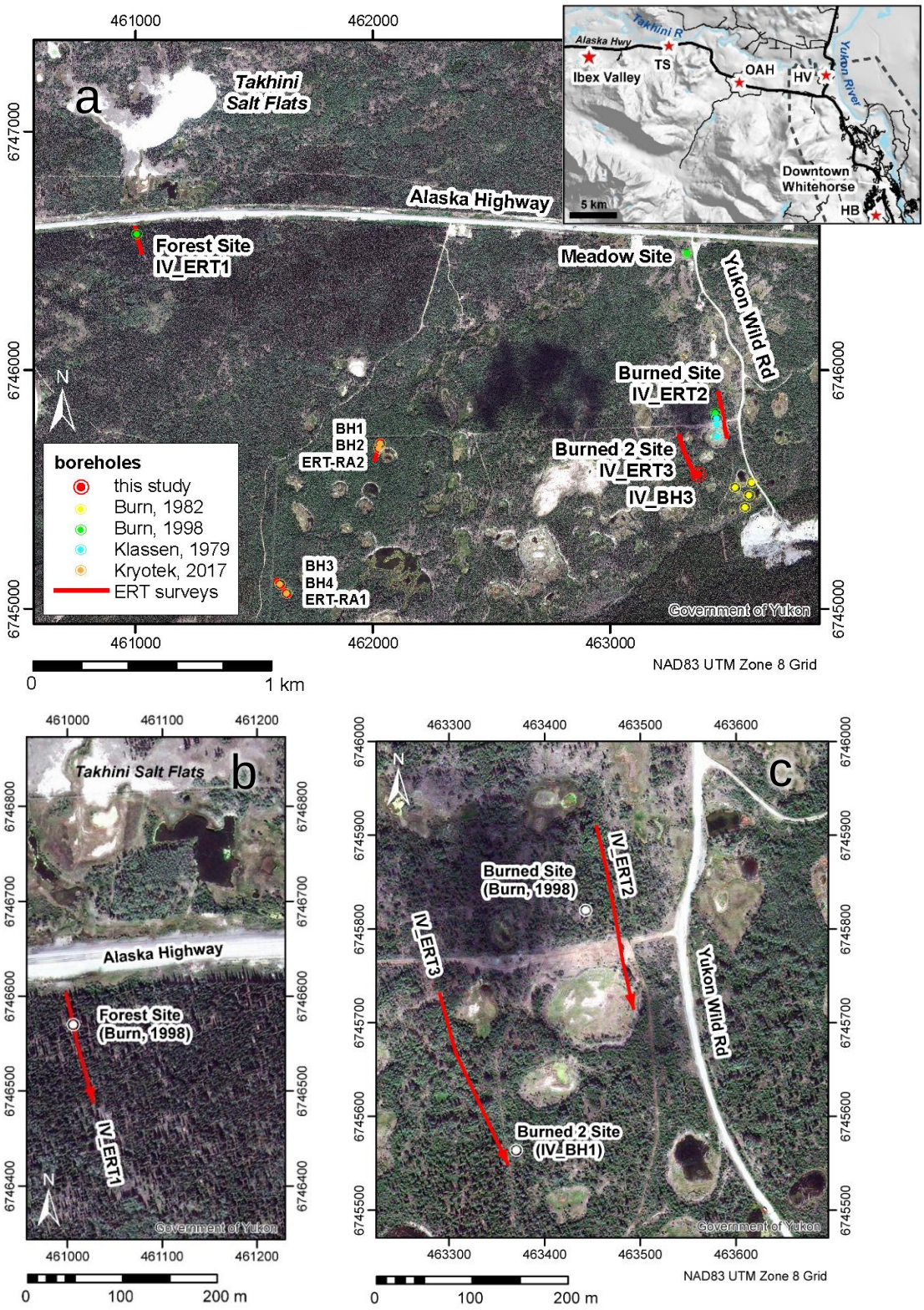

Figure 6.1 Location of the Ibex Valley case study site, and neighbouring sites in Takhini Valley, showing (a) the general locations of the three studied sites, (b) a closer view of Forest site, and (c) closer view of the Burned and Burned 2 (IV_BH1) sites. Inset map shows location relative to Whitehorse city limits (dashed line) and other nearby case study sites (TS = Takhini River thaw slump, OAH = Old Alaska Highway, HV = Hidden Valley, HB = Hamilton Blvd).

6.1.1 Climate and vegetation

An ECCC weather station located approximately 6 km east of the case study site (Takhini River Ranch station ID 2101095) indicates that mean monthly January temperatures are an average of 2.9°C cooler than Whitehorse airport (ECCC, Whitehorse A station), while mean monthly July temperatures are an average of 0.7°C cooler.

Before the wildfires of 1958, the valley was covered by white spruce forest, which dominated the vegetation of the region for at least the previous 8000 years (Keenan and Cwynar, 1992). Burned areas with intact permafrost at the Ibex Valley case study site have mixed forest cover of white spruce (*Picea glauca),* lodegepole pine (*Pinus contorta),* and aspen *(Populus tremuloides)* (Vogt, 2021, in prep). The forest at the site is in an earlier successional stage than the surrounding areas due to the occurrence of the 1958 wildfire. Surrounding unburned areas are forested with white spruce. Transitional areas are sparsely forested and degraded areas are unforested likely due to increased surface moisture and ground subsidence causing unfavourable conditions for tree growth (Vogt, 2021, in prep). Deadfall and dead standing trees are present in the area surrounding these transects. Shrubs such as willow (*Salix spp*.) and soapberry (*Shepherdia canadensis)* are present throughout much of the site. Common plant species are forbs such as fireweed (*Chamaenerion angustifolium)* and alpine sweetvetch (*Hedysarum alpinum)*, mosses, and lichens such as *Cladonia spp*.

6.1.2 Surficial geology

As outlined in Section 2.1, Glacial Lake Champagne occupied the Takhini River valley at the end of the last ice age, when glaciers readvanced westward from the Yukon River valley and blocked the mouth of Takhini River. Thus this portion of the Takhini River valley is filled by a glaciolacustrine plain (LGp) comprising thick fine-grained lake-bottom sediments. The surface of this plain undulates between elevations of 650 and 670 m in the case study area. Strandlines marking prolonged lake levels at 720 m and 736 m elevation are found between two gravel pits located just east of the case study area.

Near-surface glaciolacustrine sediments typically comprise interbedded fine sand, silt and clay (Fig 6.2a), and are capped with sandy blankets of eolian and/or glaciofluvial sediments immediately north and east of Two Horsemen Lake. Three water wells located within 1–2 km of IV_BH1 indicate that fine-grained glaciolacustrine sediment is 27–40 m thick in the immediate vicinity (Fig. 6.3; Environment Yukon, 2021, borehole ID: 204130007, 204130008 and 980000162), however over 300 m of the same material was encountered in a water well drilled in Takhini River Subdivision, located ~5 km to the west (EBA, 2014).

Figure 6.2 a) Interbedded glaciolacustrine silt and clay exposed in nearby Takhini River cutbank, b) typical thermokarst lake (note person circled for scale) with actively collapsing south-facing banks, c) fresh tension cracks and slumping along south-facing bank of thermokarst depression, and d) salt flats commonly develop in drained thermokarst lakes, such as this one along the banks of Takhini River.

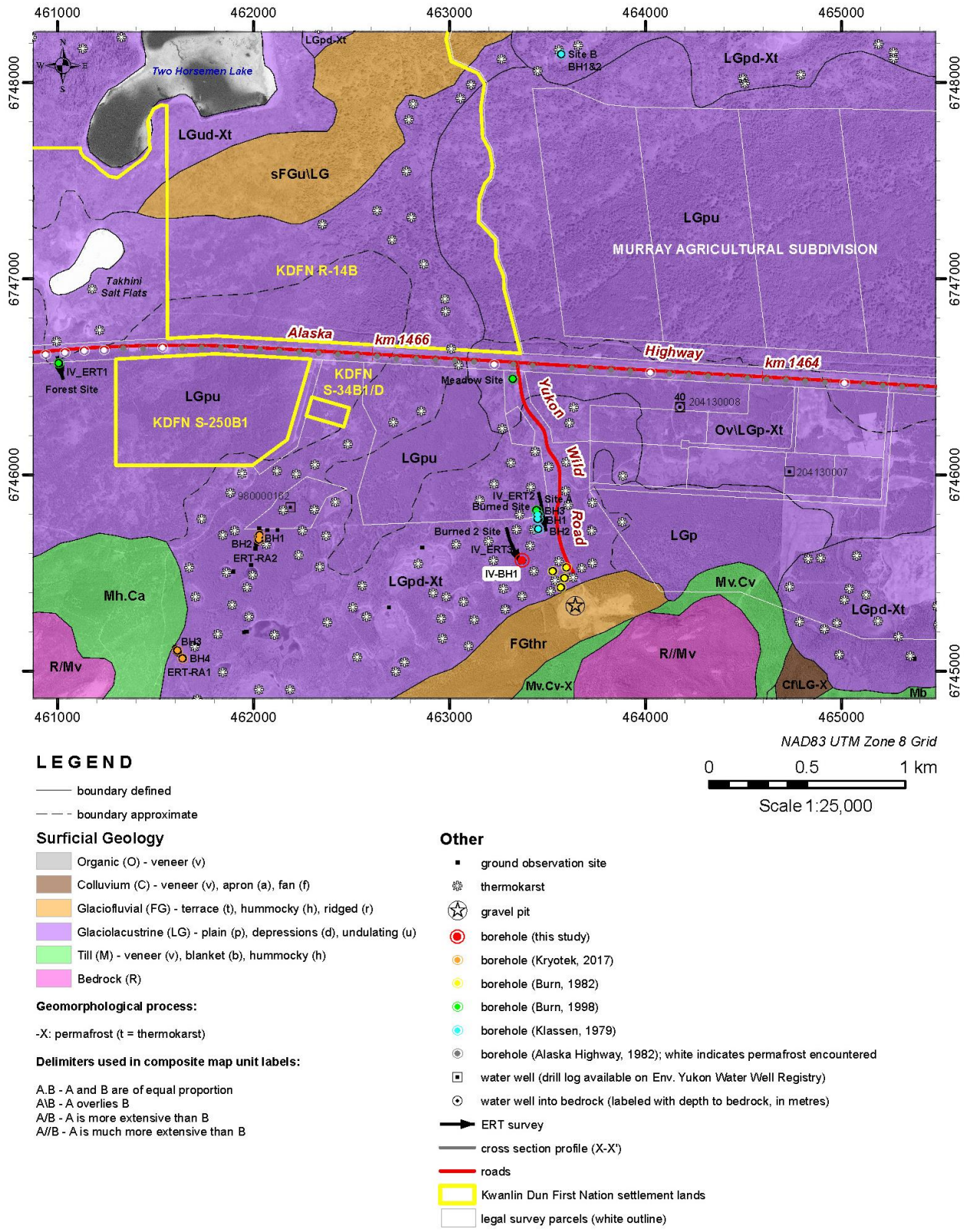

Figure 6.3 Simplified surficial geology map showing major landscape units, landforms and boreholes drilled in the vicinity of Ibex Valley.

The glaciolacustrine plain is pitted with clusters of crater-like thermokarst depressions (Fig. 6.3) where thaw of ice-rich permafrost has recently occurred (Fig. 6.2b). The depressions are rimmed by steep banks up to 5 m high (Klassen, 1979; Cherian-Hall, 2019). Thermokarst activity is particularly common along south-facing banks, as indicated by fresh bank collapse, slumping and tension cracks (Fig 6.2c). Most of the thermokarst depressions are occupied by shallow ponds, although some have drained and transformed into grassy meadows and/or salt flats (Fig 6.3d) such as Takhini Salt Flats.

Sand and gravel extraction have occurred on a glaciofluvial kame terrace (FGthr-T) located along the toe of the slope to the south. This marked the lateral margin of the ice during a period of stagnation as it retreated from the valley. Higher elevation slopes are mantled with basal till (Mv and Mb) and colluvium (Cv), and bedrock outcrop is common. Organic materials commonly veneer north-facing slopes mantled in till and accumulate in poorly-drained areas adjacent to wetlands, or in the floors of drained thermokarst lakes.

Three main bedrock units are mapped in Figure 6.3 (Yukon Geological Survey, 2021). Paleozoic (299–375 Ma) Takhini Group metabasite, amphibolite gneiss, tuff, wacke and marble underlie most of the area shown in Figure 6.3. Early Jurassic (183–186 Ma) Aishihik batholith (Long Lake Suite) granodiorite is also found in the western portion of the Figure 6.3 map area. Upper Triassic (217–229 Ma) Lewes River Group (Povoas Formation) volcanic rocks (including andesitic basalt flows, breccia, and tuff) extend to the north. Bedrock was encountered at 40 m depth 1 km northeast of IV_BH1 (Fig. 6.3; Environment Yukon, 2021, borehole ID: 204130008).

Previous surficial geological mapping for the area includes a 1:100 000 scale map by Klassen (1978), an unpublished Yukon Government 1:100 000 map completed by Morison, McKenna and Davies in 1982 for the Southern Lakes (105D NW), and a 1:20 000 scale soil survey map (Mougeot and Smith, 1992). Figure 6.3 provides an updated 1:25 000 scale map for the area, based on these previous works, in addition to 2013 lidar data, satellite imagery, and soft copy interpretation of aerial photographs between 1946 (1:30 000 scale) and 2007 (1:40 000 scale).

6.1.3 Permafrost

The area has been extensively studied by Klassen (1979) and Burn (1998) in the late 70s to late 90s, laying a baseline to characterize the permafrost distribution in the valley. James Coates (Kryotek Arctic Innovation Inc., 2017) has also provided knowledge and insight about his drilling and ERT experience in the Takhini Valley, wherein the Ibex Valley case study lies.

Klassen (1979) investigated thermokarst lakes in the case study area as part of a 1:100 000 scale surficial geology mapping program in the region (Klassen, 1979). Klassen drilled three boreholes near IV_BH1 (Site A BH1, 2 and 3 in Fig. 6.3), and two boreholes on the north side of the Alaska Highway (Site B, BH1 and 2 in Fig. 6.3). Permafrost was absent to depths of 4.5 m and 6.4 m respectively, beneath the center of the thermokarst depressions investigated. Ground ice was observed from 3 m to at least 9.5 m depth just outside these depressions.

A series of shallow geotechnical boreholes (5 m deep on average) were drilled every 100 m along the Alaska Highway centerline in this area in mid July 1982. Of the 45 Alaska Highway boreholes shown in Figure 6.3, only 8 intersected the frost table at depths ranging from 3.2 to 4.5 m. Five of these were located just west of Alaska Highway km 1467, near Burn's (1998) Forest site and the Takhini Salt Flats. Permafrost was only noted in three other boreholes between km 1463 and 1467.

Chris Burn monitored ground temperatures down to 5 m depth at three locations in this area (Forest, Meadow and Burned sites) from 1983 to 1996 (Burn, 1998). He determined most ground warming during this period occurred in winter and found summer ground temperature changes were less pronounced because large inputs of latent heat are required to initially thaw the ground before sensible heating can occur. He showed that by 1997, the active layer at the burned site had thickened by 2.4 m since the 1958 wildfire. He also suggested over a millennium would be required to completely thaw permafrost in the area under current conditions, although thin permafrost would likely disappear within centuries.

Signs of permafrost degradation are present on both burned sites (Burned and Burned 2) and comprise thermokarst ponds and leaning/dead trees (drunken trees). The wildfire of 1958 removed most of the vegetation cover which contributed to permafrost thaw. Burn (1998) indicated that following the fire, the permafrost went through a rapid thaw which eventually slowed as the permafrost table progressed deeper as the overlying soil created an insulating buffer from the surface warming.

The Forest site studied by Chris Burn in the late 1990s is not showing significant signs of degradation. Vegetation density and organic cover (15 cm) of this undisturbed forested site probably played a crucial role in preserving the permafrost. According to Burn (1998), the active layer at the undisturbed forest site was 1.4 m thick, while in 1996, 38 years after the fire, the active layer at the Burned site was 3.75 m thick. Our observations at Burned 2 (IV_BH1) suggest the depth to top of permafrost is 4.9 m. Burn estimated that over a millennium would be required to completely thaw the permafrost following the current thermal ground regime at the Burned site, implying the rate of thaw would be ~1–2 cm/yr. This rate could slow gradually due to the increasing insulating capacity of the unfrozen soil above.

The boreholes studied by Burn were completed by water jet drilling and no cryostratigraphic observations were made, however the Burned 2 site (IV_BH1) was cored, allowing the ground stratigraphy to be recorded. High ground-ice content was observed at IV_BH1, and likely occur elsewhere in the area. High ground ice presents a potential for hazards such as subsidence. When ice-rich material overlies ice-poor material, the thaw-settlement hazard is high in the short term, and the rate of change is fast. Conversely, when ice-poor material overlies ice-rich sediment, thawing of the upper layer is rapid but minimal thaw settlement occurs initially. This will be followed by slow, but constant thawing of the underlying ice-rich layer resulting in differential thaw settlement.

Kryotek (2017) conducted an ERT and borehole drilling program on 10–11 May 2017 to characterize permafrost conditions in the area (see Fig.6.3 for locations). The first 100-m ERT survey (RA1) suggested ice-rich permafrost extended from 3 to 5 m depth at the permafrost table, to a depth of 14 m within aspen forest, while no permafrost was present beneath a stabilized thermokarst depression. The second ERT survey (RA2) conducted entirely within aspen forest adjacent to an active thermokarst depression suggested ice-rich permafrost was present beneath saturated silt, between a permafrost table of 5–6 m depth to the base of permafrost at 12–15 m depth. Borehole drilling confirmed the depth to top of permafrost along both ERT surveys, and 22–96% excess ice was observed in core samples from three of the four boreholes. Ice-rich permafrost was also noted in a nearby water well from 5 to 12 m depth in 2016 (Environment Yukon, 2021, borehole ID: 980000162).

6.2 Results

6.2.1 Borehole geotechnical data

Borehole IV_BH1 (689 m asl) was drilled and instrumented to a depth of 19.8 m at the Burned 2 site, on 14 January 2019 using Midnight Sun Drilling's sonic rig under the supervision of Louis-Philippe Roy and Panya Lipovsky (Fig. 6.4 and Table 6.1). Data from pre-existing boreholes at the Burned and Forest sites drilled by Chris Burn in July 1990 were also used in this assessment (Table 6.1). ERT survey IV_ERT1, was carried out 5 June 2018 at the Forest site to assess the present ground conditions (Fig. 6.1a). ERT surveys IV_ERT2 and IV_ERT3 were conducted on 10 October 2018 and intersected the Burned and Burned 2 boreholes, respectively (Fig. 6.1).

Figure 6.4 Midnight Sun Drilling Sonic drill rig (a) and instrumented borehole (b) at IV_BH1.

Table 6.1 Location details of field surveys at the Ibex Valley study site, including three boreholes, one of which was instrumented, and three ERT surveys.

Site (Borehole)	Date	Coordinates (NAD83 UTM Zone 8)	Depth (m)	Ground Temperature Sensor Depths (m)
Forest (Forest_BH)	1/7/1990	461006 6746570	16.5	
Burned (Burned_BH)	1/7/1990	463443 6745820	21	
Burned 2 (IV_BH1)	14/1/2019	463370 6745564	19.8	0.0, 0.25, 0.5, 1.0, 2.0, 3.0, 5.0, 8.0, 10.0, 15.0, 18.8
IV_ERT1	5/6/2018	Dipole-dipole and Wenner	Length (m): 120	Electrode Spacing (m): 1.5
0 m		460998 6746604		
30 m		461004 6746581		
60 m		461011 6746547		
90 m		461021 6746513		
120 m		461027 6746487		
IV_ERT2	10/10/2018	Dipole-dipole and Wenner	Length (m): 200	Electrode Spacing (m): 2.5
0 m		463454 6745911		
50 m		463465 6745862		
100 m		463474 6745812		
150 m		463482 6745763		
200 m		463493 6745714		
IV_ERT3	10/10/2018	Wenner	Length (m): 200	Electrode Spacing (m): 2 + 4 (Extremities)
0 m		463290 6745732		
50 m		463305 6745674		
100 m		463321 6745637		
150 m		463339 6745602		
200 m		463362 6745548		

Borehole IV_BH1 is located on an agricultural grazing lease. Its location was selected based on an ERT survey (IV_ERT3), which showed evidence of ice-rich sediments at this site. Once drilling was completed, eleven thermistors were inserted (see Section 6.2.2). The borehole was cased with 1-inch PVC pipe, and backfilled to the surface.

The borehole for IV_BH1 (see Figure A4) shows layers of gray clayey-silt alternating with coarser fine sand. The borehole ends at 20 m in the sandy clayey-silt sediment. Lenticular and microlenticular cryostructures were identified along the profile and the volumetric excess ice content ranged from 23 to 97% (Table 6.2 and Fig. 6.5). The horizon from 7 to 10 m contained the highest excess ice content, ranging from 54 to 97% (Table 6.2). Overall, the borehole has a mean volumetric excess ice content of 49%. Full geotechnical laboratory results completed on this core are presented in Appendix D.

Table 6.2 Grain-size distributions and excess ice content results at various depths from borehole IV_BH1 at Ibex Valley case study site.

Sample Depth (m)	Volumetric Excess Ice (%)	Gravel (%)	Sand (%)	Silt (%)	Clay (%)
1.00	29.8	0.0	31.9	54.2	14.0
1.52	23.4	0.0	42.0	42.1	15.9
2.00	63.8	0.0	29.9	44.2	25.9
3.00	38.2	0.0	34.8	36.1	29.1
4.00	94.5	0.0	39.8	46.3	14.0
5.00	38.5	0.0	37.8	42.3	19.9
6.00	28.0	0.0	29.9	40.2	29.9
7.00	96.7	0.0	37.8	30.3	31.9
8.00	54.0	0.0	50.6	31.7	17.7
9.00	92.8	0.0	32.2	41.6	26.2
10.00	63.8	0.0	33.9	46.2	19.9
11.00	35.1	0.0	33.9	48.2	17.9
12.00	48.3	0.0	17.9	68.2	13.9
13.00	74.5	0.0	25.9	52.2	21.9
14.00	26.9	0.0	39.9	44.2	16.0
15.00	30.8	0.0	17.7	64.4	17.9
16.00	40.0	0.0	20.0	66.1	13.9
17.00	41.6	0.0	13.9	70.2	15.9
18.00	31.1	0.0	23.8	68.2	7.9
19.00	33.5	0.0	38.0	34.1	27.9
20.00	30.1	0.0	46.2	40.0	13.8

Figure 6.5 Ice-rich permafrost core taken from IV_BH1 at 6 m depth.

6.2.2 Ground temperatures

Borehole IV_BH1 was cased with PVC pipe and instrumented with one 11-channel LogR Systems logger to record ground temperatures at various depths (Table 6.1). The PVC casing was filled with silicone oil. Ground temperature recording started 16 May 2019 at 16:00 and was downloaded on 12 August 2020, providing 15 months of ground temperatures (Fig. 6.6). The annual mean ground temperature at the deepest point (18.8 m) is 0.25°C (Table 6.3). Depth of the permafrost table and base were estimated by linear extrapolation of the ground temperature envelope (Fig. 6.7). The permafrost table was estimated at a depth of 4.9 m, and the base at 17.5 m, making the permafrost ~12.6 m thick.

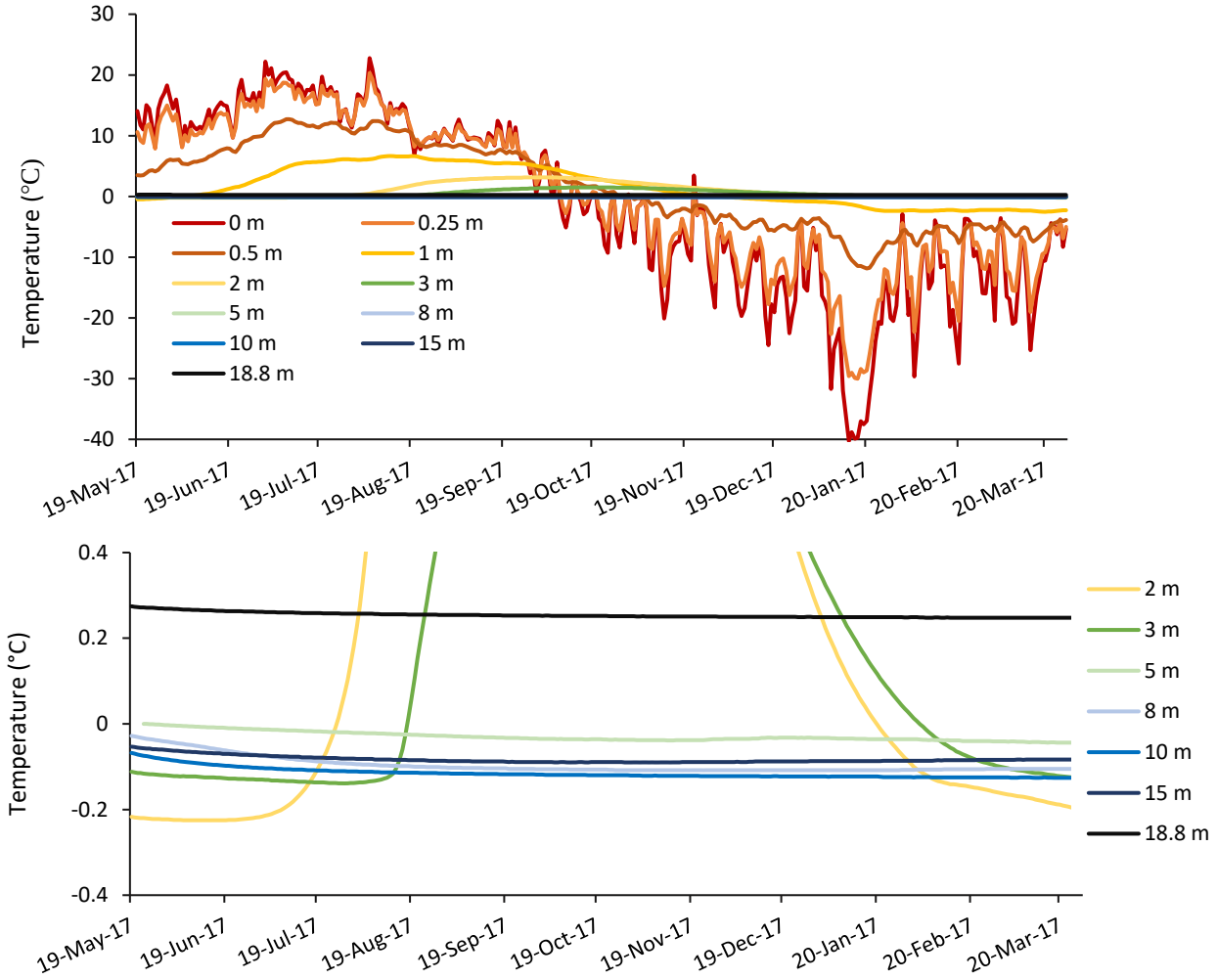

Figure 6.6 Ibex Valley daily mean ground temperatures at IV_BH1 for the period 17 May 2019 to 24 March 2020, from a) 0 to 18.8 m depth, and b) 2 to 18.8 m depth.

Table 6.3 Annual minimum, maximum and mean ground temperature (GT; from daily mean values) at IV_BH01 for the period 1 June 2019 to 31 May 2020.

Depth (m)	0.0	0.25	0.5	1.0	2.0	3.0	5.0	8.0	10.0	15.0	18.8
Annual min GT (°C)	−40.33	−30.01	−11.86	−2.52	−0.26	−0.14	−0.05	−0.11	−0.13	−0.09	0.24
Annual max GT (°C)	22.77	20.33	12.72	6.65	3.14	1.48	0.00	−0.04	−0.09	−0.06	0.27
Annual mean GT (°C)	-0.59	0.28	1.22	1.13	0.71	0.31	−0.03	−0.10	−0.12	−0.08	0.25

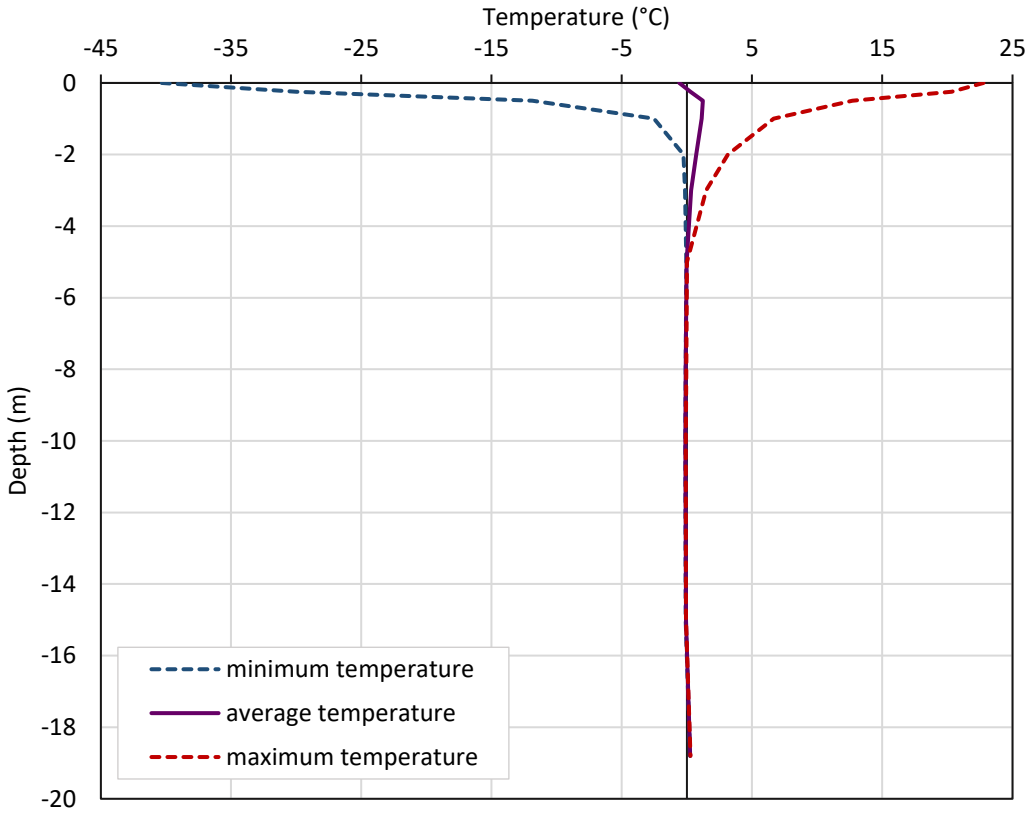

Figure 6.7 Ibex Valley ground temperature envelope at IV_BH1 (from daily mean values) for the period 1 June 2019 to 31 May 2020.

6.2.3 ERT

One ERT survey was conducted on each site, with the ERT transect intercepting a borehole at each. IV_ERT1 intercepted the Forest site, IV_ERT2 intercepted the Burned site, and IV_ERT3 intercepted the Burned 2 site (Fig. 6.1a). For surveys IV_ERT1 and IV_ERT2 both Wenner and dipole-dipole arrays were used, while only the Wenner array was used for survey IV_ERT3. The results obtained with the Wenner and dipole-dipole arrays show a similar distribution of resistivity in the subsurface, however the dipole-dipole array shows more details in the low resistivity areas.

IV_ERT1

Survey IV_ERT1 was completed at the Forest site and ran north to south, through undisturbed spruce forest (Fig. 6.8). The forest cover was open in the first third of the profile (~40 m) and dense in the last two thirds (Fig. 6.9a). The ERT survey intercepted Forest_BH at 35.5 m along the survey line (Fig. 6.9a). Both Wenner and dipole-dipole array show similar patterns (dipole-dipole results are shown in Fig. 6.9; see Figure C4 for Wenner results). It appears the high resistivity areas, shown as dark blue shades, are primarily located towards the north end of the profile from 30 to 38 m along the transect up to 5 m depth (Fig. 6.9b). It is possible that thicker organic cover along this portion of the transect could be preserving the permafrost below. No evidence of ice-rich permafrost was observed at the surface.

Figure 6.8 ERT transect (IV_ERT1) at Forest site, intercepting the Forest_BH borehole.

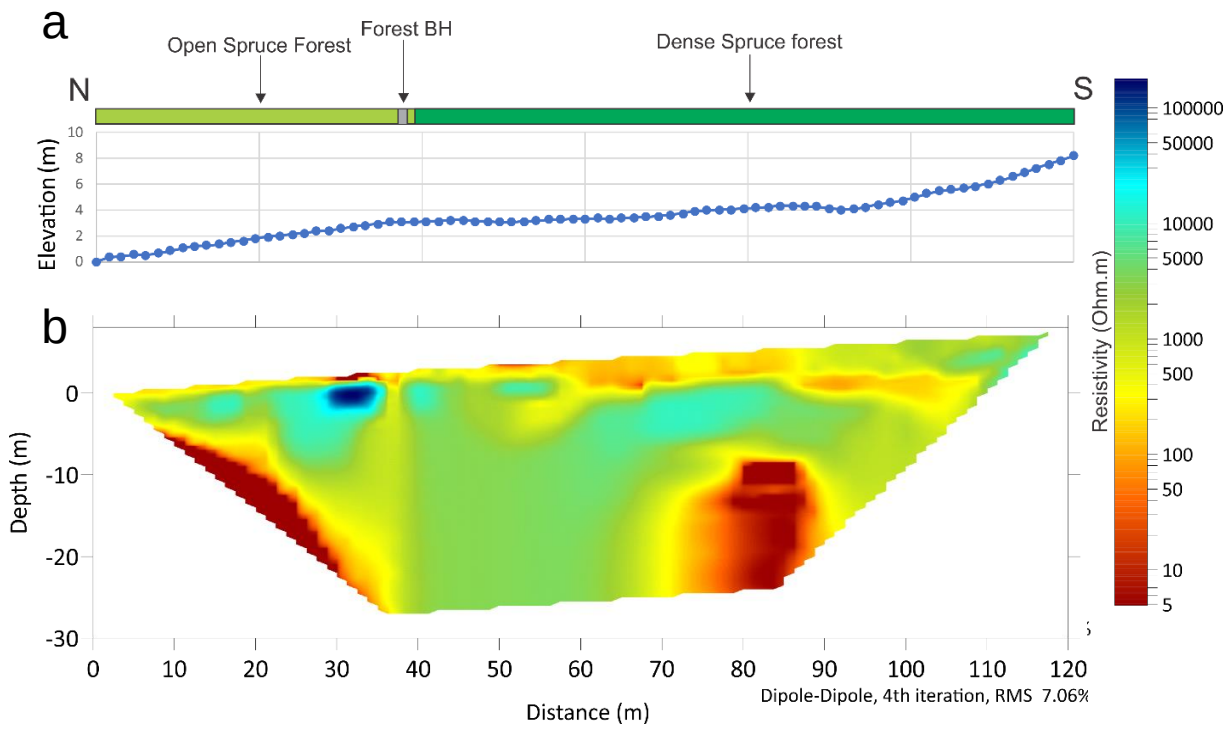

Figure 6.9 Ibex Valley ERT survey at the Forest Site (IV_ERT1) showing the (a) topographic profile, and (b) ERT profile using dipole-dipole array, 4th iteration, RMS error= 7.1%. In (b) green to blue shades are interpreted as permafrost, and orange to red shades most likely represent unfrozen ground.

Towards the south end of the profile resistivity values are still relatively high (5000 to 10 000 ohm·m, shown as blue-green shades) all the way to the surface of the ground (Fig. 6.9b), which may suggest a very shallow permafrost table. A lower resistivity area, shown as red shades, from 10 to 30 m horizontal distance could be the result of vegetation clearing on the Alaska Highway right-of-way during construction (Fig. 6.9b). Another lower resistivity zone from 70 to 90 m horizontal distance and 10 to 25 m depth could be the result of groundwater flow. It is unlikely the aquifer at the site would be completely confined because of the discontinuous distribution of permafrost in Takhini Valley. The ERT data also suggest that permafrost may be present down to 25 m depth towards the middle of the profile from 38 to 65 m horizontal distance.

IV_ERT2

Survey IV_ERT2 was conducted at the Burned site, and ran north to south, intercepting borehole Burned_BH at 100 m along the profile (Fig. 6.10a); see Figure C3 for ERT profile using Wenner array. The vegetation cover in the northern half of the profile was colonized predominantly by trembling aspen, clusters of willow, some lodgepole pine, and occasional spruce saplings. The data suggest that the permafrost table (top) is uneven, varying from 3 m depth at the north end to 5–6 m near the middle of the survey. A high resistivity area under the forest is shown as dark blue shades from 45 to 95 m distance and 5 to 15 m depth. A second, high resistivity pocket shown in light blue is located below the access road from 102 to 142 m distance. The Burned_BH borehole is located between these two high-resistivity units and appears to be unfrozen. Material below 15 m depth seems to be unfrozen as well.

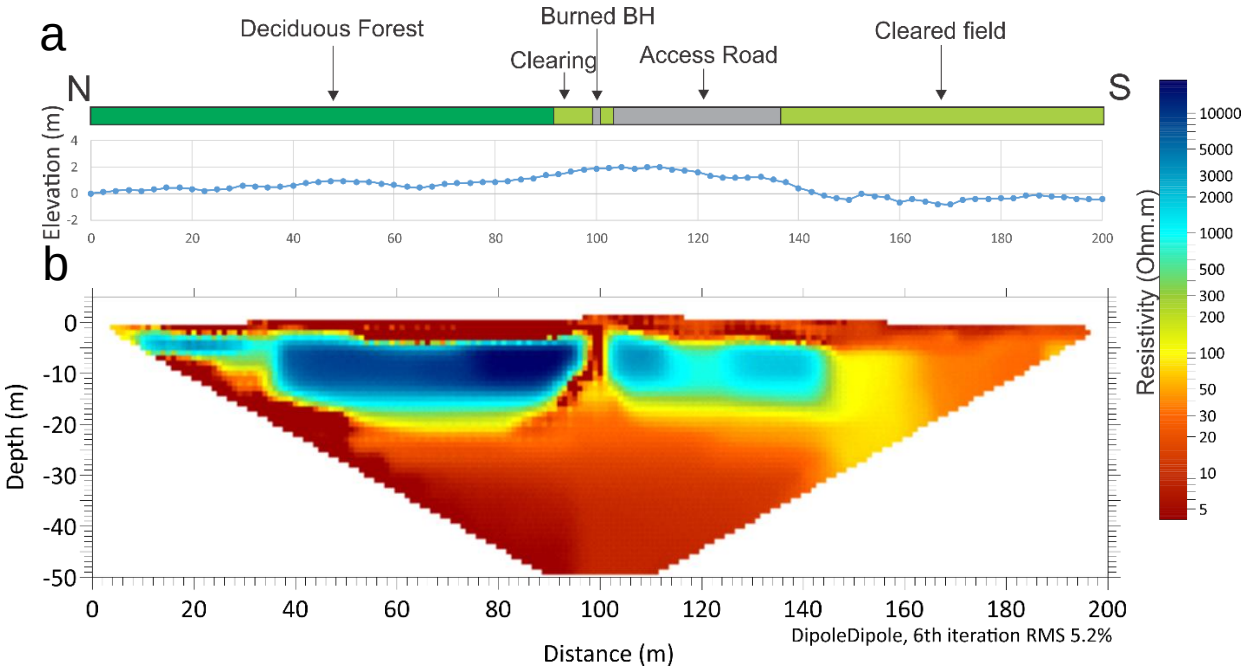

Figure 6.10 Ibex Valley ERT survey at the Burned site (IV_ERT2) showing the (a) topographic profile, and (b) ERT profile using dipole-dipole array 6th iteration, RMS error= 5.2%. In (b) blue shades are interpreted as frozen ground, and orange to red shades as unfrozen ground.

IV_ERT3

Survey IV_ERT3 was completed at the Burned 2 site within an early successional forest that has grown since the 1958 wildfires (Fig. 6.1a). The survey ran north-south going up a slight (<3°) slope and intersects borehole IV_BH1 at a ~180 m horizontal distance (Fig. 6.11a). The forest cover in the northern half of the profile was open and colonized predominantly by trembling aspen, willows, lodgepole pine, and some spruce trees. Forest cover in the southern half of the survey was denser and contained a higher concentration of mature spruce trees. The data suggest that the permafrost table is relatively even along the southern half of the survey, varying from 4 to 5 m depth. The data indicate a high resistivity area in dark blue from 100 to 200 m horizontal distance beginning at a depth of 3–4 m depth and extending to the base of the survey at 27 m. This high resistivity body is almost certainly permafrost, while material from 0 to 100 m distance along the transect is likely unfrozen.

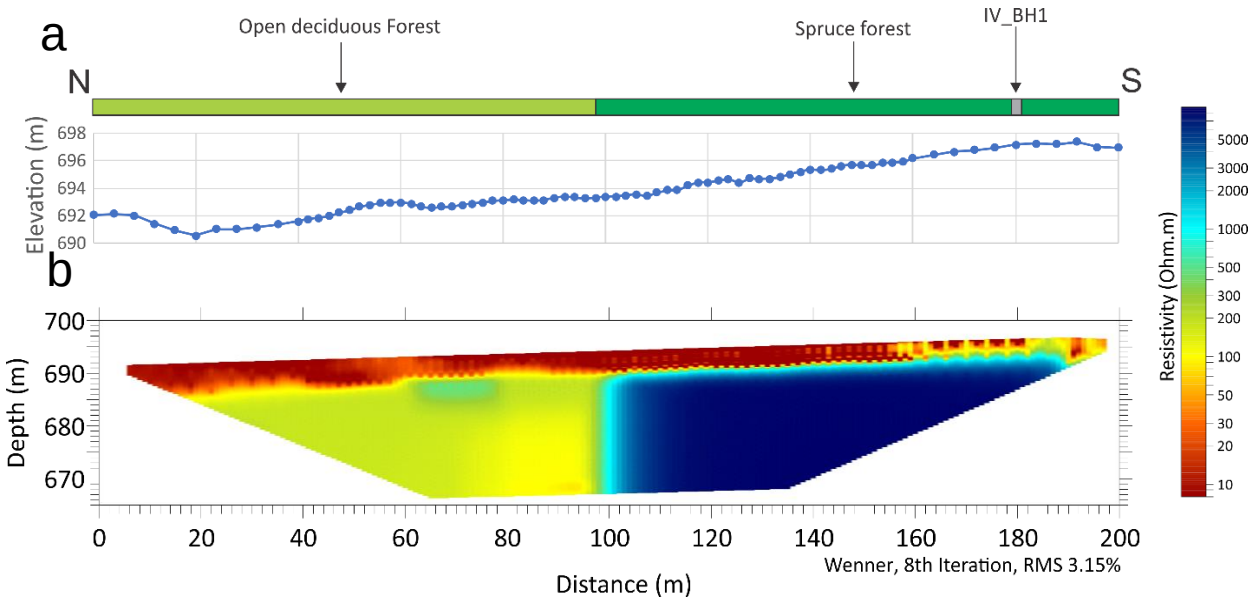

Figure 6.11 ERT survey at Ibex Valley, IV_ERT3, at the Burned 2 site showing the (a) topographic profile, and (b) Wenner array 8th iteration, RMS error= 3.1%. In (b) blue shades are interpreted as frozen ground, and yellow to red shades as unfrozen ground.

In all three surveys, very high-resistivity areas are attributable to ice-rich fine-grained sediment (clayey-silts); resistivity may also increase with depth, as permafrost becomes colder. The low resistivity values could be attributable to ice-poor and/or unfrozen material, however the lowest values may indicate the presence of groundwater, or the impact of organic cover loss after the wildfire of 1958. The geophysical and geotechnical data suggests the presence of permafrost is strongly linked to vegetation cover. Dense mature forest will preserve permafrost and open or disturbed organic cover will negatively impact permafrost thickness and distribution.

6.2.4 Synthesis

The geotechnical borehole data support the interpretation of ERT data in defining the top and thickness of permafrost. The permafrost table was estimated at a depth of 4.9 m, and the base at 17.5 m (from ground temperatures), making the permafrost ~12.6 m thick. As the borehole has a mean volumetric excess ice content of 49%, the potential subsidence is estimated at 6.2 m if all permafrost were to thaw at that location. The cores collected on site show the presence of clayey silts, a frost susceptible sediment, down to at least 20 m depth. Ground temperature records from IV_BH1 suggest the permafrost is warm and vulnerable to thaw. The areas that were subject to burning by wildfire lack insulating organic material at the surface which allowed the active layer to deepen and permafrost to thaw. The presence of numerous thermokarst lakes in historical aerial photos also indicates that widespread permafrost degradation has likely been occurring in the area since well before the 1958 wildfire.

Permafrost at the Ibex Valley case study site is warm with average temperatures between 0.0 and −0.1°C. Permafrost (shown as high resistivity pockets in the ERT surveys) is currently being preserved because the ground is ice-rich and therefore requires a high amount of energy for ice to melt. Temperature data indicate that the permafrost table at IV_BH1 in 2019–2020 is 1.11 m deeper than Burned_BH at the Burned site in 1997 (Burn, 1998). Borehole IV_BH1 and Burned_BH are geographically close (roughly 200 m apart) and can be used for comparison. Assuming IV_BH1 had a comparable active layer depth to Burned_BH in 1997, a 1.11 m increase in active layer depth would correspond to permafrost thaw on the order of 5 cm/yr. Permafrost thaw could cause subsidence of ~24% of the permafrost thickness at the Burned site and ~50% at the Forested and Burned 2 site. Ground subsidence is therefore the main hazard for this site and similar terrain units around Ibex Valley.

7 TAKHINI RIVER THAW SLUMP

7.1 Site setting

Retrogressive thaw slumps are slope failures caused by the thaw of ice-rich permafrost. They have steep headwalls which gradually retreat due to ongoing thaw of the headwall face, while periodic debris flows transport thawed sediment away. They usually occur along the shorelines of lakes, rivers and coastlines and in areas underlain by massive ice bodies, or ice-rich silts. The Takhini River Thaw Slump case study site is in the Takhini Valley at km 1456.45 of the Alaska Highway, about 34 km west of Whitehorse airport by road (Fig. 7.1). This retrogressive thaw slump developed in 2014 on the southern bank of the Takhini River, and is actively retrogressing towards the Alaska Highway. Continued retrogression may eventually impact the highway.

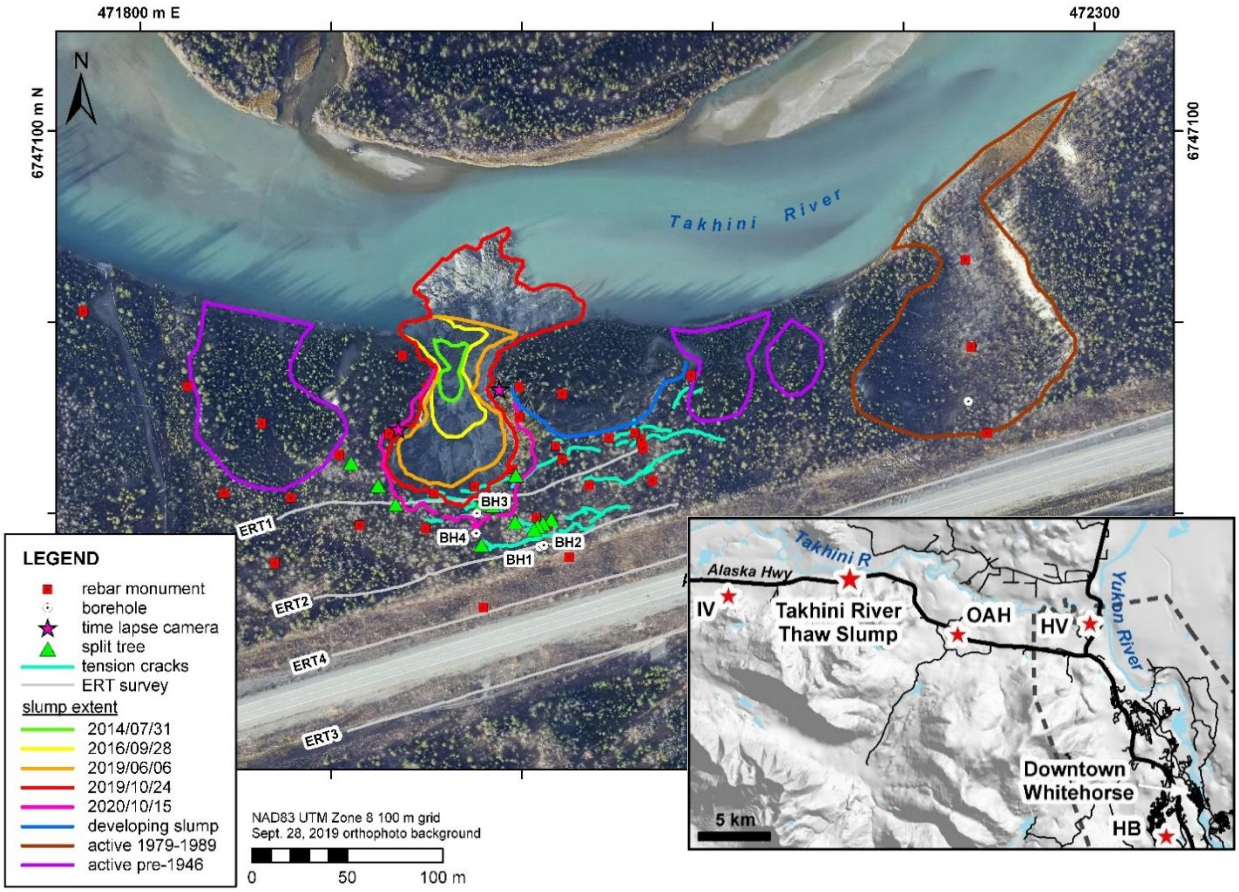

Figure 7.1 Location of the Takhini River Retrogressive Thaw Slump (km1456) case study site with past retrogressive thaw slumps, as well as locations of boreholes, ERT surveys, tension cracks and split trees. Inset map shows location relative to Whitehorse city limits (dashed line) and other nearby case study sites (IV = Ibex Valley, OAH = Old Alaska Highway, HV = Hidden Valley, HB = Hamilton Blvd).

The thaw slump was most likely initiated by erosion on the outer bend of a meander. A tributary creek and alluvial fan enter the Takhini River on the opposite (north) bank 100-m upstream, forcing the thalweg (deepest part of the channel) further to the outer (south) bank of the bend (Fig. 7.1). The thaw slump has been retreating towards the highway at a rate of up to 11 m/yr between 2014 and 2020. Several tension cracks, ranging from metres to tens of metres, are also present between the headscarp and the road; the closest being 20 m from the road embankment (marked in Fig. 7.1). The slump currently extends a horizontal distance of 160 m, and vertical distance of roughly 25 m; from ~666 m elevation at the top of its headscarp to 640 m at the toe of the debris fan in the Takhini River (Fig. 7.2).

Figure 7.2 Panoramic view of thaw slump bowl on 24 August 2020, looking northeast. The headscarp retreats as mudflows transport thawed material into Takhini River.

Agricultural development and activity in this portion of Takhini Valley has increased in recent years. A farm 2 km long and 0.8 km wide is located about 200 m upslope (south) of the thaw slump, on the south side of the Alaska Highway. Aerial photos show that clearing of pastures on this farm began around the year 2000 and was largely completed by 2005. Several of the pastures are also intensively irrigated during the growing season (B. Barton, EMR Agriculture Branch, pers. comm., 2019).

Retrogressive thaw slumps represent a rapid erosive process in present-day periglacial environments, and typically become stable between 30 and 50 years after their initiation (French and Egginton, 1973). Older aerial imagery shows several older retrogressive thaw slumps of similar size have occurred on the adjacent slope, and several earth slopes on the opposing bank (Fig. 7.3). One retrogressive thaw slump located 200 m to the east was active from 1979 to 1989. This 40 000 m^3 retrogressive thaw slump (Huscroft *et al.,* 2004) was also likely initiated by riverbank erosion. The headscarp retreated 112 m and stabilized a few meters short of the highway. Another slump located 100 m to the west was also active in the 1940s. These older slumps have since stabilized likely due to depletion of ground ice near the road and/or covering or insulation of their headwalls. However, cracks in the road surface continue to propagate parallel to the headscarp behind the slump which was active in the 1980s.

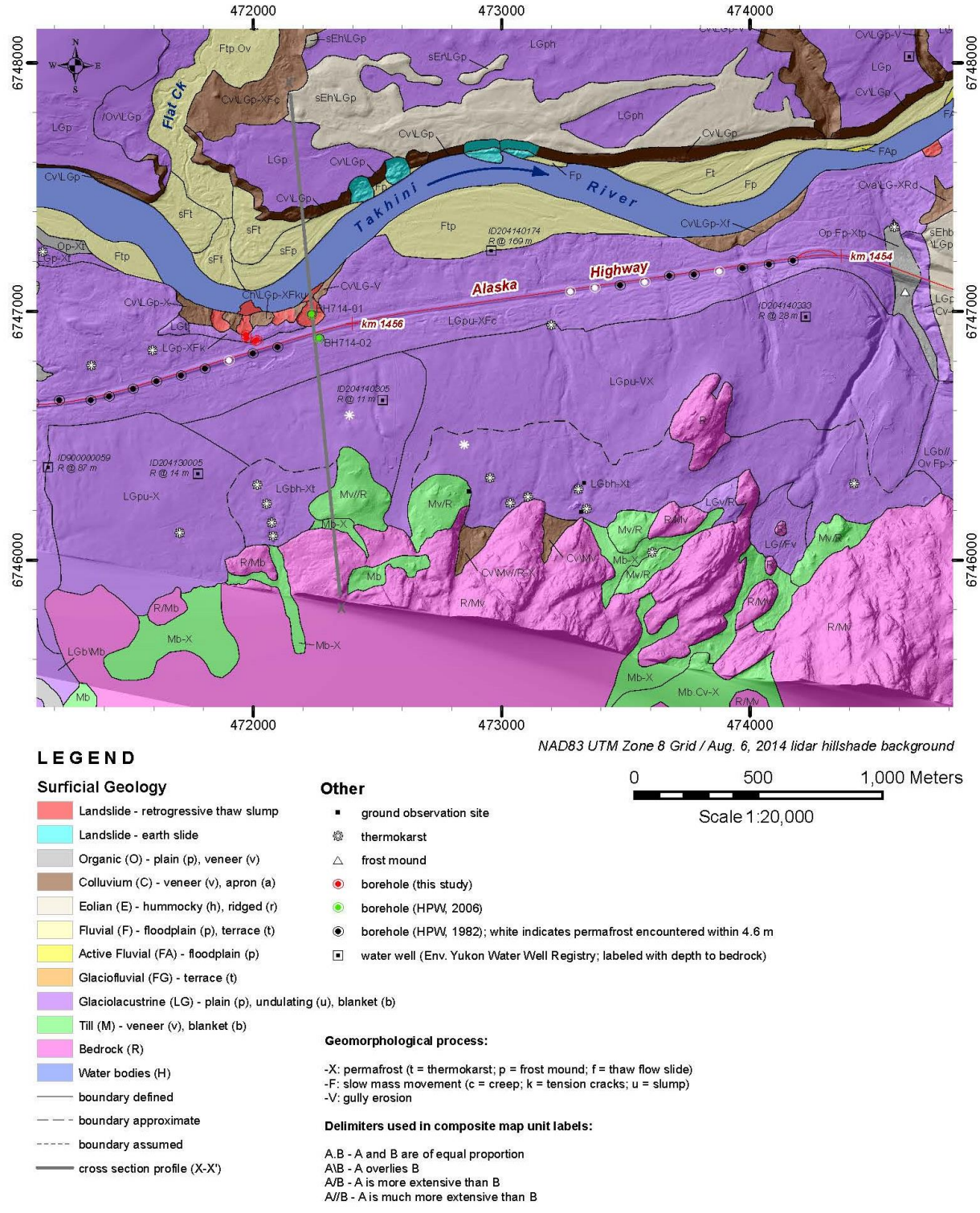

Figure 7.3 Simplified surficial geology map showing major landscape units, landforms and boreholes drilled in the vicinity of the Takhini River Retrogressive Thaw Slump, near km 1456 of the Alaska Highway.

7.1.1 Climate and vegetation

A weather station located 900 m west of the thaw slump at km 1457 (Yukon Department of Highways and Public Works) recorded MAATs an average of 2.1°C cooler than Whitehorse airport (ECCC, Whitehorse A station) for the period 2015–2020 (excluding 2018). Another weather station located 3.5 km west of the Takhini River Thaw Slump (ECCC, Takhini River Ranch station) indicates that mean monthly January temperatures are an average of 2.9°C cooler than Whitehorse airport (ECCC, Whitehorse A station), while mean monthly July temperatures are an average of 0.7°C cooler.

The site has a mixed forest cover primarily composed of white spruce (*Picea glauca*) and aspen (*Populus tremuloides*). Shrubs such as willow (*Salix spp.*) and soapberry (*Shepherdia canadensis*) are present throughout much of the site. Common plant species are forbs such as fireweed (*Chamaenerion angustifolium*) and alpine sweetvetch (*Hedysarum alpinum*), mosses, and lichens such as *Cladonia spp*. The case study site was also burned in the 1958 wildfire that burned much of Takhini Valley, which is likely responsible for the lack of thick organic cover on site.

7.1.2 Surficial geology

The primary surficial material (Figs. 7.3 and 7.4) in this area is a thick package of Glacial Lake Champagne glaciolacustrine sediments which filled much of lower Takhini River valley as described in Section 2.1. Near the thaw slump, these sediments extend up to an elevation of 700 m. The sediment largely comprises finely laminated silt and clay lake bottom deposits (Fig. 7.5). The thaw slump headscarp also exposes a thin layer (<50 cm) of fluvial fine sand capping the glaciolacustrine sediments (Fig. 7.6). This sand was likely deposited during drainage of Glacial Lake Champagne. Following drainage of the lake, eolian activity also deposited a layer of wind-blown fine sandy silt at surface.

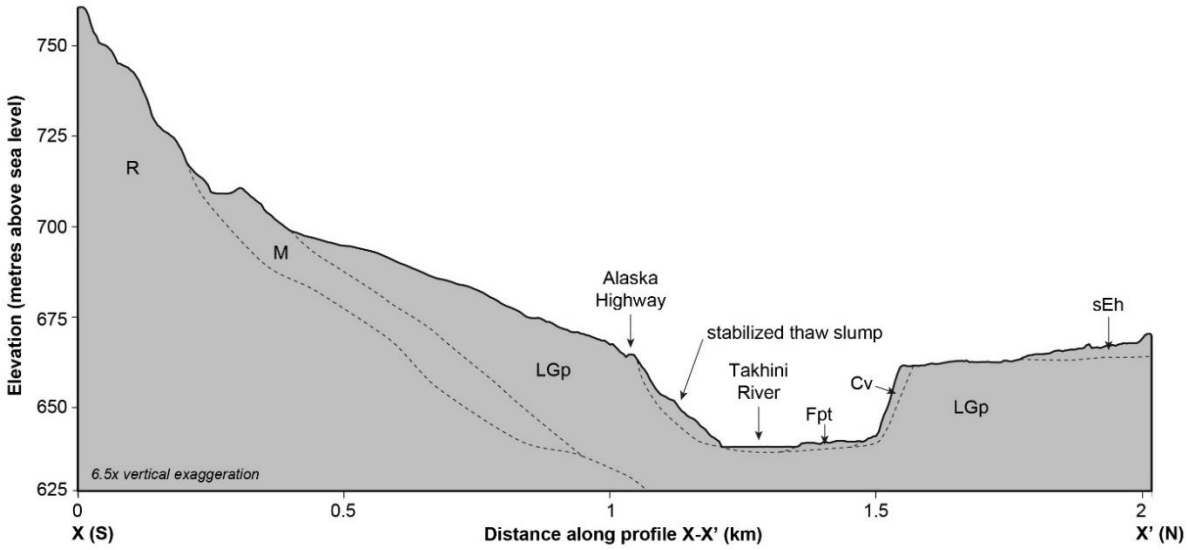

Figure 7.4 Generalized stratigraphic cross section from 2013 LiDAR DEM along transect X-X' (shown in Fig. 7.2) Note, this cross section extends through the nearby stabilized thaw slump that was active in the 1980s, not the one investigated in this study (which is located 200 m to the west).

Figure 7.5 Roughly 8 m of laminated glaciolacustrine sediments are exposed in the thaw slump headwall near borehole WH_1456_BH3, 15 October 2020. Broken borehole casing is circled.

Figure 7.6 Near-surface stratigraphy exposed in thaw slump headwall near WH_1456_BH3. The uppermost unit comprises ~1.3 m of massive eolian silty sand. This is underlain by ~0.5 m of stratified fluvial sand. The lower unit comprises beds of ice-rich glaciolacustrine silt and clay.

Glaciolacustrine sediments were up to 127 m thick in a water well located 1 km northeast of the thaw slump near the modern Takhini River (Environment Yukon, 2021, borehole ID: 204140174). Closer to the bedrock

hills immediately south of the thaw slump, glaciolacustrine sediments range from 5 to 87 m thick, as indicated in 4 other water wells located within 2 km of the thaw slump. Till and colluvium mantle the lower slopes of the nearby bedrock hills above an elevation of 700 m.

Bedrock outcrop south of the thaw slump comprises Jurassic (168–200 Ma) Whitehorse trough Laberge Group sedimentary and volcaniclastic units (Richtofen and Nordenskiold formations). Upper Triassic (217–229 Ma) Lewes River Group volcanic rocks extend to the west (Yukon Geological Survey, 2021). A deep trough in the underlying bedrock topography likely extends beneath the Takhini River floodplain, where the thickness of overburden is at least 169 m (Environment Yukon, 2021, borehole ID: 204140174). Depth to bedrock in other nearby water wells south of the Alaska Highway range from 11 to 87 m (Fig. 7.3).

7.1.3 Permafrost

Permafrost in the thick glaciolacustrine sediments occupying the floor of Takhini Valley likely formed in different environmental conditions than the present day, *i.e.,* a colder and wetter environment after the drainage of Glacial Lake Champagne. Thus the case study site likely overlies relict permafrost that is out of equilibrium with the current climate, and is sensitive to surface disturbance. In many locations along the slump headwall, finely-bedded glaciolacustrine deposits are deformed by slope movement (Fig. 7.6), but ice-lenses are parallel to the topography, indicating that permafrost formed after the original slope disturbance. Rampton *et al.* (1983) suggested ice-rich permafrost in this area may have also formed where high hydraulic gradients promote movement of groundwater from the uplands and valley sides to the glaciolacustrine sediments in the valley floor. The thermokarst depressions near the base of valley side bedrock slopes shown in Figure 7.3 support this hypothesis.

A series of shallow (4.6 m) geotechnical boreholes were drilled every 100 m along the Alaska Highway centerline in this area in July 1982. Of the 21 boreholes drilled between km 1454 and 1457.5 (Fig. 7.3), only 5 intersected the frost table at depths of 3.3–4.6 m. Frozen ground was also encountered from 6 to 12 m depth in an 18 m deep borehole drilled in October 2006 near the headscarp of the large thaw slump which was active in the 1980s (Yukon Highways and Public Works, borehole log 714-01) approximately two hundred metres to the east.

In 2014, Highways and Public Works (HPW) installed a ground temperature monitoring array at km 1457.4 as part of their intelligent transportation system (ITS) network. This installation comprises a meteorological station and three instrumented boreholes (in the road, at the toe of the embankment, and at a “Field Site” in relatively undisturbed ground at the edge of the right-of-way). Thermistors in the Field Site extend to 10 m depth and have been recording hourly ground temperatures since November 2014; these data indicate that permafrost is present at this site from ~8 to 10 m depth, with a mean annual ground temperature (MAGT) of −0.05°C and a mean annual air temperature (MAAT) of −1.2°C between 2015 and 2020.

Permafrost creep is evident on north-facing gully or riverbank slopes where the Takhini River and tributaries have incised through the fine-grained sediments, as indicated by a furrowed surface texture visible on lidar imagery (Fig. 7.3). Creep movement of survey corner posts at rates of up to ~1 m/decade have also been noted by land surveyors in the vicinity of Alaska Highway km 1455, complicating boundary and highway right of way surveys in the area (P. Burbidge, pers. comm., 2018; B. Thompson, pers. comm., 2005). Features associated with the development of the retrogressive thaw slump were the main indicators of permafrost degradation on site. This includes metre-wide tension cracks and split trees due to ground movements. Some shallow ponds and depressions were also present in the cleared right-of-way beside the road embankment and may have formed from thermokarst activity.

7.2 Results

7.2.1 Slump progression

The retrogressive thaw slump likely initiated because of exposure of ice-rich permafrost due to bank erosion along an outer meander bend of the Takhini River. The exact date of initiation is unknown, however aerial photographs show the slump as ~10 m wide by 30 m long on 31 July 2014, suggesting an initiation date not long before. As of September 2020, the slump had grown to 70 m wide and 150 m long (Fig. 7.7). The retrogressive thaw slump's amphitheater-shaped source zone is surrounded by a steep headwall up to 12 m high as of fall 2020, which exposes ice-rich permafrost within glaciolacustrine silt and clay sediments (Figs. 7.5 and 7.6). Groundwater springs seep from the headwall at several locations from 2 to 3 m below the top of the face. Ongoing thaw of exposed ice has caused the headwall to retreat at rates of up to 19 m/yr since 2014 toward the Alaska Highway. The edge of the highway shoulder was located 55 m from the closest point on the headwall on 29 September 2020 (Table 7.1 and Fig. 7.1).

Table 7.1 Measured rate of expansion of the retrogressive thaw slump since 2016. Distance to road is measured to the edge of the shoulder at the top of road embankment (see Fig. 7.19).

Date	Distance to road (m)	Full size area (m²)	Area to original river bank (m²)
7/27/2016	105.8	1321.9	1257.8
8/18/2018	80.9	2816.3	2705.8
5/16/2019	80.9	N/A	N/A
8/22/2019	71.8	4777.8	4018.5
9/11/2019	69.7	6652.4	4355.5
9/25/2019	68	6942.5	4524.8
10/30/2019	68.8	6816.1	4324.6
5/20/2020	68	6982.9	4590.7
8/26/2020	57.5	7453.2	5466.7
9/29/2020	55.1	7462.02	5499.65

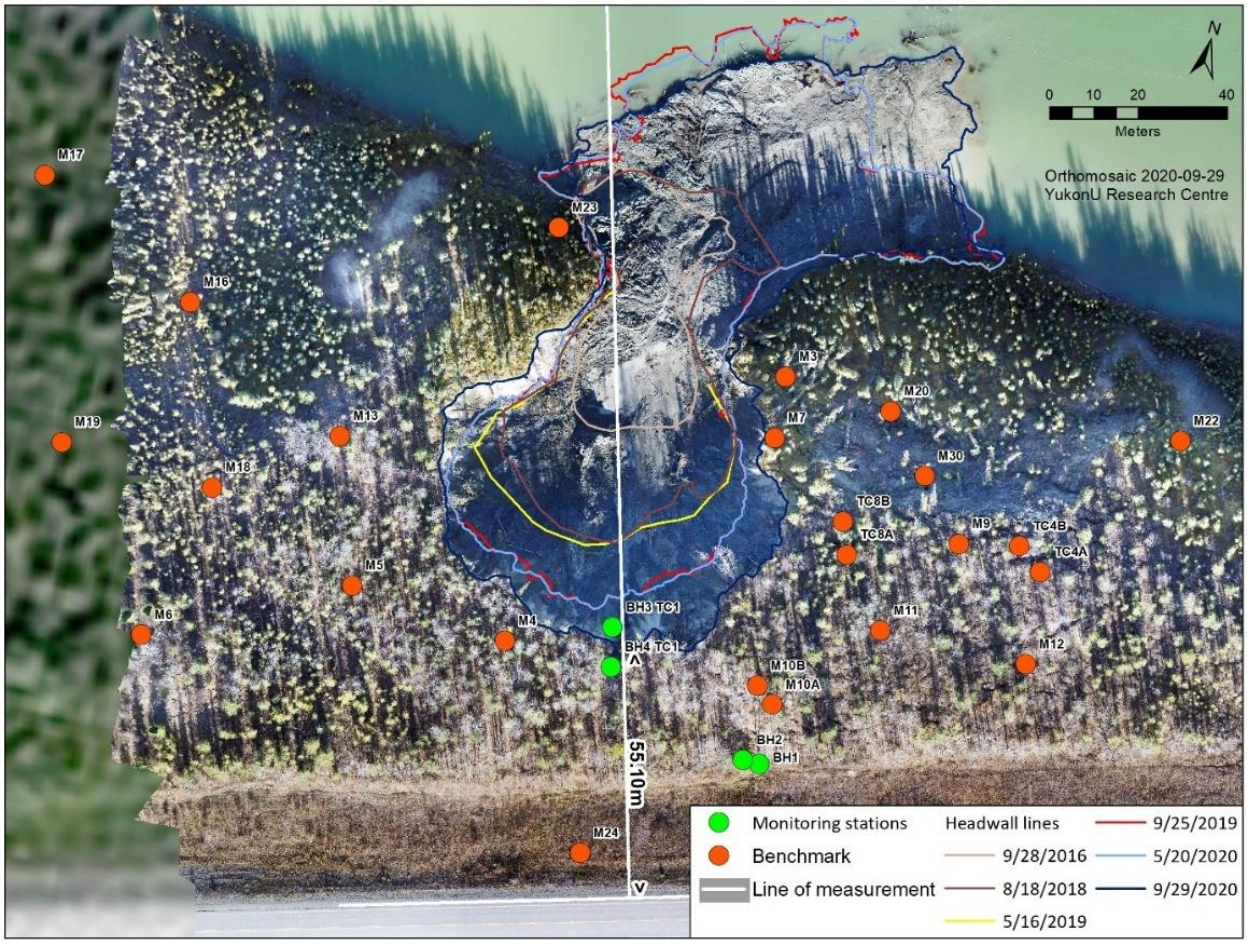

Figure 7.7 Benchmark survey monument locations and retrogressive thaw slump progression.

Thawed debris accumulates at the base of the headwall and is mobilized by periodic mudflows that have travelled toward or into Takhini River. On 2 September 2019, a large mudflow event deposited a low-angle tongue of debris more than halfway across the Takhini River, which is ~100 m wide at this location (Fig. 7.1). Tension cracks up to 1.4 m deep and 1.8 m wide are prevalent on adjacent slopes east and south of the slump (Fig. 7.1), indicating widespread slope instability that extends beyond the footprint of the slump. The tension cracks likely developed due to ongoing creep or solifluction processes active on the slope. Tree roots and split trunks extend across the tension cracks in several locations (Fig. 7.8). The crack widths of twelve split trees were measured at regular intervals throughout the summer and fall of 2019 and 2020, with cracks expanding at rates of up to 1–2 cm/month.

Figure 7.8 Tension cracks (a) splitting trees, with (b) person for scale.

To quantify and monitor long term slope deformation in the area, thirty-seven rebar survey benchmarks (monuments) were installed on adjacent and up-slope areas of the thaw slump (Fig. 7.1). In addition, air photo analysis and repeat drone surveys were used to provide snapshots of the slump extent. Survey monuments have been monitored by DGPS measurement since May 2019. A statistical analysis was to quantify movement and understand the level of error reported by DGPS measurements using R Studio software (R Core Team, 2020). To quantify error, orthogonal dispersion of points (*i.e.,* dispersion in x and y dimensions) is used to calculate the standard deviation (SD) of points in the x and y direction. Figure 7.9 illustrates the displacement of survey monuments from 24 May 2019 to 29 September 2020. The most displacement occurred on a deforming slope located immediately east of the existing thaw slump (see M30, M3, M22, M20, and M7 in Fig. 7.10). With continued slope deformation, it is possible this entire zone will develop into an additional thaw slump and eventually merge with the existing thaw slump.

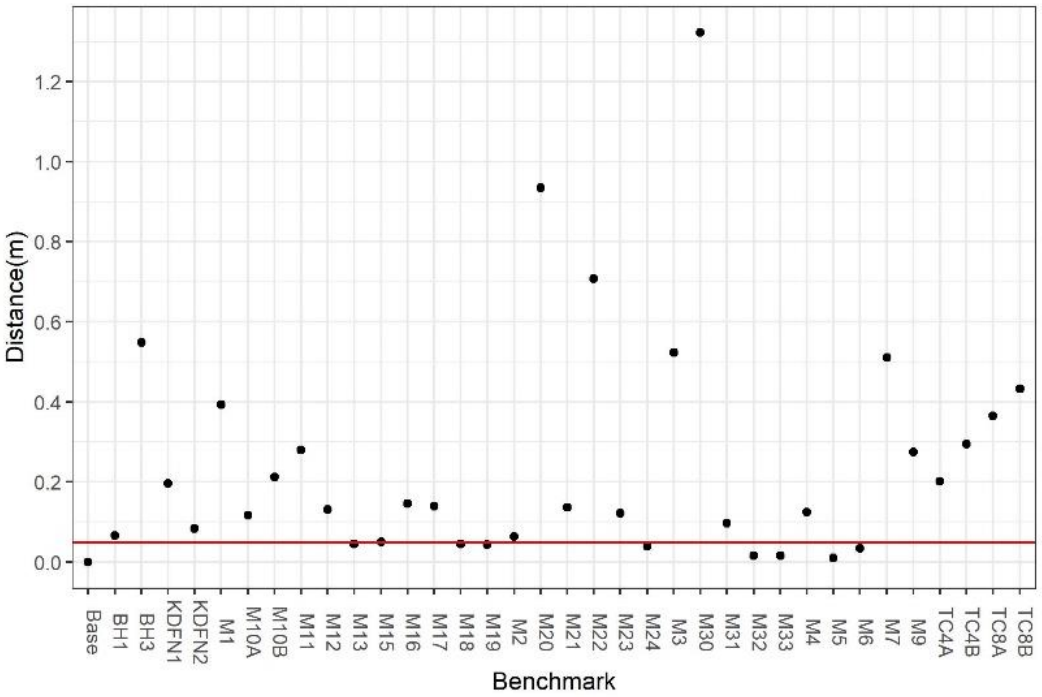

Figure 7.9 Benchmark movement for the period 24 May 2019 to 29 September 2020. The red line corresponds to the point movement versus SDy, i.e., *standard deviation of points in the y direction.*

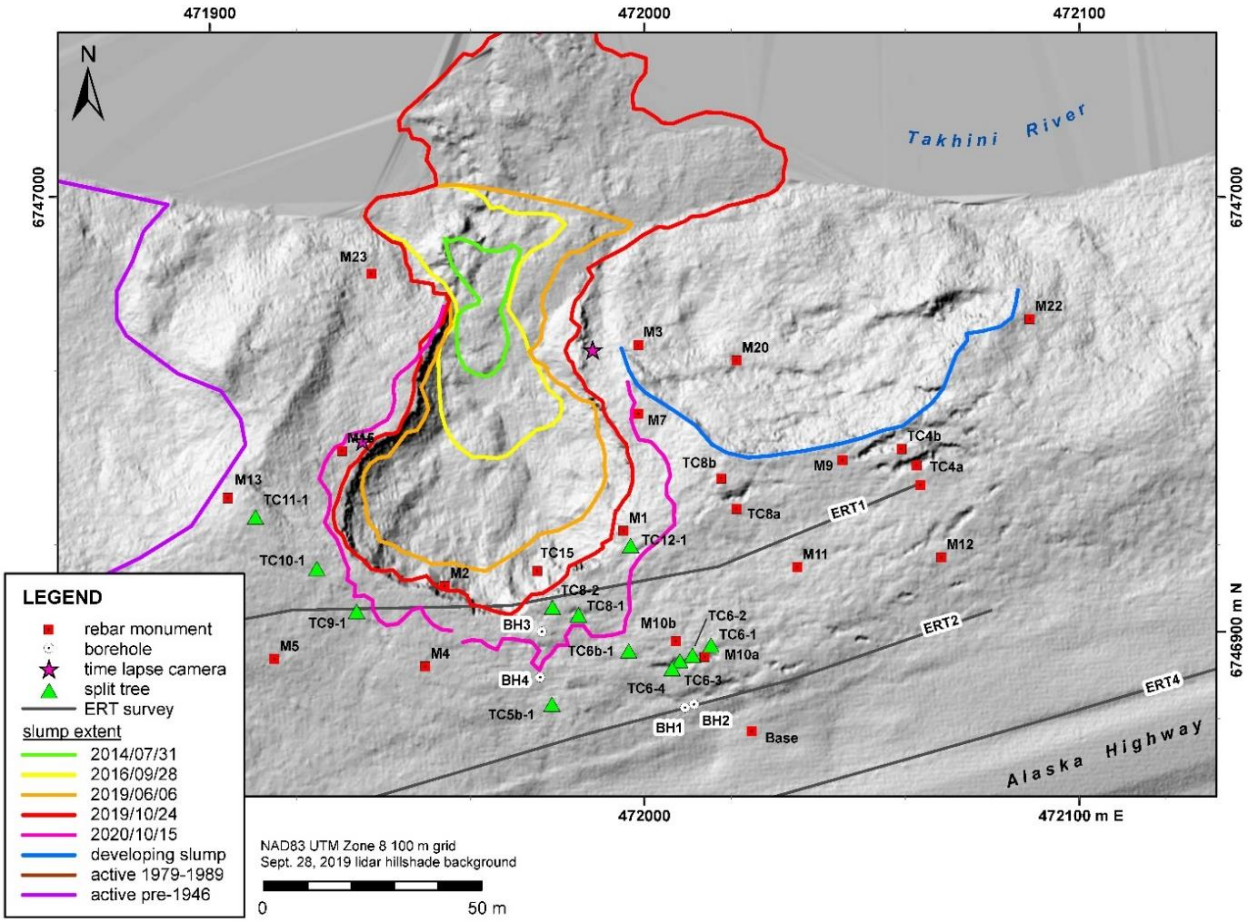

Figure 7.10 High resolution lidar hillshade image of area surrounding Takhini River thaw slump, showing development of new slump, marked by blue line. Monuments immediately above and below the developing slump show the most movement.

7.2.2 Borehole geotechnical data

Boreholes WH_1456_BH1 and WH_1456_BH2 were drilled on 16 and 24 October 2019, respectively, by Midnight Sun Drilling under the supervision of Louis-Philippe Roy and Panya Lipovsky (Table 7.2 and Figs. 7.1 and 7.11). These boreholes are located on crown land in a forested area ~30 m north of the Alaska Highway embankment. Borehole locations were selected based on ERT survey WH_1456_ERT2 which suggested ice-rich sediments at this location. The purpose of the boreholes was to provide a cryostratigraphic record and geotechnical properties of permafrost and soils in the area to better understand the hazard the retrogressive thaw slump poses to the Alaska Highway.

Table 7.2 Location details of field surveys at Alaska Highway km 1456 study site, including four boreholes, two of which were instrumented, and four ERT surveys.

Site	Date	Coordinates (NAD83 UTM Zone 8)	Depth (m)	Ground Temperature Sensor Depths (m)
WH_1456_BH1	16/10/2019	471985 6746876	10	
WH_1456_BH2	24/10/2019	472000 6746887	26	AT, 0.0, 0.5, 1.0, 1.5, 2.0, 3.0, 4.0, 5.0, 6.0, 7.0, 8.0, 9.0, 10.0, 15.0, 20.0
WH_1456_BH3	13/05/2020	471970 6746905	6	0.0, 0.5, 1.0, 2.0, 3.0, 4.0, 5.0, 6.0.
WH_1456_BH4	22/05/2020	471973 6746893	3	
WH_1456_ERT1	30/5/2019	Dipole-dipole and Wenner	Length (m): 200	Electrode Spacing (m): 2.5
0 m		472063 6746934		
50 m		472017 6746915		
100 m		471969 6746906		
150 m		471919 6746905		
200 m		471871 6746896		
WH_1456_ERT2	27/06/2019	Dipole-dipole and Wenner	Length (m): 200	Electrode Spacing (m): 2.5
0 m		472080 6746905		
50 m		472034 6746889		
100 m		471985 6746876		
150 m		471938 6746862		
200 m		471887 6746857		
WH_1456_ERT3	20/08/2019	Dipole-dipole	Length (m): 500	Electrode Spacing (m): 2.5
0 m		471908 6746785		
100 m		472003 6746814		
200 m		472098 6746843		
300 m		472194 6746871		
400 m		472290 6746898		
500 m		472385 6746927		
WH_1456_ERT4	11/9/2019	Dipole-dipole	Length (m): 500	Electrode Spacing (m): 2.5
0 m		471900 6746826		
100 m		471998 6746853		
200 m		472093 6746880		
300 m		472184 6746907		
400 m		472280 6746935		
500 m		472378 6746964		

Figure 7.11 (a) Midnight Sun Drilling CRREL drill rig and (b) permafrost cores at WH_1456_BH1.

WH_1456_BH1 was drilled to 10.00 m depth. The uppermost 3.35 m of unfrozen material was drilled with a 6-inch auger. Once the frost table was encountered, a CCREL drill was used to collect core of the frozen ground below. The hole was abandoned at 10.00 m depth, because unfrozen saturated sandy material above the frost table started to collapse and threatened to trap the CRREL core barrel in the borehole. Borehole log WH_1456_BH1 (see Figure A5 and Table 7.3) shows a stratigraphy composed predominantly of clayey silt. The borehole ends at 10.00 m in silty sediment (99.9% silt). Lenticular, microlenticular, reticulate and suspended cryostructures (Fig. 7.12) were identified throughout the profile and the volumetric excess ice content ranged from 13 to 41% (Table 7.3). Based on field drilling observations, the active layer extended from 0.00 to 3.35 m, and excess ice was noted at the time of drilling from 3.35 to 7.9 m depth. Overall, the borehole had a mean volumetric excess ice content of 32.5%, which represents a potential subsidence of 1.96 m if permafrost were to thaw to 9.4 m depth (the lowest depth that excess ice content was measured).

Table 7.3 Grain-size distributions and excess ice content results at various depths from borehole WH_1456_BH1 at Takhini River RTS case study site.

Depth (m)	Volumetric Excess Ice (%)	Cobble (%)	Gravel (%)	Sand (%)	Silt (%)	Clay (%)
0.0	0.0	0.0	0.0	4.1	72.5	23.4
1.52	0.0	0.0	0.1	91.8	7.5	0.6
3.04	0.0	0.0	0.0	5.5	79.8	14.7
3.35	14.1	0.1	0.0	2.7	78.7	18.6
4.57	30.7	0.0	0.0	2.9	83.6	13.5
4.80	34.6	0.0	0.0	8.0	81.7	10.3
5.63	35.8	0.0	0.0	0.2	90.3	9.5
5.96	36.2	0.0	0.0	0.6	76.7	22.7
6.57	39.2	0.0	0.0	0.4	85.7	13.9
7.03	36.4	0.0	0.0	0.1	64.3	35.6
7.45	34.6	0.0	0.0	0.2	92.2	7.7
7.85	13.4	0.0	0.0	1.2	87.1	11.8
8.22	39.5	0.0	0.0	0.0	67.7	32.3
8.50	36.6	0.0	0.0	1.7	87.4	10.9
8.78	41.6	0.0	0.0	0.1	68.1	31.8
9.15	26.3	0.0	0.0	0.1	70.1	29.8
9.40	33.9	0.0	0.0	0.2	99.9	0.0

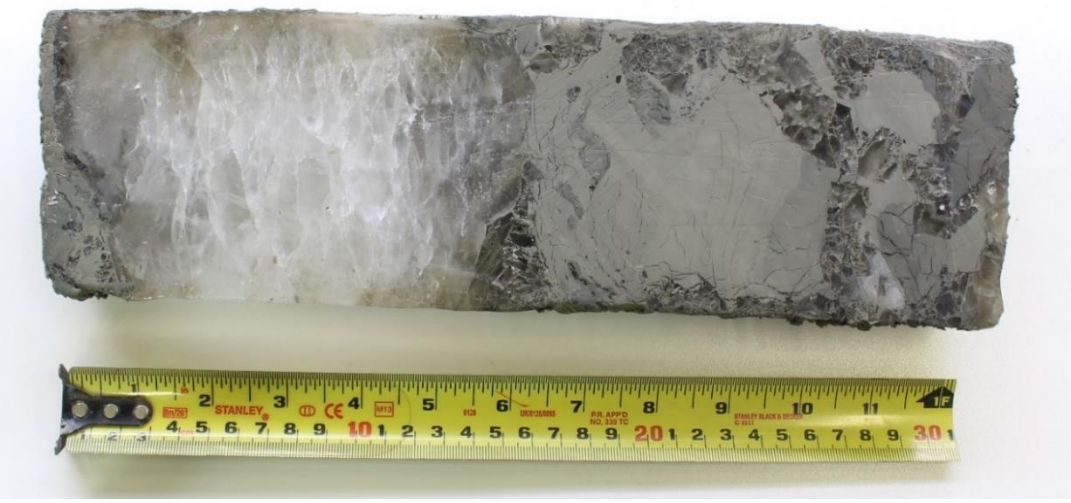

Figure 7.12 Ice-rich permafrost showing thick layered (left) and suspended (right) cryostructures in a core from WH_1456_BH1 at 6.57 m depth.

Borehole WH_1456_BH2 was drilled 2 m east of WH_1456_BH1 using a destructive ODEX hollow stem drill with a 4-inch casing, reaching a depth of 26 m. Once drilling was completed, the boreholes were cased with two 1-inch PVC pipes and backfilled to the surface using filter sand. A 16-channel thermistor string connected to a LOGR logger was installed. A 24 m-long Measurand SAAV-001 ShapeArray inclinometer was also installed in one of the PVC pipes. This instrument will enable monitoring of soil deformation induced by the retrogressive thaw slump in the next few years. More detailed information on this case study, including inclinometer results are presented in the recently published report “Assessment and monitoring of a new retrogressive thaw slump at km 1456 of the Alaska Highway: a rare opportunity” by Calmels *et al.* (2020).

Two shallow boreholes, WH_1456_BH3 and WH_1456_BH4, were drilled on 13 and 22 May 2020, respectively, by Louis-Philippe Roy, Fabrice Calmels and Cyrielle Laurent following the methodology outlined in Appendix E. Borehole WH_1456_BH3 was located 10 m upslope (south) of the thaw slump headwall at ~100 m distance along the WH_1456_ERT1 survey. It was drilled to 6.0 m depth using a GÖLZ MT portable core-drill system. The borehole was initiated by removing the unfrozen active layer using a shovel down to the thaw front at 0.3 m.

The borehole log for WH_1456_BH3 (see Figure A6) shows layers of ice-rich gray clayey silt alternating with some very ice-rich layers. While starting the drilling in frozen ground, an unfrozen area with groundwater was encountered at roughly 2 m depth before the drilling resumed in frozen ground. The borehole ended at 6 m in clayey-silt sediment. Lenticular and microlenticular cryostructures were identified along the profile (Fig. 7.13). Once drilling was completed, the borehole was cased with two 1-inch PVC pipe, and backfilled to the surface. Eight thermistors were inserted as described in Section 7.2.2. A 6 m-long Measurand SAAV-001 ShapeArray inclinometer was also installed in one of the PVC pipes (for results see Calmels *et al*., 2020). On 12 August 2020, the retrogressive thaw slump retreated to the location of the borehole, causing it to collapse into the thaw slump bowl (Fig. 7.14).

Figure 7.13 Ice-rich permafrost core from WH_1456_BH3, showing glaciolacustrine sediment suspended within ground ice.

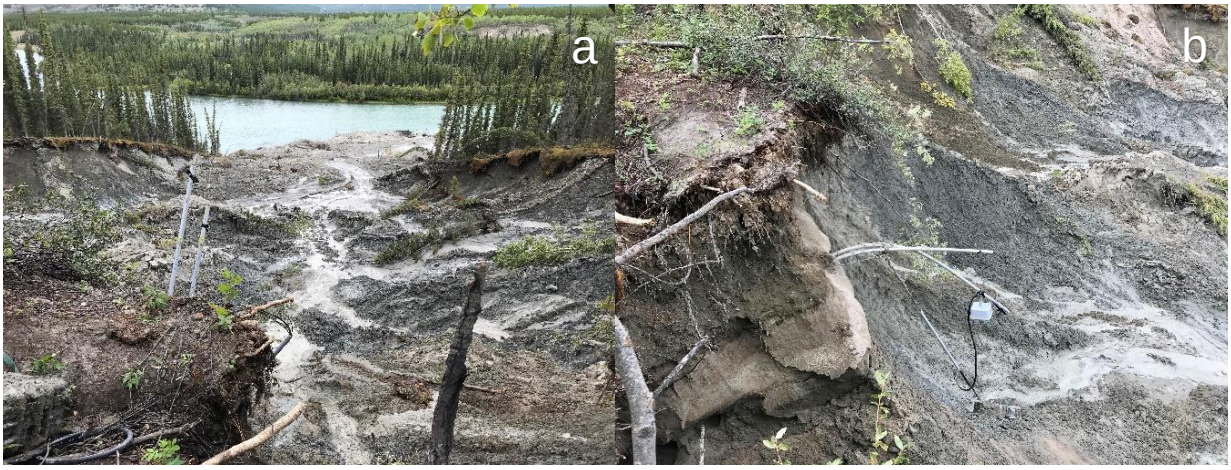

Figure 7.14 WH_1456_BH3 borehole casing and instrumentation (a) prior to, and (b) following collapse into the slump on 13 August 2020.

WH_1456_BH4 was drilled 13 m south of WH_1456_BH3 and 23 m upslope (south) of the thaw slump headwall. The borehole was initiated by removing the unfrozen active layer using a shovel down to the thaw front at 0.50 m. The borehole was drilled using a GÖLZ MT portable core-drill system down to 2.97 m where a point a refusal was reached. The dry sediment made it extremely difficult for the core barrel to cut through the material. The ground profile showed a thin discontinuous layer of organics at the surface (0–0.05 m depth) overlying layers of sand (0.05–0.20 m depth) and wet silt (0.20–0.50 m depth). Gray clayey silt was identified down to 1.71 m depth. From 1.71 to 2.69 m depth, the stratigraphy became coarser, and layers of fine sand were observed. The borehole ended at 2.97 m in clayey-silt sediment. No visible ice was identified along the profile. Once drilling was completed, the borehole was cased with a 1-inch PVC pipe, and backfilled to the surface. No thermistors were installed.

The grain size distribution of sediments determines the porosity and hydraulic conductivity of the ground. Coarse material (medium sand and coarser) has a high hydraulic conductivity and readily drains water as ice melts, whereas fine-grained material drains poorly once it thaws due to its low hydraulic conductivity. Fine-grained sediments commonly contain excess ice and may form ice lenses or layers by ice segregation; whereby ice lenses develop from the migration of pore water to the freezing front (the warmest isotherm where pore ice exists). On flat terrain, ground with excess ice will undergo severe thaw settlement if it thaws; likewise, on slopes, silt and clay deposits may experience highly mobile mass movement when the pore water pressure increases from ice melting. For slope deposits, the plastic and liquid limits of the material are used to evaluate the potential of ground failure.

Ground ice is segregated with the dominant cryostructures being suspended and thick layered ice. These types of cryostructures form in ground where the freezing front progress slowly (under a low thermal gradient, with a sufficient groundwater supply). Typically, the thickness of the ice layers increases with depth. This is because the freezing front slows down (*i.e.,* its progression downward does not occur as quickly), so there is more time for pore water to migrate to the freezing front. This type of cryostratigraphical record is typical of epigenetic discontinuous permafrost, which forms after the deposition of the soil material in which it occurs.

7.2.3 Ground temperatures

Borehole WH_1456_BH2 was lined with PVC pipe and instrumented with one 16-channel LogR Systems logger to record ground temperatures at various depths. The PVC casing was filled with silicone oil. The recording started 28 February 2020 at 24:00, and data was last downloaded on 28 February 2021, providing one year of ground temperatures data (Fig 7.15 and Table 7.4). Ground temperature data suggests permafrost does not remain in the borehole below 8 m depth.

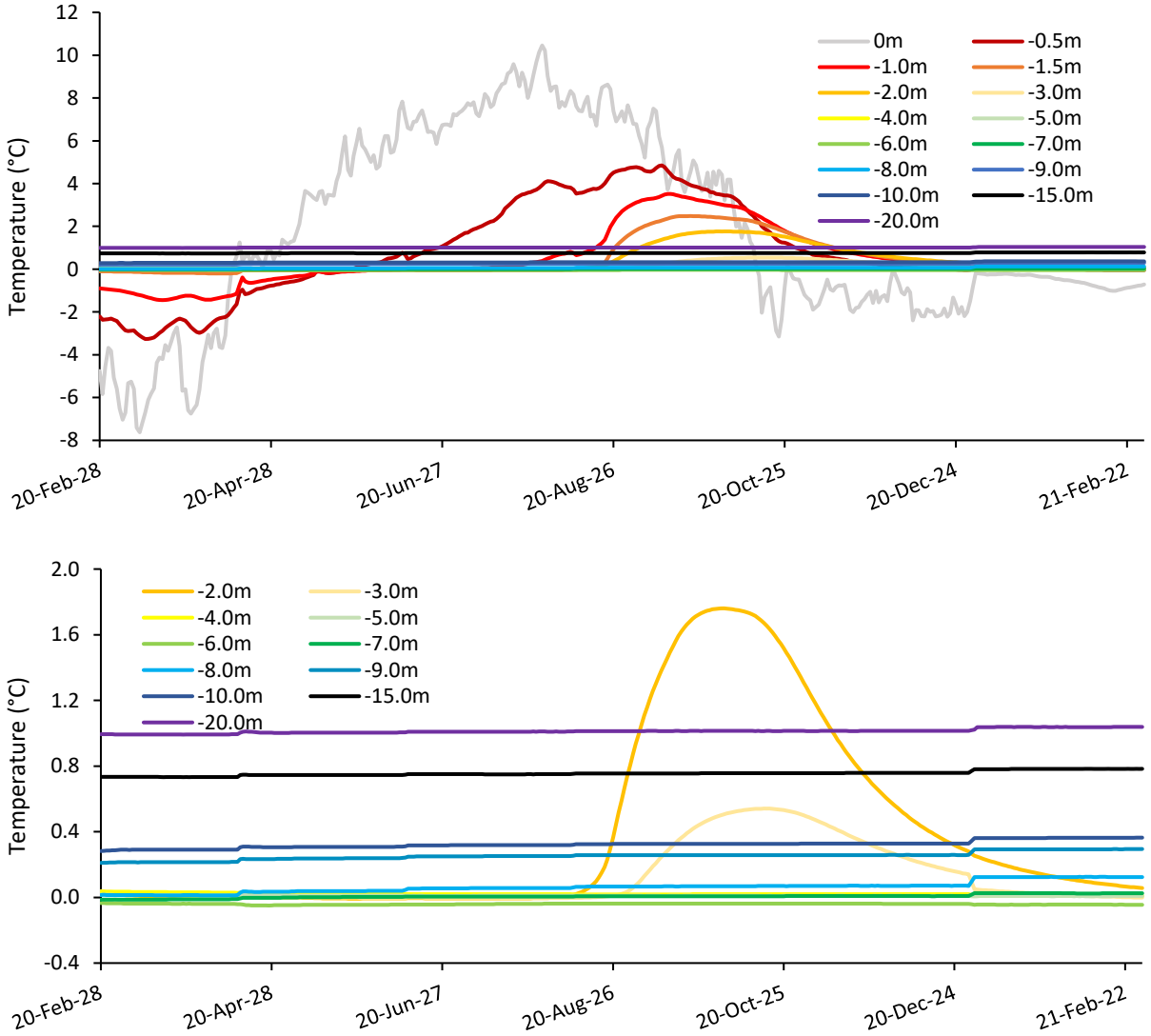

Figure 7.15 Takhini River Thaw Slump daily mean ground temperatures at WH_1456_BH2 for the period 28 February 2020 to 28 February 2021 from a) 0 to 20 m depth, and b) 2 to 20 m depth.

Table 7.4 Annual minimum, maximum and mean ground temperature (from daily mean values) at WH_1456_BH2 for the period 1 March 2020 to 28 February 2021.

Depth (m)	0	0.5	1.0	1.5	2.0	3.0	4.0	5.0	6.0	7.0	8.0	9.0	10.0	15.0	20.0
Annual min GT(°C)	−7.62	−3.26	−1.45	−0.20	−0.01	0.00	0.01	0.01	−0.05	−0.01	0.01	0.21	0.28	0.73	0.99
Annual max GT(°C)	10.45	4.85	3.52	2.48	1.76	0.54	0.04	0.02	−0.04	0.03	0.13	0.29	0.36	0.78	1.04
Annual mean GT(°C)	1.80	0.80	0.50	0.47	0.40	0.12	0.02	0.01	−0.04	0.01	0.06	0.25	0.32	0.76	1.01

Geotechnical drilling observations from WH_1456_BH1 allow the depth to the permafrost table to be estimated at 3.4 m, while the base of permafrost was estimated at 7.9 m depth, making it ~4.5 m thick. However, the ground temperature data from WH_1456_BH2, located 2 m to the east, suggests that permafrost is thinner and does not extend past 6 m depth (Fig 7.16). A potential explanation for this discrepancy is that in warm (very close to 0°C) and ice-poor frozen material, the drilling process may upset the thermal and hydrogeological regimes, thawing local permafrost around the borehole. Temperatures may recover to pre-drilling conditions over time, or may remain permanently disturbed. It should also be noted that groundwater was intercepted during the drilling process, which may have caused further permafrost thaw around the borehole from thermal erosion. The significant ice content in the surrounding ground will, however, help to dampen the rate of further thaw because of latent heat effects (whereby a large amount of additional heat is required to melt the remaining ice before ground warming can occur).

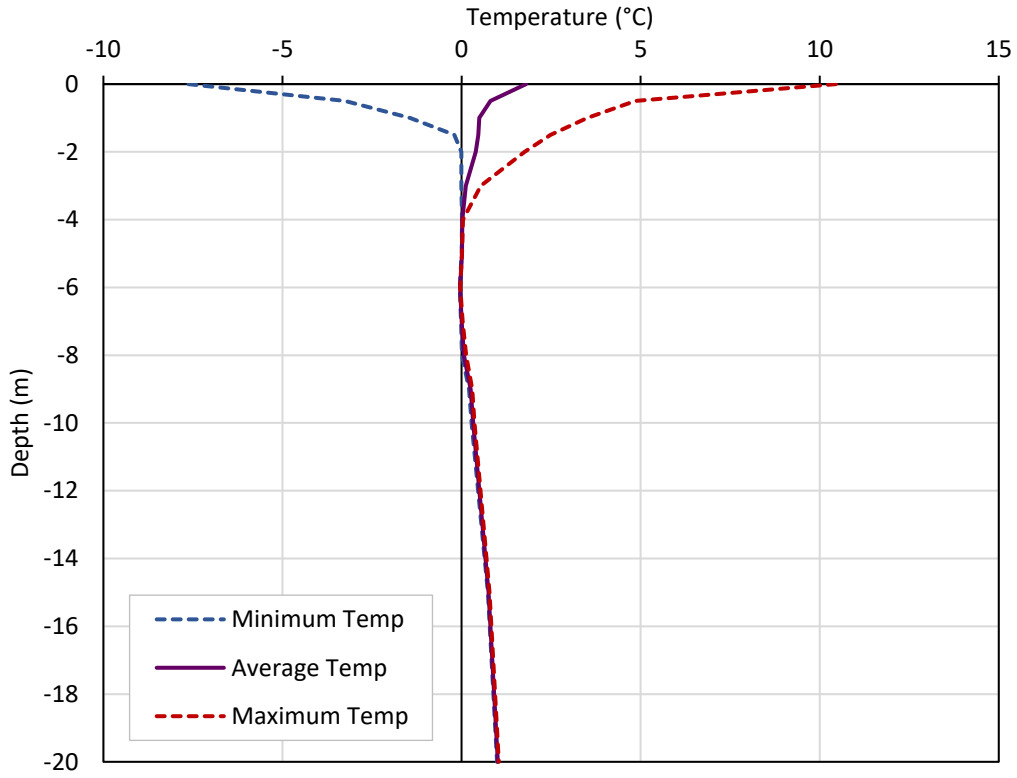

Figure 7.16 Takhini River Thaw Slump ground temperature envelope at WH_1456_BH2 for the period 1 March 2020 to 28 February 2021.

Borehole WH_1456_BH3 was cased with PVC pipe and instrumented with two 4-channel Hobo UX120 loggers to record ground temperatures at various depths (Table 7.2). The pipe was filled with silicone oil. The recording started 1 June 2020 at 18:00 and ended on 12 August 2020 at 08:00. Ground temperatures remained below 0°C from 1 to 6 m depth until early July. Ground temperature at 1 and 2 m depth slowly rose above 0°C as the thaw slump headwall approached closer to the borehole, until the entire installation collapsed into the slump on 12 August 2020 (Fig. 7.17), at which point the instrumentation was recovered from the borehole.

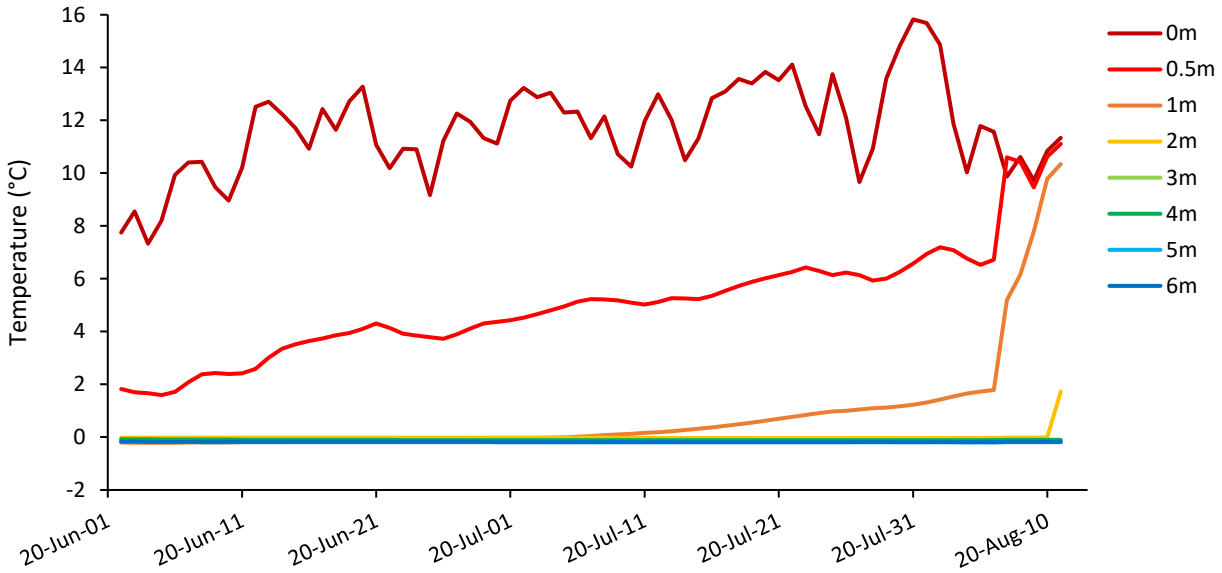

Figure 7.17 Takhini River Thaw Slump daily mean ground temperatures at WH_1456_BH3 for the period 1 June to 12 August 2020.

7.2.4 ERT

Four ERT surveys were conducted at this site (Table 7.2). Two 200-m-long ERT surveys, WH_1456_ERT1 and WH_1456_ERT2, were conducted close to the thaw slump on 30 May and 27 June 2019, respectively (Table 7.2 and Fig. 7.18). Two subsequent 500-m-long ERT surveys, WH_1456_ERT3 and WH_1456_ERT4, were conducted on 20 August and 11 September 2019. The latter two surveys were carried out on either side of the Alaska Highway embankment to assess the ground ice distribution at this monitoring site (Fig. 7.18). The results below present 2D ERT profiles. However, 3D ERT survey results for this case study are presented in the report “Assessment and monitoring of a new retrogressive thaw slump at km 1456 of the Alaska Highway: a rare opportunity” by Calmels *et al.* (2020).

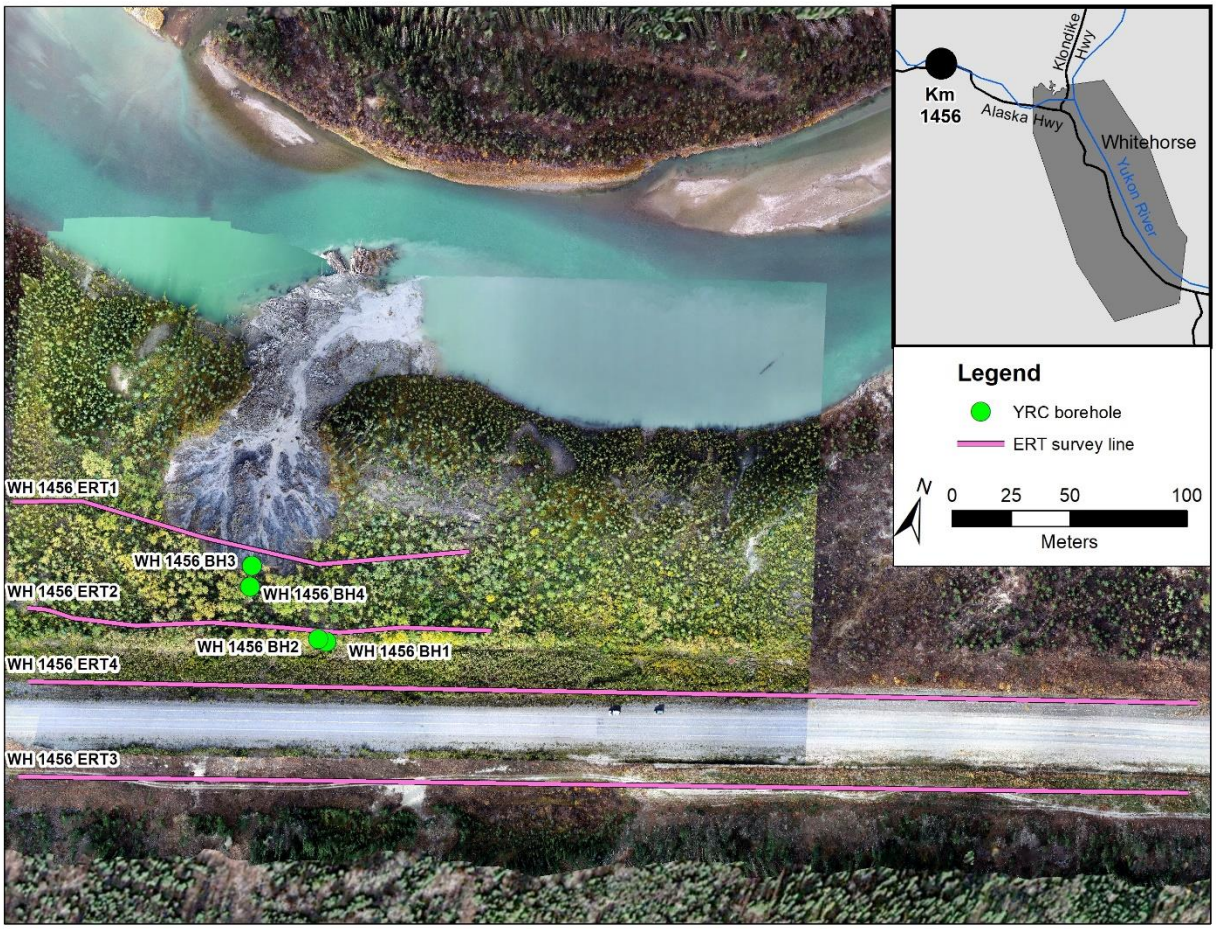

Figure 7.18 Takhini River RTS ERT survey and borehole locations.

For the WH_1456_ERT1 and WH_1456_ERT2 surveys, both the Wenner and dipole-dipole array were measured. For WH_1456_ERT3 and WH_1456_ERT4 only the dipole-dipole array was measured. The results obtained with the Wenner and dipole-dipole arrays show a similar distribution of resistivity in the ground, however the dipole-dipole array shows more detail for the low resistivity areas (see Figures C7 and C8 for Wenner results).

Overall, the very high-resistivity areas, shown as darker blue shades, were interpreted as ice-rich fine-grained sediment (clayey-silts). The presence of this fine-grained ice-rich sediment is greatest close to the slump headwall and becomes increasingly discontinuous towards the highway. The low resistivity values, mainly orange and red shades, suggest ice-poor and/or unfrozen material, and the lowest values, shown as red shades, may indicate the presence of ground water.

WH_1456_ERT1

The WH_1456_ERT1 survey was completed on 30 May 2019. It ran from east to west, through a dense mixed forest, 12 m south of the headwall at the time (Fig. 7.18). The ERT data, shown in Figure 7.19, suggests permafrost could be as deep as 30 m towards the eastern part of the survey. The highest resistivity pocket represented in dark blue shades is located from 25 to 50 m along the survey at a depth of about 5 m. Tension cracks were observed at the ground surface. The permafrost table appears to be shallowest towards the eastern end of the profile, where the resistivity values remain relatively high (2500 ohm·m). A lower resistivity body shown in orange, is observed at 40 m horizontal distance and could be the result of a ghosting effect from the high resistivity material above or it may be associated with water movement. Another lower resistivity zone from 180 m horizontal distance and 8–12 m depth could be the result of groundwater flow adjacent to permafrost bodies. This is expected given the discontinuous distribution of permafrost in the Takhini Valley.

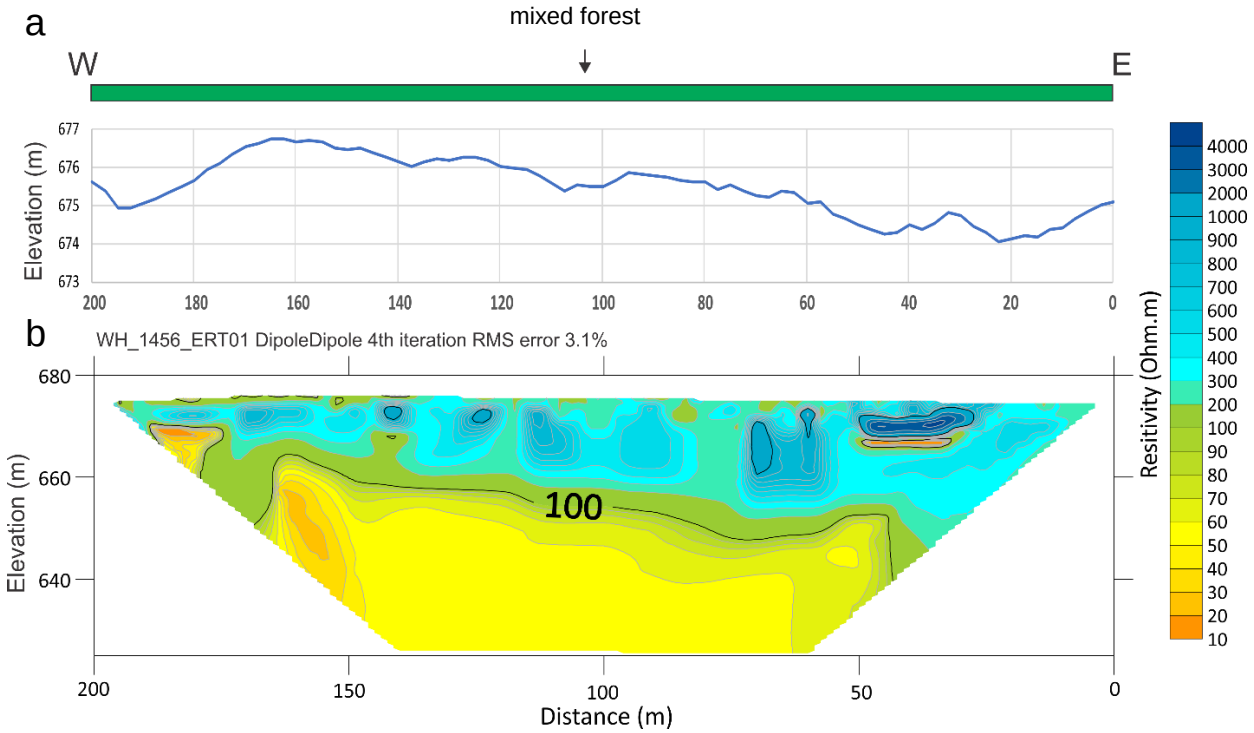

Figure 7.19 Takhini River Retrogressive Thaw Slump E–W ERT survey (WH_1456_ERT1) showing the (a) elevation profile, and (b) ERT profile using dipole-dipole array, 4th iteration, RMS error=3.1%. Note that WH_1456_BH3 is nearby the profile at 98 m distance. Resistivities above the 100 ohm·m isoline in (b) suggest a higher likelihood of permafrost (blue to dark green shades), while yellow to orange shades have a low likelihood.

WH_1456_ERT2

WH_1456_ERT2 was conducted on 27 June 2019. This survey ran east to west in a mixed forest, about 25 m north of the toe of the Alaska Highway embankment (Fig. 7.18), just outside the cleared portion of the Alaska Highway right of way, and 30 m away from the headwall at the time. The survey intercepted the borehole location of WH_1456_BH2 at 75 m horizontal distance (electrode 31) and WH_1456_BH1 at 77.5 m (electrode 32). Vegetation along the profile was predominantly trembling aspen, and white spruce forest. The understory, composed mainly of aspen saplings, willow and soapberry, was dense in the first and last quarter of the profile, but was more open from 60 to 80 m. The survey intercepted meter deep tension cracks at 5 and 135 m along the profile (Fig. 7.20a).

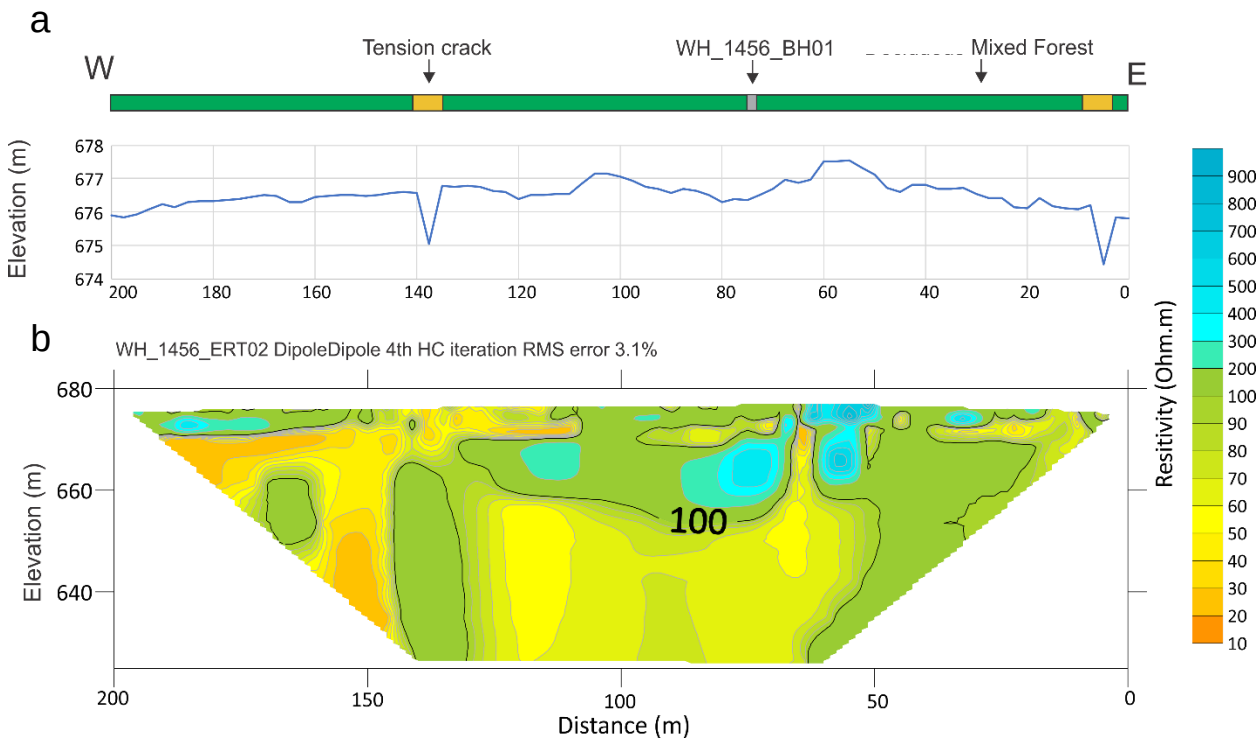

Figure 7.20 Takhini River Retrogressive Thaw Slump E–W ERT Survey (WH_1456_ERT2), showing the (a) elevation profile, and (b) ERT profile using dipole-dipole array, 4th iteration, RMS error= 3.1%. Resistivities above the 100 ohm·m isoline in (b) suggest a higher likelihood of permafrost (blue to dark green shades), while yellow to orange shades have a low likelihood.

In Figure 7.20b the darkest blue highest resistivity pockets concentrated between 50 and 80 m, likely indicate ice-rich permafrost, which is similar to the distribution observed in WH_1456_ERT1. Permafrost distribution seems more discontinuous than along ERT1 profile and does not likely extend deeper than 20 m at its deepest point (77.5 m along the profile). Some small high resistivity pockets shown in light blue can be observed at 30, 115 and 180 m. The low resistivity area in orange shades at 35 m and from 115 to 200 m may indicate ice-poor and/or unfrozen material, or the presence of liquid ground water circulating around permafrost. It is not impossible to have permafrost in areas with resistivity as low as 100 ohm·m. Near 0°C temperature in fine-grained material results in higher liquid water content and low resistivity values.

WH_1456_ERT3

WH_1456_ERT3 was completed on 20 August 2019. The 500 m-long survey ran west-east along the south side of the Alaska Highway embankment, going down a slight hill slope (Fig. 7.18). The vegetation along the profile was open and predominantly small trembling aspen, willows and some spruce saplings. ERT data, presented in Figure 7.21b, suggests permafrost is present in localized high resistivity areas, shown as dark blue shades, from 20 to 200 m distance along the profile and up to 7 m deep and again from 420 to 500 m up to 20 m deep. Permafrost is unlikely from 200 to 280 m, and within deep low resistivity pockets (orange shades) extending vertically at 265 and 365 m. These pockets are likely associated with groundwater flow (see Figure C7 for larger profile)

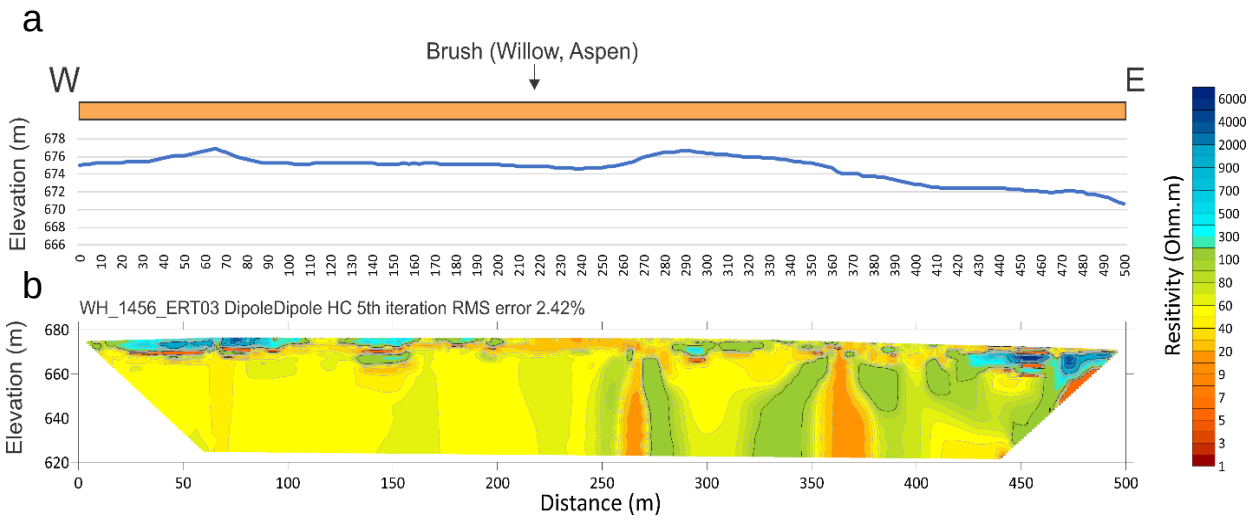

Figure 7.21 Takhini River Retrogressive Thaw Slump W–E ERT Survey (WH_1456_ERT3), showing the (a) elevation profile, and (b) ERT profile using dipole-dipole array, 5th iteration, RMS error= 2.4%. In (b) blue shades are interpreted as permafrost, while orange shades are likely unfrozen.

WH_1456_ERT4

WH_1456_ERT4 was completed on 11 September 2019. The 500 m survey ran west to east along the north side of the Alaska Highway embankment, going down a slight hill slope (Fig. 7.18). The vegetation cover was very similar to WH_1456_ERT, which included trembling aspen saplings, willows and some spruce saplings. The ERT data, presented in Figure 7.22b, suggests the presence of permafrost within high resistivity areas (shaded blue) along most of the profile down to 7 m depth. Permafrost is unlikely at the west end of the profile from 0 to 70 m. The largest high resistivity pocket extends from 450 to 500 m at the east end of the profile where ice-rich permafrost is likely present from 17 to 35 m depth. Some shallow low resistivity pockets along the length of the profile between 5 and 10 m depth could be associated with groundwater flow around permafrost (see Figure C8 for larger profile).

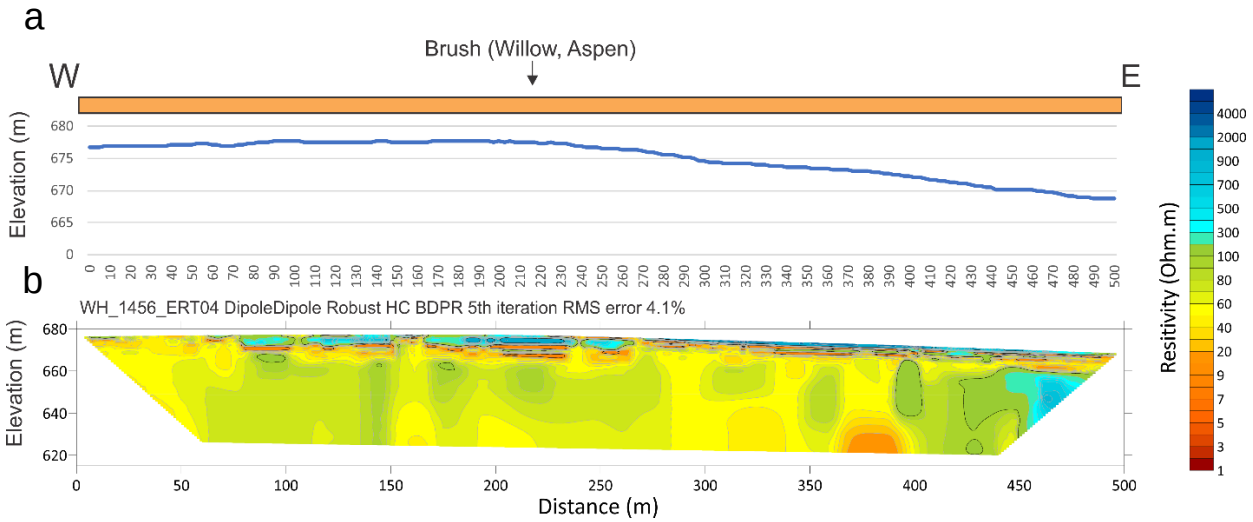

Figure 7.22 Takhini River Retrogressive Thaw Slump W–E ERT Survey (WH_1456_ERT4), showing the (a) elevation profile, and (b) ERT profile using dipole-dipole array, 5th iteration, RMS error= 4.1%. In (b) blue shades are interpreted as permafrost, while orange shades are likely unfrozen.

7.2.5 Synthesis

Geotechnical drilling indicated that permafrost is 4.5 m thick and extends from 3.4 to 7.9 m depth at BH1. Borehole drilling at BH2 confirmed the presence of frost susceptible clayey silt down to at least 26 m depth. The ground temperature data from BH2 show that permafrost is warm (>−0.1°C) and only extends to ~6 m depth in the borehole. ERT data, however, suggest that permafrost is much thicker (up to 20 m depth at the east end of the ERT2 profile). The discrepancy in permafrost thickness estimates by ground temperature and ERT results may be a result of the drilling process causing localized permafrost thaw immediately adjacent to the borehole. The geophysical and geotechnical data showed thick (up to 30 m) ice-rich permafrost at the headwall of the thaw slump and thinner (up to 7 m) and more sporadic bodies of ice-rich permafrost closer to the road. While the ERT data suggest that permafrost may still be present at several locations on both sides of the highway, it may be thinner and more sporadic due to decades of permafrost degradation beneath the Alaska Highway embankment and cleared right of way since its construction in 1942. The 1958 wildfire and recent agricultural development have also likely altered the local surface energy balance, groundwater flow, and evapotranspiration rates in the area, potentially contributing further to permafrost degradation.

The cryostratigraphical observations from the core samples and the headwall are typical of epigenetic permafrost; *i.e.,* permafrost that formed after the deposition of the soil material in which it occurs. The formation of this type of ground ice, with suspended and thick layered cryostructures in fine-grained material, requires ample water supply, a slow thermal gradient, and usually an organic cover. Such conditions may have existed in glaciolacustrine sediments occupying the floor of Takhini Valley after drainage of Glacial Lake Champagne. This type of permafrost is generally associated with permafrost plateaus and frost heave mound environments (Calmels *et al.,* 2007). Although the vegetation and the topography have changed on site since permafrost first developed, the original cryostratigraphy remains intact. The lack of thick organic cover and the abundance of deciduous trees on site (a result of forest regeneration following the 1958 wildfire) is atypical in comparison to other sites where similar ice-rich epigenetic permafrost is found in the discontinuous permafrost zone. The shading provided by the forest may have helped preserve relict permafrost at this site.

8 OLD ALASKA HIGHWAY

8.1 Site setting

The Old Alaska Highway case study site is located at km 1446.5 of the Alaska Highway, approximately halfway between the two endpoints of the Old Alaska Highway (Fig. 8.1), and 24 km west of Whitehorse airport by road. The case study site is situated at an elevation of ~740 m asl, southwest of a large dip in the road. The highway embankment is up to 10 m thick where it crosses a small creek.

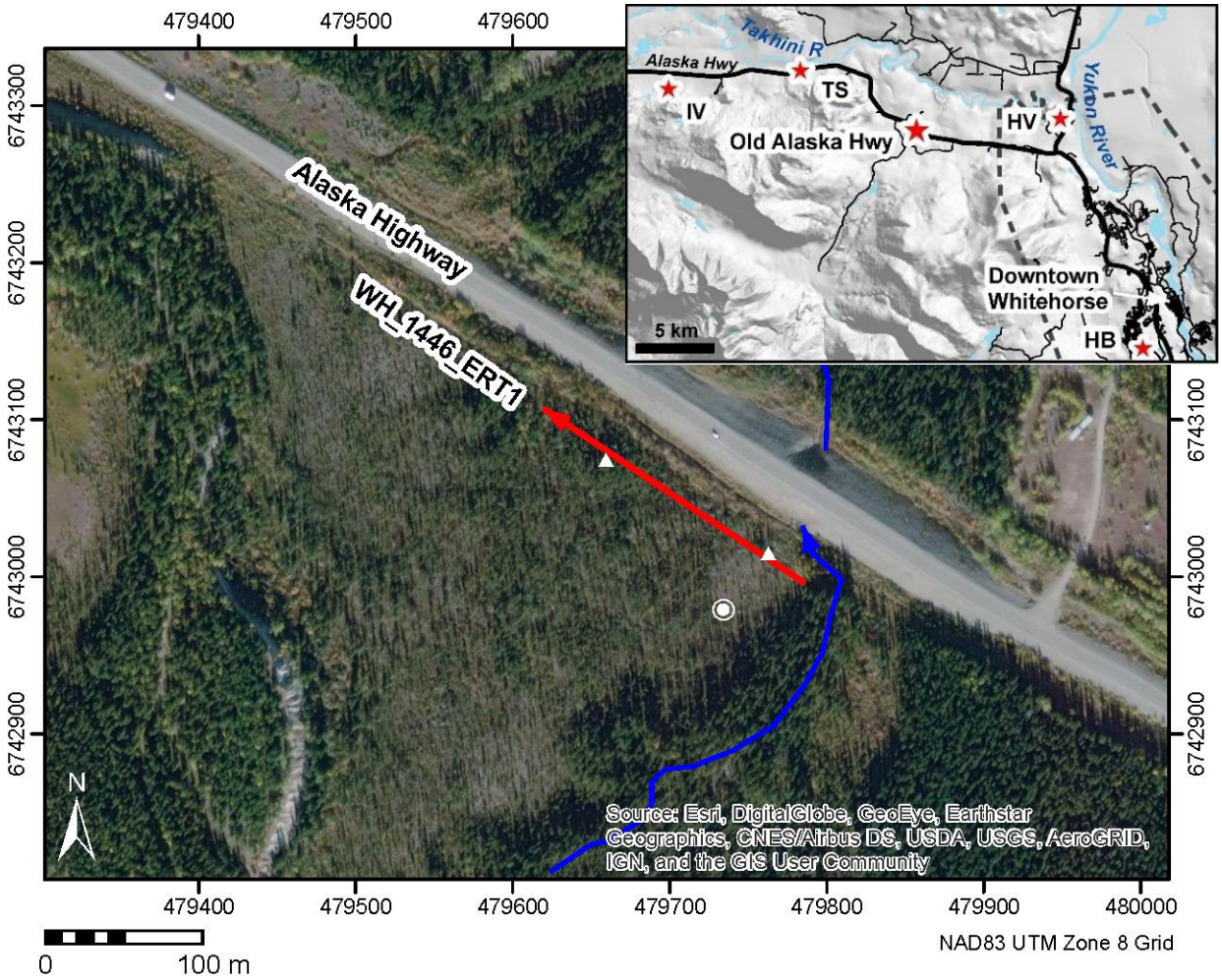

Figure 8.1 Location of the Old Alaska Highway (km 1446) case study site with ERT survey location (red line). Blue line shows location of small creek which flows northward under the highway, white triangles represent permafrost mounds (lithalsas), and the white circle indicates the location of borehole drilled by Quantum Machine works in late April 2019. WorldView2 (20 September 2018) background satellite image. Inset map shows location with respect to Whitehorse city limits (dashed line) and nearby case study sites (IV = Ibex Valley, TS = thaw slump; HV = Hidden Valley, HB = Hamilton Boulevard).

8.1.1 Climate and vegetation

The climate of the Old Alaska Highway case study site is assumed to be similar to that described for the Takhini River thaw slump, located 10 km to the west (see Section 7.1.1). The open mature forest consists mainly of white spruce (*Picea glauca*), which are “drunken” or tilted in many places. Willow (*Salix spp*.), labrador tea, and soapberry (*Shepherdia canadensis)* shrubs commonly occur. Common plant species include forbs such as fireweed (*Chamaenerion angustifolium)* and alpine sweetvetch (*Hedysarum alpinum)*, mosses, and lichens such as *Cladonia spp*. A 15 cm mat of feather moss and lichen was observed in two soil pits located near the eastern end of the ERT transect (Fig. 8.1).

8.1.2 Surficial geology

The case study site (Fig. 8.2, circled in white) is located on a gentle (5–10°) northeast-facing slope mantled by a veneer of organic cover overlying a dense stony basal till. The till is well exposed in a glacial meltwater-carved escarpment at the top of the slope, about 250 m southwest of the ERT transect. The slope is ~350 m long by 400 m wide and extends from ~720 to 750 m elevation (Fig. 8.3) and drains into the headwaters of a large gully system incised into the nearby glaciolacustrine plain to the north.

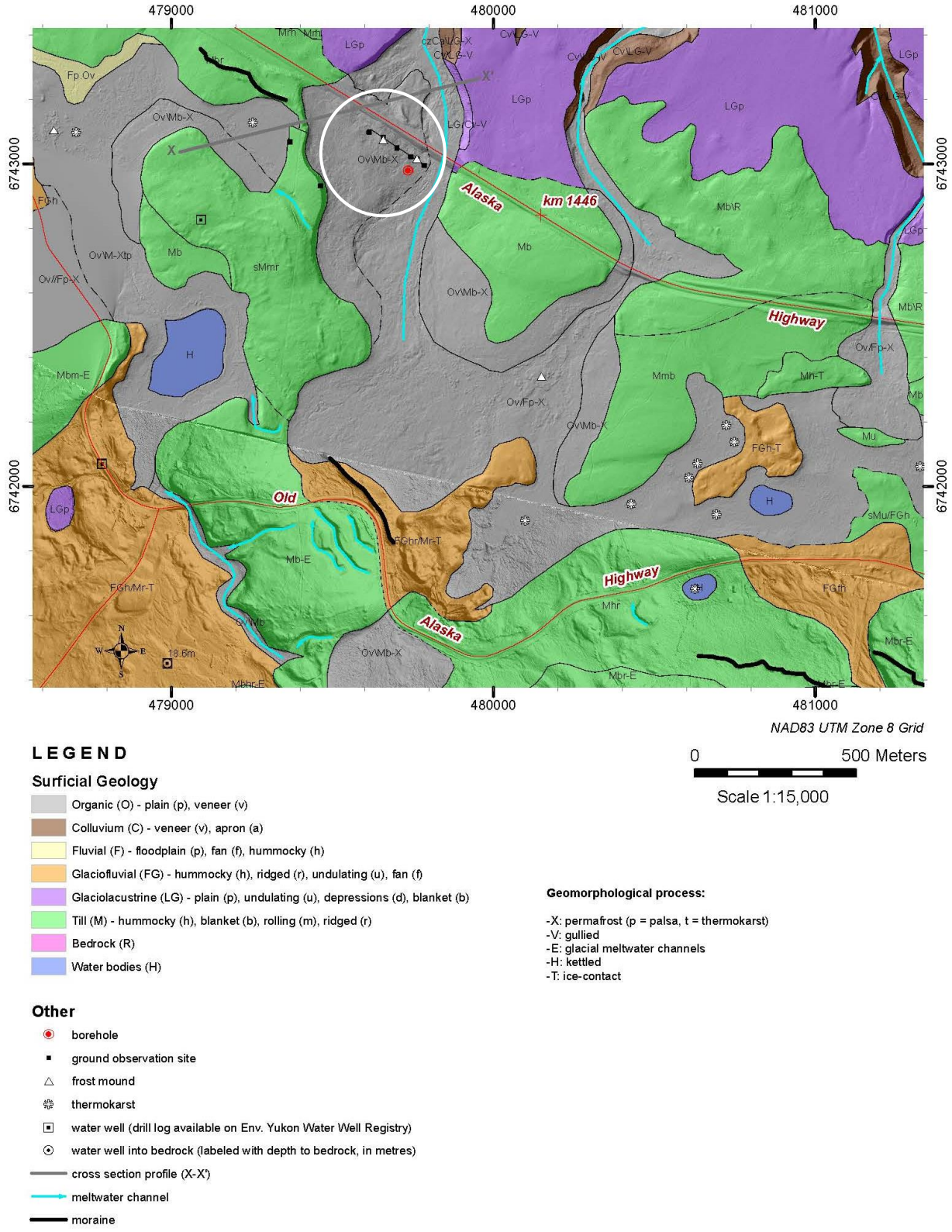

Figure 8.2 Simplified surficial geology map showing major landscape units, landforms and boreholes drilled in the vicinity of the Old Alaska Highway case study site, km 1446. White circle highlights study area location.

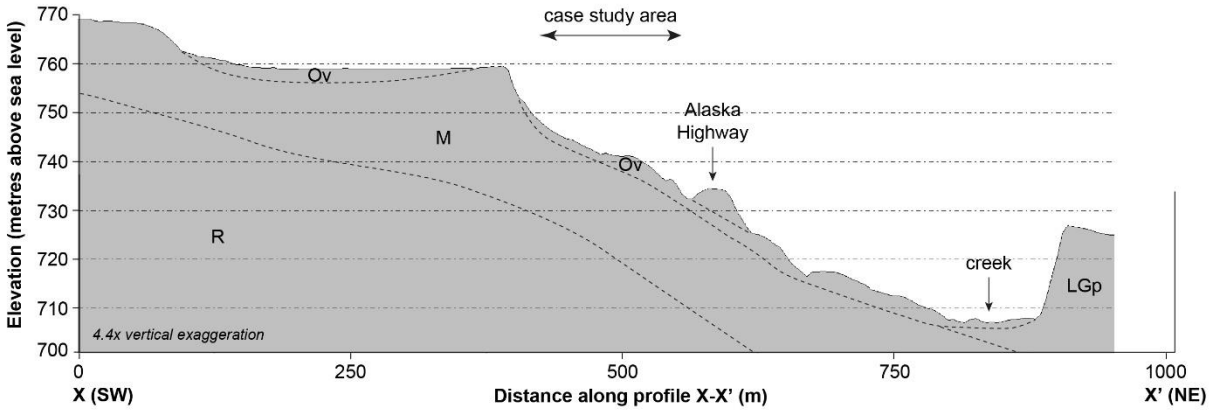

Figure 8.3 Generalized stratigraphic cross section from 2013 LiDAR DEM along transect X-X' (shown in Fig. 8.2).

More broadly, as outlined in Section 2.1, Glacial Lake Champagne occupied Takhini River valley at various levels as ice readvanced westward and blocked the mouth of Takhini River. A series of recessional moraines (Mr) in the valley bottom, and lateral meltwater channels along the valley sides in the Scout Lake area mark the intermediate extents of the ice as it paused before fully retreating to the east (Bond *et al*., 2005-8). Strandlines rimming several recessional moraine ridges located immediately to the north of the study site indicate that water levels extended up to at least 750 m elevation in this area. A glaciolacustrine plain (LGp) comprising thick fine-grained sand, silt and clay lake-bottom sediments extends up to elevations of ~720 m in this portion of the Takhini River valley. Coarse-grained (sand and gravel) glaciofluvial sediments (FGh, FGf) were also deposited by glacial meltwater in the Old Alaska Highway area during periods of ice-stagnation and retreat. At higher elevations, the valley sides are generally mantled with basal till (Mb, Mm) and colluvium (Cv). Organic materials (Ov, Op) have accumulated on many north-facing slopes, and adjacent to wetland areas and tributaries which drain into Takhini River; the presence of thermokarst thaw ponds and permafrost mounds confirms the presence of permafrost within these units.

Upper Triassic (200–204 million years old) Lewes River Group Mandanna member sedimentary rocks (Aksala Formation green and red greywacke, pebble conglomerate and mudstone) are found along both sides of the Alaska Highway east of km 1444. The bedrock hills immediately west of Alaska Highway km 1449 comprise Lower Jurassic (168–200 million years old) Laberge Group units of the Whitehorse Trough (Richthofen Formation turbiditic sandstone-siltstone-mudstone, and conglomerate; and Nordenskiold Formation dacite crystal tuff and volcaniclastic sandstone; Yukon Geological Survey, 2021). Only 2 out of 15 water well logs examined from the Old Alaska Highway area encountered bedrock, at depths of 18.6 and 27.4 m (Environment Yukon, 2021).

8.1.3 Permafrost

At this location, the road embankment is subject to frequent maintenance to repair periodic deformation and tension cracks (Fig. 8.4a). Similar cracks were observed in the natural ground adjacent to the highway (Fig. 8.4b), around the margins of degrading ice-rich permafrost mounds (lithalsas). Lithalsas (Fig. 8.5a, b) are mounds formed in mineral soil with segregated ice in their cores (Harris, 1993). The widespread presence of drunken forest (tilted trees due to thawing permafrost) at this site also indicates the presence of permafrost. At least 2 m of ice-rich permafrost was also encountered at this site, ~40 m SW of the ERT transects east end (Fig. 8.6), as indicated in a portable drilling system demonstration conducted at this site (Quantum Machine Works, April 2019).

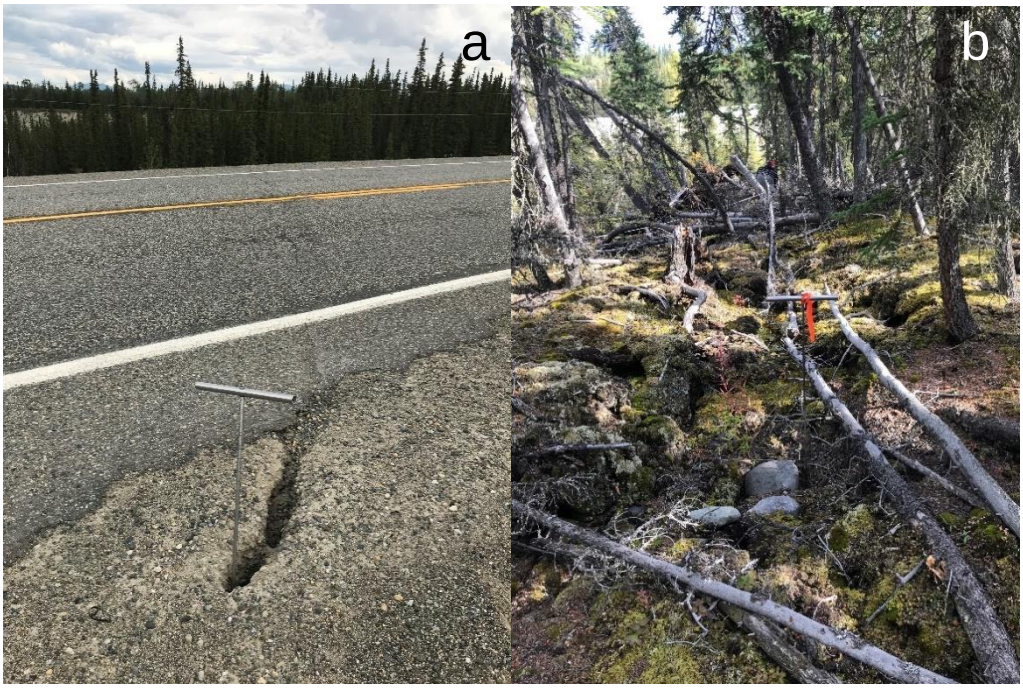

Figure 8.4 Tensions cracks a) on the embankment of the Alaska Highway, and b) on the margin of degrading lithalsa (permafrost mound) near X=150 m of ERT transect. Probe handle is 40 cm wide.

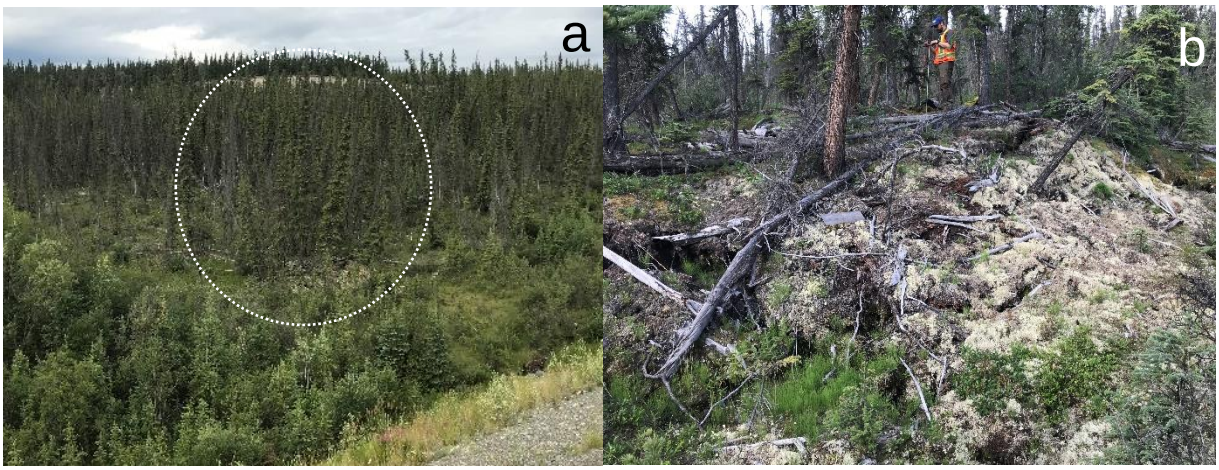

Figure 8.5 Lithalsa a) viewed from the Alaska Highway (feature circled in white), and b) close-up view.

The frost table on 17 July 2019 ranged from 49 to 60 cm depth in two soil pits dug into the side of a small 16 m-wide by 22 m-long permafrost mound near the east end of the ERT transect. Nearby frost probing on the same day revealed the frost table ranged from 55 to 75 cm depth immediately to the south of the mound, while further upslope it ranged from 40 to 55 cm depth on raised mossy mounds to >130 depth in small micro-depressions. This suggests active layer depths by late summer would likely remain less than 1 m, except beneath micro-depressions.

8.2 Results

8.2.1 ERT

One 200-m ERT survey, WH_1446_ERT1, was conducted on undisturbed ground on the southern side of the highway on 28 August 2019 (Fig. 8.1 and Table 8.1), using both the Wenner and dipole-dipole arrays. The results obtained with both arrays show a similar distribution of resistivity in the ground, however the dipole-dipole array shows more details within the low resistivity areas. The survey ran from east to west through a white spruce forest, traversing two permafrost mounds from 20 to 40 m (Fig. 8.6a) and 145 to 165 m horizontal distance (Fig. 8.2). Some ponding and surface seepage were observed as well as some wide tension cracks from 145 to 162 m along the profile (Fig. 8.7).

Table 8.1 Location details of the one ERT survey at the Old Alaska Highway study site.

Site	Date	Coordinates (NAD83 UTM Zone 8)	Array	Length (m)	Electrode Spacing (m)
WH_1446_ERT1	28/8/2019		Dipole-dipole and Wenner	200	2.5
0 m		479786 6742996			
50 m		479745 6743024			
100 m		479703 6743051			
150 m		479662 6743079			
200 m		479620 6743107			

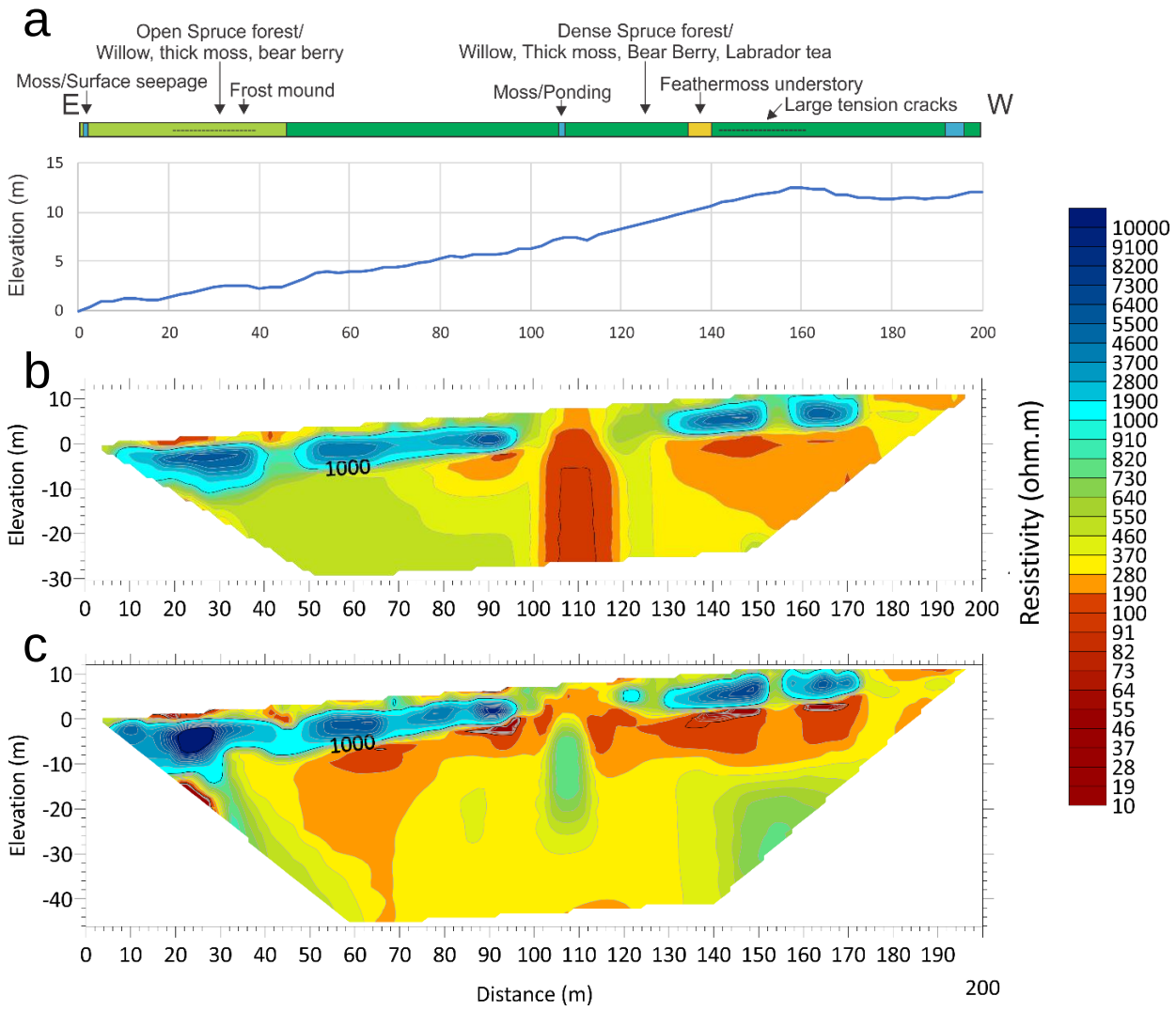

Figure 8.6 Old Alaska Highway E-W ERT Survey (WH_1446_ERT1) showing the (a) elevation profile, (b) ERT profile using Wenner array, 5th iteration, RMS error= 2.7%, and (c) ERT profile using dipole-dipole array, 4th iteration, RMS error= 2.5%. In (b) and (c) blue shades are interpreted as permafrost, and orange or red shades as unfrozen ground. Resistivities above the 1000 ohm·m isoline in (b) and (c) suggest a higher likelihood of ice-rich permafrost.

Figure 8.7 WH_1446_ERT1 survey, along margin of degrading permafrost mound (lithalsa), at X= ~150 m.

The ERT data suggest the permafrost table is relatively shallow with an active layer between 0.5 and 2 m thick, and the base of permafrost is up to 10 m deep. High resistivity pockets shown as dark blue shades, are present from 4 to 8 m depth along the survey, except for a deep low resistivity area, shown by red shades in the middle of the profile which is interpreted to indicate groundwater flow between discontinuous patches of permafrost. Based on field observation, the high-resistivity blue shaded areas are most likely attributable to ice-rich stony till (cobbles and boulders were observed near the surface in both permafrost mounds). Low resistivity values (<100 ohm·m) could be attributable to ice-poor and/or unfrozen material, and the lowest values may indicate the presence of liquid ground water. Shallow elongate and intermittent high-resistivity bodies overlying low resistivity ground are typical indicators of a permafrost mound environment.

8.2.2 Synthesis

Permafrost at the Old Alaska Highway case study site has formed on a gentle north-facing slope within stony till that is covered in a thick organic mat. Field observations and geophysical data collected at the Old Alaska Highway case study site suggest that permafrost at this location is on the order of 8 m thick. The presence of lithalsa permafrost mounds and the high-resistivity pattern in the ERT results suggest that permafrost is likely ice-rich. Degradation indicators such as tension cracks and drunken forest suggest the permafrost is warm, out of equilibrium with the current climate, and prone to degradation. Low-resistivity areas in the ERT profile are attributed to the presence of groundwater, which may be the cause of degradation. It is unclear whether ongoing movement observed in the road embankment is the result of permafrost degradation *(i.e.,* subsidence due to the melt of ground ice) or the deformation and creep of ice-rich permafrost under the weight of the embankment. No conclusions can be drawn at this point, but it is expected that permafrost thaw will eventually affect the road embankment at this location.

9 FISH LAKE

9.1 Site setting

The Fish Lake case study site is located west of Whitehorse city limits, 950 m north of Fish Lake (Fig. 9.1). The site lies at an elevation of 1124 m above sea level in a subalpine peat plateau with hummocky microtopography. Palsas and shallow thermokarst ponds are the dominant geomorphologic landforms indicating the presence of permafrost (Fig. 9.2). The study site is located on Kwanlin Dün First Nation settlement land (block R-4A).

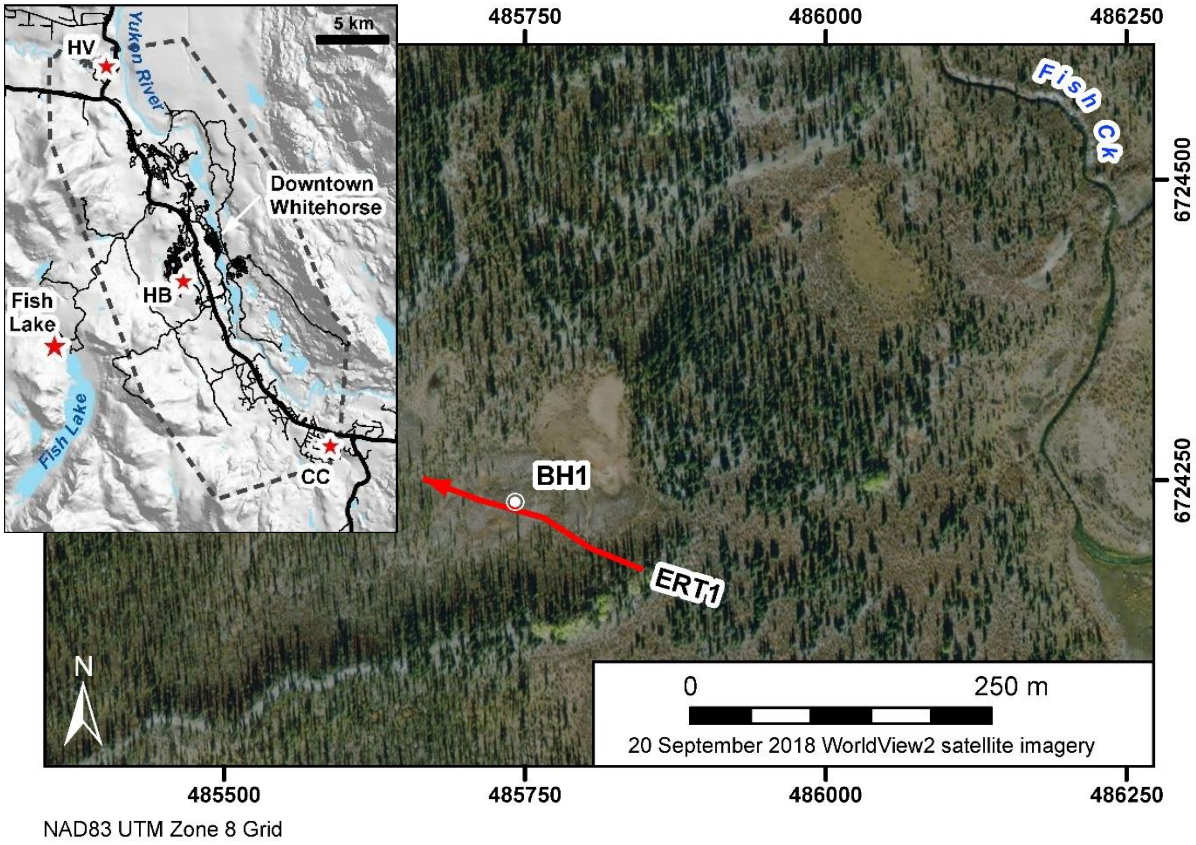

Figure 9.1 Location of the Fish lake case study site with borehole (white circle) and ERT survey location (red line). Inset map shows location with respect to Whitehorse city limits (dashed line) and nearby case study sites (HV = Hidden Valley, HB = Hamilton Boulevard, CC = Cowley Creek).

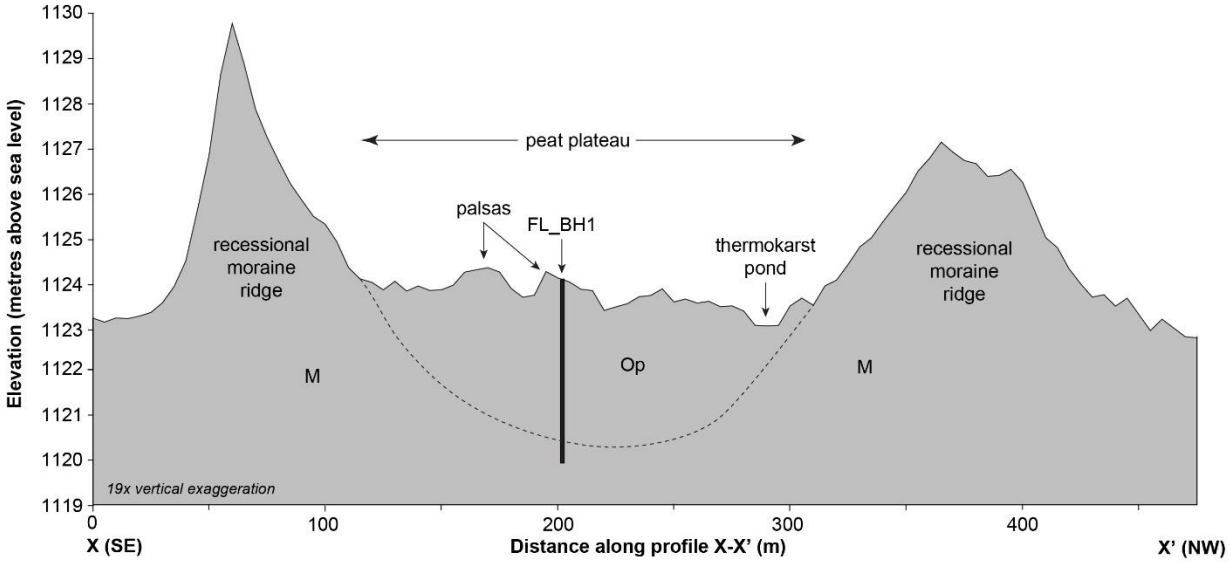

Figure 9.2 Generalized stratigraphic cross section, illustrating palsa peat plateau microtopography, from 2018 LiDAR DEM along transect X-X' (shown in Fig. 9.3).

9.1.1 Climate and vegetation

The Fish Lake case study site lies within the Boreal High bioclimate zone (Flynn, 2017). The ecosite is classified as a BOLsl/F04P-SW51 fen wetland (McKenna, *et al.,* 2017). This classification is characterized by hydric to hygric soils, dominated by shrub birch (*Betula glandulosa*), sedges (*Carex aquatilis*), and brown mosses (*Aulacomium, Tomenthypnum)* (McKenna, *et al.,* 2017). The area is sparsely forested with white spruce (*Picea glauca*). Vegetation is dominated by moss, lichen, sphagnum and dwarf birch. Raised permafrost mounds exist within the ecosite, lifting vegetation above the water table and leading to drier conditions and the presence of lichens and higher cover of lowbush cranberry (*vaccinium vitis-idaea*).

9.1.2 Surficial geology

During glacial maximum (~18 ka), the western margin of the Cassiar Lobe of the Cordilleran Ice Sheet covered the entire Fish Lake area and flowed in a northwesterly direction (Bond, 2004). The presence of erratics on the summit of nearby Mount Granger (2087 m elevation) indicates that ice was at least 1 km thick above the modern level of Fish Lake (1112 m) at that time.

Deglaciation was characterized by a complex history of ice retreat, stagnation and readvance (Bond, 2004). The northern ridge of Mount McIntyre was ice-free at 1377 m elevation by about 15 500 years ago (Menounos *et al.,* 2017). Following this initial phase of ice thinning and retreat in the Whitehorse area, a lobe of ice readvanced up-valley from the Yukon River valley toward Jackson Lake, and veered southward through the Fish Lake valley to the foot of Ibex Mountain (Bond, 2005-7). Streamlined basal till landforms just north of Fish Lake clearly indicate that the most recent ice-flow direction in the area was southwesterly to southeasterly (Fig. 9.3). This phase of ice-flow deposited most of the sediment (till) found at surface within the study area.

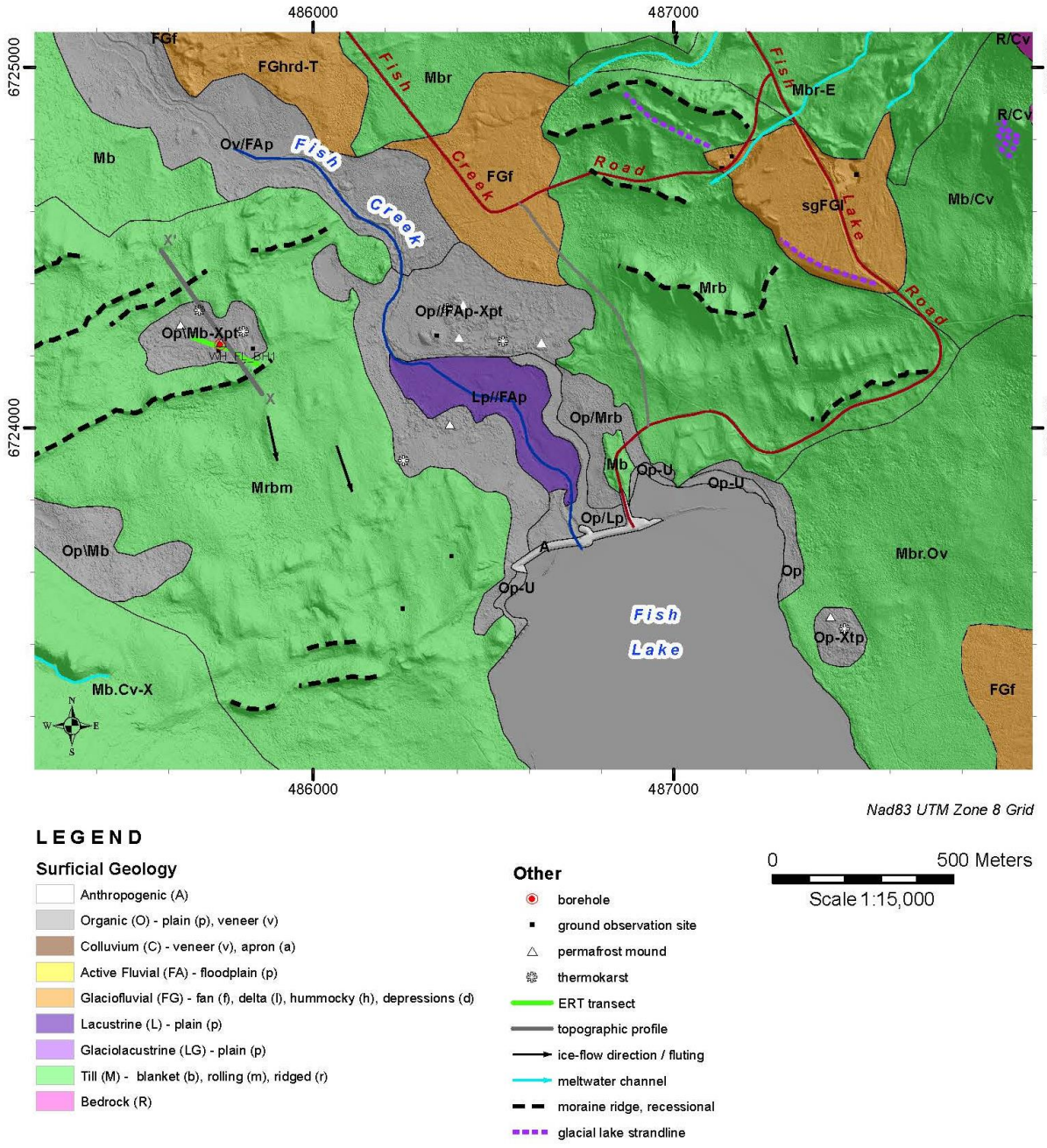

Figure 9.3 Simplified surficial geology map showing major landscape units, landforms and boreholes drilled in the vicinity of the Fish Lake case study site. White box indicates location of Fig. 9.1.

As this ice lobe retreated, it blocked meltwater drainage to the north, damming Glacial Lake McIntyre in the Fish Lake basin up to a maximum elevation of ~1250 m (140 m higher than the modern lake level at 1112 m elevation). Flights of paleo-shorelines (strandlines) from this former lake are visible above modern Fish Lake, on the western slopes of Mount McIntyre (Fig. 9.3). The strandlines were created as the ice thinned and retreated and lake levels gradually dropped. The outlet of Glacial Lake McIntyre was at the south end of the lake, into the Ibex River valley. Fine-grained (sand, silt and clay) glaciolacustrine deposits are interpreted to underlie low-lying areas at the north and south ends of the modern Fish Lake. The presence

of thermokarst ponds in these areas suggests that these fine-grained materials were likely susceptible to ice-segregation and the growth of ice-rich permafrost after Glacial Lake McIntyre drained ~11 000 years ago.

Vast amounts of meltwater drained the margins of the retreating ice, as indicated by subparallel sequences of incised gullies north of Fish Lake. To the east, meltwater from ice filling the Yukon River valley overtopped the low ridge at the north end of Mount McIntyre and carved the deep channels visible today on the slopes above northeastern Fish Lake. Glaciofluvial fans (FGf) and raised deltas (FGl) (Fig. 9.3) comprising well-drained sand and gravel are found at the foot of many of the larger meltwater channels.

The Fish Lake case study site is located within a small peat plateau (~1124 m elevation, see Fig. 9.2) that formed in a poorly-drained depression contained by a set of low (up to 10 m high) recessional moraine ridges. These moraine ridges were deposited at the ice front when it stagnated for short periods during its retreat to the north.

Yukon Electrical Company Ltd. built a dyke at the north end of Fish Lake in the late 1940s to control water levels in the Fish Creek outlet, which drains into a small hydro facility that has operated since 1949 (Yukon Energy, 2009). The dyke caused water levels to rise slightly in Fish Lake, drowning shorelines around the perimeter of the lake. The dyke also caused drainage of a former bay that previously extended 700 m downstream of the structure (Lp in Fig. 9.3).

The entire study area depicted in Figure 9.3 is underlain by Upper Triassic (200–217 million years old) Lewes River Aksala Formation sedimentary rocks (mostly Hancock member, with some Mandanna member), including conglomerate, sandstone, limestone and chert (Yukon Geological Survey, 2021). A water well drilled at the end of Fish Creek Road indicates that overburden (presumably till) is at least 31 m thick, 3 km northwest of the Fish Lake dyke (Environment Yukon, 2021, borehole ID: 900000048).

9.1.3 Permafrost

Thermokarst ponds and permafrost mounds (palsas) are the most obvious indicators of permafrost at the case study site and in the surrounding area; the Fish Lake case study site is within a field of palsas (Fig. 9.4). Near the case study site, thermokarst ponds and palsas occupy areas within or adjacent to low-lying, poorly-drained wetland areas with thick organic cover (Op-X in Fig. 9.3). A palsa is a peaty permafrost mound containing a core of alternating layers of ice and peat (van Everdingen, 2005). These low-relief (<10 m) hummocky landforms are from the permafrost mound family. These landforms are epigenetic and form by the action of downward freezing (*i.e.*, lowering of the permafrost base) through a previously deposited organic, peaty substrate. Ground ice accumulates within the peat through the process of ice segregation, fed by groundwater movement or the migration of soil moisture. Palsas share the same genetic processes as lithalsas, the main difference being the substrate of palsas is organic while lithalsas is mineral. Although both lithalsas and palsas are considered permafrost mounds, they should not be confused with other mounds such as frost blisters, icing blisters and pingos, which form from different genetic processes. Permafrost mounds are commonly identifiable by their bumpy raised appearance, particularly in lidar hillshade imagery (Fig. 9.4). Permafrost was also interpreted to be present on north-facing slopes mantled with till and colluvium and thick organic cover. Permafrost is likely absent within coarse-grained glaciofluvial materials in the area, and on steep south and south-west facing slopes mantled with till and colluvium.

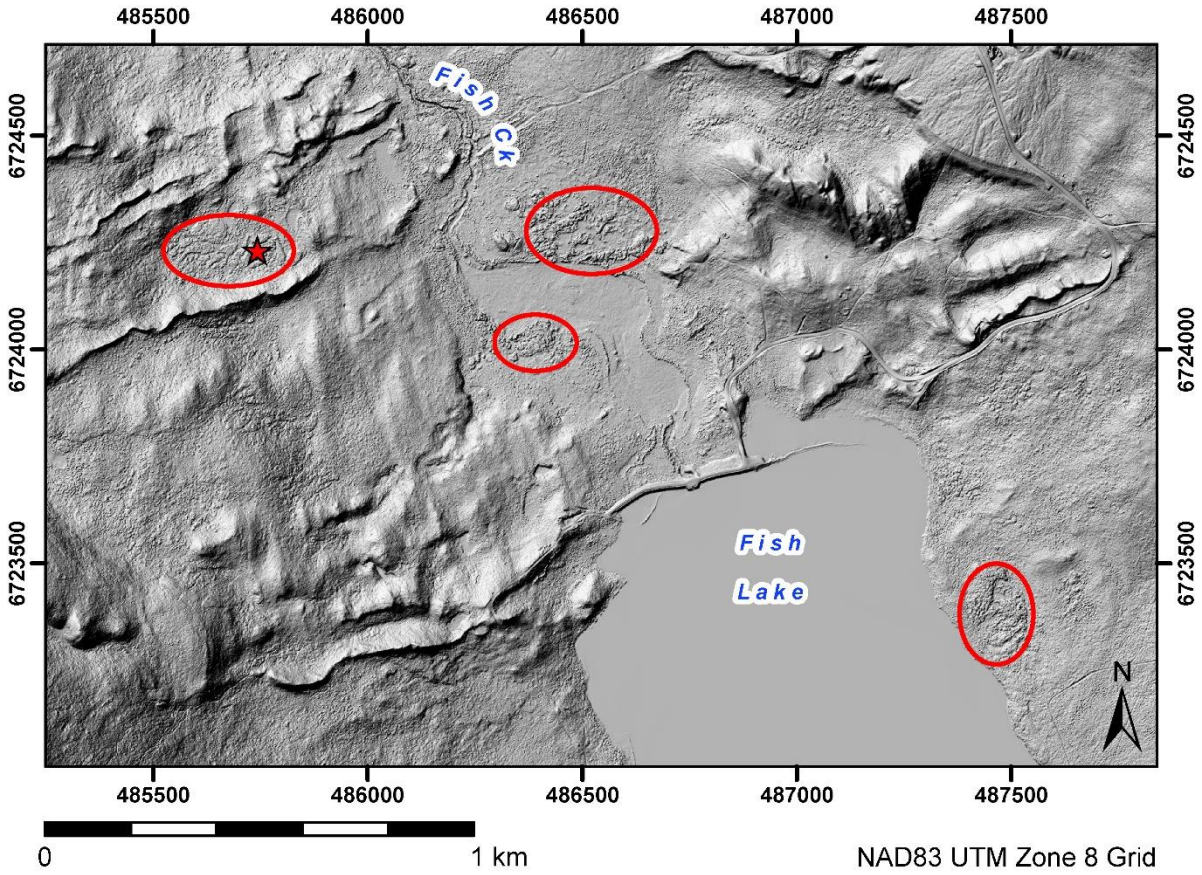

Figure 9.4 Palsa fields (circled in red) are easily identifiable in high resolution lidar hillshade imagery, based on their low relief bumpy appearance. Red star indicates Fish Lake case study location.

9.2 Results

9.2.1 Borehole geotechnical data

One 200 m long ERT survey, WH_FL_ERT1, was conducted at the Fish Lake case study site on 30 August 2019 (Table 9.1 and Fig. 9.1). Borehole WH_FL_BH1 was subsequently drilled on 8 October 2020 by the YGS with the participation of Fabrice Calmels (Fig. 9.5a), using a Talon drill system. Borehole WH_1456_BH1, is in the centre of an undisturbed peat plateau wetland (Fig. 9.5b). The purpose of the borehole was to provide a cryostratigraphic record and enable installation of ground temperature logging equipment to monitor the temperature of permafrost over time. The location selected was based on the ERT survey results, within the largest body of ice-rich permafrost indicated along the survey (at ~120 m).

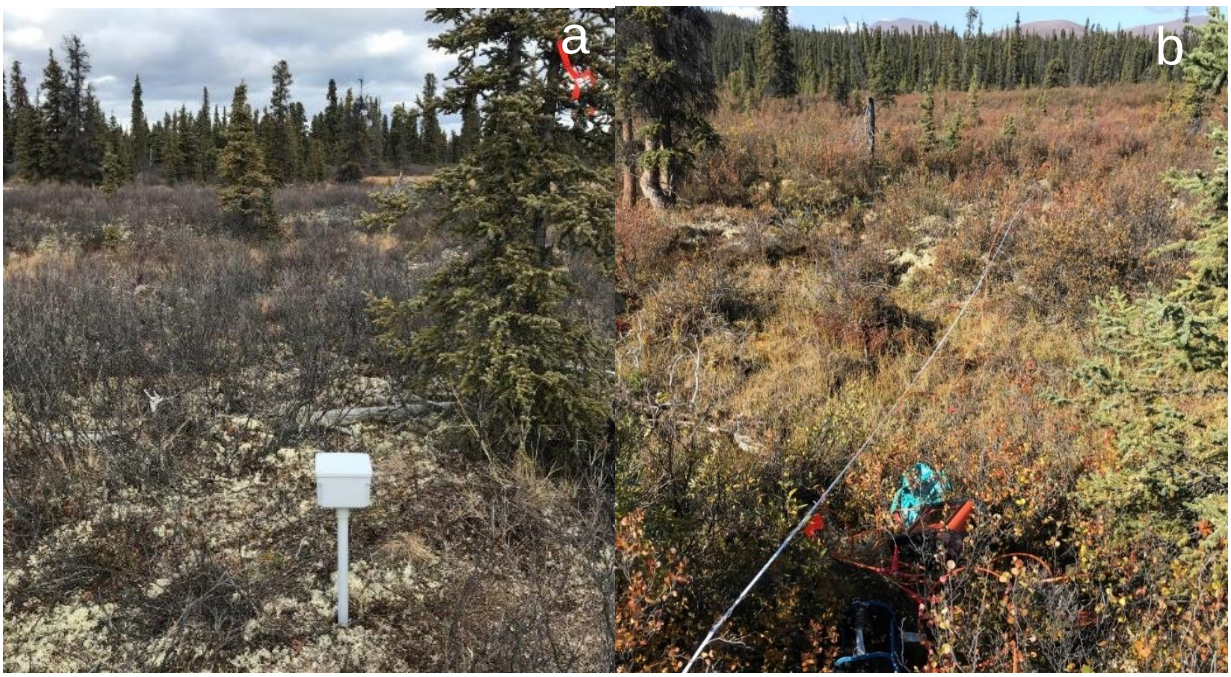

Figure 9.5. Fish Lake (a) borehole WH_FL_BH1 location and (b) ERT survey WH_FL_ERT1, location and environment.

Table 9.1 Location details of field surveys at the Fish Lake study site, including one instrumented borehole, and one ERT survey.

Site	Date	Coordinates (NAD83 UTM Zone 8)	Depth (m)	Ground Temperature Sensor Depths (m)
WH_FL_BH1	8/10/2020	485742 6724232	4.1	0.0, 1.0, 2.0, 4.1
WH_FL_ERT1	30/08/2019	Dipole-dipole and Wenner	Length (m): 200	Electrode Spacing (m): 2.5
0 m		485848 6724175		
50 m		485804 6724193		
100 m		485766 6724219		
150 m		485713 6724233		
200 m		485665 6724251		

Borehole WH_FL_BH1 was drilled to a depth of 4.11 m where a point of refusal was reached in gravelly till. The borehole stratigraphy comprises a layer of unfrozen peat at the surface (0–0.50 m depth; assumed to represent the active layer) overlying a thick layer of frozen fibric peat (0.50–3.36 m depth) with very little visible ice (occasional ice crystals). Gray silty clay extended from 3.36 to 3.73 m depth, with lenticular and suspended cryostructures, including 3 to 6 cm ice lenses (Fig. 9.6a). Frozen till was encountered from 3.73 to 4.11 m depth, with pebbles in a dense matrix of sand, silt, and clay (Fig. 9.6b).

Figure 9.6 Ice-rich permafrost core WH_FL_BH1, showing a) thick lenticular cryostructures in a core from 3.36 to 3.73 m depth, and b) lenticular cryostructure collected from the till at the base of borehole at a depth of 4.11 m.

9.2.2 Ground temperatures

Borehole WH_FL_BH1 was lined with PVC pipe and instrumented with one 4-channel HOBO (UX120-006M) data logger to record ground temperatures at 0, 1.0, 2.0, and 4.1 m depths. The recording started 8 October 2020 at 13:00, and data was last collected 18 February 2021 (Fig. 9.7). Active layer depths were probed and were found to vary from 0 to 1.2 m depth in August 2020, with an average depth of 0.5 m. Ground temperatures support the results from probing, suggesting a shallow active layer less than 1.0 m below the ground surface. Stable ground temperatures of −0.4°C at 4.1 m depth over the four-month period (Table 9.2 and Figs. 9.7–9.8) suggest permafrost extends beyond that depth.

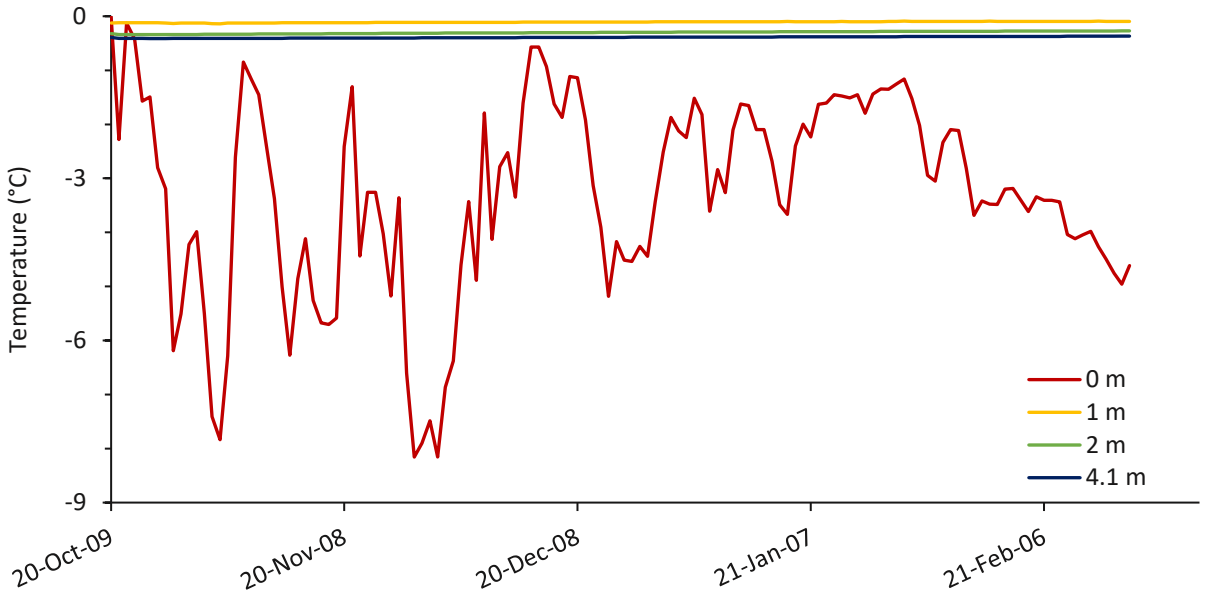

Figure 9.7 Fish Lake daily mean ground temperatures at FL_BH1 for the period 9 October to 17 February 2021.

Table 9.2 Minimum, maximum and mean ground temperatures (from daily mean values) over ~five months at FL_BH1 for the period 9 October 2020 to 17 February 2021.

Depth (m)	0.0	1.0	2.0	4.1
Min GT (°C)	−8.16	−0.14	−0.34	−0.41
Mean GT (°C)	−3.28	−0.11	−0.30	−0.39
Max GT (°C)	−0.01	−0.09	−0.27	−0.37

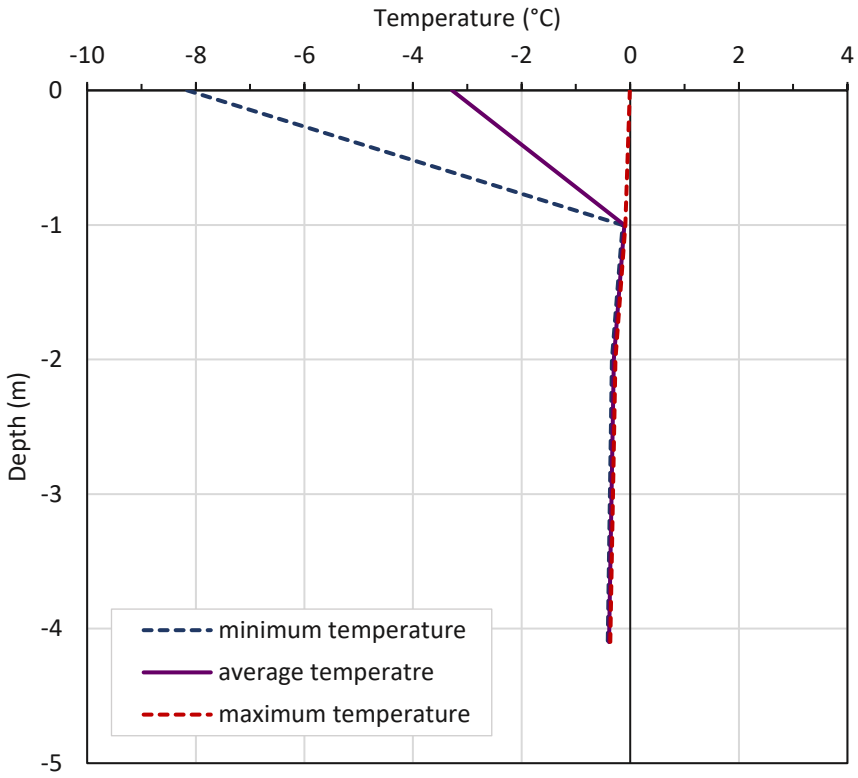

Figure 9.8 Ground temperature envelope at FL_BH1 for the period 19 October 2020 to 17 February 2021.

9.2.3 ERT

One ERT survey, WH_FL_ERT1, was conducted at Fish Lake on 30 August 2019 (Fig. 9.1). Both the Wenner and dipole-dipole array were measured. The results obtained with the Wenner and dipole-dipole arrays show a similar distribution of resistivity in the ground, however the dipole-dipole array shows more detail in low resistivity areas. The survey ran southeast to northwest, through an open peat plateau (Fig. 9.9).

The survey data suggests the permafrost base is typically 10 m deep but is up to 15 m deep at certain locations (30–35 m distance along the ERT profile) (Fig. 9.9). Some highly resistive material is present as deep as 30 m from 100 to 145 m along the profile (Fig. 9.9), but it could be due to the presence of coarser sediment or to an artefact generated by the inversion process. High resistivity pockets shown as dark blue shades in Figure 9.9, are concentrated between 2 and 6 m depth along the survey profile, which likely indicated the ice-richest horizons in the profile. Near-surface lower resistivity bodies shown in yellow and red shades coincide with the presence of depressions along the elevation profile (Fig. 9.9a). Water ponding at these locations corresponds to areas where permafrost is degrading. Another very low resistivity area can be observed at 170–180 m along the profile, extending from the ground surface to a depth of 20 m and is likely the result of groundwater flow.

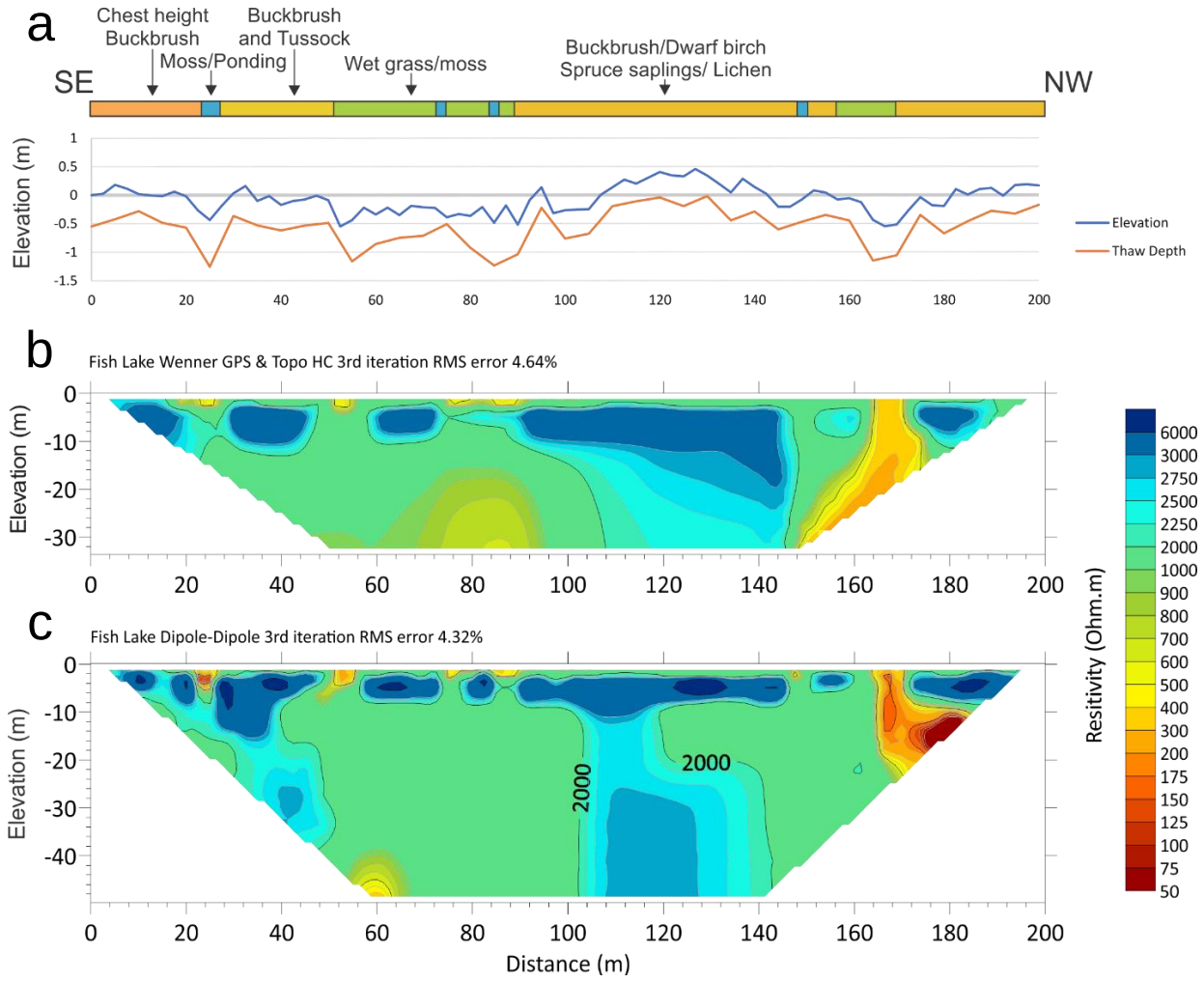

Figure 9.9 Fish Lake SE-NW ERT Survey (FL_ERT1) showing the (a) elevation profile and frost probe thaw depths, (b) ERT profile using Wenner array, 3rd iteration, RMS error= 4.6%, and (c) ERT profile using dipole-dipole array, 3rd iteration, RMS error= 4.3%. In (b) and (c) blue shades are interpreted as permafrost, and yellow to orange shades as unfrozen ground. Resistivities above the 2000 ohm·m isoline in (b) and (c) suggest a higher likelihood of permafrost.

9.2.4 Synthesis

The geotechnical boreholes and ERT data agreed well in defining the top of permafrost at ~0.5 m depth. The cores collected on site show peat, followed by clayey silts and till down to at least 4.1 m. The geophysical data showed ice-rich permafrost from 0.5 m to a maximum depth of ~15 m. High resistivity pockets at ~30 m depth suggest deeper permafrost may be possible in some locations. Some ponds are present in the area, likely of thermokarst origin. Long-term ground temperature monitoring will determine if permafrost is in balance with its current local environment or degrading.

10 DISCUSSION

Summary of permafrost conditions

Local environmental conditions such as elevation, vegetation, and terrain features vary across the seven case studies, but several similarities are also observed across the sites (Table 10.1).

Six of the case study sites lie in valley bottom settings between 655 and 750 m asl, while the Fish Lake site lies at 1138 m asl and serves as an example of subalpine peatland permafrost. Case study sites were often gently sloped and north-facing (Table 10.1). A thick organic layer was observed only at the Hamilton Boulevard (0.60 m) and Fish Lake (3.36 m) case study sites, while the remaining sites had thinner organic layers up to 0.15 m.

All seven case study sites are within the Southern Lakes Ecoregion and all but the Fish Lake site are located in the Boreal Low bioclimate zone, Southern Lakes subzone (BOLsl). The Fish Lake site is in the Boreal High bioclimate zone (BOH). All except the Fish Lake site were forested, generally with white spruce as the most abundant species. The Fish Lake site is located in a fen wetland peat plateau environment, with a vegetation cover of moss, lichen, sphagnum, dwarf birch and scattered white spruce. Areas where permafrost has degraded commonly show fallen or tilted trees (drunken forests) and a reduction in white spruce forest cover, as well as an increasing presence of water tolerant species (Vogt, 2021, in prep.).

Generally, the geologic settings in which permafrost is found in the GWA are: subalpine peat plateaus (*e.g.,* Fish Lake), north-facing slopes underlain by till (*e.g.*, Old Alaska Highway and Hamilton Boulevard), areas underlain by fine-grained glaciolacustrine sediment *(e.g.,* Hidden Valley, Ibex Valley, and Takhini Retrogressive Thaw Slump), and low-lying fine-grained or organic-rich terrain, particularly within abandoned meltwater channels (*e.g.,* Cowley Creek). Permafrost in all settings most likely began to form near the end of the last ice age, sometime after 15,000 years ago, once glacier cover disappeared and ice-dammed lakes had drained. Ice-rich permafrost is most strongly associated with thick organic materials and fine-grained sediments (such as glaciolacustrine materials, and silt and/or clay-rich basal till) in close proximity to abundant groundwater sources (*i.e.*, in low-lying areas close to streams or water bodies, and near the foot of bedrock slopes). Ice-rich permafrost generally does not occur in coarse-grained surficial materials that are primarily composed of sand, gravel and/or rubble (*i.e.*, glaciofluvial deposits, ablation or meltout till, and weathered bedrock) or on most south-facing slopes. The most common landforms indicating the presence of permafrost at the case study sites were hummocky permafrost mound terrain (lithalsas and palsas), thermokarst ponds and tension cracks.

Depending on the definition used, permafrost is considered vulnerable to thaw when mean annual ground temperature (T_p) is greater than −2.0 or −3.0°C. Using either definition, permafrost at all case study sites is particularly vulnerable, given that the lowest observed mean annual ground temperature was −0.28°C at Hamilton Boulevard. While ground temperatures of −0.40°C were observed at Fish Like, data at this site were only available for a five-month period (Table 10.1). Across all sites, mean annual ground temperature typically ranged from 0.0 to −0.2°C (Table 10.1).

Table 10.2 summarizes the nature and condition of permafrost at the seven case study sites. ERT and borehole geotechnical data reinforce the sporadic, shallow (<30 m deep) and thin nature of permafrost in the area. Many of the ERT resistivity profiles suggest the presence of permafrost in isolated pockets or zones on the order of 1-10's of metres in length. Only a few ERT surveys (*e.g.,* CC_ERT1 at Cowley Creek, WH_1456_ERT1 at the Takhini River thaw slump, and HV_ERT2 in Hidden Valley) show continuous high resistivity along their entire lengths, where permafrost appears to extend >100 m.

Table 10.1 Summary of the environmental and permafrost conditions across the seven case study sites. Permafrost depth and potential subsidence were determined from borehole geotechnical data and thermistors, not ERT. T_p represents the annual mean temperature of permafrost, V_{ice} the average volumetric excess ice content, and P_{Table}, P_{Base} and $P_{Thickness}$ the depth to top and bottom of permafrost, and total thickness, respectively.

Case Study	Cowley Creek	Hamilton Blvd	Hidden Valley	Ibex Valley	Takhini River RTS	Old Alaska Hwy	Fish Lake
Elev. (m asl)	718	750	650	680–690	640–670	720–750	1120–1125
Slope	flat	gentle (3–5°)	gentle to moderate (6–25°)	flat	gentle to moderate (3–25°)	gentle (5–10°)	flat
Aspect	n/a	northeast	north	n/a	north	north	n/a
Ecosite	BOLsl/01Z-Sw27s	BOLsl/33P-Sw39z	BOLsl/01-APSw25z	BOLsl	BOLsl	BOLsl	BOLsl/F04P-SW51
Organic Layer (m)	0.10	0.60	0.10	Forest: 0.10	unknown	0.15	3.36
Intact Veg.	white spruce	w. spruce	bench: cleared, escarpment: grassy, gentle slope: spruce	Forest: w. spruce Burned: lodgepole pine, w. spruce, aspen	w. spruce, aspen	mature w. spruce	moss, lichen, sphagnum, dwarf birch and w. spruce
Degraded Veg.	Reduced tree density	No change	-	Forest: reduced tree density	removed on slump	-	fen wetland, grasses
Terrain features	permafrost mounds, hummocky	poor drainage, frost mounds, hummocky	subsidence	thermokarst lakes, salt flats, drunken trees	slumping, tension cracks	drunken forest, lithalsas, tension cracks	hummocky, palsas, thermokarst ponds, fen wetland
Surficial Geology	silty fluvial terrace	depression in basal till	glaciolacustrine terrace	glaciolacustrine plain	glaciolacustrine terrace	organic veneer overlying basal till	peat plateau overlying basal till
T_p (°C)	−0.03 to −0.13	−0.03	> 0.00	−0.03 to −0.12	-0.04	-	−0.11 to −0.39‡
V_{ice} (%)	42	36	36	49	33	-	-
P_{Table} (m)	1.5	0.5	8.0^{+}	4.9	3.4	~1	0.5
P_{Base} (m)	5.1†	2.0	18.8^{+}	17.5	8.0	-	4.1†
$P_{Thickness}$ (m)	3.6	1.5	10.8^{+}	12.6	4.6	~2	3.6
Subsidence (m)	1.5	0.5	3.9^{+}	6.2	1.5	-	-

$^{+}$ Temperature from 8 to 19 m depth at Hidden Valley was between 0.1 and 1.1°C and cannot be considered permafrost, however, may be considered ice-rich ground in disequilibrium and therefore presents a risk of subsidence.
† Permafrost base likely extends beyond this depth however was restricted by the depth of the borehole.
‡ Ground temperatures at Fish Lake were only recorded for approximately five months and represent an incomplete year of data.

Table 10.2 Summary of permafrost conditions and considerations for future development at the seven case study sites. Generalized permafrost conditions were determined mainly from ERT surveys and borehole ground temperatures.

Case Study	Generalized Permafrost Conditions	Considerations for Development
Cowley Creek	• Warm, thaw-sensitive, ice-rich • Shallow (~5–15 m), continuous high resistivity across ERT profile; may extend as deep as 25–30 m in some locations	• Subsidence
Hamilton Boulevard	• Warm, thaw-sensitive, ice-rich • Shallow (1–8 m), and continuous across ERT profile; may extend to 15 m in some locations	• Thermokarst
Hidden Valley	• Warm, thaw-sensitive, ice-rich • Shallow (>5 m) pockets at top of slope, and continuous across W-E ERT profile downslope of house • Shallow permafrost may have thawed following veg. removal and drilling	• Subsidence • Creep on slope • Slope instability • Settlement
Ibex Valley	• Warm, thaw-sensitive, ice-rich • Forest: shallow (0–5 m) preserved pocket in open spruce forest, with discontinuous permafrost potentially up to 25 m depth • Burned: shallow (~5–15 m) permafrost in deciduous forest and under access road • Burned 2: deeper (5–27 m) permafrost in mature spruce forest only (absent beneath open deciduous forest) • Dense mature forest acts to preserve permafrost, fire disturbed areas led to a deepening active layer	• Subsidence and differential settlement
Takhini River RTS	• Warm, thaw-sensitive, ice-rich • Epigenetic permafrost becomes thinner and more discontinuous closer to highway (20–25 m deep near RTS headwall) • Generally present in local, shallow pockets (up to 7 m) immediately south of the highway, and more continuous (up to 7 m) immediately north of the highway.	• Widespread slope instability (slumping and creep) • Tension cracks
Old Alaska Highway	• Likely warm, thaw-sensitive, ice-rich • Shallow pockets (up to 8 m) in ice-rich stony till	• Subsidence
Fish Lake	• Warm, thaw-sensitive, ice-rich • Shallow pockets (~1–10 m), with a maximum depth of ~15 m • Low resistivity areas in local depressions with water ponding	• Subsidence

The case studies demonstrate that permafrost in the greater Whitehorse area is patchy, shallow, vulnerable to thaw, and thaw-sensitive where excess ice was observed. Permafrost is restricted to locations where vegetation, environmental and ground thermal conditions favour the maintenance of frozen ground (e.g. north-facing aspects, mature forest cover and/or thick organic layers, fine-grained surficial materials, peat plateaus, and low-lying areas with poor drainage).

Impacts of climate change

Past climate trends have shown seasonal differences in warming, with the most significant warming occurring in winter. Daily winter minimum temperatures rose 3.4°C/century from 1942 to 2009 while daily summer maximum temperatures rose only 1.1°C/century. This winter warming can also be seen in a reduction in the number of days below −40°C and increases in frost-free days. The number of days below −40°C has decreased at a rate of 5 days/century for the period 1942–2009, and the number of frost-free days per year has increased at a rate of 42 days/century from 1980 to 2010. Projected air temperatures show between the current decade (2020–2029) and 2090–2099, air temperatures for Whitehorse are predicted to rise between 1.2°C and 3.5°C in January, and 1.6°C and 4.0°C in July (Fig. 2.5a, b and Table 2.1).

Past climate trends of Whitehorse have also shown decreased winter precipitation (14 mm/century for the period 1942–2009), and increased summer precipitation (20 mm/century for the same period). Overall, the total annual precipitation of Whitehorse has increased slightly at a rate of 11 mm/century for the period 1943–2009. Total depth of snow on February 28 decreased by 13 cm/century for the years 1955–2010. While historic data have shown decreases in winter precipitation, projected climate trends show increases in winter precipitation. From 2020–2029 to 2090–2099, precipitation is projected to increase between 0 and 2 mm (0–10.5%) in January, and 2 and 6 mm (4.3–14.6 %) in July. This could be a result of the high variability in precipitation data. As historic climate trends disagree with projections, the change in future precipitation is less certain.

It is important to understand that the principal control on the formation and persistence of permafrost is climate. Local environmental characteristics of a site such as snow cover, vegetation, organic cover, proximity to water bodies, groundwater flow, aspect and surficial materials then act to modify the energy balance and determine the spatial distribution, thickness, and temperature of permafrost. So, while a change in climate will result in a change in ground temperature, the effect will vary depending on the local environmental conditions. Additionally, while increasing air temperature alone may increase ground temperature, climate change will also impact several other factors such as changes in snowfall, rainfall, and their timing. These additional climate change effects will further contribute to changes in vegetation and snow cover, and subsequently ground temperatures.

As climate is the main control on permafrost, as air temperature warms, we expect permafrost to as well. An increase in air temperature will lead to an increase in the ground surface temperature that will propagate downwards. The greatest increases would be seen at the ground surface and lessen with depth. Higher ground surface temperatures would lead to gradual deepening of the active layer and degradation at the top of permafrost. Warm permafrost, (*i.e.,* >−2°C), responds slower to surface warming than cool permafrost. When ground is near 0°C, energy from the surface is used to melt ground ice (*i.e.,* latent heating), however when ground temperatures are cooler, the surface energy is used to raise the ground temperature (*i.e.*, sensible heating). While warm permafrost like that in the GWA may be slower to respond, once ground ice has melted, the soil strength will rapidly decline.

Detailed estimates of thaw are not available at each site, however general rates of thaw can be deduced from previous research. Climate change may thaw shallow permafrost less than 7 m within the next century, however thicker and ice-rich permafrost will take longer to thaw (CSA, 2019). Analysis from Takhini Valley by Burn (1998) re-affirm the time-scale at which complete thaw would occur. Using a simplified model Burn (1988) estimated that complete thaw of 14 m of ice-rich permafrost would require 1300 years under 1998 climate conditions. This analysis acts as a partial analogue for climate change however the analysis is limited in that it only considers thaw following a surface disturbance (wildfire) and the model does not consider convective heat transfer. For thinner permafrost, between 4 and 5 m thick, complete thaw would occur over a century or less. Additional results by James *et al.* (2013) highlight significant permafrost degradation has occurred in the southern Yukon since the 1960s, over which only relatively minor changes to climate have been observed. These studies indicate that active layer deepening and the complete thaw of thin permafrost could occur quite rapidly, on the order of decades to centuries, while thicker permafrost would require a much longer time scale, on the order of millennia, to thaw completely.

Development considerations

Warming ground temperatures and the degradation of permafrost is important for a number of reasons, the most pertinent of which in the GWA is the loss of volume that accompanies thawing of ice-rich permafrost and the loss of soil strength. The strength of frozen soils increases inversely with their temperature due to ice bonding; soil strength generally increases as ground temperatures cool and weaken as they warm (CSA, 2019). Another major factor affecting permafrost strength is unfrozen water content, which is influenced not only by ground temperature, but also soil grain size distribution, clay content, and pore water quality (e.g. dissolved solids and salinity) (van Everdingen, 2005). Thaw of frozen soils with excess ice may lead to the loss of soil strength as ground ice thaws and excess water causes pore-water pressures to rise (CSA, 2019). The loss of soil strength following thaw is particularly important on sloping grounds because it can cause landslides.

When soils with ground ice thaw, the excess water content drains, volume is lost, and the soil settles, *i.e.,* consolidates. The loss of volume and associated settlement of the ground surface is called subsidence. Higher ice contents mean greater potential subsidence upon thawing. Variable excess ice contents and soil drainage leads to differential thaw settlement, which is of particular concern for agricultural development in the Takhini Valley area. Thaw-sensitive permafrost refers to soils that will experience significant thaw settlement and a loss strength (Harris *et al.,* 1988). Soils can also be thaw-stable if no significant thaw settlement or loss of strength is expected. Thaw-sensitive soils are often fine-grained soils such as silt or clay because these soils are frost-susceptible, *i.e.*, will form segregated ice if given adequate moisture supply and temperature. It is implied that any ice-rich soil is frost-susceptible and thaw-sensitive. Thaw stable soils are more often coarse-grained, with minimal excess ice. For example, most bedrock is thaw stable (CSA, 2019).

Frost heave is the displacement of soil (commonly upwards) during the freezing season, as ice forms in the soil. The main cause of frost heave is the formation of ice lenses by ice segregation. The amount of frost heave that occurs depends on soil type, available moisture, and freezing rate (CSA, 2019), with the largest displacements occurring in ground with a thick active layer, composed of silty (frost-susceptible) material, and a moist environment (Murton, 2021). In areas where permafrost is degrading, a deepening active layer and a greater availability in soil moisture may increase the frost heave potential at a site. Seasonal frost heave may also occur in frost-susceptible (fine sandy) soils in non-permafrost areas, sometimes causing damage to near-surface infrastructure and pavement.

Overall, thawing of permafrost is important because it accompanies a significant loss of soil strength, may lead to thaw settlement, and increases the potential for frost heaving (CSA, 2019). All of which are problematic from a development perspective. At the case study sites in the GWA, the most noted development consideration noted was potential subsidence (Table 10.2), due to the high excess ice contents of the permafrost. Slope instability and creep were also noted as potential development considerations at case studies with sloping ground (*i.e.*, Hidden Valley and Takhini River Retrogressive Thaw Slump; Table 10.2).

Several remediation techniques can be applied to different foundation types with the purpose of mitigating ground warming. These techniques have been outlined in detail by CSA (2014), tailored to the North Alaska Highway (Calmels *et al.,* 2016a) and summarized in relation to Ross River (Calmels *et al.,* 2016b), and include shading, drainage, snow management, ground insulation, thermosyphons, mechanized refrigeration, and adjustment or replacement of foundation. The remediation techniques work similar to local environmental characteristics such as vegetation, organic thickness, *etc*., discussed throughout the report, as they modify the surface or ground thermal regime to be more favourable for maintaining permafrost. The applicability of each mitigation techniques depends heavily on the site characteristics, and requires information on the extent of permafrost, soil properties and the thermal regime (CSA, 2019). CSA (2019) provides a detailed step-by-step approach to plan and design infrastructure in permafrost environments.

An additional development consideration is that regardless of climate change, site preparation and construction can disturb the ground surface (*e.g.,* vegetation clearing, grading, removal of the organic layer, leading to increased ground temperatures). Therefore, in areas underlain by permafrost, minimizing disturbances to the ground surface as much as possible throughout the development process is important to reduce ground warming. A number of publications and standards address good building practices in permafrost environments, including ‘Geotechnical site investigation for building foundations in permafrost zones’ (BNQ, 2017), ‘Guidelines for Development and Management of Transportation Infrastructure in Permafrost Regions’ (TAC, 2010), and ‘Geotechnical site investigation guidelines for building foundations in permafrost’ (GNWT, 2009), as well as a homeowners guide produced by GNWT (2015).

11 CONCLUSIONS

This report gives an account of field investigations on the permafrost conditions at seven case study sites in the Greater Whitehorse Area. Field investigations began in May 2018 and continued up to February 2021. Permafrost conditions were evaluated based on ground temperature profiles, excess ice content and material type from borehole logs, and resistivity profiles of the subsurface. Ground temperatures were monitored at eight boreholes over six case study sites. Extraction of cores and subsequent geotechnical analysis was possible at seven boreholes. Between one and four ERT surveys were completed at each of the sites, with a total of thirteen surveys completed. Permafrost conditions were contextualized by considering environmental conditions of the case study sites such as vegetation, terrain features and surficial materials. Generalized permafrost conditions were then used to explore impacts of climate change and potential rates of thaw, as well as considerations for future development. The following conclusions can be drawn from examination of permafrost conditions in the greater Whitehorse area (GWA):

- Permafrost at the seven case study sites is warm, with the coolest mean annual ground temperatures reaching −0.13°C at 2 m depth at Cowley Creek CC_BH2. Annual temperatures of permafrost so close to the melting point suggest permafrost throughout the GWA is in disequilibrium with its environment and is particularly vulnerable to thaw by disturbance or environmental change.
- Permafrost was associated with four primary geologic settings: (1) low-lying fine-grained or organic-rich terrain, particularly within abandoned meltwater channels; (2) fine-grained glaciolacustrine sediments; (3) north-facing slopes underlain by fine-grained till; and (4) subalpine peat plateaus. Features associated with the presence of permafrost were thermokarst lakes, subsidence, drunken forests, permafrost mounds (hummocks and palsas), slope creep, and tension cracks.
- Estimates of the active layer depth and base of permafrost varied depending on if they were defined using boreholes or ERT surveys. Generally, active layer depth ranged from as shallow as ~0.5 m to more than 4 m, while the base of permafrost ranged from 2 m depth at isolated borehole locations up to 30 m depth as suggested in ERT surveys.
- The Ibex Valley case study site had the highest potential for ground subsidence with an average ground ice content of 49% and an estimated permafrost thickness of 12.6 m. This equates to 6.2 m of potential subsidence should this entire thickness of permafrost thaw. Because ground ice content can vary spatially, differential thaw settlement will pose a major challenge to future development in this area, particularly as agricultural land-use increases.
- The case study sites with the thinnest permafrost were Old Alaska Highway and Hamilton Boulevard, while thicker and more spatially extensive permafrost was seen at Ibex Valley and Cowley Creek.
- The lowest ground temperatures in permafrost (−0.39°C over a 5 month period) were found at the Fish Lake site, which is located at the highest elevation and has the thickest organic layer.
- In several boreholes, ground ice was encountered during drilling, but subsequent monitoring indicated ground temperatures slightly above 0°C. This suggests that while permafrost was present prior to drilling, it subsequently thawed in the immediate vicinity of the borehole as a result of the drilling process, highlighting how vulnerable warm permafrost is to thaw when disturbed. Warm ice-rich permafrost in undisturbed areas is generally only preserved due to the ice's high latent heat of fusion (melting) (*i.e.*, a large amount of heat is required to change ice from solid to liquid phase, during which no change in temperature occurs).

12 GLOSSARY

Surficial geology deposits

- Note: surficial material descriptions are based on definitions from Howes and Kenk (1997), which may be consulted for further details (https://www2.gov.bc.ca/assets/gov/environment/natural-resource-stewardship/nr-laws-policy/risc/terclass_system_1997.pdf)
- Yukon-specific modifications to the BC classification system are outlined here: https://ygsftp.gov.yk.ca/YGSIDS/compilations/Surficial_2014_04_08/Yukon_Digital_Surficial_Geology_Release1_08Apr2014.pdf

Colluvium: Sediment that has been transported and deposited by gravity-induced mass movement (*e.g.,* slope creep, sloughing or landslides), involving no other agent of transportation such as water or ice. Generally consists of massive to moderately well–stratified, non–sorted to poorly–sorted sediments with any range of particle sizes from clay to boulders and blocks. Colluvium varies widely in character, depending on the nature of the material from which it was derived and its specific mode of deposition.

Eolian: sediments transported and deposited by wind. Generally consists of medium to fine sand and coarse silt that is well–sorted, non–compacted, and may contain internal structures such as cross–bedding or ripple laminae, or may be massive. The most common eolian features that occur in the Greater Whitehorse area are sand dunes and loess (a surface veneer or blanket of largely homogenous non-stratified fine sand and/or silt).

Fluvial: Sediments that have been transported and deposited by streams and rivers (synonymous with alluvial). Fluvial deposits generally consist of moderately to well-sorted stratified beds of gravel and/or sand and/or silt. Gravel is typically rounded and contains interstitial sand. Fluvial materials generally occur as floodplains, terraces and fans.

Glaciofluvial: Material deposited by glacial meltwater streams either on, within, adjacent to, or in front of a glacier. Glaciofluvial material generally comprises gravel and sand with varying degrees of sorting and stratification. Landscape features commonly associated with glaciofluvial materials include outwash plains, terraces, fans, deltas, and ice-contact features such as kettle holes, kames and eskers.

Glaciolacustrine: Material deposited in or along the margins of glacial (ice–dammed) lakes, including sediments that were released by the melting of floating ice. Lake bed sediments generally consist of well-stratified fine sand, silt and/or clay, and may contain ice-rafted stones and lenses of till and/or glaciofluvial material. Coarse-grained beach deposits transported by wave action along the margins of the glacial lakes are also considered to be glaciolacustrine.

Kettle hole: a depression in glacial sediment caused by the melting of a buried detached block of stagnant glacier ice. Kettle holes often contain a lake or swamp.

Lacustrine: Sediments that have settled in and along the shorelines of lakes which have not been dammed by glaciers. Most commonly consists of well-stratified fine sand, silt and/or clay deposited on the lake bed from suspension and underwater gravity flows. Includes coarse-grained beach deposits that have accumulated along shorelines through wave action.

Morainal (till): sediment deposited directly from glacial ice without further modification by other agents of transportation such as wind or water. Till may be transported beneath, beside, on, within and in front of a glacier. Its composition, structure, and surface expression are highly variable depending on the source of the sediment transported by the glacier, and the mode of deposition. Till generally consists of well–compacted to non–compacted material that is non–stratified and contains a heterogeneous mixture of particle sizes, often in a matrix of sand, silt and clay.

Organic: Materials resulting from the accumulation of vegetative matter that may range in level of decomposition. Most commonly found in and around wetlands or on gentle slopes, where the rate of accumulation exceeds that of decay. Organic materials that are commonly saturated with water consist mainly of the remains of mosses, sedges or other hydrophytic vegetation. Organic materials in drier environments are commonly associated with more fibric remnants of leaf litter, twigs, branches and mosses.

Tephra: Tephra is a general term for all pyroclastic materials ejected from a volcano. The White River tephra commonly occurs in the Greater Whitehorse area just below the ground surface in a distinctive white layer of silt to sand-sized volcanic ash on the order of 1 cm thick. This tephra was deposited in an eruption from Mount Churchill ~1200 years ago.

Permafrost and related ground ice features

- Note: most permafrost and ground ice terms are based on definitions from Harris *et al.,* (1988), which may be consulted for further details (https://ipa.arcticportal.org/images/Glossary/Glossary_of_Permafrost_and_Related_Ground-Ice_Terms_1998.pdf)

Active layer: The layer of ground subject to annual thawing and freezing in areas underlain by permafrost. In the continuous permafrost zone, the active layer generally reaches the permafrost table however in the zone of discontinuous permafrost it often does not. The active layer includes the uppermost part of the permafrost if either the salinity or clay content of the permafrost allows it to thaw and refreeze annually, even though the material remains below 0°C.

Aggradational ice: Ground ice formed as a direct result of permafrost aggradation.

Buried ice: Ice formed or deposited on the ground surface and later covered by sediments. Buried ice likely represents buried glacier ice or snowbanks, or less likely, lake, river or sea ice.

Discontinuous permafrost: Describes permafrost distribution in a geographic region, where permafrost occurs in some areas beneath the land surface where other areas are free of permafrost. The zone of discontinuous permafrost occurs between the zone of continuous permafrost zone and the southern limit of permafrost in lowlands. Permafrost is widespread near the northern boundary, while near the southern boundary it occurs in isolated patches where surface conditions are favourable and is often referred to as “sporadic” permafrost. Depending on the scale of mapping, several subzones can often be distinguished, based on the percentage of the land surface underlain by permafrost.

Epigenetic permafrost: Permafrost that formed after the deposition of the soil material in which it occurs, through the lowering of the permafrost base.

Excess ice: This the volume of ice in the ground exceeding the total pore volume the ground would have under natural unfrozen conditions. In standard geotechnical terminology, a soil is considered normally consolidated when its total pore volume or its total water content is in equilibrium with the acting gravity stresses. Due to the presence of ground ice, the total water content of a frozen soil may exceed that corresponding to its normally consolidated state when unfrozen. As a result, upon thawing, a soil containing excess ice will settle under its own weight until it attains its consolidated state.

Frost heave: The upward or outward movement of the ground surface (or objects on or in the ground) caused by the formation of ice in the soil (Murton, 2021). It is the volume increase in soil and accompanying surface displacement from the accumulation of ice in the soil profile. Heave normally occurs upwards, perpendicular to ice lenses. The main cause of frost heave is ice segregation, though other minor causes may be the volumetric expansion of water freezing within ground, and the injection of water under high pressure into frozen ground. Frost heave tends to be greatest in moist, silty, thick active layers commonly found in areas of discontinuous permafrost.

Frost mound: Any mound-shaped landform produced by the ground freezing, combined with the accumulation of ground ice due to groundwater movement or the migration of soil moisture. Various types of frost mounds (*e.g.*, frost blisters, icing blisters, palsas and pingos), can be distinguished based on their structure and duration and the character of the ice contained in them.

Frost-susceptible ground: Ground (soil or rock) in which *segregated ice* will form (causing frost heave) if the appropriate moisture supply and temperature conditions are provided. Frost-susceptible ground will eventually become ice-rich, regardless of its initial total water content. By implication, frost-susceptible ground may also be susceptible to thaw weakening effects when it thaws.

Ice-rich permafrost: Permafrost that contains ice in excess of pore space is considered ice-rich. Ice-rich permafrost is *thaw-sensitive.*

Ice-wedge: A massive, usually wedge-shaped body of ice with a downward pointing apex, commonly foliated or vertically banded, and white, ice. The width of the wedge can vary from less than 10 cm to 3 m at the top, and commonly tapers to a feather edge at a depth between 1 and 10 m. Ice wedges occur in thermal contraction cracks into which snowmelt penetrates in the spring. Repeated contraction cracking of the ice in the wedge, followed by freezing of the water in the crack, gradually increases the size of the wedge.

Lenticular Cryostructure: Lens-shaped ice in sediment, generally continuously shaped. They are typically horizontal (form parallel to the freezing plane) but may be straight, wavy, inclined or interlaced. They may contain ice bubbles. Lenses are usually ≥ than 1 mm thick and present in ice-rich sediment (Murton and French, 1994). The length of lenticular cryostructures vary from mm to cm in syngenetic permafrost, and cm to decimetres (dm) in epigenetic permafrost.

Massive ice: A comprehensive term used to describe large masses of ground ice, including ice wedges, pingo ice, buried ice and large ice lenses. Massive ice beds typically have an ice content of at least 250 percent (on an ice-to-dry-soil weight basis).

Microlenticular Cryostructure: Lens-shaped ice in sediment, generally discontinuously shaped. They are typically horizontal (forming parallel to the freezing plane) but may be straight, wavy, inclined or interlaced. They contain very few ice bubbles. Lenses are usually less than 1 mm thick and present in ice-rich sediment (Murton and French, 1994). In syngenetic permafrost microlenticular cryostructures compose >50% volume, while in epigenetic permafrost they make up 30–50% volume.

Permafrost: Ground (soil, rock, organic material and ice) that remains at or below 0°C for at least two consecutive years. Permafrost is defined on the basis of temperature. It is not necessarily frozen, because the freezing point of water may be below 0°C, and moisture (water or ice) may or may not be present. Permafrost does not include glacier ice, icings or bodies of surface water with temperatures perennially below 0°C, however it does include human-made perennially frozen ground around or below chilled pipelines, hockey arenas, *etc.*

Permafrost aggradation: An increase in the thickness and/or areal extent of permafrost. It can occur from an increase in the ground surface from sediment deposition, or from climatic cooling and changes in terrain such as vegetation succession or decreased snow cover. It can also occur under ice arenas, road and airfield embankments, *etc*. It may be expressed as a thinning of the *active layer* and a thickening of the *permafrost table*, or by an increase in the areal extent of permafrost.

Permafrost degradation: An increase in the thickness and/or areal extent of permafrost. It may be expressed as a thickening of the *active layer*, a lowering of the *permafrost table*, a raising of the *permafrost base*, or a reduction in the areal extent of permafrost.

Permafrost base: The lower boundary surface of permafrost, above which temperatures are perennially below 0°C and below which temperatures are perennially above 0°C.

Permafrost table: The upper boundary surface of permafrost. The depth of this boundary below the land surface, whether exposed or covered by a water body or glacier ice, varies according to such local factors as topography, exposure to the sun, insulating cover of vegetation and snow, drainage, grain size and degree of sorting of the soil, and thermal properties of the soil and rock.

Permafrost thickness: The vertical distance between the *permafrost table* and the *permafrost base*.

Relict ice: Ice formed in, and remaining from, the geologically recent past.

Reticulate Cryostructure: Net-like cryostructure of interconnected sub-horizontal ice lenses and sub-vertical ice veins. Usually ice-rich to very ice rich sediment (35–95% volume)**.** (Murton and French, 1994).

Segregated ice: Ice formed by the migration of pore water to the frozen fringe where it forms into discrete layers or lenses within soil. Segregated ice can range in thickness from a hairline to more than 10 m. It commonly occurs in alternating layers of ice and soil.

Suspended Cryostructure: Suspended aggregates in ice. Usually very ice-rich sediment (up to 90–95% volume). Common in upper part of permafrost (Murton and French, 1994).

Syngenetic permafrost: Permafrost that formed simultaneously with the deposition of the soil material in which it occurs. It formed through a rise in the permafrost table during the deposition of additional sediment or earth material on the ground surface.

Talik: A layer or body of unfrozen ground in a permafrost area.

Thaw-sensitive permafrost: Perennially frozen ground which, when it thaws, will experience significant thaw settlement and lose strength to a value significantly lower than a similar material in an unfrozen condition. Ice-rich permafrost is thaw-sensitive.

Thawing front: The advancing boundary between thawed ground and frozen ground. The thawing front may be advancing into either seasonally or perennially frozen ground during progressive thawing. In non-permafrost areas there will be two thawing fronts during the annual thawing period: one moving downward from the surface, the other moving upward from the bottom of the seasonally frozen ground.

Thermal erosion: The erosion of ice-rich permafrost by both the thermal (*i.e.*, the melting of ice) and mechanical (*i.e.,* moving water) action of moving water. Thermal erosion is distinct from the development of *thermokarst* terrain, which develops from thermal melting followed by subsidence of the ground but occurs without mechanical erosion.

Thermokarst: The process by which characteristic landforms result from the thawing of ice-rich *permafrost* or the melting of *massive ice*. Landforms include alasses, thermokarst lakes and thermokarst mounds.

Thermokarst lake: A lake that occupies a depression formed by the ground settling following the thawing of ice-rich *permafrost* or the melting of *massive ice*. Thermokarst lakes are generally shallow. The depressions may expand by the failure of the active layer and the lakes may expand by thermokarst processes. In glaciated terrain they may be similar in appearance to kettle lakes.

13 REFERENCES

ASTM Standard C29 – 09, 2000. Standard test method bulk density (“unit weight”) and voids in aggregate. West Conshohocken, PA, ASTM International.

ASTM Standard D422 – 63, 2000. Standard test method for particle-size analysis of soils. West Conshohocken, PA, ASTM International.

Barnes, S.D., 1997. The sedimentology and paleogeography of Glacial Lake Champagne, southern Yukon Territory. MA thesis, Carleton University, Ontario, Canada, 109 p.

Benkert, B.E., Kennedy, K., Fortier, D., Lewkowicz, A., Roy, L.-P., de Grandpré, I., Grandmont, K., Drukis, S., Colpron, M., Light, E. and Williams, T., 2016. Old Crow landscape hazards: Geoscience mapping for climate change adaptation planning. Northern Climate ExChange, Yukon Research Centre, Yukon College. 136 p. and 2 maps.

Bond, J., 2004. Late Wisconsinan McConnell glaciation of the Whitehorse map area (105D), Yukon. *In:* Yukon Exploration and Geology 2003, D.S. Emond and L.L. Lewis (eds.), Yukon Geological Survey, p. 73–88.

Bond, J.D., Morison, S. and McKenna, K., 2005. Surficial geology of Whitehorse. Yukon Geological Survey, Geoscience Map 2005-7, 1:50 000 scale.

Bonnaventure, P.P. and Lewkowicz, A.G., 2008. Mountain permafrost probability mapping using the BTS method in two climatically dissimilar locations, northwest Canada. Canadian Journal of Earth Sciences, pp. 443–455, doi: 10.1139/E08-013.

Bonnaventure, P.P. and Lewkowicz, A.G., 2013. Impacts of mean annual air temperature change on a regional permafrost probability model for the southern Yukon and northern British Columbia, Canada. The Cryosphere, vol. 7, p. 935–946, doi:10.5194/tc-7-935-2013.

Bonnaventure, P.P., Lewkowicz, A.G., Kremer, M. and Sawada, M.C., 2012. A permafrost probability model for the southern Yukon and northern British Columbia, Canada. Permafrost and Periglacial Processes, vol. 23, p. 52–68, https://doi.org/10.1002/ppp.1733.

Brown, R.J.E., 1967. Permafrost investigations in British Columbia and Yukon Territory. National Research Council of Canada, Ottawa, ON, 55 p.

Bureau de normalisation du Québec (BNQ). 2017. Geotechnical site investigation for building foundations in permafrost zones (CAN/BNQ 2501-500), 88 p., https://www.bnq.qc.ca/en/standardization/civil-engineering-and-urban-infrastructure/geotechnical-site-investigation-for-building-foundations-in-permafrost-zones.html.

Burgess, M.M., Judge, A.S. and Taylor, A.E., 1982. Yukon ground temperature data collection -1966 to August 1981. Energy, Mines and Resources Canada, Ottawa, ON, Open File 82-1.

Burn, C.R., 1987. Thermokarst ponds and ground temperatures in Takhini Valley. *In*: XIIth INQUA Congress field excursions A20 and A20b Research in Yukon, S.R. Morison and C.A.S. Smith (eds.), National Research Council of Canada, Ottawa, ON, p. 34.

Burn, C.R., 1998. The response (1958-1997) of permafrost and near-surface ground temperatures to forest fire, Takhini River valley, southern Yukon Territory. Canadian Journal of Earth Sciences, vol. 35, p. 184–199.

Burn, C.R., 2001. Permafrost. *In*: Occasional Papers in Earth Sciences no. 2. Field guide to Quaternary research in central and western Yukon Territory. D.G. Froese, A. Duk-Rodkin and J.D. Bond (eds.), Yukon Heritage Branch, p. 10–14.

Burn, C.R., 2004. Permafrost. *In*: Ecoregions of the Yukon Territory: Biophysical properties of Yukon landscapes, C.A.S. Smith, J.C. Meikle and C.F. Roots (eds.), Agriculture and Agri-Food Canada, PARC Technical Bulletin No. 04-01, Summerland, British Columbia, p. 42–45.

Calmels, F. and Allard, M., 2007. Segregated ice structures in various heaved permafrost landforms through CT scan. Earth Surface Processes and Landforms, vol. 33, p. 209–225, doi: 10.1002/esp.1538

Calmels, F., Doré, G., Kong, X., Roy, L., Lemieux, C. and Horton, B., 2016a. Vulnerability of the north Alaska Highway to permafrost thaw: Design options and climate change adaptation. Northern Climate ExChange, Yukon Research Centre, Yukon College, 130 p.

Calmels, F., Horton, B., Roy, L.P., Lipovsky, P. and Benkert, B., 2016b. Assessment of risk to infrastructure from permafrost degradation and a changing climate, Ross River. Northern Climate Exchange, Yukon Research Centre, Yukon College, 100 p., http://scholar.yukonu.ca/fcalmels/publications/assessment-risk-infrastructure-permafrost-degradation-and-changing-climate.

Camels, F., Roy, L.P., Grandmont, K. and Pugh, R., 2018. ERT and Temperature Monitoring to Assess the Effectiveness of Insulating Culverts on Northern Highways. Yukon Research Centre, Yukon College, 39 p.

Calmels, F., Roy, L.P, Laurent, C., Amyot, F. and Lipovsky, P., 2020. Assessment and monitoring of a new retrogressive thaw slump at km 1456 of the Alaska Highway: A rare opportunity. Yukon University Research Centre, 62 p.

Canadian Standards Association (CSA Group), 2014. Moderating the effects of permafrost degradation on existing building foundations (CAN/CSA-S501 Standard). Toronto: CSA Group, http://shop.csa.ca/en/canada/infrastructure-andpublic-works/cancsa-s501-14/invt/27037462014.

Canadian Standards Association (CSA Group), 2019. Technical Guide: Infrastructure in permafrost: A guideline for climate change adaptation (CSA PLUS 4011:19). Toronto: CSA Group, https://climatechange.toolkitnwtac.com/.

Cherian-Hall, A., 2019. Thermokarst lake evolution in a discontinuous permafrost zone near Whitehorse, Yukon, Canada. Quest University undergraduate research project poster.

De Pascale, G.P., Pollard, W.H. and Williams, K.K., 2008. Geophysical mapping of ground ice using a combination of capacitive coupled resistivity and ground-penetrating radar, Northwest Territories, Canada, Journal of Geophysical Research, vol. 113, F02S90, doi:10.1029/2006JF000585.

EBA Engineering Consultants Ltd., A Tetra Tech Company (EBA), 2013. Geotechnical evaluation of road settlement Hamilton Boulevard section 4+640 to 4+860, Whitehorse, YT. Internal report to Government of Yukon, Community Services, Infrastructure Development Branch, File: W14103046-02. Dec. 24, 2013.

EBA Engineering Consultants Ltd., A Tetra Tech Company (EBA), 2014. Preliminary aquifer and wellhead protection plan, Takhini River Subdivision, Yukon. Prepared for Champagne Aishihik First Nation.

EBA Engineering Consultants Ltd., A Tetra Tech Company (EBA), 2015. End of year status report – ground temperature cable readings, Hamilton Boulevard Station 4+730. Internal report to Government of Yukon, Community Services, Infrastructure Development Branch, File: W14103383-08. Dec. 10, 2015.

Environment and Climate Change Canada (ECCC), 2021a. Historical data, http://climate.weather.gc.ca/historical_data/search_historic_data_e.html, [accessed February 8, 2021].

Environment and Climate Change Canada (ECCC), 2021b. Canadian climate normals, http://climate.weather.gc.ca/climate_normals/index_e.html, [accessed February 8, 2021].

Environment Yukon, 2021. Yukon water well registry, webmap. Water Resources Branch, https://www.arcgis.com/apps/webappviewer/index.html?id=51322dfb133d42c4ad184fee9986048b, [accessed January 13, 2021].

Flynn, N. and McKenna, K., 2017. Chapter 6: Subzones of the Boreal Low Zone. *In*: Southern Lakes Boreal Low Subzone (BOLsl): A field guide to ecosite identification. Department of Environment, Government of Yukon, Whitehorse, Yukon.

Foothills Pipe Lines (South Yukon) Ltd., 1979. Environmental Impact Statement for the Alaska Highway Gas Pipeline, https://www.arlis.org/thepipefiles/Record/1476125, [accessed February 1, 2021].

French, H., 2007. The Periglacial Environment. Third Edition. Online ISBN: 9781118684931

French. H.M. and Egginton. P., 1973. Thermokarst Development, Banks Island, Western Arctic. *In:* Permafrost, North American Contribution, 2nd International Conference Permafrost, Yakutsk, U.S.S.R. National Academy of Science Publ. 2115, Washington, D.C., p. 203–12.

Gilbert, R. and Desloges, J.R., 2005. The record of Glacial Lake Champagne in Kusawa Lake, southwest Yukon Territory. Canadian Journal of Earth Sciences, vol. 42, p. 2127–2140.

Government of the Northwest Territories (GNWT). 2009. Geotechnical site investigation guidelines for building foundations in permafrost. Prepared by I. Holubec Consulting Inc., Department of Government Works and Services, Government of the Northwest Territories, Yellowknife, NT, 48 p., https://geocryology.files.wordpress.com/2013/05/for-lecture-geotechnical-guidelines-for-construction-on-permafrost.pdf.

Government of the Northwest Territories (GNWT). 2015. A homeowner's guide to permafrost in the Northwest Territories. Environment Division, Department of Environment and Natural Resources, Government of the Northwest Territories, 22 p., https://www.enr.gov.nt.ca/sites/enr/files/permafrost-homeowners-guide.pdf.

Government of Yukon, 2019. Permafrost probability model, https://yukon.maps.arcgis.com/apps/webappviewer/index.html?id=534f141ffa5f4796954627dc98f82b99, [accessed February 7, 2021].

Harris, S.A., French, H.M., Heginbottom, J.A., Johnston, G.H., Ladanyi, B., Sego, D.C. and van Everdingen, R.O., 1988. Glossary of permafrost and related ground-ice terms. National Research Council of Canada, Associate Committee on Geotechnical Research, Technical Memorandum No. 142, https://doi.org/10.4224/20386561.

Harris, S.A. 1993. Palsa-like mounds developed in a mineral substrate, Fox Lake, Yukon Territory. *In*: Proceedings of the Sixth International Conference on Permafrost, Beijing, China. South China University of Technology Press, vol. 1, p. 248–253.

Hart, C.J.R., 1997. Geology of Thirty-seven Mile Creek map area, southern Yukon Territory, (NTS 105D/13). Indian and Northern Affairs Canada/Department of Indian and Northern Development: Exploration and Geological Services Division, Geoscience Map 1997-4.

Heffner, T., 2008. The role of glacial lakes in the pre-contact human history of southwest Yukon Territory: a late drainage hypothesis. The Northern Review, vol. 29, p. 85–104.

Heginbottom, J.A., 1995. National Atlas of Canada (5th edition), Canada Permafrost, Plate 2.1 (MCR 4177), 1:7 500 000 scale.

Holloway, J., 2020. Impacts of forest fire on permafrost in the discontinuous zones of northwestern Canada. Unpublished PhD thesis, University of Ottawa, Ontario, Canada, 213 p.

Horton, S., 2007. The Paleogeography of Glacial Lake Lebarge, south central Yukon Territory. Unpublished BSc Honours thesis, University of Victoria, British Columbia, Canada, 53 p.

Howes, D.E. and Kenk, E., 1997. Terrain classification system for British Columbia (version 2). Province of British Columbia, Resource Inventory Branch, Ministry of Environment, Lands and Parks; Recreational Fisheries Branch, Ministry of Environment; and Surveys and Mapping Branch, Ministry of Crown Lands, 104 p., https://www2.gov.bc.ca/assets/gov/environment/natural-resource-stewardship/nr-laws-policy/risc/terclass_system_1997.pdf.

Huscroft, C.A., Lipovsky, P.S. and Bond, J.D., 2004. A regional characterization of landslides in the Alaska Highway corridor, Yukon. Yukon Geological Survey, Open File 2004-18.

James, M., Lewkowicz, A.G., Smith, S.L. and Miceli, C.M., 2013. Multi-decadal degradation and persistence of permafrost in the Alaska Highway corridor, northwest Canada. Environmental Research Letters, vol. 8, 045013, doi:10.1088/1748-9326/8/4/045013.

Keenan, T. and Cwynar, L., 2011. Late Quaternary history of black spruce and grasslands in southwest Yukon Territory. Canadian Journal of Botany, vol. 70, p. 1336–1345. doi: 10.1139/b92-168.

Klassen, R.W., 1979. Thermokarst terrain near Whitehorse, Yukon Territory. *In:* Current research, part A. Geological Survey of Canada, Paper 79-1A, p. 385–388.

Krautblatter, M. and Hauck, C., 2007. Electrical resistivity tomography monitoring of permafrost in solid rock walls, Journal of Geophysical Research, vol. 112, F02S20, doi:10.1029/2006JF000546.

Kryotek Arctic Innovation Inc., 2017. Geophysical and drilling results, GR AGR 577, Agricultural Disposition, Takhini River Valley, Yukon. May 19, 2017 report to Yukon Government, Agriculture Branch (Department of Energy, Mines and Resources), 20 p.

Lewkowicz, A.G. and Bonnaventure, P.P., 2011. Equivalent elevation: a new method to incorporate variable lapse rates into mountain permafrost modelling. Permafrost and Periglacial Processes, vol. 22, p. 153–162.

Lewkowicz, A.G., Bonnaventure, P.P., Smith, S.L. and Kuntz, Z., 2012. Spatial and thermal characteristics of mountain permafrost, Northwest Canada, Geografiska Annaler, vol. 94, p. 195–213. doi:10.1111/j.1468-0459.2012.00462.x.

Lewkowicz, A.G. and Coultish TL. 2004. Beaver damming and palsa dynamics in a subarctic mountainous environment, Wolf Creek, Yukon, Canada. Arctic, Antarctic and Alpine Research, vol. 36, p. 208–218.

Lewkowicz, A.G. and Ednie, M., 2004. Probability mapping of mountain permafrost using the BTS method, Wolf Creek, Yukon Territory, Canada. Permafrost and Periglacial Processes vol. 15, p. 67–80.

Lewkowicz, A.G., Etzelmüller, B.E. and Smith, S.L., 2011. Characteristics of discontinuous permafrost from ground temperature measurements and electrical resistivity tomography, southern Yukon, Canada. Permafrost and Periglacial Processes, vol. 22, p. 320–342.

Lipovsky, P.S., 2014. Summary of Yukon Geological Survey permafrost monitoring network results, 2008-2013. *In*: Yukon Exploration and Geology 2014, K.E. MacFarlane, M.G. Nordling and P.J. Sack (eds.), Yukon Geological Survey, p. 113–122.

Lipovsky, P.S. and Yoshikawa, K., 2009. Initial results from the first year of the Permafrost Outreach Program, Yukon, Canada. *In*: Yukon Exploration and Geology 2008, L.H. Weston, L.R. Blackburn and L.L. Lewis (eds.), Yukon Geological Survey, p. 161–172.

McKenna, K., Meidinger, D., Kennedy, C.E. and Flynn, N. 2017. Part 2, Chapter 3: Guides/keys to BOLsl ecosites. *In*: Southern Lakes Boreal Low Subzone (BOLsl): A Field Guide to Ecosite Identification. Department of Environment, Government of Yukon, Whitehorse, Yukon.

Menounos, B., Goehring, B.M., Osborn, G., Margold, M., Ward, B., Bond, J., Clarke, G.K.C., Clague, J.J., Lakeman, T., Koch, J., Caffee, M.W., Gosse, J., Stroeven, A.P., Seguinot, J. and Heyman, J., 2017. Cordilleran Ice Sheet mass loss preceded climate reversals near the Pleistocene Termination. Science, vol. 358, p. 781–784.

Mougeout GeoAnalysis and Agriculture and Agri-Food Canada, 1997. Soil, terrain and wetland survey of the City of Whitehorse. Planning Services, City of Whitehorse, Whitehorse, Yukon Territory, 160 p.

Mougeot, C.M. and Smith, C.A.S., 1992. Soil survey of the Whitehorse Area. Vol 1. Takhini Valley. Centre for Land and Biological Resources Research, Research Branch, Agriculture Canada, 3 maps (1:20 000 scale).

Murton, J., 2021. Periglacial Processes and Deposits. *In*: Encyclopedia of Geology (Second Edition), D. Alderton and S.A. Elias (eds.), Academic Press, p. 857–875, https://doi.org/10.1016/B978-0-12-409548-9.11925-6.

Murton, J.B. and French, H.M., 1994. Cryostructures in permafrost, Tuktoyaktuk coastlands, western arctic Canada. Canadian Journal of Earth Sciences, vol. 31, no. 4, p. 737–747.

Oke, T.R., 1987. Boundary layer climates, Second Edition. Routledge, London, 435 p. Master e-book ISBN 0-203-40721-0.

Osterkamp, T.E. and Burn, C.R., 2003. PERMAFROST. *In:* Encyclopedia of Atmospheric Sciences, J.R. Holton (eds). Academic Press, p. 1717–1729, https://doi.org/10.1016/B0-12-227090-8/00311-0, ISBN 9780122270901.

Purves, M., 2006. Climate Change in the Yukon, Some Observations. Yukon Weather Centre Internal report YWC-06-109, 57 p. Private correspondence from the author, https://emrlibrary.gov.yk.ca/ebooks/climate-change-in-the-yukon-some-observations-2006.pdf.

Purves, M., 2010. Climate Change in the Yukon, Updated Observations. Yukon Weather Centre Internal Report YWC-10-110, 81 p. Private correspondence from the author.

Quantum Machine Works, 2019. Talon portable drill for drilling, coring, sampling and exploration, https://youtu.be/7QRkyxYAGtg, [accessed April 22, 2019].

Rampton, V.N., 1972. Surficial deposits, Alaska Highway, Whitehorse, to Alaska-Yukon boundary. Geological Survey of Canada, Paper 72-1.

Rampton, V.N., Ellwood, J.R. and Thomas, R.D., 1983. Distribution and geology of ground ice along the Yukon portion of the Alaska Highway gas pipeline. *In*: Proceedings, 4th International Conference on Permafrost, Fairbanks, Alaska, July 1722, 1983. National Academy Press, Washington, D.C., Vol. 1, p. 1030–1035.

R Core Team, 2020. R: A language and environment for statistical computing. R Foundation for Statistical Computing, Vienna, Austria, http://www.R-project.org/.

Smith, C.A.S., Meikle, J.C. and Roots, C.F. (editors), 2004. Ecoregions of the Yukon Territory: Biophysical properties of Yukon landscapes. Agriculture and Agri-Food Canada, PARC Technical Bulletin No. 04-01, Summerland, British Columbia, 313 p.

Smith, M.W. and Riseborough, D.W., 2002. Climate and the limits of permafrost: a zonal analysis. Permafrost and Periglacial Processes, vol. 13, p. 1–15.

Smith, S.L. Roy, L.-P., Lewkowicz, A.G. and Chartrand, J., 2017. Ground thermal data collection along the Alaska Highway corridor (KP1559–1895), Yukon, summer 2016. Geological Survey of Canada, Open File 8311, 29 p., https://doi.org/10.4095/306304.

Scenarios Network for Alaska + Arctic Planning (SNAP), 2021. Community Climate Charts. https://www.snap.uaf.edu/tools/community-charts, [accessed February 18, 2021].

Stephani, E., Fortier, D. and Shur, Y., 2010. Applications of cryofacies approach to frozen ground engineering – Case study of a road test site along the Alaska Highway (Beaver Creek, Yukon, Canada). GEO2010: 63rd Canadian Geotechnical Conference and 6th Canadian Permafrost Conference, Calgary, Canada.

Transportation Association of Canada (TAC), 2010. Guidelines for Development and Management of Transportation Infrastructure in Permafrost Regions. Transportation Association of Canada, Ottawa, ON. 177 p., https://www.tac-atc.ca/en/publications/ptm-permafrost.

Van Everdingen, R.O., 2005. Multi-language glossary of permafrost and related ground-ice terms, International Permafrost Association, Terminology Working Group, 90 p., https://globalcryospherewatch.org/reference/glossary_docs/Glossary_of_Permafrost_and_Ground-Ice_IPA_2005.pdf, [accessed February 26, 2021].

Vogt, N., 2021 (in prep). Influence of permafrost characteristics on vegetation change in Yukon and Northwest Territories, Canada. Unpublished Masters thesis, University of Alberta, Edmonton, Canada.

Wahl, H., 2004. Climate. *In*: Ecoregions of the Yukon Territory: Biophysical properties of Yukon landscapes, C.A.S. Smith, J.C. Meikle and C.F. Roots (eds.), Agriculture and Agri-Food Canada, PARC Technical Bulletin No. 04-01, Summerland, British Columbia, p. 19–23.

Wahl, H.E., Fraser, D.B., Harvey, R.C. and Maxwell, J.B., 1987. Climate of Yukon. Climatological Studies Number 40, Ottawa, Ontario, Atmospheric Environment Service, Environment Canada, 233 p.

Way, R.G. and Lewkowicz, A.G., 2015. Investigations of discontinuous permafrost in coastal Labrador with DC electrical resistivity tomography. I*n:* Proceedings of the 68th Canadian Geotechnical Conference & 7th Canadian Permafrost Conference. Canadian Geotechnical Society.

Wolfe, S.A., Burgess, M., Douma, M., Hyde, C. and Robinson, S., 1997. Geological and geophysical investigations of ground ice in glaciofluvial deposits, Slave Province, District of Mackenzie, Northwest Territories. *In:* Current Research 1997-C, Geological Survey of Canada, p. 39–50.

Yukon Energy, 2009. The History of Power in Yukon, https://yukonenergy.ca/about-us/news-events/the_history_of_power_in_yukon, [accessed February 1, 2021].

Yukon Geological Survey, 2021. Yukon Digital Bedrock Geology, http://www.geology.gov.yk.ca/update_yukon_bedrock_geology_map.html, [accessed January 28, 2021].

APPENDIX A – BOREHOLE LOGS

A1 Cowley Creek borehole log for CC_BH2, with volumetric excess ice content and grain size distribution.

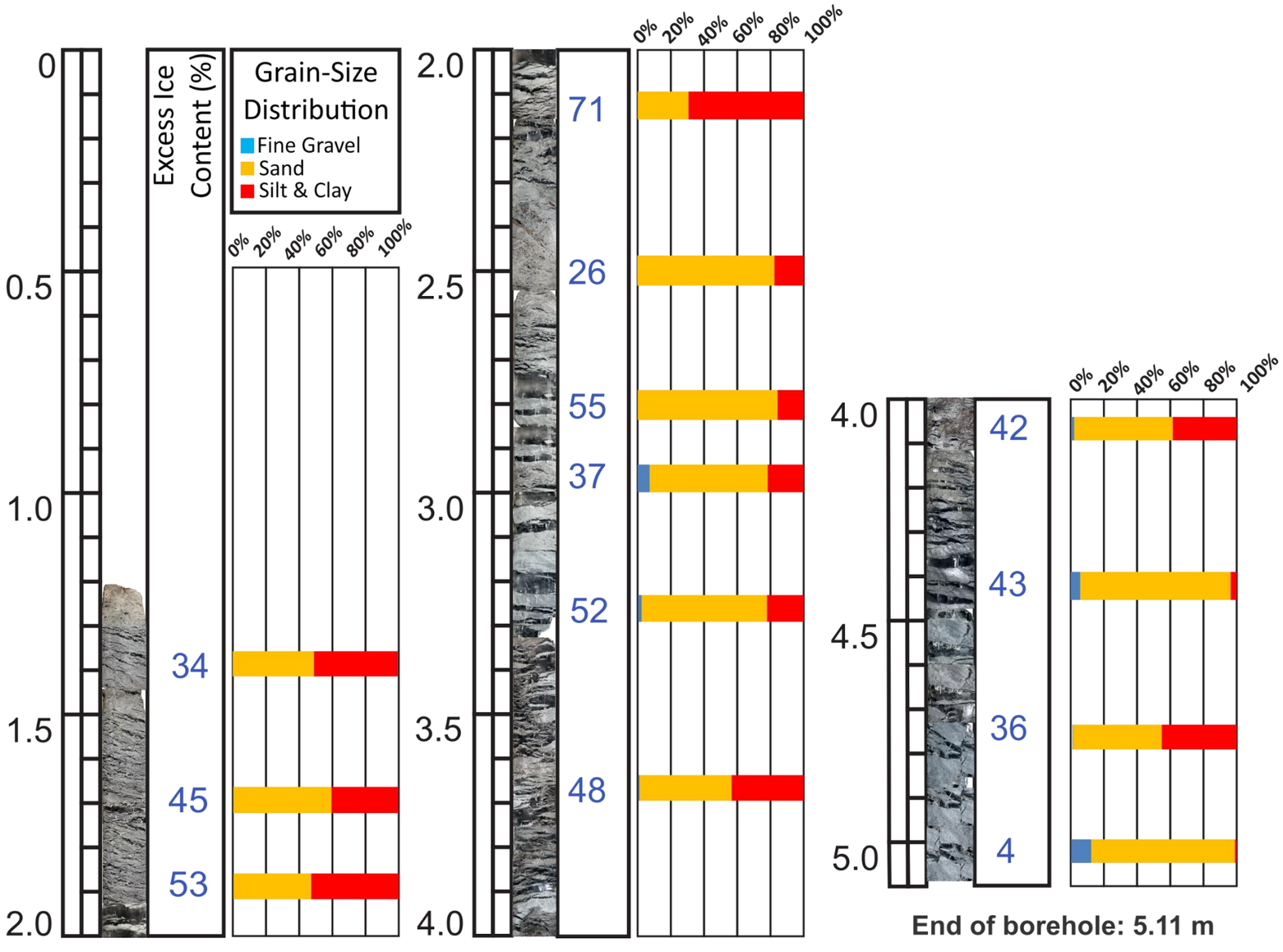

A2 Hamilton Boulevard borehole log for HB_BH1, with volumetric excess ice content and grain size distribution.

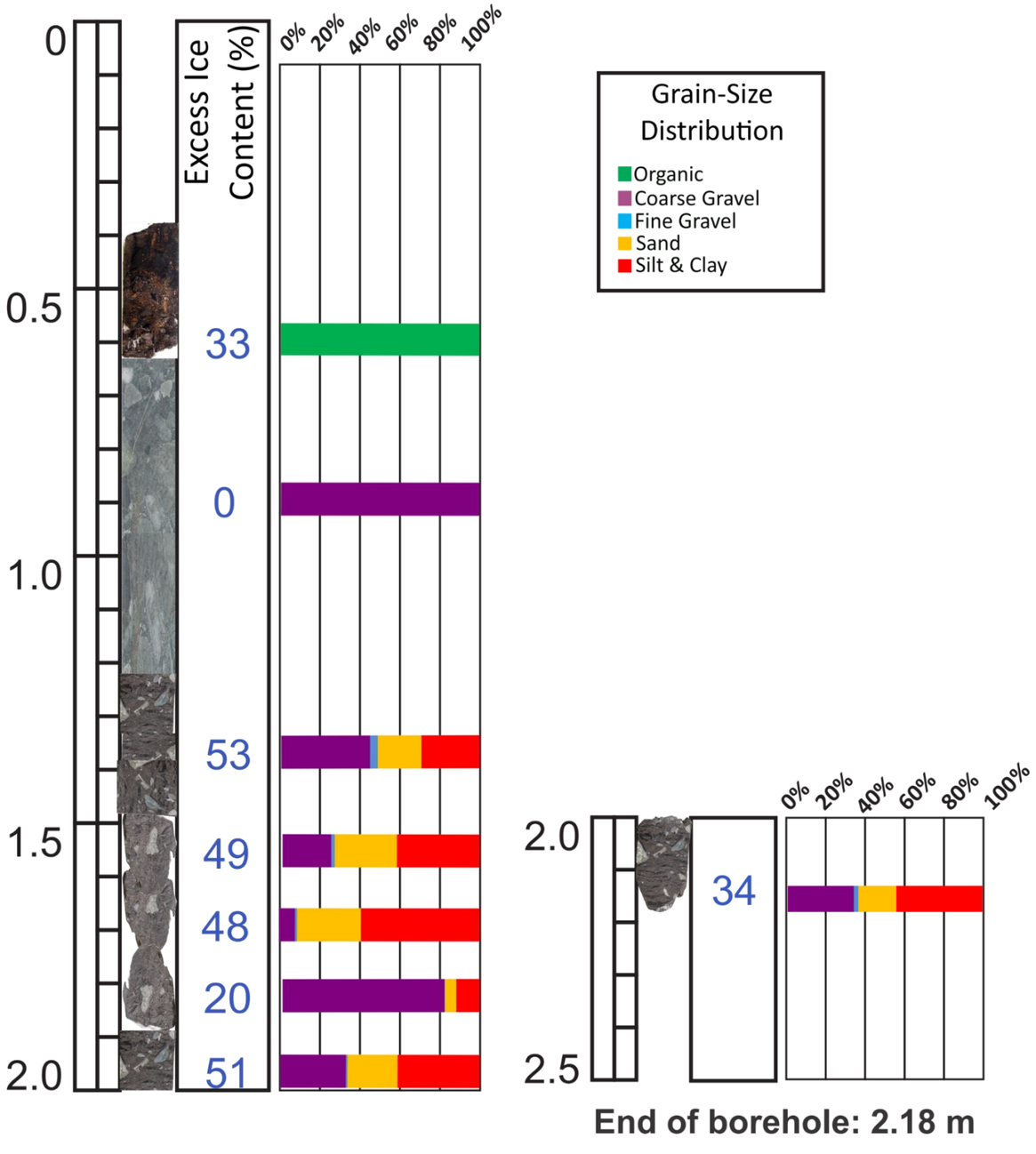

A3 Hidden Valley borehole log for HV_BH1, with volumetric excess ice content and grain size distribution.

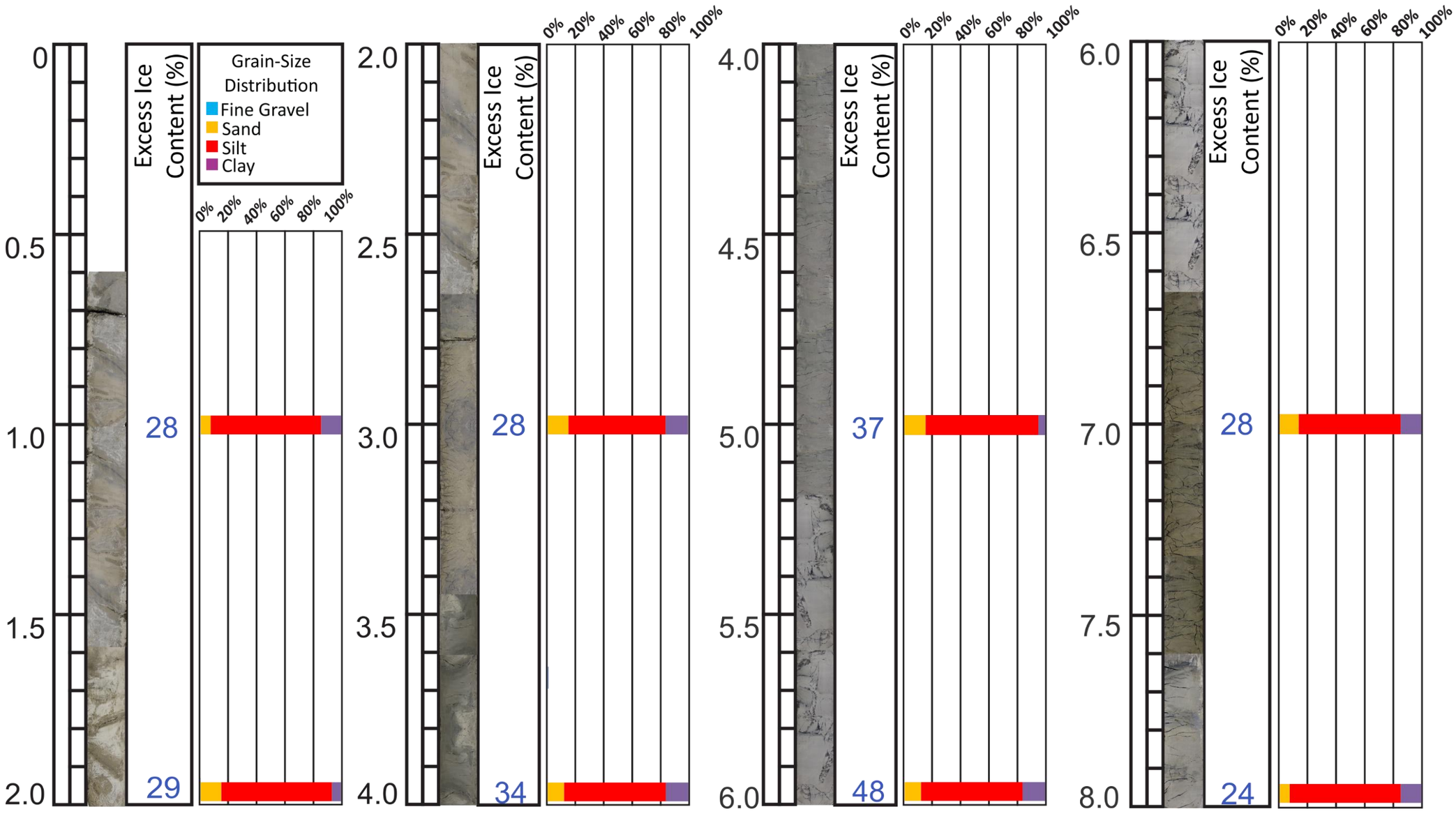

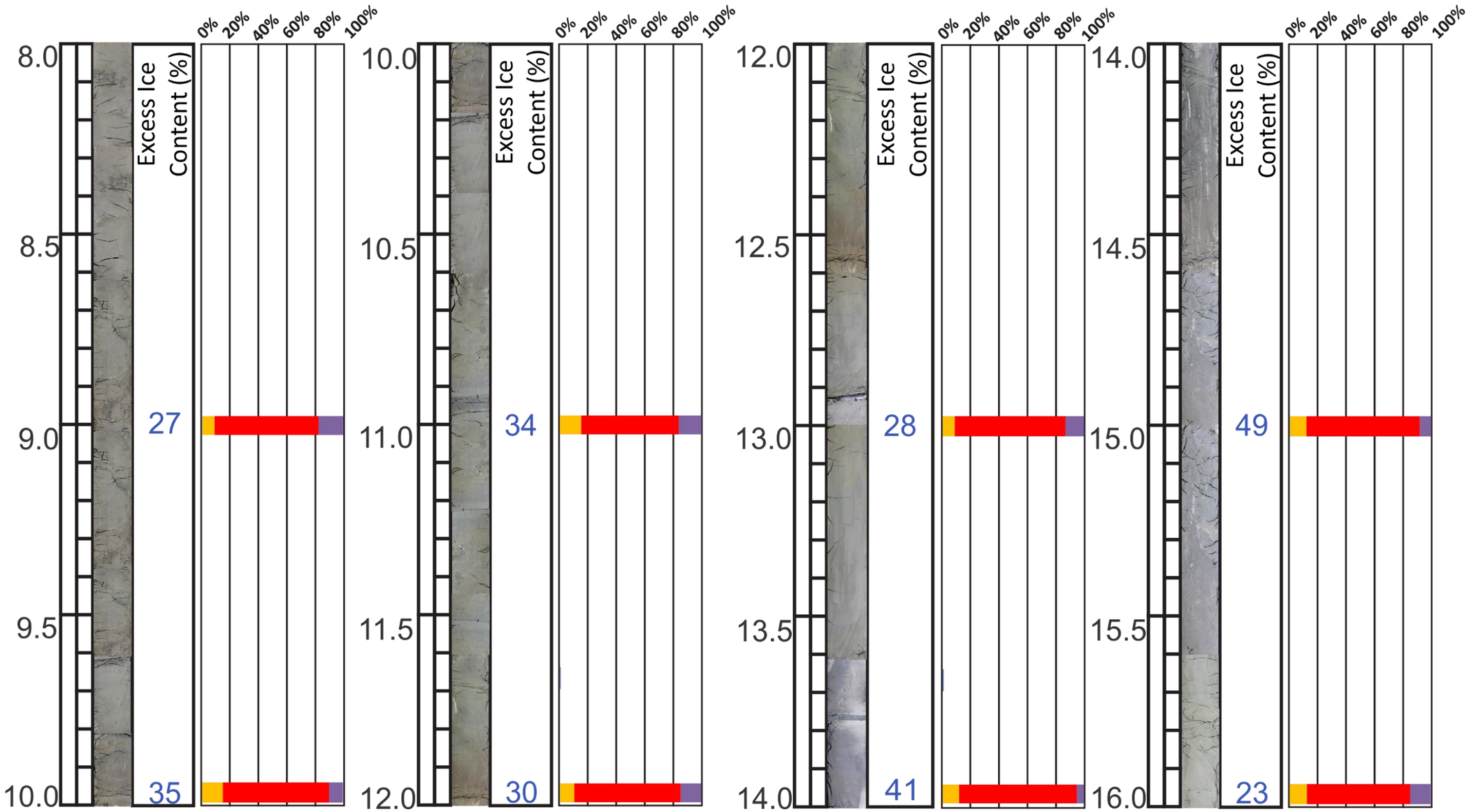
0%
20%
40%
60%
80%
100%
Excess Ice Content (%)
8.0
8.5
9.0
9.5
10.0
27
35
10.0
10.5
11.0
11.5
12.0
34
30
12.0
12.5
13.0
13.5
14.0
28
41
14.0
14.5
15.0
15.5
16.0
49
23

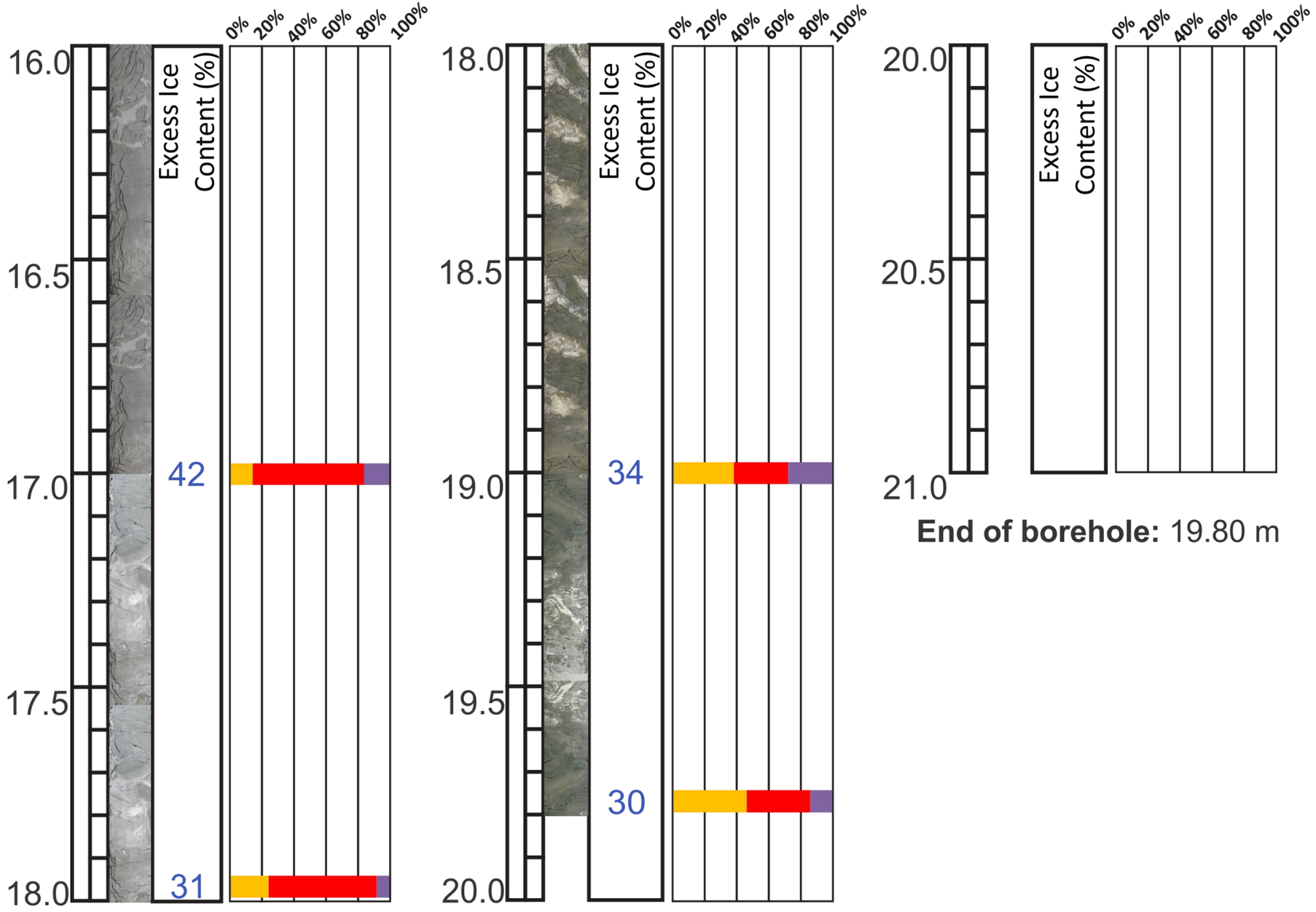

End of borehole: 19.80 m

A4 Ibex Valley borehole log for IV_BH1, with volumetric excess ice content and grain size distribution.

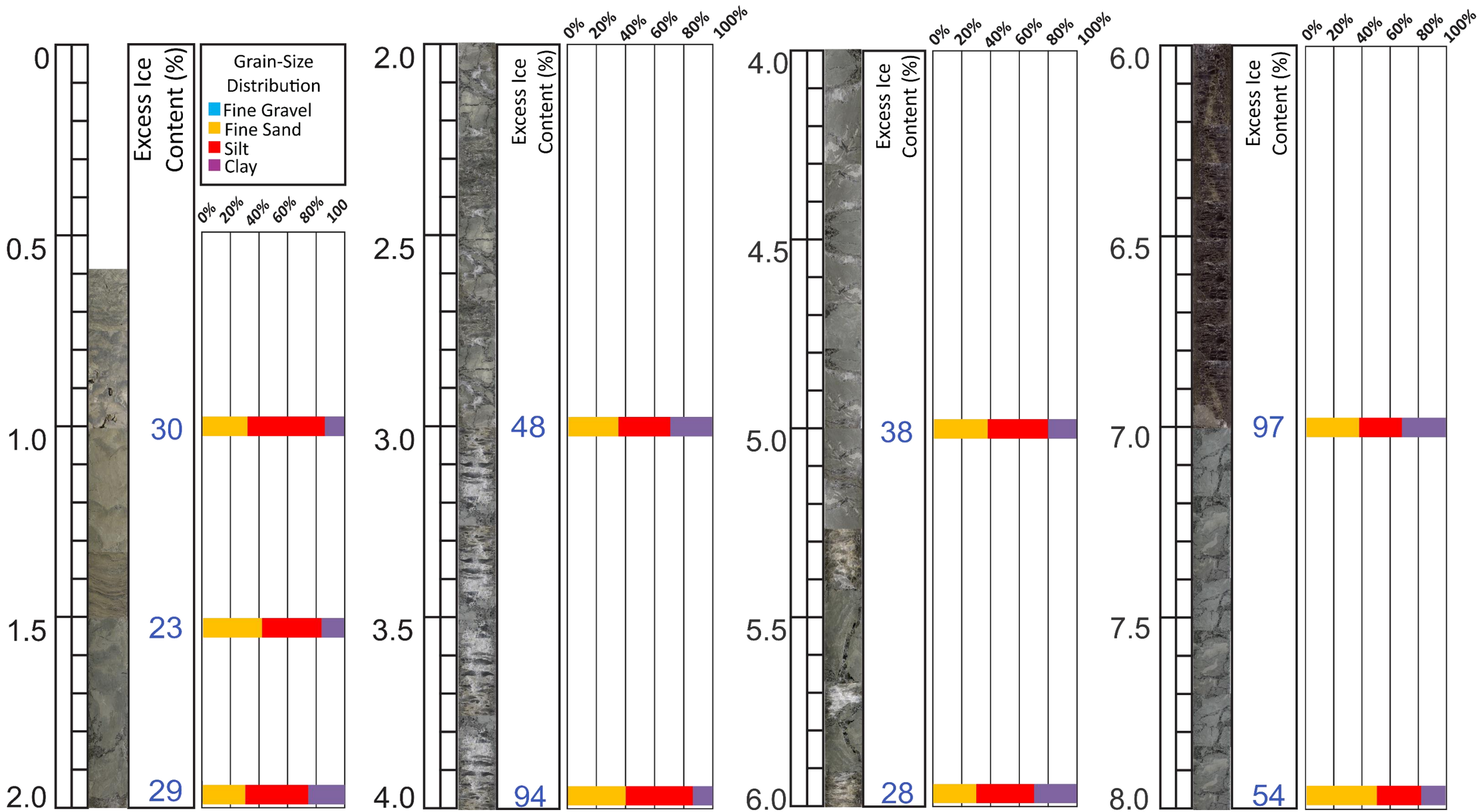

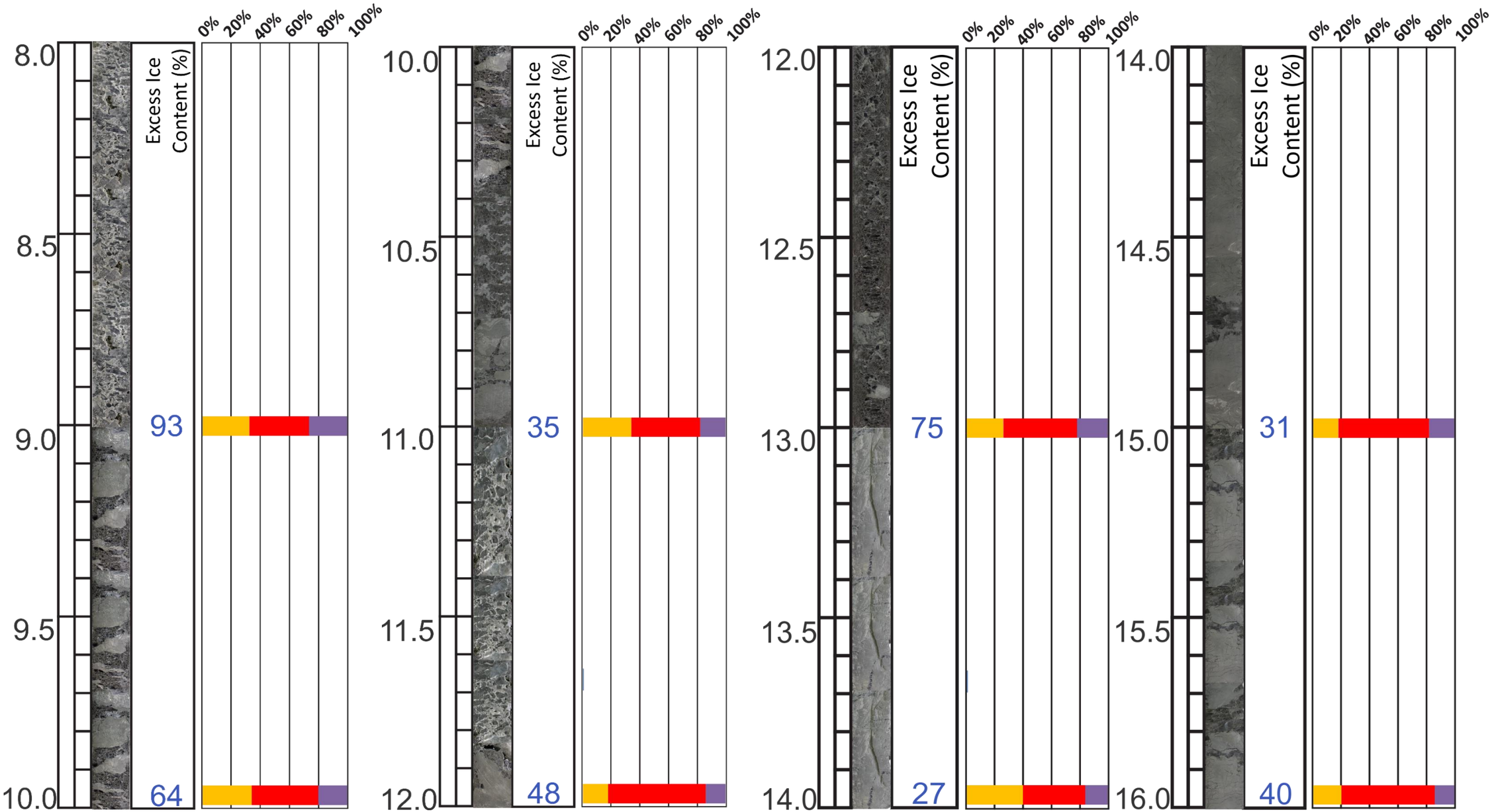
8.0
8.5
9.0
9.5
10.0
Excess Ice Content (%)
93
64
0%
20%
40%
60%
80%
100%
10.0
10.5
11.0
11.5
12.0
35
48
12.0
12.5
13.0
13.5
14.0
75
27
14.0
14.5
15.0
15.5
16.0
31
40

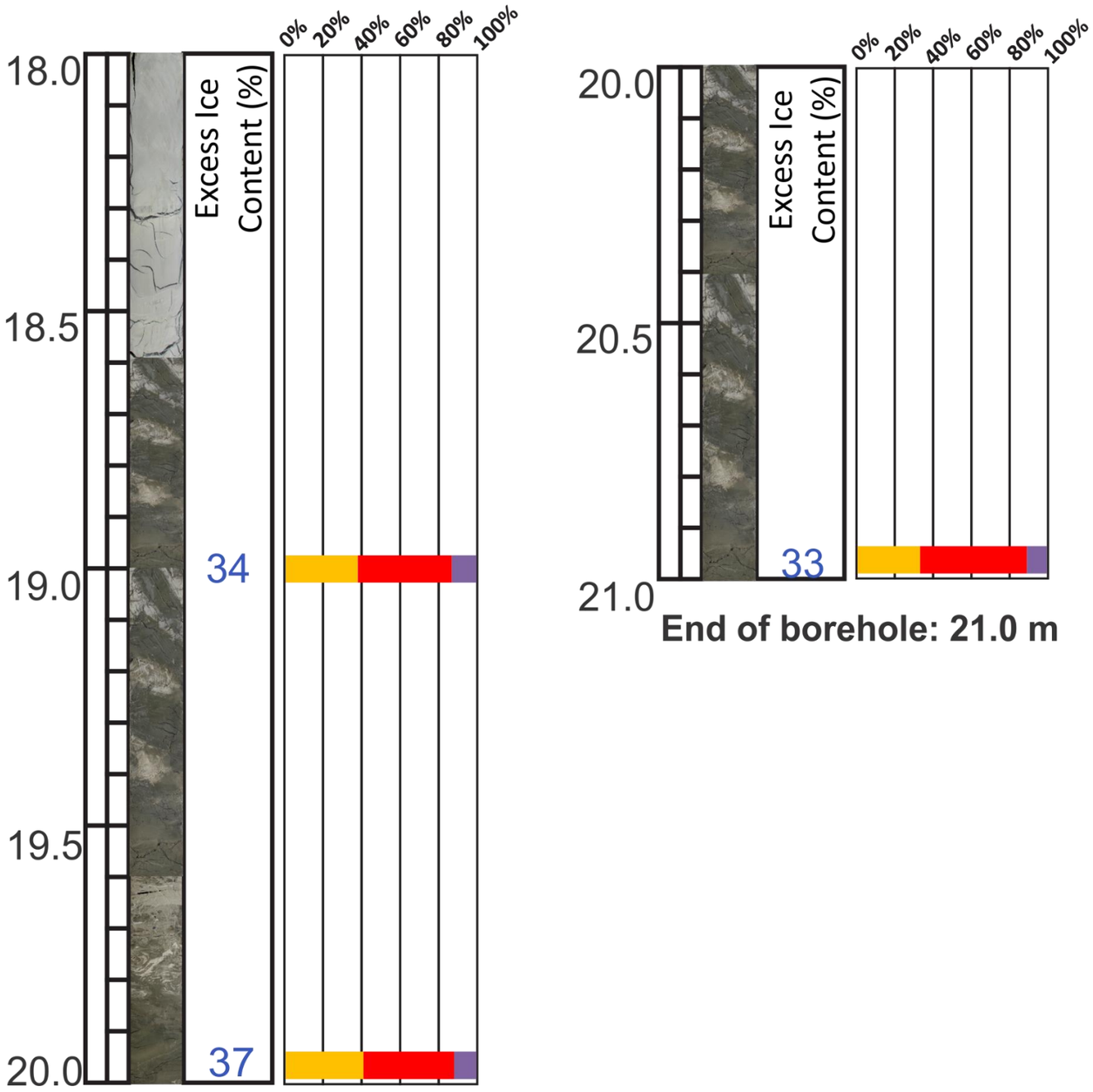
18.0
18.5
19.0
19.5
20.0
Excess Ice Content (%)
0%
20%
40%
60%
80%
100%
34
37
20.0
20.5
21.0
33
End of borehole: 21.0 m

A5 Takhini River Retrogressive Thaw Slump borehole log for WH_1456_BH1, with volumetric excess ice content and grain size distribution.

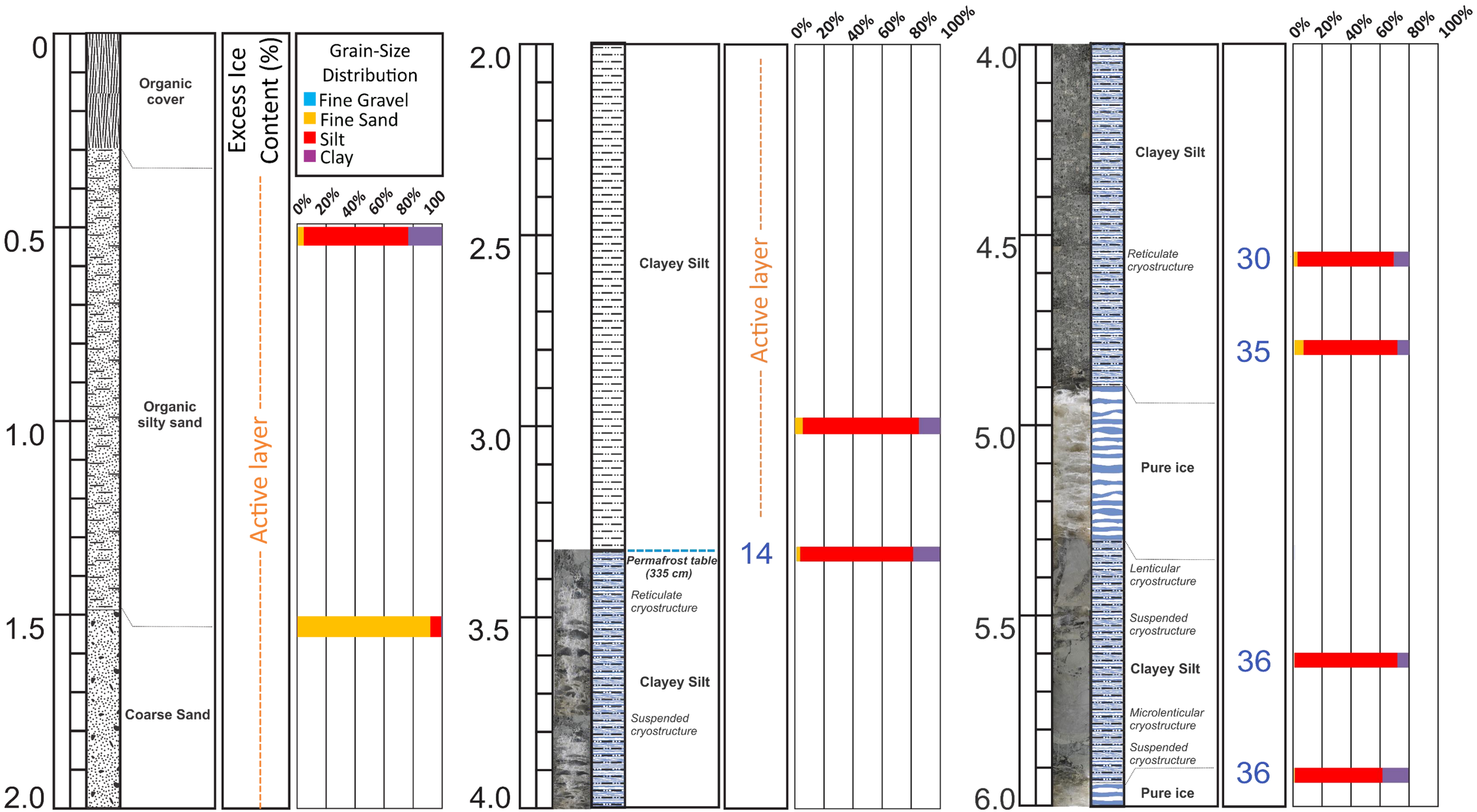

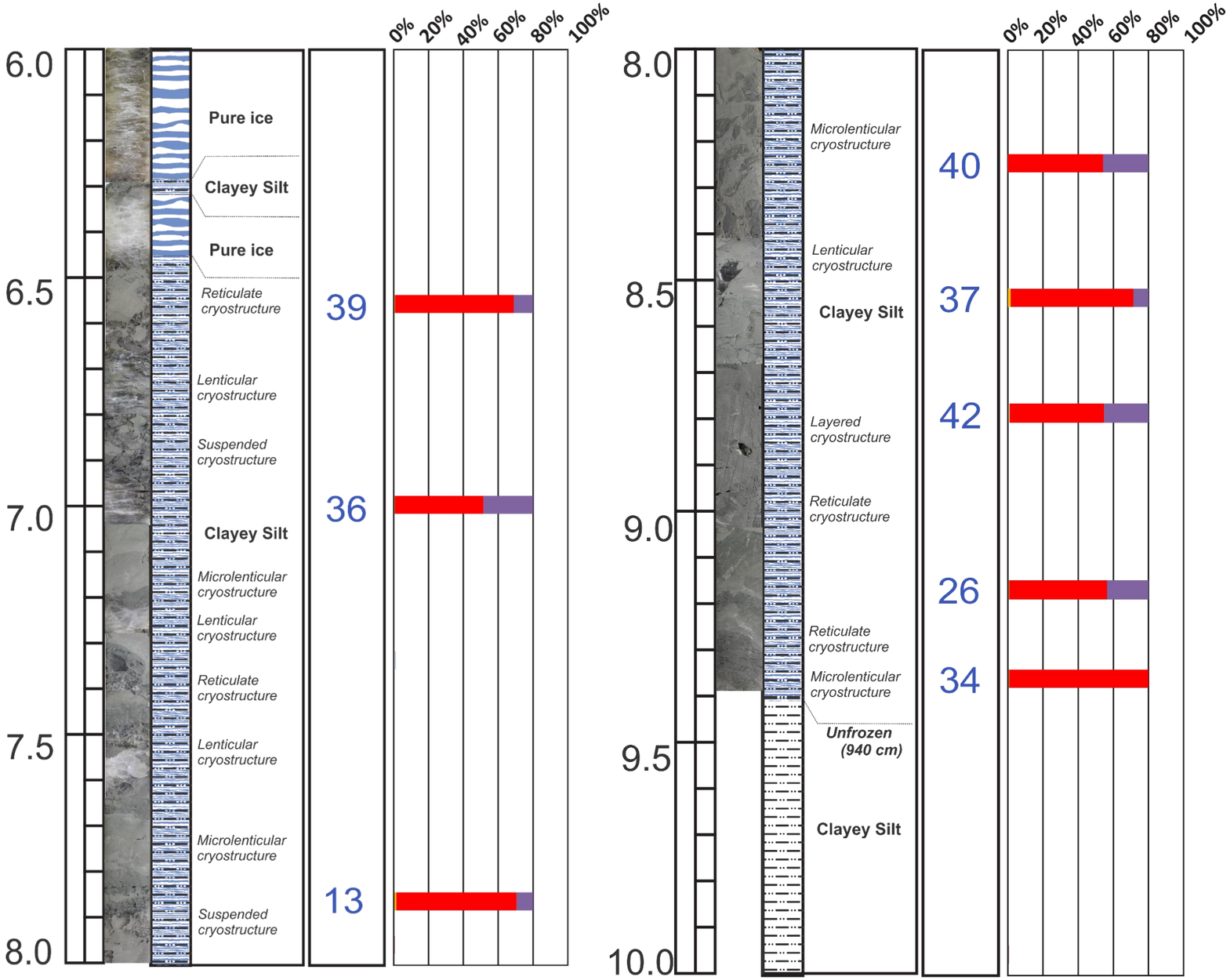

End of Borehole: 10 meters

A6 Takhini River Retrogressive Thaw Slump borehole log for WH_1456_BH3, with sediment type.

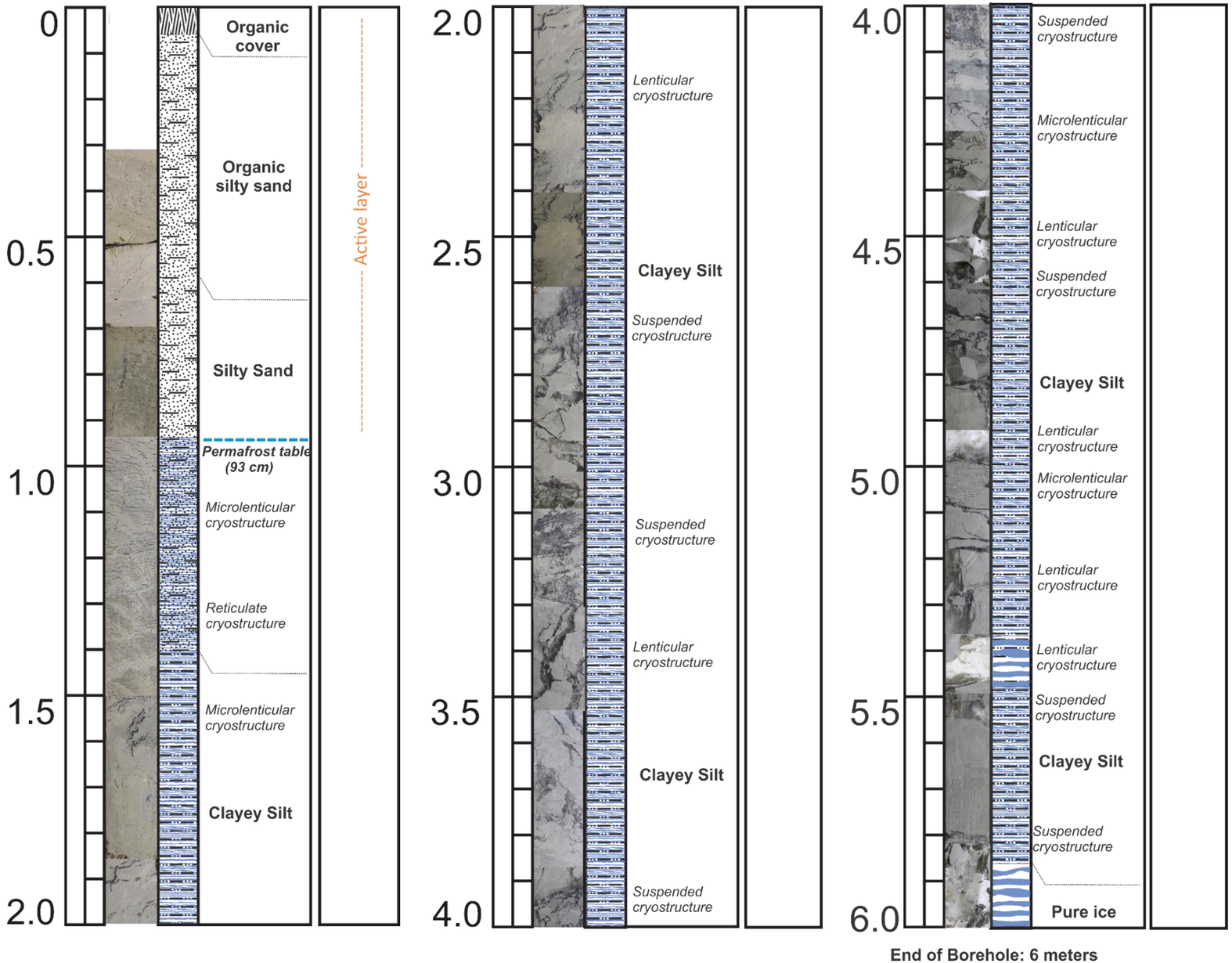

A7 Fish Lake borehole log for WH_FL_BH1, with sediment type.

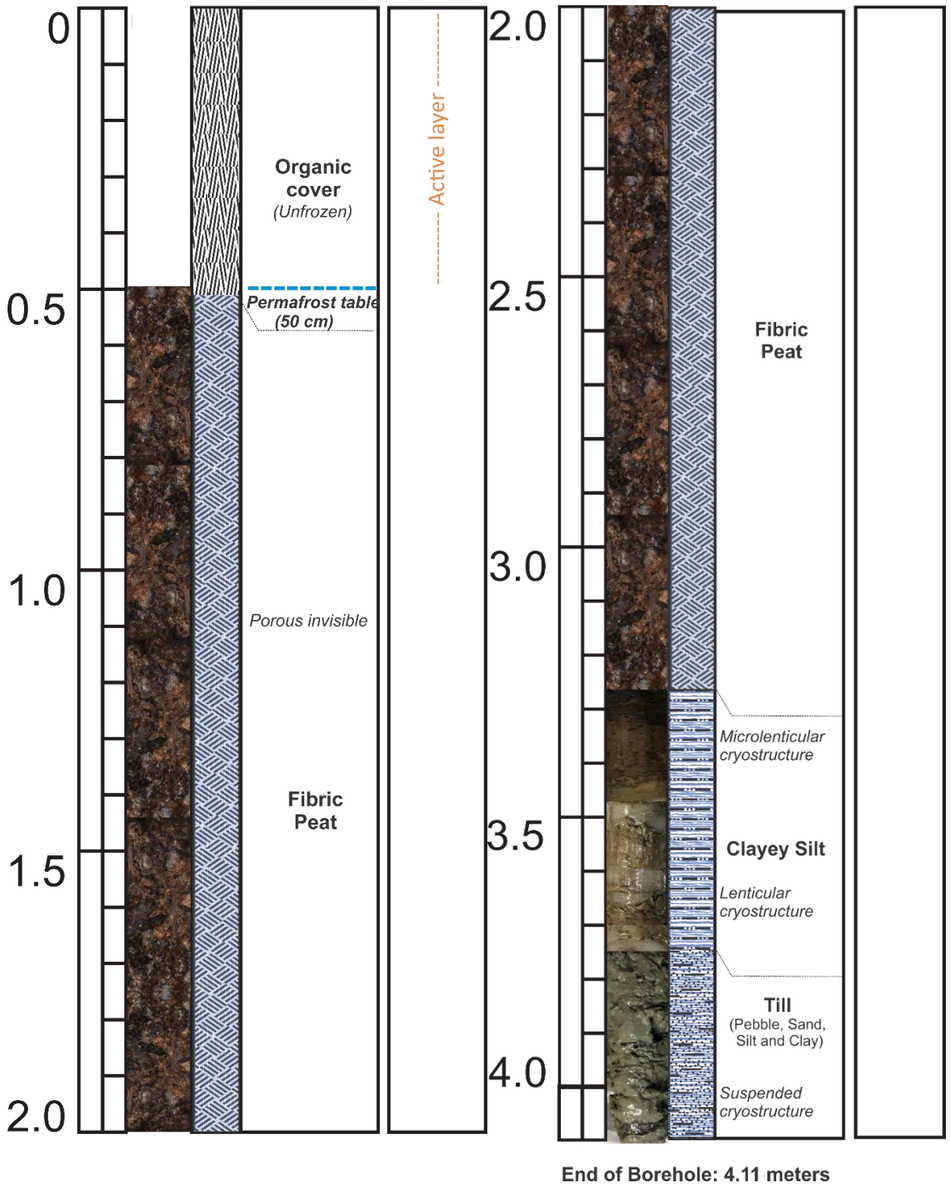

APPENDIX B – GROUND TEMPERATURE FIGURES

B1 Ground temperature profile for EBA_BH03 in 2013–2014 at Hamilton Boulevard (EBA , 2015).

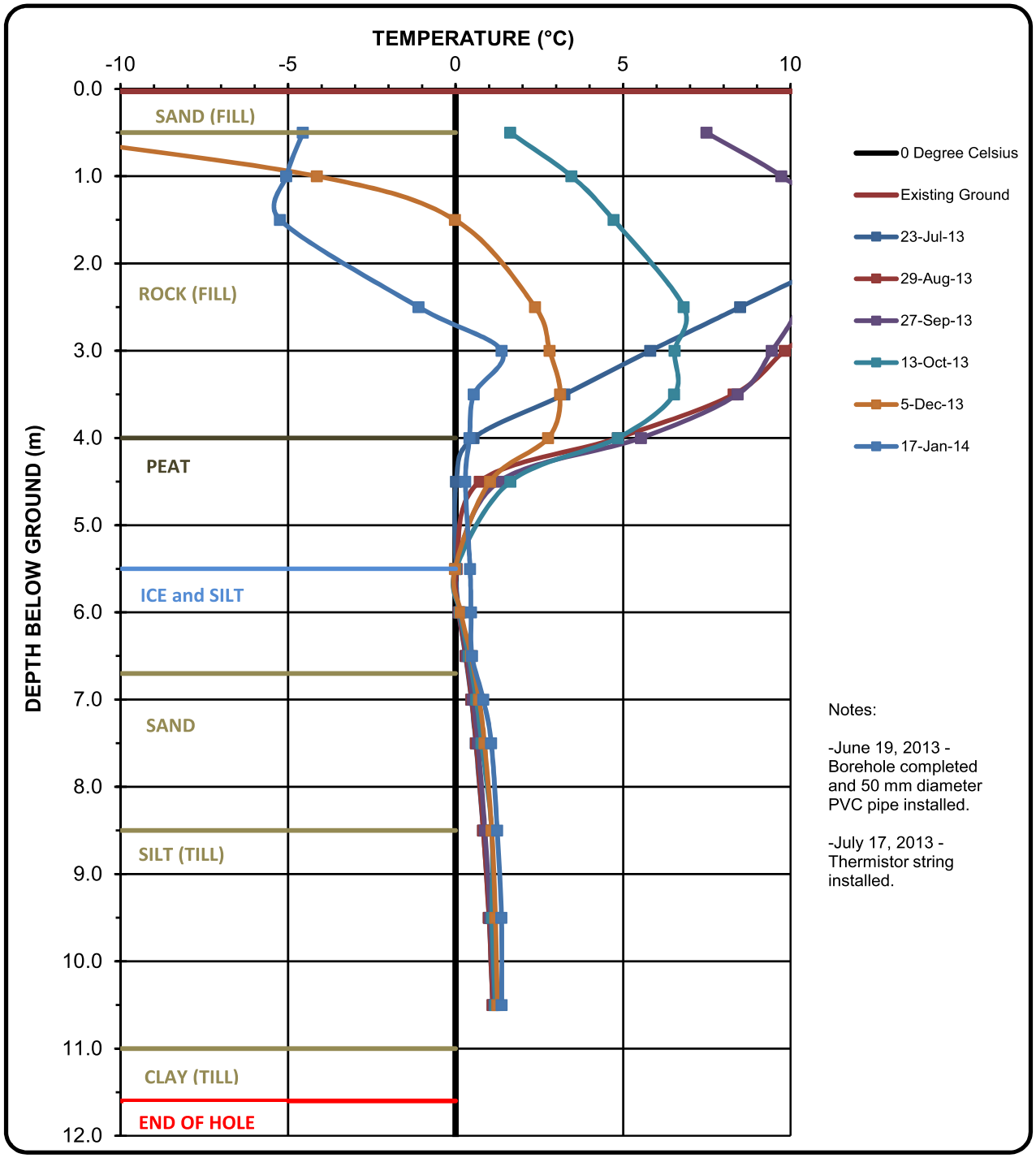

B2 Ground temperature profile for EBA_BH03 in 2015 at Hamilton Boulevard (EBA, 2015).

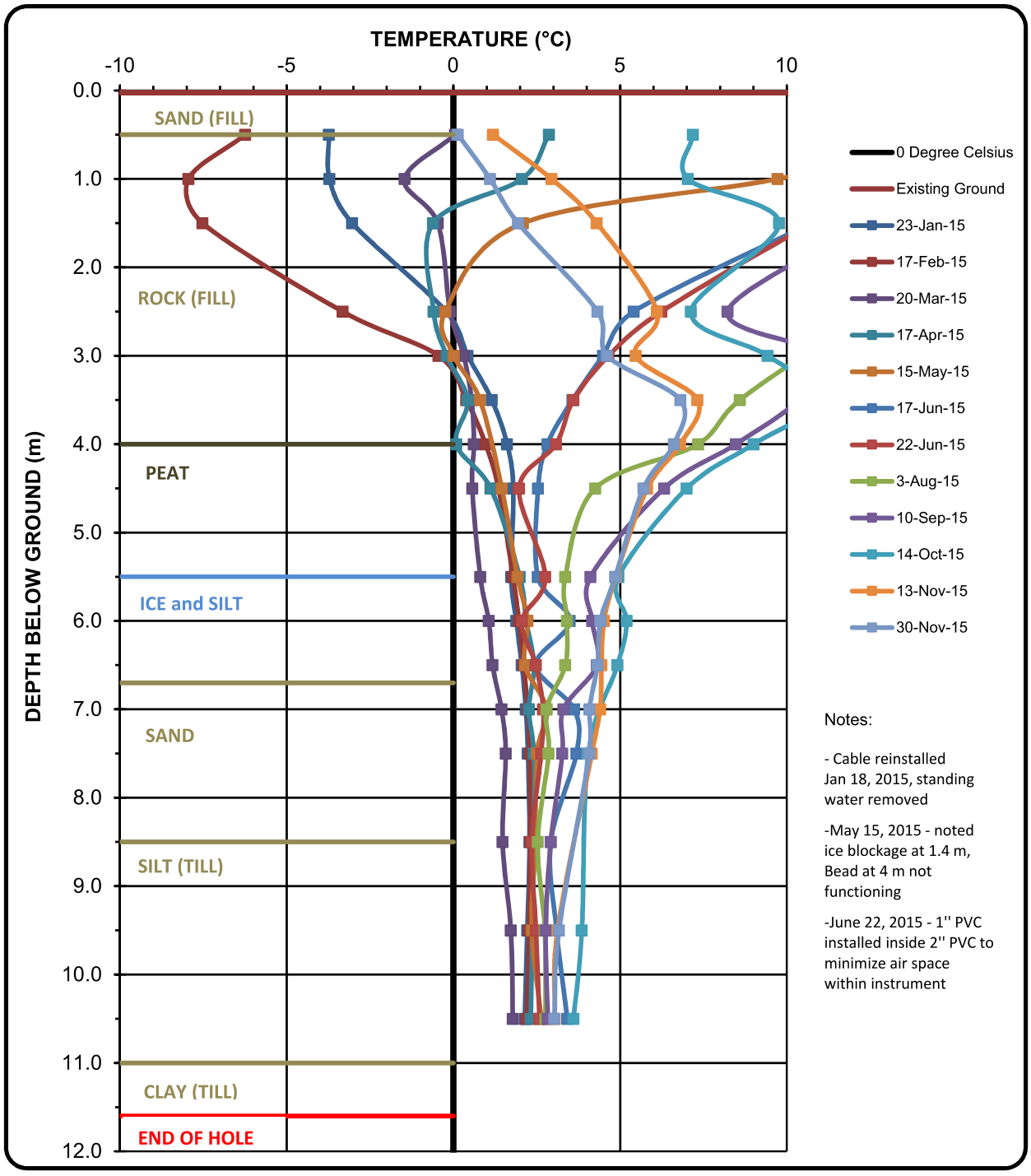

APPENDIX C – ERT FIGURES

C1 Hidden Valley S-N ERT profile (HV_ERT1) using (a) Wenner array, 4th iteration, and (b) dipole-dipole array, 5th iteration.

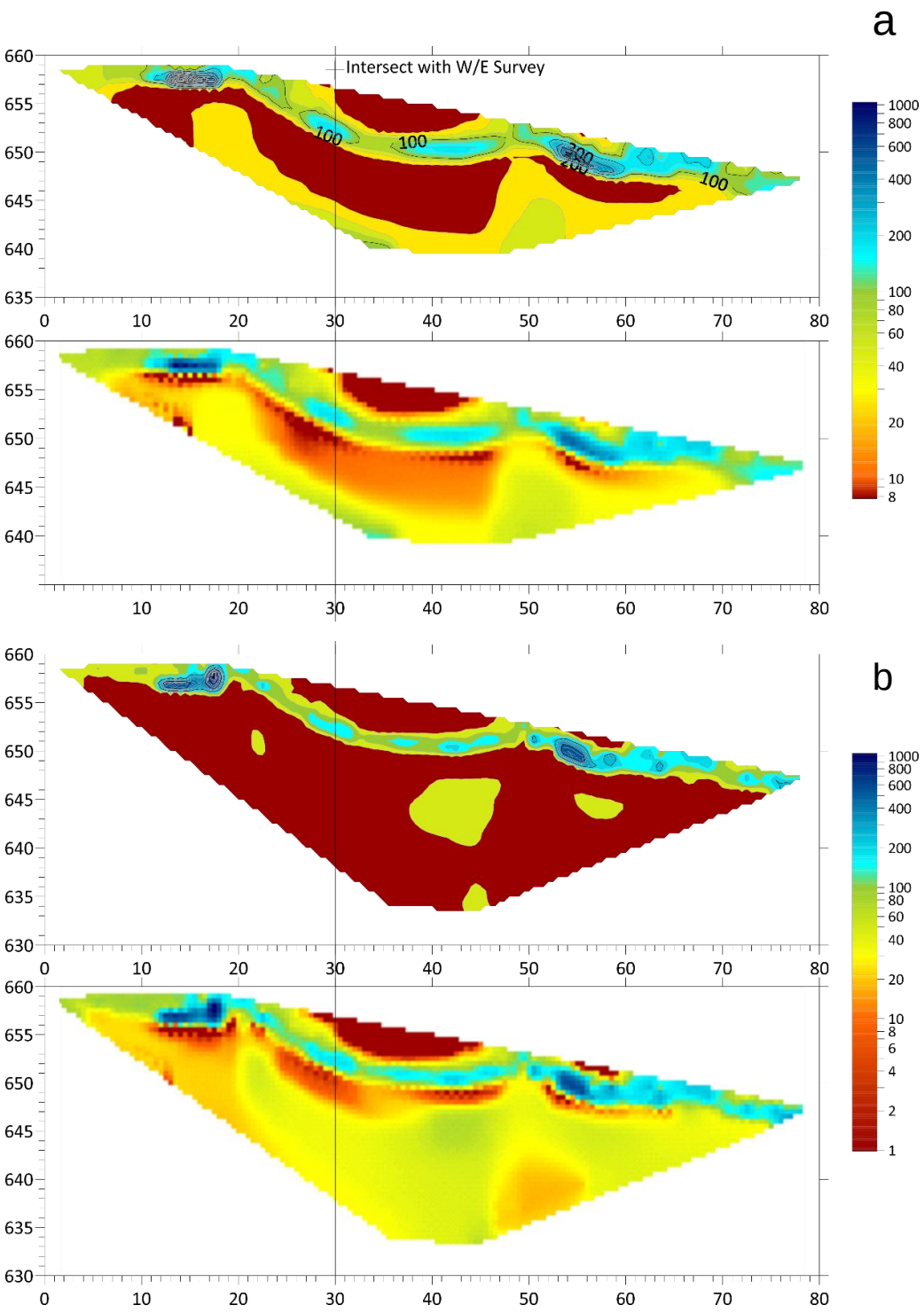

C2 Hidden Valley W-E ERT profile (HV_ERT2) using (a) Wenner array, 4th iteration, RMS error= 4.7%, and (b) dipole-dipole array, 3rd iteration, RMS error =9.4%.

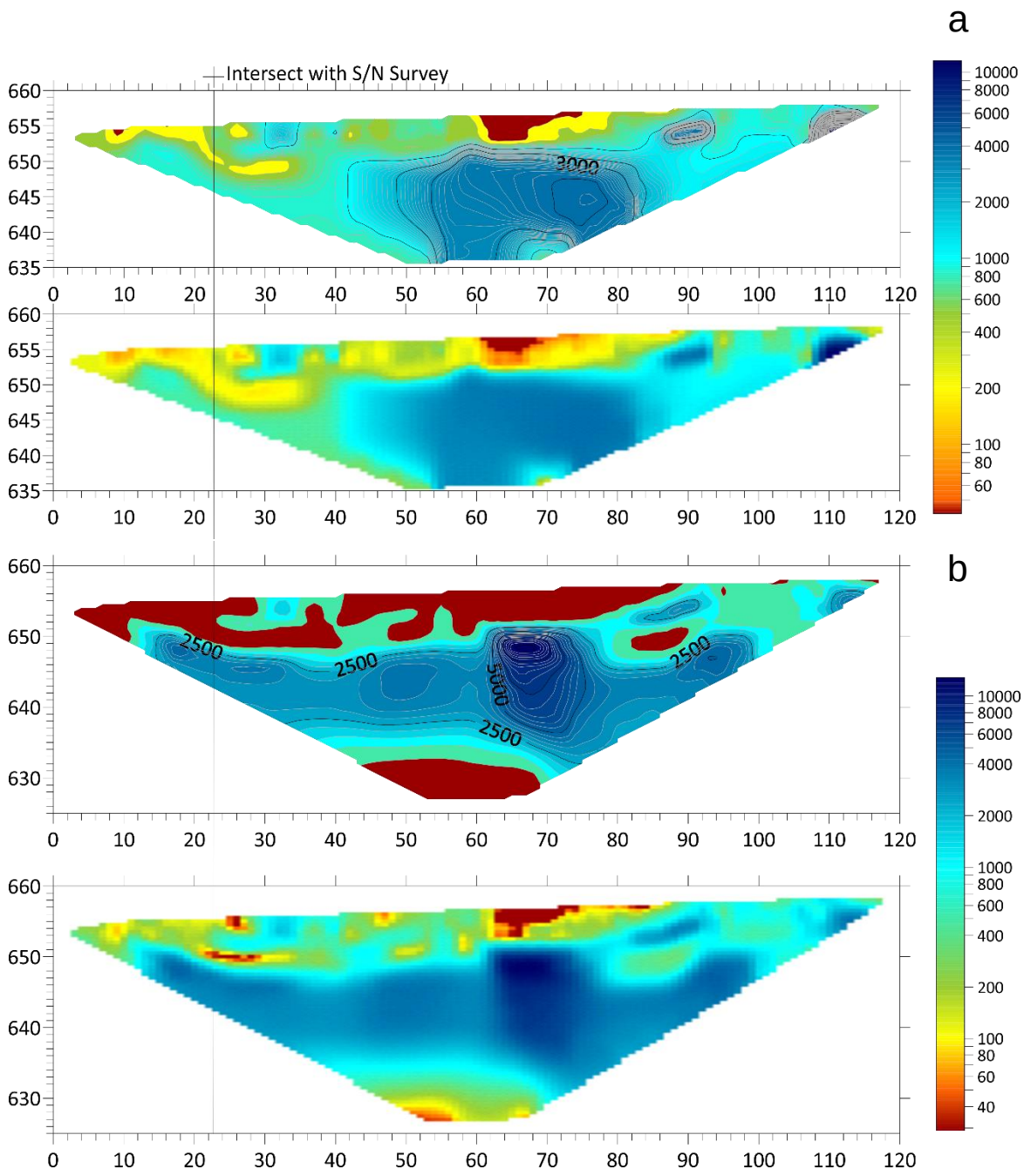

C3 Ibex Valley ERT profile at Burned site (IV_ERT2) using (a) Wenner array, 6th iteration, RMS error = 5.2% and (b) dipole-dipole array, 7th iteration, RMS error=3.0%.

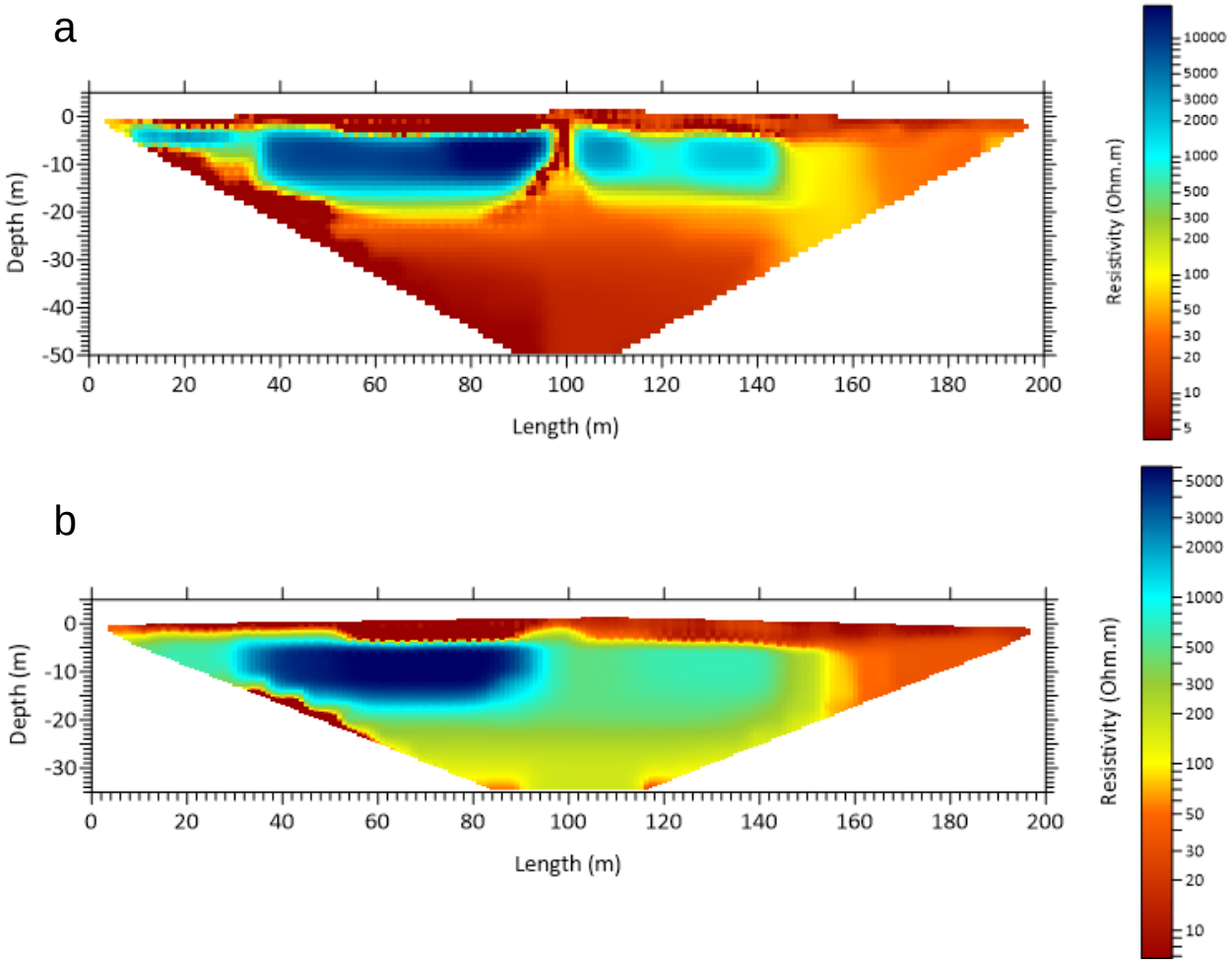

C4 Ibex Valley ERT profile at Forest site (IV_ERT1) using (a) Wenner array, 4th iteration, RMS error=4.8%, and (b) dipole-dipole array, 4th iteration, RMS error=7.1%.

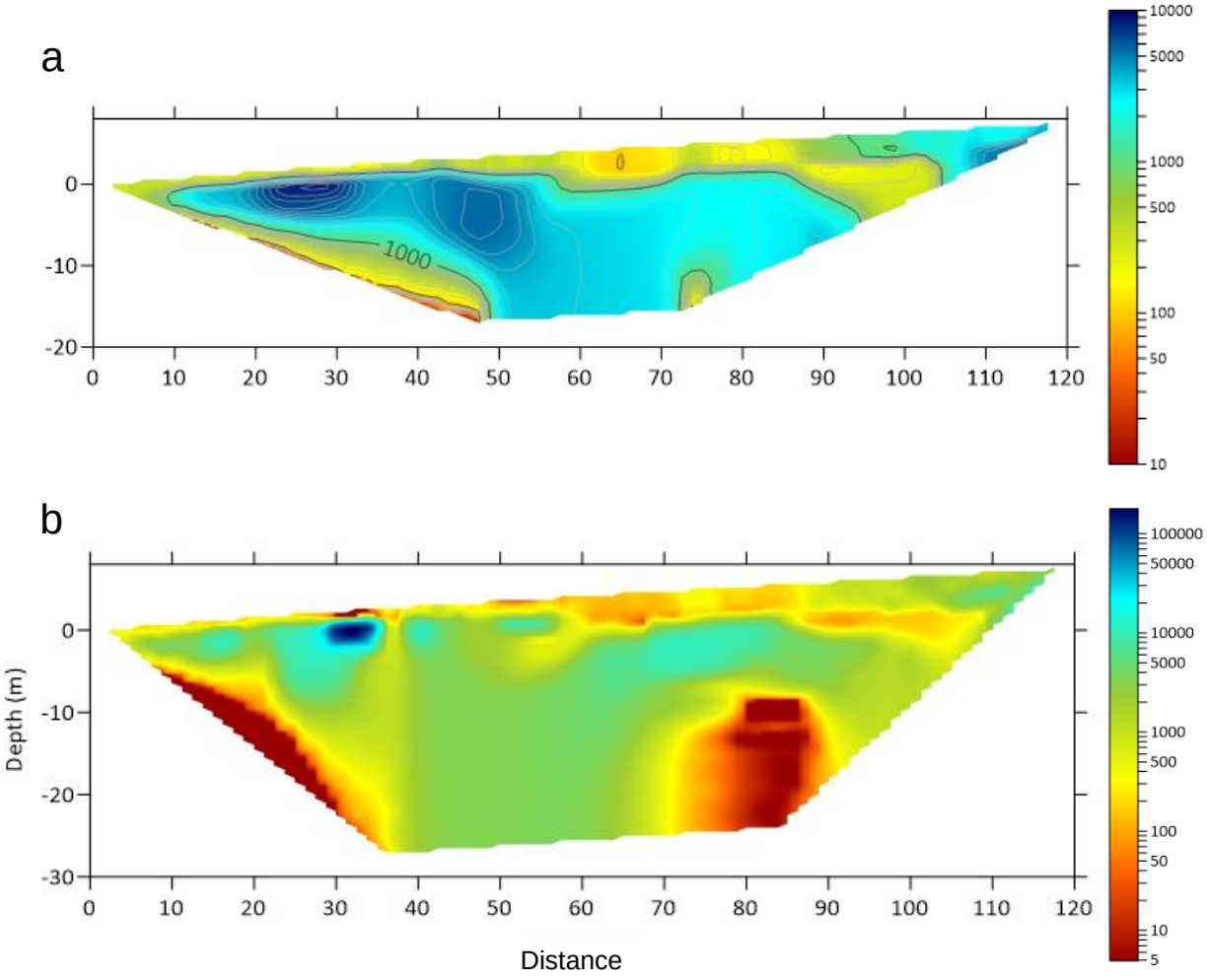

C5 Takhini River Retrogressive Thaw Slump E-W ERT profile (WH_1456_ERT1) using (a) Wenner array, 4th iteration, RMS error= 4.0%, and (b) dipole-dipole array, 4th iteration, RMS error= 3.1%.

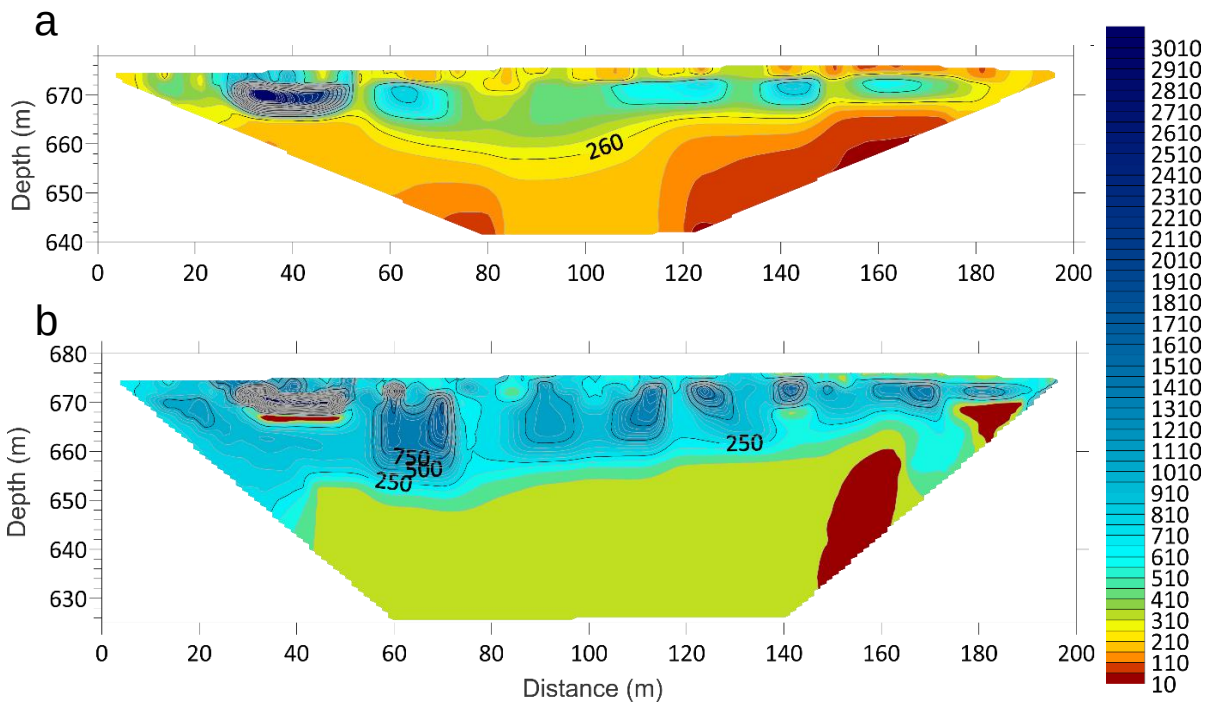

C6 Takhini River Retrogressive Thaw Slump E-W ERT profile (WH_1456_ERT2) using (a) Wenner array, 4th iteration, RMS error=4.0%, and (b) dipole-dipole array, 4th iteration, RMS error=3.1%.

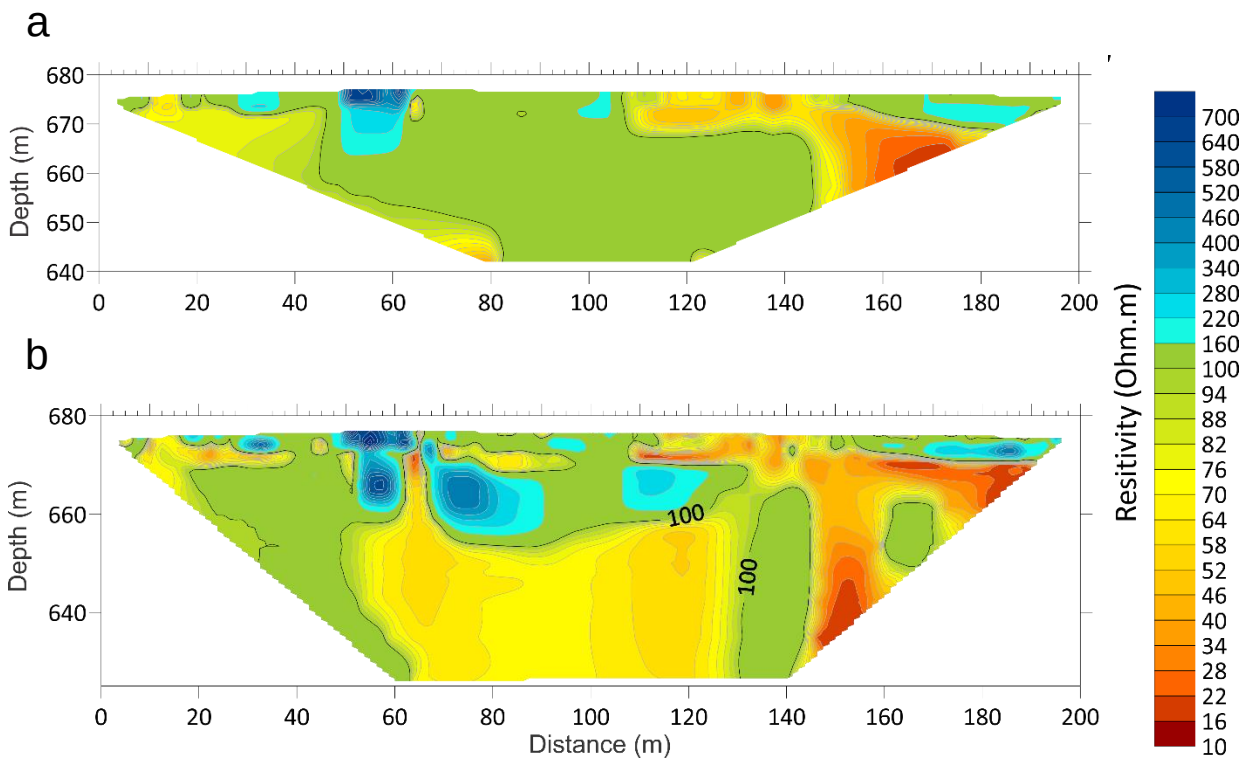

C7 Takhini River Retrogressive Thaw Slump ERT profile (WH_1456_ERT3) using dipole-dipole array, 5th iteration, RMS error=2.4%.

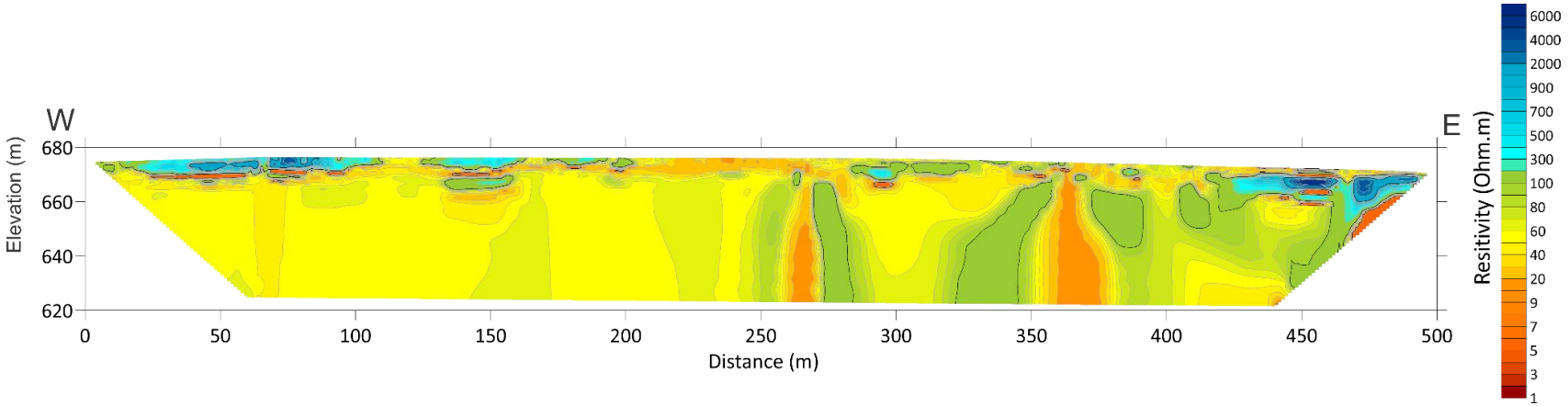

C8 Takhini River Retrogressive Thaw Slump ERT profile (WH_1456_ERT4) using dipole-dipole array, 5th iteration, RMS error=4.1%.

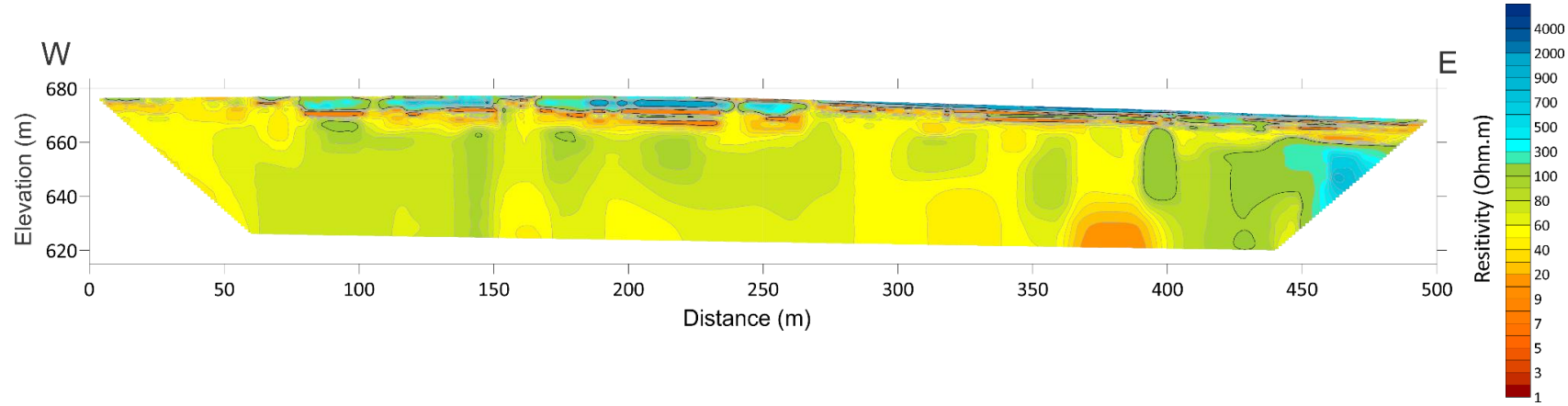

APPENDIX D – LABORATORY RESULTS

D1 Cowley Creek grain-size analysis results at CC_BH1. Analysis completed on the 16-17 November 2018 and compiled with Gradistat.

Cowley Creek sediment type (CC_BH1)

Sample Depth	Sieving Error	Sample Type	Textural Group	Sediment Type
1.46 m	1%	Bimodal, Moderately Sorted	Slightly Gravelly Muddy Sand	Slightly Very Fine Gravelly Very Coarse Silty Very Fine Sand
1.72 m	0%	Trimodal, Moderately Sorted	Muddy Sand	Very Coarse Silty Very Fine Sand
1.97 m	0%	Trimodal, Moderately Sorted	Slightly Gravelly Sandy Mud	Slightly Very Fine Gravelly Very Fine Sandy Very Coarse Silt
2.18 m	0%	Bimodal, Moderately Sorted	Slightly Gravelly Sandy Mud	Slightly Very Fine Gravelly Very Fine Sandy Very Coarse Silt
2.55 m	0%	Polymodal, Poorly Sorted	Slightly Gravelly Muddy Sand	Slightly Very Fine Gravelly Very Coarse Silty Fine Sand
2.87 m	0%	Trimodal, Poorly Sorted	Slightly Gravelly Muddy Sand	Slightly Very Fine Gravelly Very Coarse Silty Very Fine Sand
3.00 m	0%	Polymodal, Poorly Sorted	Gravelly Muddy Sand	Very Fine Gravelly Very Coarse Silty Very Fine Sand
3.34 m	0%	Polymodal, Poorly Sorted	Slightly Gravelly Muddy Sand	Slightly Very Fine Gravelly Very Coarse Silty Very Fine Sand
3.72 m	0%	Polymodal, Poorly Sorted	Slightly Gravelly Muddy Sand	Slightly Very Fine Gravelly Very Coarse Silty Very Fine Sand
4.07 m	0%	Polymodal, Poorly Sorted	Slightly Gravelly Muddy Sand	Slightly Very Fine Gravelly Very Coarse Silty Very Fine Sand
4.36 m	0%	Polymodal, Poorly Sorted	Gravelly Sand	Very Fine Gravelly Very Fine Sand
4.74 m	0%	Trimodal, Poorly Sorted	Slightly Gravelly Muddy Sand	Slightly Very Fine Gravelly Very Coarse Silty Very Fine Sand
5.11 m	0%	Polymodal, Poorly Sorted	Gravelly Sand	Fine Gravelly Very Fine Sand

Cowley Creek grain-size distribution (CC_BH1)

Size Class	Grain Size (mm)	1.46 m	1.72 m	1.97 m	2.18 m	2.55 m	2.87 m	3.00 m	3.34 m	3.72 m	4.07 m	4.36 m	4.74 m	5.11 m
very coarse gravel (%)	32 to 64	0.00	0.00	0.00	0.00	0.00	0.00	0.00	0.00	0.00	0.00	0.00	0.00	0.00
coarse gravel (%)	16 to 32	0.00	0.00	0.00	0.00	0.00	0.00	0.00	0.00	0.00	0.00	0.00	0.00	0.00
medium gravel (%)	8 to 16	0.00	0.00	0.00	0.00	0.00	0.00	0.00	0.00	0.00	0.00	0.00	0.00	0.00
fine gravel (%)	4 to 8	0.00	0.00	0.00	0.00	0.00	0.00	0.20	0.00	0.00	0.00	2.00	0.00	6.10
very fine gravel (%)	2 to 4	0.36	0.00	0.07	0.36	0.60	0.89	6.32	1.97	0.52	1.35	3.19	0.37	4.72
very coarse sand (%)	1 to 2	0.93	0.58	0.67	1.52	1.36	3.66	9.64	5.66	1.93	4.95	9.21	1.52	11.05
coarse sand (%)	0.5 to 1	1.40	2.09	2.60	3.03	5.39	6.21	10.03	9.69	6.37	7.90	14.06	3.91	15.94
medium sand (%)	0.25 to 0.5	4.27	8.04	6.39	4.73	18.08	8.71	10.12	12.60	14.84	12.99	17.17	11.20	19.28
fine sand (%)	0.125 to 0.25	15.03	23.69	14.38	8.67	34.69	19.42	12.48	19.59	15.06	17.63	19.28	18.75	17.00
very fine sand (%)	0.063 to 0.125	28.85	26.08	24.27	14.87	22.97	46.39	31.98	29.99	19.52	18.97	31.87	20.22	24.95
very coarse silt (%)	0.031 to 0.063	49.16	39.52	51.62	66.82	16.90	14.72	19.22	20.51	41.75	36.21	3.22	44.03	0.94
coarse silt (%)	0.016 to 0.031	0.00	0.00	0.00	0.00	0.00	0.00	0.00	0.00	0.00	0.00	0.00	0.00	0.00
medium silt (%)	0.008 to 0.016	0.00	0.00	0.00	0.00	0.00	0.00	0.00	0.00	0.00	0.00	0.00	0.00	0.00
fine silt (%)	0.004 to 0.008	0.00	0.00	0.00	0.00	0.00	0.00	0.00	0.00	0.00	0.00	0.00	0.00	0.00
very fine silt (%)	0.002 to 0.004	0.00	0.00	0.00	0.00	0.00	0.00	0.00	0.00	0.00	0.00	0.00	0.00	0.00
clay (%)	0.00006 to 0.002	0.00	0.00	0.00	0.00	0.00	0.00	0.00	0.00	0.00	0.00	0.00	0.00	0.00
gravel (%)		0.36	0.00	0.07	0.36	0.60	0.89	6.53	1.97	0.52	1.35	5.19	0.37	10.82
sand (%)		50.48	60.48	48.31	32.81	82.50	84.40	74.25	77.52	57.73	62.44	91.59	55.60	88.23
mud (%)		49.16	39.52	51.62	66.82	16.90	14.72	19.22	20.51	41.75	36.21	3.22	44.03	0.94

Cowley Creek grain-size distribution curve (CC_BH1)

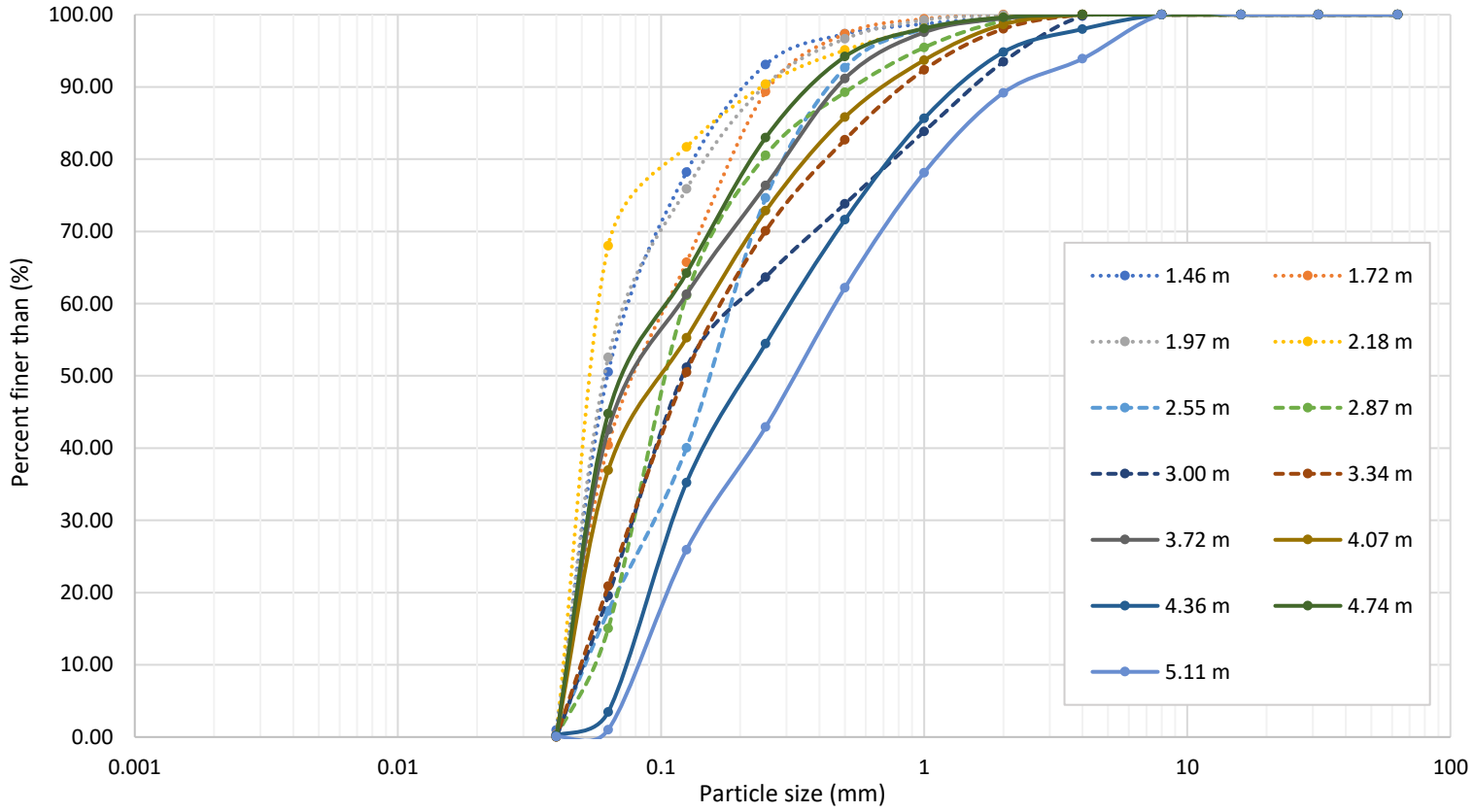

D2 Hamilton Boulevard grain-size analysis results at HB_BH1. Analysis was completed on 15 March 2020 and compiled with Gradistat.

Hamilton Boulevard sediment type (HB_BH1)

Sample Depth	Sieving Error	Sample Type	Textural Group	Sediment Type
1.40 m	0.0%	Bimodal, Very Poorly Sorted	Muddy Gravel	Coarse Silty Fine Gravel
1.58 m	0.0%	Trimodal, Very Poorly Sorted	Gravelly Mud	Fine Gravelly Coarse Silt
1.73 m	0.0%	Trimodal, Very Poorly Sorted	Gravelly Mud	Fine Gravelly Coarse Silt
1.85 m	0.0%	Unimodal, Very Poorly Sorted	Gravel	Fine Gravel
2.00 m	0.0%	Trimodal, Very Poorly Sorted	Muddy Gravel	Coarse Silty Fine Gravel
2.18 m	0.0%	Bimodal, Very Poorly Sorted	Muddy Gravel	Coarse Silty Fine Gravel

Hamilton Boulevard grain-size distribution (HB_BH1)

Size Class	Grain Size (mm)	1.40 m	1.58 m	1.73 m	1.85 m	2.00 m	2.18 m
very coarse gravel (%)	32 to 64	0.00	0.00	0.00	0.00	0.00	0.00
coarse gravel (%)	16 to 32	0.00	0.00	0.00	0.00	0.00	0.00
medium gravel (%)	8 to 16	0.00	0.00	0.00	0.00	0.00	0.00
fine gravel (%)	4 to 8	43.87	23.99	7.93	82.10	32.64	33.55
very fine gravel (%)	2 to 4	3.82	1.83	0.99	0.24	0.86	2.42
very coarse sand (%)	1 to 2	2.09	2.71	1.20	0.25	0.95	1.07
coarse sand (%)	0.5 to 1	2.78	3.75	2.77	0.55	2.05	1.19
medium sand (%)	0.25 to 0.5	3.77	5.21	5.79	1.03	4.67	2.69
fine sand (%)	0.125 to 0.25	4.97	6.83	8.01	1.59	7.40	5.38
very fine sand (%)	0.063 to 0.125	10.04	15.06	15.03	2.54	10.73	10.00
very coarse silt (%)	0.031 to 0.063	0.00	0.00	0.00	0.00	0.00	0.00
coarse silt (%)	0.016 to 0.031	28.66	40.62	58.28	11.70	40.69	43.70
medium silt (%)	0.008 to 0.016	0.00	0.00	0.00	0.00	0.00	0.00
fine silt (%)	0.004 to 0.008	0.00	0.00	0.00	0.00	0.00	0.00
very fine silt (%)	0.002 to 0.004	0.00	0.00	0.00	0.00	0.00	0.00
clay (%)	0.00006 to 0.002	0.00	0.00	0.00	0.00	0.00	0.00
gravel (%)		47.69	25.82	8.92	82.34	33.50	35.97
sand (%)		23.65	33.56	32.80	5.96	25.80	20.33
mud (%)		28.66	40.62	58.28	11.70	40.69	43.70

Hamilton Boulevard grain-size distribution curve (HB_BH1)

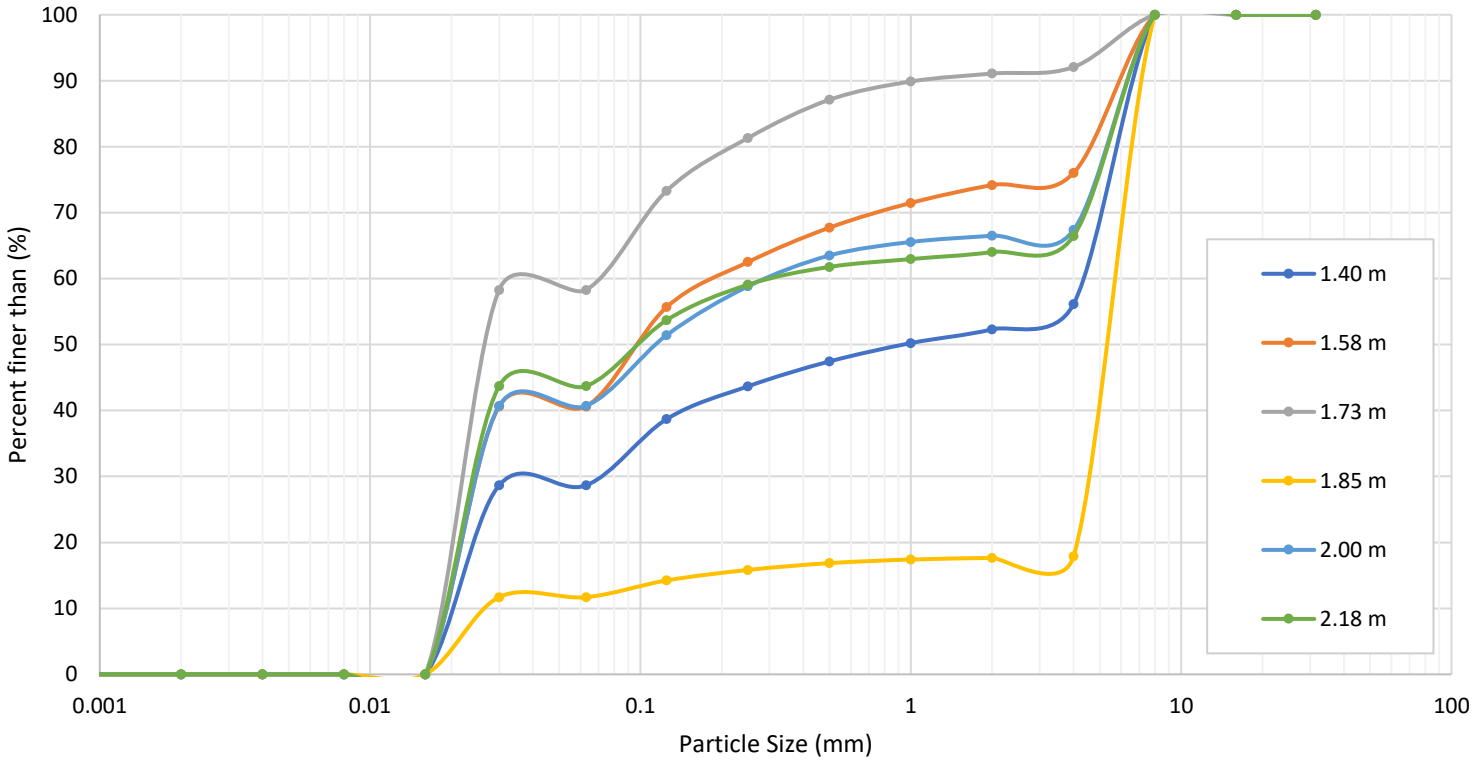

D3 Hidden Valley grain-size analysis results at HV_BH1. Analysis was completed on 4 February 2020 and compiled with Gradistat.

Hidden Valley sediment type (HV_BH1)

Sample Depth	Sieving Error	Sample Type	Textural Group	Sediment Type
1.00 m	0.0%	Trimodal, Very Poorly Sorted	Slightly Gravelly Sandy Mud	Slightly Very Fine Gravelly Medium Sandy Medium Silt
2.00 m	0.0%	Trimodal, Very Poorly Sorted	Slightly Gravelly Muddy Sand	Slightly Very Fine Gravelly Medium Silty Coarse Sand
3.00 m	0.0%	Trimodal, Very Poorly Sorted	Slightly Gravelly Muddy Sand	Slightly Very Fine Gravelly Fine Silty Coarse Sand
4.00 m	0.0%	Trimodal, Very Poorly Sorted	Slightly Gravelly Muddy Sand	Slightly Very Fine Gravelly Fine Silty Medium Sand
5.00 m	0.0%	Trimodal, Very Poorly Sorted	Slightly Gravelly Muddy Sand	Slightly Very Fine Gravelly Medium Silty Medium Sand
6.00 m	0.0%	Trimodal, Very Poorly Sorted	Slightly Gravelly Muddy Sand	Slightly Very Fine Gravelly Fine Silty Medium Sand
7.00 m	0.0%	Trimodal, Very Poorly Sorted	Slightly Gravelly Muddy Sand	Slightly Very Fine Gravelly Fine Silty Medium Sand
8.00 m	0.0%	Trimodal, Very Poorly Sorted	Slightly Gravelly Muddy Sand	Slightly Very Fine Gravelly Medium Silty Coarse Sand
9.00 m	0.0%	Trimodal, Very Poorly Sorted	Slightly Gravelly Muddy Sand	Slightly Very Fine Gravelly Medium Silty Coarse Sand
10.00 m	0.0%	Polymodal, Very Poorly Sorted	Slightly Gravelly Muddy Sand	Slightly Very Fine Gravelly Medium Silty Medium Sand
11.00 m	0.0%	Trimodal, Very Poorly Sorted	Slightly Gravelly Muddy Sand	Slightly Very Fine Gravelly Medium Silty Coarse Sand
12.00 m	0.0%	Trimodal, Very Poorly Sorted	Muddy Sand	Medium Silty Coarse Sand
13.00 m	0.0%	Trimodal, Very Poorly Sorted	Slightly Gravelly Muddy Sand	Slightly Very Fine Gravelly Medium Silty Coarse Sand
14.00 m	0.0%	Trimodal, Very Poorly Sorted	Slightly Gravelly Sandy Mud	Slightly Very Fine Gravelly Medium Sandy Medium Silt
15.00 m	0.0%	Trimodal, Very Poorly Sorted	Slightly Gravelly Sandy Mud	Slightly Fine Gravelly Medium Sandy Medium Silt
16.00 m	0.0%	Trimodal, Very Poorly Sorted	Slightly Gravelly Sandy Mud	Slightly Very Fine Gravelly Medium Sandy Fine Silt
17.00 m	0.1%	Trimodal, Very Poorly Sorted	Sandy Mud	Medium Sandy Fine Silt
18.00 m	0.0%	Trimodal, Very Poorly Sorted	Sandy Mud	Medium Sandy Fine Silt
19.00 m	0.0%	Bimodal, Very Poorly Sorted	Slightly Gravelly Sandy Mud	Slightly Very Fine Gravelly Medium Sandy Fine Silt
20.00 m	0.0%	Trimodal, Very Poorly Sorted	Sandy Mud	Medium Sandy Fine Silt
21.00 m	0.0%	Trimodal, Very Poorly Sorted	Sandy Mud	Medium Sandy Fine Silt

Hidden Valley grain-size distribution (HV_BH1)

Size Class	Grain Size (mm)	1.00 m	2.00 m	3.00 m	4.00 m	5.00 m	6.00 m	7.00 m	8.00 m	9.00 m	10.00 m	11.00 m	12.00 m	13.00 m	14.00 m	15.00 m	16.00 m	17.00 m	18.00 m	19.00 m	20.00 m	21.00 m
very coarse gravel (%)	32 to 64	0.00	0.00	0.00	0.00	0.00	0.00	0.00	0.00	0.00	0.00	0.00	0.00	0.00	0.00	0.00	0.00	0.00	0.00	0.00	0.00	0.00
coarse gravel (%)	16 to 32	0.00	0.00	0.00	0.00	0.00	0.00	0.00	0.00	0.00	0.00	0.00	0.00	0.00	0.00	0.00	0.00	0.00	0.00	0.00	0.00	0.00
medium gravel	8 to 16	0.00	0.00	0.00	0.00	0.00	0.00	0.00	0.00	0.00	0.00	0.00	0.00	0.00	0.00	0.00	0.00	0.00	0.00	0.00	0.00	0.00
fine gravel (%)	4 to 8	0.00	0.00	0.00	0.00	0.00	0.00	0.00	0.00	0.00	0.00	0.00	0.00	0.00	0.00	0.12	0.00	0.00	0.00	0.00	0.00	0.00
very fine gravel (%)	2 to 4	0.01	0.07	0.05	0.02	0.02	0.06	0.09	0.03	0.05	0.01	0.02	0.00	0.03	0.02	0.12	0.23	0.00	0.00	0.09	0.00	0.00
very coarse sand (%)	1 to 2	0.01	15.14	13.19	7.95	6.15	8.51	6.02	8.48	8.77	5.66	6.52	8.12	7.02	5.13	4.89	0.00	0.00	0.00	0.08	0.00	0.00
coarse sand (%)	0.5 to 1	1.62	22.14	26.45	23.43	16.93	21.75	22.69	24.00	24.53	19.46	23.27	21.64	20.11	16.19	17.65	0.21	0.00	0.09	0.17	0.51	0.11
medium sand (%)	0.25 to 0.5	24.68	18.38	22.04	24.58	21.86	22.43	25.08	22.08	22.86	22.40	23.23	20.38	19.87	17.48	20.16	29.97	31.57	33.19	32.97	32.83	26.44
fine sand (%)	0.125 to 0.25	0.00	0.00	0.00	0.00	0.00	0.00	0.00	0.00	0.00	0.00	0.00	0.00	0.00	0.00	0.00	0.00	0.00	0.00	0.00	0.00	0.00
very fine sand (%)	0.063 to 0.125	5.05	6.59	5.71	5.18	8.25	5.51	6.16	3.15	3.71	7.81	7.03	5.03	4.53	7.14	6.67	8.49	5.94	3.61	4.62	7.47	6.56
very coarse silt (%)	0.031 to 0.063	4.41	1.29	1.73	2.66	2.44	1.38	2.04	1.35	1.34	2.38	2.83	2.18	3.20	5.44	4.26	1.01	1.00	1.98	3.02	5.95	8.74
coarse silt (%)	0.016 to 0.031	8.76	5.90	3.13	4.32	7.35	3.30	3.96	5.09	4.74	6.80	4.97	6.12	9.83	13.07	11.67	6.11	2.78	6.70	7.05	7.37	9.86
medium silt (%)	0.008 to 0.016	16.76	10.18	6.46	7.44	12.66	8.91	8.47	10.11	9.00	11.17	8.62	11.70	12.04	15.10	12.83	13.89	10.88	12.41	12.89	10.01	11.83
fine silt (%)	0.004 to 0.008	14.27	8.88	7.68	8.83	11.04	10.46	9.57	9.74	8.78	9.80	8.12	8.97	8.43	8.89	8.68	15.31	16.53	14.29	13.37	12.32	13.17
very fine silt (%)	0.002 to 0.004	13.86	8.60	7.45	8.57	10.68	10.15	9.29	9.45	8.54	9.50	7.89	8.71	8.19	8.60	8.41	14.85	16.07	13.90	13.00	11.97	12.79
clay (%)	0.00006 to 0.002	10.58	2.82	6.10	7.02	2.63	7.54	6.62	6.52	7.68	5.03	7.49	7.16	6.76	2.93	4.55	9.93	15.24	13.83	12.75	11.57	10.51
gravel (%)		0.01	0.07	0.05	0.02	0.02	0.06	0.09	0.03	0.05	0.01	0.02	0.00	0.03	0.02	0.24	0.23	0.00	0.00	0.09	0.00	0.00
sand (%)		31.36	62.26	67.40	61.14	53.19	58.20	59.95	57.71	59.88	55.33	60.06	55.16	51.52	45.94	49.36	38.67	37.50	36.89	37.84	40.81	33.10
mud (%)		68.63	37.67	32.55	38.84	46.79	41.74	39.96	42.26	40.07	44.66	39.92	44.84	48.45	54.04	50.40	61.10	62.50	63.11	62.07	59.19	66.90

Hidden Valley grain-size distribution curve (HV_BH1)

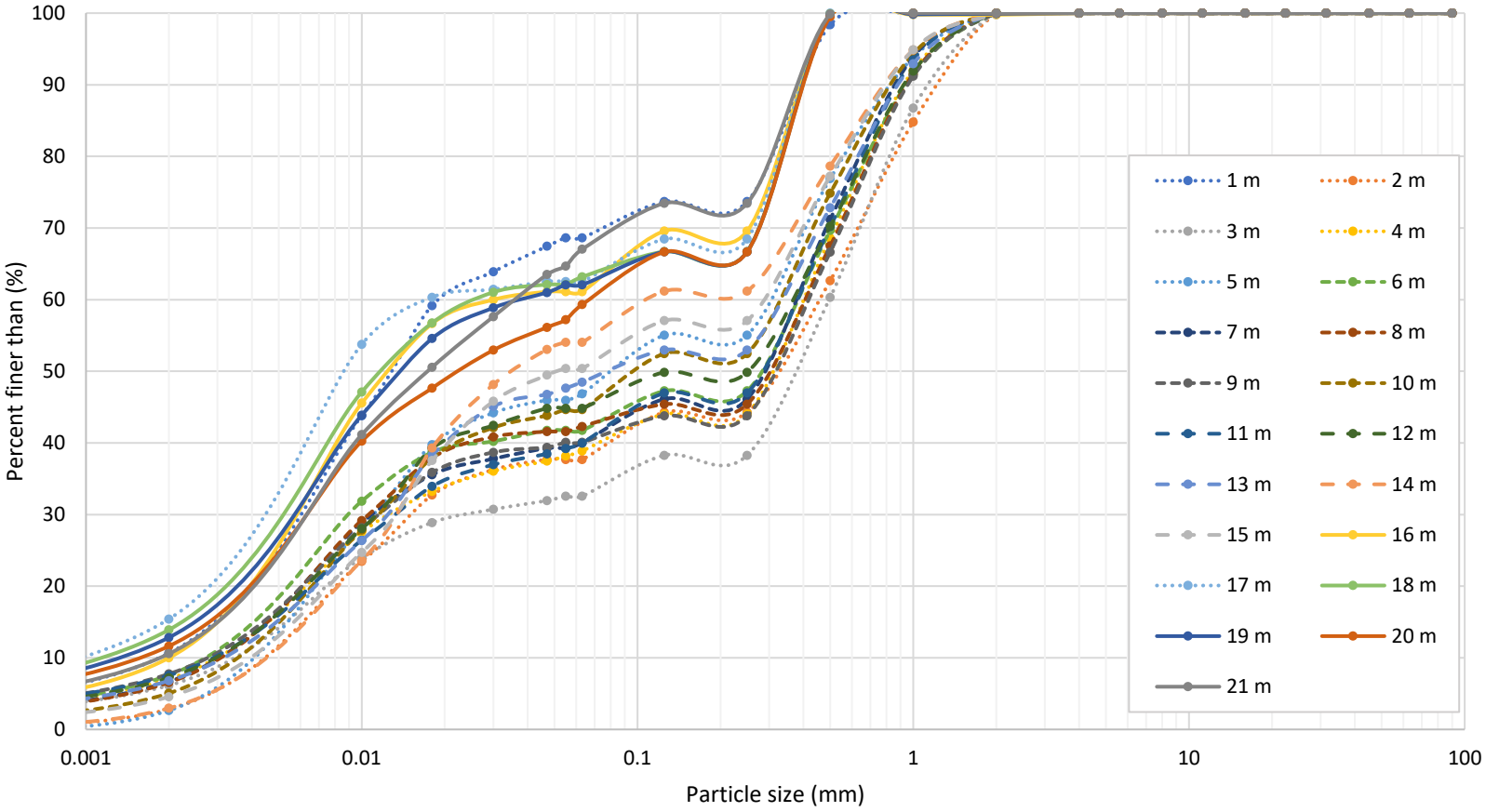

Hidden Valley sand, silt, clay diagram (HV_BH1)

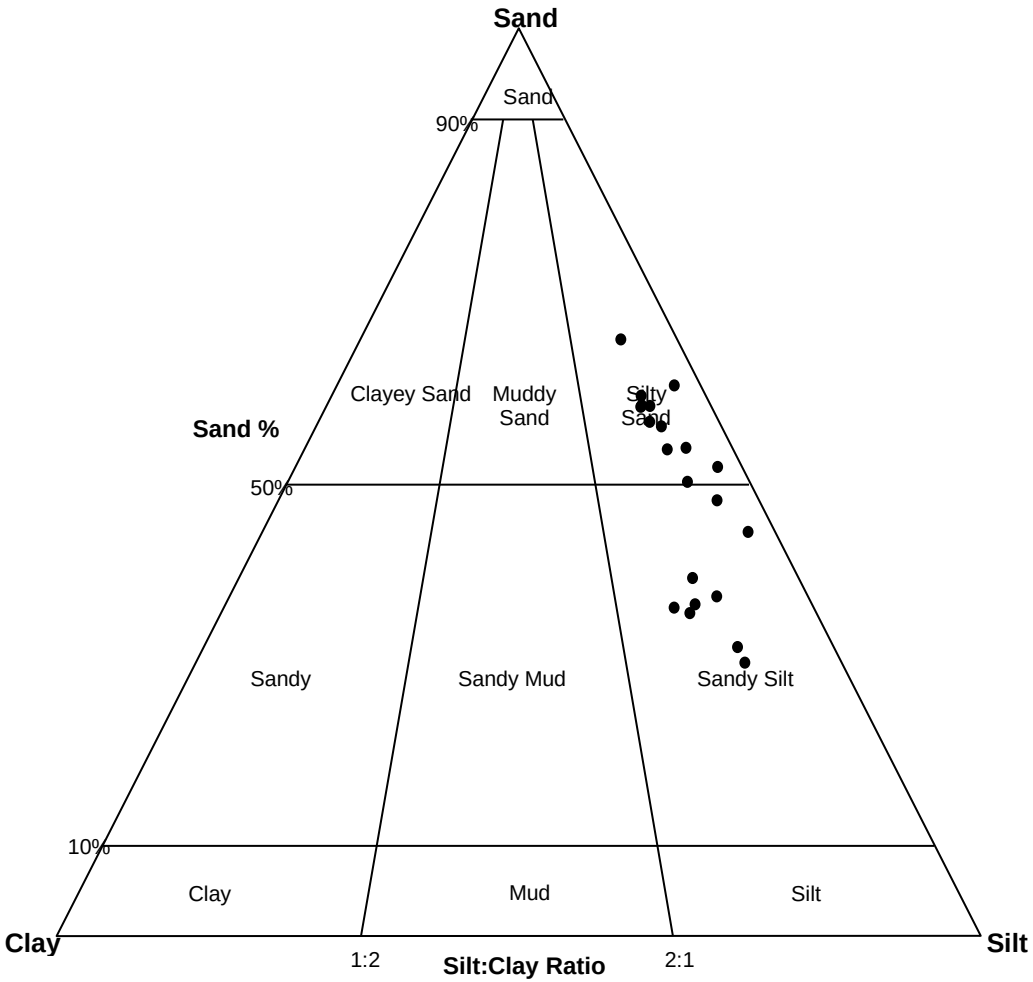

D4 Ibex Valley grain-size analysis results at IV_BH1. Analysis completed on 30 March 2020 and compiled with Gradistat.

Ibex Valley sediment type (IV_BH1)

Sample Depth	Sieving Error	Sample Type	Textural Group	Sediment Type
1.00 m	0.0%	Trimodal, Very Poorly Sorted	Sandy Mud	Very Fine Sandy Fine Silt
1.52 m	0.0%	Unimodal, Very Poorly Sorted	Sandy Mud	Very Fine Sandy Fine Silt
2.00 m	0.0%	Bimodal, Very Poorly Sorted	Sandy Mud	Very Fine Sandy Mud
3.00 m	0.0%	Bimodal, Very Poorly Sorted	Slightly Gravelly Sandy Mud	Slightly Fine Gravelly Very Fine Sandy Mud
4.00 m	0.0%	Bimodal, Very Poorly Sorted	Sandy Mud	Very Fine Sandy Fine Silt
5.00 m	0.0%	Bimodal, Very Poorly Sorted	Slightly Gravelly Sandy Mud	Slightly Very Fine Gravelly Very Fine Sandy Fine Silt
6.00 m	0.0%	Trimodal, Very Poorly Sorted	Sandy Mud	Very Fine Sandy Mud
7.00 m	0.0%	Unimodal, Very Poorly Sorted	Sandy Mud	Very Fine Sandy Mud
8.00 m	0.0%	Unimodal, Very Poorly Sorted	Muddy Sand	Muddy Very Fine Sand
9.00 m	0.0%	Bimodal, Very Poorly Sorted	Sandy Mud	Very Fine Sandy Mud
10.00 m	0.0%	Bimodal, Very Poorly Sorted	Sandy Mud	Very Fine Sandy Fine Silt
11.00 m	0.0%	Bimodal, Very Poorly Sorted	Sandy Mud	Very Fine Sandy Fine Silt
12.00 m	0.0%	Trimodal, Very Poorly Sorted	Sandy Mud	Very Fine Sandy Fine Silt
13.00 m	0.0%	Trimodal, Very Poorly Sorted	Sandy Mud	Very Fine Sandy Fine Silt
14.00 m	0.0%	Bimodal, Very Poorly Sorted	Sandy Mud	Very Fine Sandy Fine Silt
15.00 m	0.0%	Trimodal, Very Poorly Sorted	Sandy Mud	Very Fine Sandy Medium Silt
16.00 m	0.0%	Trimodal, Very Poorly Sorted	Sandy Mud	Very Fine Sandy Fine Silt
17.00 m	0.0%	Trimodal, Very Poorly Sorted	Sandy Mud	Very Fine Sandy Fine Silt
18.00 m	0.0%	Trimodal, Very Poorly Sorted	Sandy Mud	Very Fine Sandy Fine Silt
19.00 m	0.0%	Unimodal, Very Poorly Sorted	Sandy Mud	Very Fine Sandy Mud
20.00 m	0.0%	Unimodal, Very Poorly Sorted	Slightly Gravelly Sandy Mud	Slightly Very Fine Gravelly Very Fine Sandy Fine Silt

Ibex Valley grain-size distribution (IV_BH1)

Size Class	Grain Size (mm)	1.0 m	1.5 m	2.0 m	3.0 m	4.0 m	5.0 m	6.0 m	7.0 m	8.0 m	9.0 m	10.0 m	11.0 m	12.0 m	13.0 m	14.0 m	15.0 m	16.0 m	17.0 m	18.0 m	19.0 m	20.0 m
very coarse gravel (%)	32 to 64	0.00	0.00	0.00	0.00	0.00	0.00	0.00	0.00	0.00	0.00	0.00	0.00	0.00	0.00	0.00	0.00	0.00	0.00	0.00	0.00	0.00
coarse gravel (%)	16 to 32	0.00	0.00	0.00	0.00	0.00	0.00	0.00	0.00	0.00	0.00	0.00	0.00	0.00	0.00	0.00	0.00	0.00	0.00	0.00	0.00	0.00
medium gravel (%)	8 to 16	0.00	0.00	0.00	0.00	0.00	0.00	0.00	0.00	0.00	0.00	0.00	0.00	0.00	0.00	0.00	0.00	0.00	0.00	0.00	0.00	0.00
fine gravel (%)	4 to 8	0.00	0.00	0.00	0.65	0.00	0.00	0.00	0.00	0.00	0.00	0.00	0.00	0.00	0.00	0.00	0.00	0.00	0.00	0.00	0.00	0.00
very fine gravel (%)	2 to 4	0.00	0.00	0.00	0.20	0.00	0.02	0.00	0.00	0.00	0.00	0.00	0.00	0.00	0.00	0.00	0.00	0.00	0.00	0.00	0.00	0.22
very coarse sand (%)	1 to 2	0.00	0.00	0.00	0.11	0.00	0.00	0.00	0.00	0.00	0.00	0.00	0.00	0.00	0.00	0.00	0.00	0.00	0.00	0.00	0.00	0.00
coarse sand (%)	0.5 to 1	0.00	0.02	0.00	0.41	0.00	0.02	0.00	0.02	0.30	0.00	0.00	0.00	0.00	0.01	0.00	0.00	0.00	0.01	0.01	0.05	0.31
medium sand (%)	0.25 to 0.5	0.04	0.13	0.22	1.28	0.08	0.06	0.11	0.06	0.94	0.07	0.00	0.00	0.02	0.01	0.00	0.00	0.00	0.01	0.01	0.09	0.27
fine sand (%)	0.125 to 0.25	0.00	0.00	0.00	0.00	0.00	0.00	0.00	0.00	0.00	0.00	0.00	0.00	0.00	0.00	0.00	0.00	0.00	0.00	0.00	0.00	0.00
very fine sand (%)	0.063 to 0.125	31.83	41.82	29.67	32.95	39.74	37.73	29.80	37.73	49.34	32.16	33.91	33.89	17.87	25.86	39.88	17.73	20.01	13.83	23.82	37.84	45.58
very coarse silt (%)	0.031 to 0.063	6.18	8.70	4.28	4.58	2.54	4.54	6.45	4.54	4.38	7.87	6.71	6.45	4.45	6.45	6.18	6.82	2.43	6.81	6.45	4.43	6.66
coarse silt (%)	0.016 to 0.031	2.71	6.18	2.70	6.49	4.93	4.93	4.93	4.93	4.86	5.10	6.19	4.44	6.37	5.41	3.19	9.09	6.36	8.11	6.38	4.93	6.14
medium silt (%)	0.008 to 0.016	9.51	6.73	8.27	7.45	9.80	8.88	8.26	7.03	7.24	9.21	7.66	8.28	16.51	11.32	9.19	17.73	16.49	16.19	16.22	7.64	6.68
fine silt (%)	0.004 to 0.008	18.15	10.36	14.66	8.42	14.69	12.09	10.36	6.91	7.68	9.76	12.95	14.69	20.72	14.69	12.97	15.56	20.70	19.85	19.88	8.63	10.28
very fine silt (%)	0.002 to 0.004	17.62	10.11	14.34	8.33	14.28	11.81	10.21	6.89	7.54	9.60	12.65	14.31	20.11	14.34	12.63	15.15	20.08	19.27	19.25	8.53	10.02
clay (%)	0.00006 to 0.002	13.95	15.94	25.86	29.14	13.95	19.92	29.88	31.88	17.71	26.24	19.92	17.94	13.94	21.91	15.95	17.94	13.93	15.92	7.98	27.87	13.84
gravel (%)		0.00	0.00	0.00	0.85	0.00	0.02	0.00	0.00	0.00	0.00	0.00	0.00	0.00	0.00	0.00	0.00	0.00	0.00	0.00	0.00	0.22
sand (%)		31.87	41.97	29.89	34.75	39.82	37.81	29.91	37.81	50.58	32.23	33.91	33.89	17.89	25.88	39.88	17.73	20.01	13.85	23.84	37.98	46.16
mud (%)		68.13	58.03	70.11	64.40	60.18	62.17	70.09	62.19	49.42	67.77	66.09	66.11	82.11	74.12	60.12	82.27	79.99	86.15	76.16	62.02	53.62

Ibex Valley grain-size distribution curve (IV_BH1)

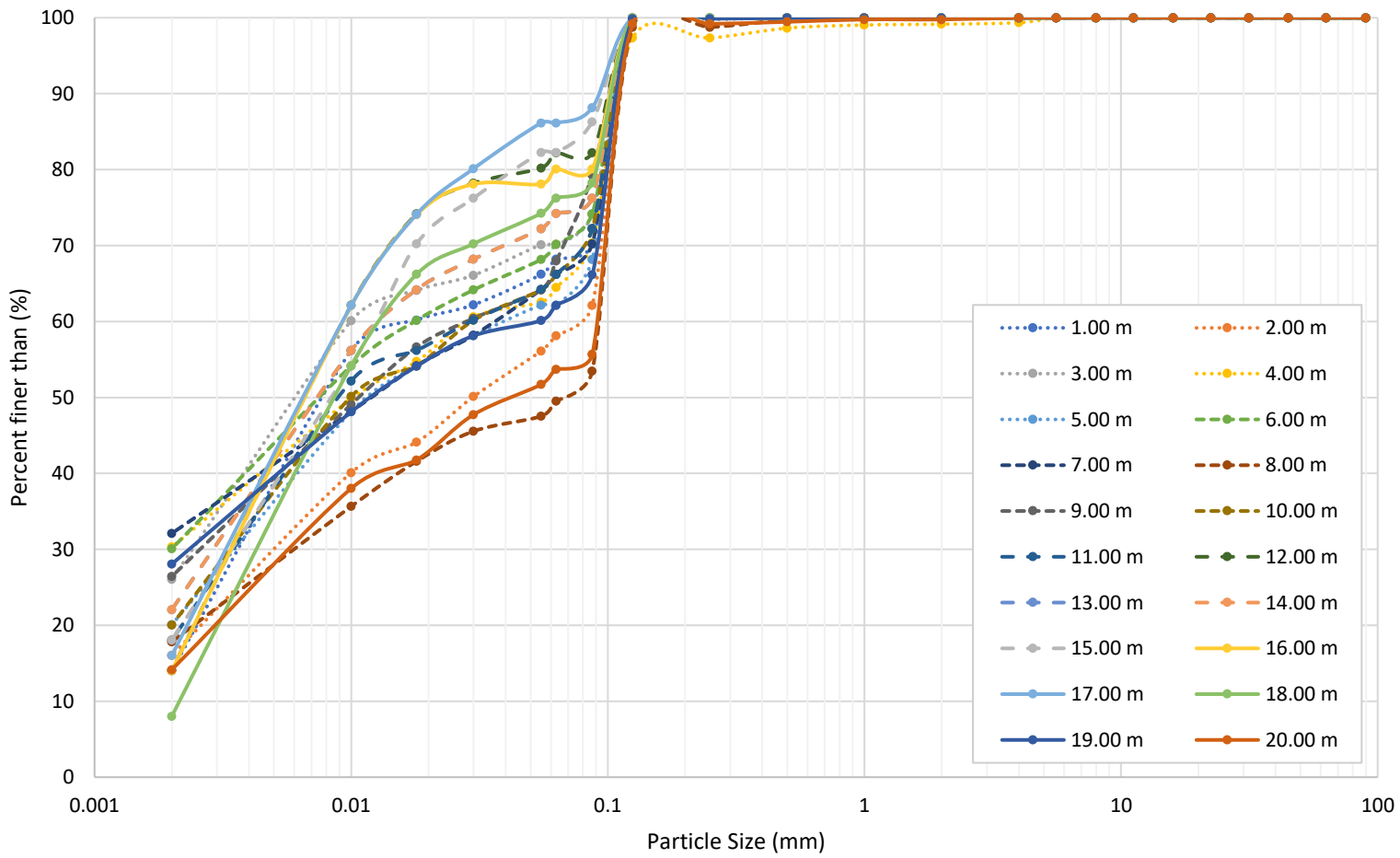

D5 Takhini River Retrogressive Thaw Slump grain-size analysis results at WH_1456_BH1. Analysis completed 18 December 2020 and compiled with Gradistat.

Takhini River Retrogressive Thaw Slump sediment type (WH_1456_BH1)

Sample Depth	Sieving Error	Sample Type	Textural Group	Sediment Type
0.00 m	0.0%	Trimodal, Very Poorly Sorted	Slightly Gravelly Sandy Mud	Slightly Very Fine Gravelly Very Fine Sandy Fine Silt
1.52 m	0.0%	Bimodal, Poorly Sorted	Slightly Gravelly Sand	Slightly Very Fine Gravelly Medium Sand
3.04 m	0.0%	Trimodal, Very Poorly Sorted	Sandy Mud	Very Fine Sandy Medium Silt
3.35 m	0.0%	Bimodal, Very Poorly Sorted	Slightly Gravelly Sandy Mud	Slightly Fine Gravelly Very Fine Sandy Fine Silt
4.57 m	0.0%	Bimodal, Very Poorly Sorted	Slightly Gravelly Sandy Mud	Slightly Very Fine Gravelly Medium Sandy Medium Silt
4.80 m	0.0%	Trimodal, Very Poorly Sorted	Sandy Mud	Very Fine Sandy Medium Silt
5.96 m	0.0%	Trimodal, Very Poorly Sorted	Slightly Gravelly Mud	Slightly Very Fine Gravelly Fine Silt
6.57 m	0.0%	Trimodal, Very Poorly Sorted	Sandy Mud	Very Fine Sandy Fine Silt
7.03 m	0.0%	Trimodal, Very Poorly Sorted	Sandy Mud	Very Fine Sandy Mud
7.45 m	0.0%	Unimodal, Poorly Sorted	Mud	Medium Silt
7.85 m	0.0%	Bimodal, Very Poorly Sorted	Sandy Mud	Very Fine Sandy Fine Silt
8.22 m	0.0%	Bimodal, Very Poorly Sorted	Mud	Mud
8.50 m	0.0%	Trimodal, Very Poorly Sorted	Sandy Mud	Very Fine Sandy Medium Silt
8.78 m	0.0%	Bimodal, Very Poorly Sorted	Sandy Mud	Very Fine Sandy Mud
9.15 m	0.0%	Bimodal, Poorly Sorted	Sandy Mud	Very Fine Sandy Medium Silt
9.40 m	0.0%	Bimodal, Poorly Sorted	Sandy Mud	Very Fine Sandy Fine Silt

Takhini River Retrogressive Thaw Slump grain-size distribution (WH_1456_BH1)

Size Class	Grain Size (mm)	0.00 m	1.52 m	3.04 m	3.35 m	4.57 m	4.80 m	5.96 m	6.57 m	7.03 m	7.45 m	7.85 m	8.22 m	8.50 m	8.78 m	9.15 m	9.40 m
very coarse gravel (%)	32 to 64	0.00	0.00	0.00	0.00	0.00	0.00	0.00	0.00	0.00	0.00	0.00	0.00	0.00	0.00	0.00	0.00
coarse gravel (%)	16 to 32	0.00	0.00	0.00	0.00	0.00	0.00	0.00	0.00	0.00	0.00	0.00	0.00	0.00	0.00	0.00	0.00
medium gravel (%)	8 to 16	0.00	0.00	0.00	0.00	0.00	0.00	0.00	0.00	0.00	0.00	0.00	0.00	0.00	0.00	0.00	0.00
fine gravel (%)	4 to 8	0.00	0.00	0.00	0.12	0.00	0.00	0.00	0.00	0.00	0.00	0.00	0.00	0.00	0.00	0.00	0.00
very fine gravel (%)	2 to 4	0.04	0.09	0.00	0.00	0.12	0.00	0.01	0.00	0.00	0.00	0.00	0.00	0.00	0.00	0.00	0.00
very coarse sand (%)	1 to 2	0.18	1.05	0.04	0.02	0.46	0.15	0.07	0.02	0.00	0.01	0.04	0.00	0.01	0.00	0.00	0.00
coarse sand (%)	0.5 to 1	0.29	13.71	0.48	0.41	1.11	1.00	0.10	0.01	0.01	0.01	0.13	0.00	0.13	0.00	0.01	0.02
medium sand (%)	0.25 to 0.5	0.96	50.83	3.45	1.59	23.93	4.97	0.24	0.22	0.04	0.08	0.72	0.01	1.12	0.01	0.03	0.06
fine sand (%)	0.125 to 0.25	0.00	0.00	0.00	0.00	0.00	0.00	0.00	0.00	0.00	0.00	0.00	0.00	0.00	0.00	0.00	0.00
very fine sand (%)	0.063 to 0.125	16.42	32.58	10.95	12.38	0.00	18.41	9.06	18.22	19.52	5.05	12.00	8.98	21.08	26.34	12.44	19.81
very coarse silt (%)	0.031 to 0.063	2.98	0.00	2.56	3.06	1.28	1.34	2.71	3.62	4.28	1.39	1.53	1.34	4.39	5.44	3.84	1.40
coarse silt (%)	0.016 to 0.031	7.45	0.00	14.63	10.71	8.14	10.25	4.28	1.80	3.76	11.73	5.94	4.08	9.82	4.20	16.34	6.94
medium silt (%)	0.008 to 0.016	14.42	0.18	21.91	17.91	17.57	19.49	16.62	13.38	6.64	30.05	16.89	14.78	21.07	7.73	26.67	20.94
fine silt (%)	0.004 to 0.008	17.24	0.50	15.90	17.92	17.35	17.34	22.50	24.83	15.34	22.40	25.95	19.60	16.02	12.45	18.57	25.86
very fine silt (%)	0.002 to 0.004	16.80	0.49	15.46	17.44	16.84	16.82	21.89	24.08	15.05	21.68	25.14	19.14	15.55	12.24	17.96	24.97
clay (%)	0.00006 to 0.002	23.22	0.58	14.61	18.43	13.20	10.24	22.52	13.83	35.37	7.60	11.67	32.07	10.82	31.59	4.14	0.00
gravel		0.04	0.09	0.00	0.12	0.12	0.00	0.01	0.00	0.00	0.00	0.00	0.00	0.00	0.00	0.00	0.00
sand		17.85	98.17	14.92	14.40	25.50	24.53	9.47	18.47	19.57	5.15	12.89	8.99	22.34	26.35	12.48	19.89
mud		82.11	1.74	85.08	85.48	74.38	75.47	90.52	81.53	80.43	94.85	87.11	91.01	77.66	73.65	87.52	80.11

Takhini River Retrogressive Thaw Slump grain-size-distribution curve (WH_1456_BH1)

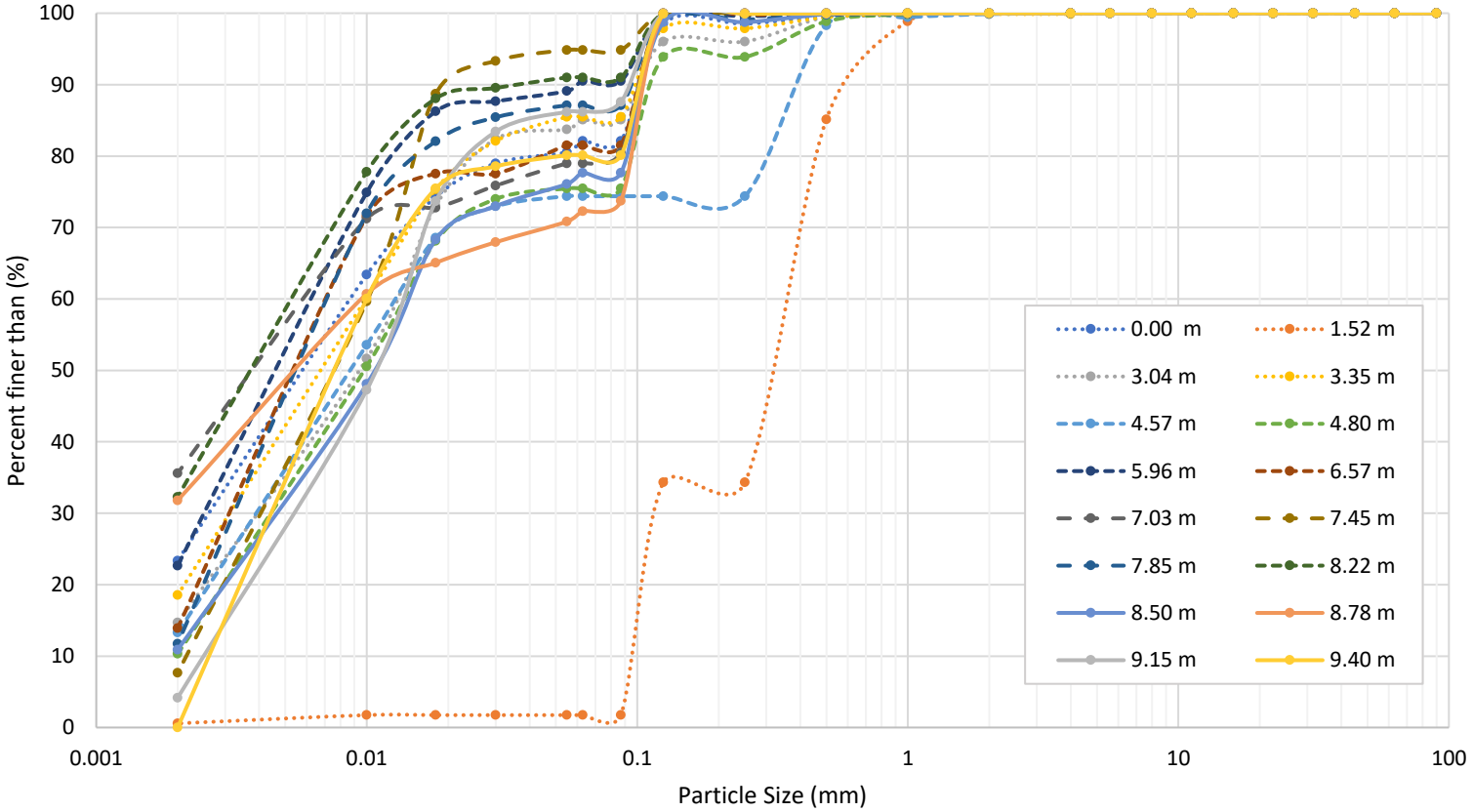

Takhini River Retrogressive Thaw Slump sand, silt, clay diagram (WH_1456_BH1)

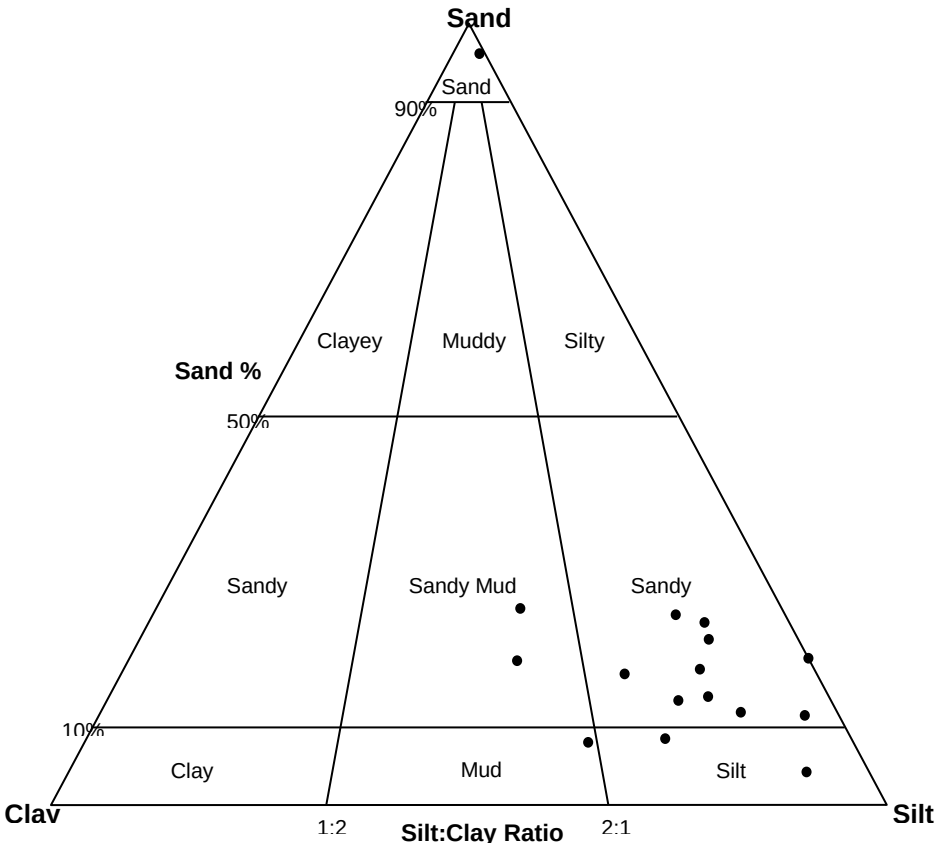

APPENDIX E – METHODS

Assessment of existing data

Surficial geology maps prepared by the YGS, along with aerial and satellite images were interpreted as part of this project. These data were supplemented with geotechnical reports from consultants and discussion with civil engineers and maintenance crew from HPW. Data and personal communications were combined, analyzed, and interpreted to complement previous permafrost studies.

Field surveys

Field investigation focused largely on the acquisition of new geophysical information using electrical resistivity tomography (ERT) surveys. In addition, shallow drilling was used to verify interpretations of geophysical information and to develop cryostratigraphic logs. This information is key because it allowed project researchers to infer the probability of permafrost presence.

Electrical resistivity and tomography

ERT is a geophysical method that passes electrical current through stainless steel electrodes (conductors used to provide current through non-metal materials) driven into the ground surface. A terrameter located at a central station measures the resistivity distribution of the subsurface between electrode pairs. Calmels *et al.,* (2018) explain “Resistivity is the mathematical inverse of conductivity and indicates the ability of an electrical current to pass through a material. Mineral materials (except for specific substances such as metallic ores) are mostly non-conductive. Therefore, variation in the resistivity of a soil or rock profile is governed primarily by the amount and resistivity of pore water present in the profile, and the arrangement of the pores. This makes ERT very well suited to permafrost and hydrology applications. Because most water content in frozen ground is in the solid phase and typically has a higher resistivity than unfrozen water content, permafrost distribution can be inferred based on changes in resistivity between frozen and unfrozen ground.”

An ERT system consists of an automated imaging unit and a set of wires connected to an electrode array. The system used for the surveys presented in this report is an ABEM Terrameter LS electrical resistivity and tomography system, consisting of a 4-channel imaging unit and 4 electrode cables, each with 21 take-outs at 5 m intervals. To conduct a survey, 81 electrodes are driven into the ground along a survey line and connected to the electrode cables (Fig. 1).

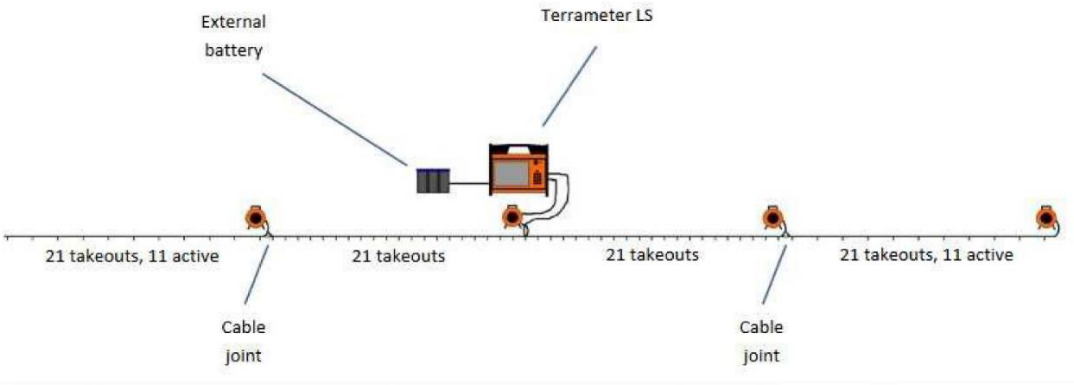

Figure 1. Instrument set-up for ERT surveying.

Two different types of electrode configurations or arrays were used during the surveys: Wenner and dipole-dipole. These arrays differ in how they pair current and potential electrodes (Figure 2). A direct current electrical pulse is sent from the resistivity meter along the survey line in two current electrodes (C1 and C2), and the measurement is performed by two potential electrodes (P1 and P2). The resulting data consists of a cross-sectional (2D) plot of the ground's resistivity (ohm·m) versus depth (m) for the length of the survey.

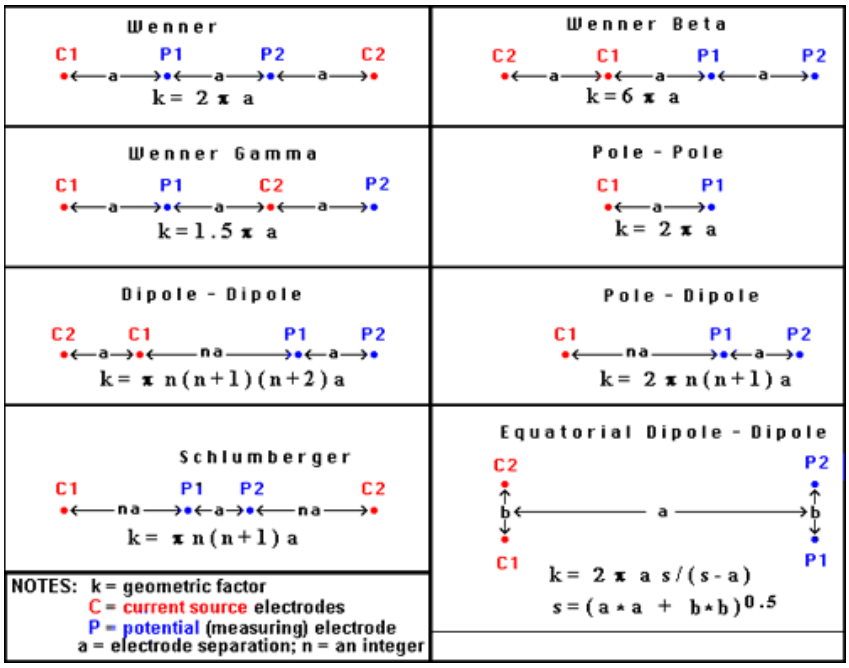

Figure 2. Survey configurations or "arrays" for ERT surveying.

In general, the Wenner array is good in resolving vertical changes (*i.e.*, horizontal structures), but relatively poor in detecting horizontal changes (*i.e.*, narrow vertical structures). Compared to other arrays, the Wenner array has a moderate depth of investigation. Among the common arrays, the Wenner array has the strongest signal strength. This can be an important factor if the survey is carried in areas with high

background noise. Relatively small current magnitudes are needed to produce measurable potential differences. The disadvantage is it is necessary to use longer current cables to image deep into the earth. The Wenner array is also very sensitive to near surface heterogeneities which may skew deeper electrical responses. One disadvantage of this array for 2-D surveys is the relatively poor horizontal coverage as the electrode spacing is increased, which can be a problem when using a system with a relatively small number of electrodes.

The dipole-dipole array is very sensitive to horizontal changes in resistivity, but relatively insensitive to vertical changes in the resistivity. Meaning it is good for mapping vertical structures, such as dykes and cavities, but relatively poor in mapping horizontal structures such as sills or sedimentary layers. This array can have a shallower depth of investigation compared to the Wenner array, but it has better horizontal data coverage than the Wenner, which can be an advantage when the number of nodes available with the multi-electrode system is small. One possible disadvantage can be a very weak signal strength. With the proper field equipment and survey techniques, this array has been successfully used in many areas to detect structures such as cavities where the good horizontal resolution of this array is a major advantage.

No single model fits the observed resistivities instead the modelled results converge by iteration with the measured values. The choice of when to stop iteration in the RES2DINV software is made by the operator. Too few iterations lead to large Root Mean Square (RMS) errors, *i.e.*, the model does not fit the measurements. Too many iterations can result in model 'over-fit' in which the broad patterns are lost. Analyses for this study were stopped after the 8th iteration as RMS errors were all very low (less than 5%) by that point. The profiles are presented with a linear depth scale and no vertical exaggeration. ERT profiles were interpreted in conjunction with the results of frost probing along the profiles, field descriptions of vegetation cover at the site, borehole and laboratory analyses undertaken by the research team, and surficial mapping. Results of the surveys are post-treated and analyzed at the NCE using inversion software (Res2DInv 64 and Res3DInv 32).

Drilling and sample collection

The objective of the drilling program was to core and collect permafrost samples from predetermined study sites. The drilling locations were selected in advance through interpretation of ERT surveys in combination with desktop interpretation of available maps, aerial photos, satellite images and consultation with community members (property owners, infrastructure and land managers, consultants, and industry). Commercial drill rigs were contracted to drill deep (>5 m) boreholes. Hand portable drilling and coring operations used for shallow (<5 m) boreholes generally required the use of two different drills to account for changes in subsurface conditions: a core-drill (a custom GÖLZ^{TM} portable core-drill system), and a hand auger.

The hand auger is used to sample the thawed active layer; it has a 10.2 cm diameter sampling core barrel, and three 1 m-long extension rods. It is ideal for sampling near-surface, fine-grained, unfrozen soil (*e.g.*, clay, silt, sand and fine gravel containing pebbles with a maximum diameter of 25 mm).

The GÖLZTM portable core-drill system is a light hand drill with a high rotation speed (600 rpm) that can be controlled by two people and is therefore used with minimal impact on the environment. Stainless steel rods measuring 1 m long and 4.5 cm in diameter, and a core barrel 40 cm long and 10 cm in diameter were used, making it possible to drill up to 5 m into unconsolidated, fine to medium grained material (sand to clay). A core catcher was used to extract the frozen core out of the borehole, which allows for continuous undisturbed permafrost sampling.

Using a combination of these drills, boreholes were drilled along ERT survey lines in representative areas (*e.g.*, forested areas, open fields) or in an area belonging to a particular surficial geology unit. For each borehole, the same sampling and drilling procedures were followed. The site was first described (*e.g.*, vegetation type and density, and topography), photos were taken, and locations were recorded using a handheld GPS. The boreholes were initiated using a hand auger if the ground was soft or an auger drill if the ground was gravelly or compacted. As soon as the permafrost table was reached, the GÖLZTM portable core-drill system was used. Frozen core samples were collected and briefly described on site. Each core was cleaned to remove the drilling mud, packaged in poly bags, and transported to a storage facility for laboratory processing.

Geotechnical analysis of permafrost

Laboratory analyses were carried out to measure geotechnical properties of active layer and permafrost samples, and additional tests were conducted to evaluate the mechanical behavior of the permafrost upon thawing. Both soil characteristics and ice characteristics were evaluated. To evaluate soil characteristics, a grain-size analysis was performed on every sample. Additionally, plasticity index, remolded bulk density, porosity, specific gravity and thaw settlement potential were calculated for representative samples. To evaluate ice characteristics in permafrost samples, the cryostructure, volumetric ice content, gravimetric ice content and settlement potential were quantified. These methods are described below.

Dry or unsaturated frozen materials or soils do not present a high risk upon thawing, as the water will remain in the soil porosity or will drain away. In contrast, when a saturated soil thaws, it presents a much higher risk of settlement, mass movement, or ponding in response to poor drainage. The thawing of ice-rich materials or soils is affected by factors such as stratigraphy and the grain size distribution of the stratigraphic layers, as well as external factors such as slope, surface roughness, and vegetation (Stephani *et al.,* 2014).

For thaw-settlement assessments, cryostratigraphy is used to locate and describe ice-rich and ice-poor layers and determine the geometry and distribution of massive ice. The presence of ice-rich deposits usually raises concern in terms of hazard potential. Where ice-rich deposits overlie ice-poor layers, the thaw-settlement hazard is high in the short term, and the rate of change is fast. Conversely, when ice-poor deposits overlie ice-rich sediment, the thawing of the upper layer is rapid but with minimal thaw settlement and will be followed by the slow, but constant thawing of the underlying ice-rich layer resulting in differential thaw settlement.

The grain size distribution of sediments determines the porosity and hydraulic conductivity of the ground. Coarse material (medium sand and coarser) has a high hydraulic conductivity and readily drains water as ice melts, whereas fine-grained material drains poorly once it thaws due to its low hydraulic conductivity. Furthermore, fine-grained sediments commonly contain excess ice (*i.e.,* the volume of ice in excess of the total pore volume of the ground when unfrozen) and may form ice lenses or layers by ice segregation. On flat terrain, ground with excess ice will undergo severe thaw settlement; likewise, on slopes, silt and clay deposits may experience mass movement when the pore water pressure created by melting ice is high. For slope deposits, the plastic and liquid limits of the material are used to evaluate the potential of ground failure.

Grain-size Analysis

Sieve and hydrometer analysis of grain size were performed following a specifically modified American Standard and Testing Method protocol (ASTM D422-63, 2000). The sieves used were 4, 2, 1, 0.5, 0.25, 0.125 and 0.063 mm. The data was then compiled in GRADISTAT to generate the statistical analysis.

A hydrometer test was performed on a 40 g subsample passing through 0.25 mm openings; after sedimentation started, readings were taken after 0.25, 0.50, 0,75, 1, 1.5, 2, 5, 15, 30, 60, 120, 180, 300 and 1440 minutes.

Cryostructure

Cryostructure (the geometry of the ice in the permafrost) depends on water availability, as well as the soil's ice-segregation potential and the time of freezing, resulting in the development of ice structures in the soil matrix. Information such as soil genesis, climate conditions at the time of freezing, permafrost development history, and ground vulnerability when permafrost degrades can be interpreted from cryostructure, cryofacies analysis, and general cryostratigraphy.

The cryostructure of the cores was described in the Yukon University laboratory using a standard terminology (Stephani *et al*., 2010; Murton and French, 1994). High-resolution pictures of the samples were taken in the laboratory.

where $M_{S+B}$is the weight of the beaker full of compacted sediment, M_B is the weight of the empty beaker, and V_B is the beakers internal volume.

Gravimetric Ice content

Ice content was calculated using:

$$u_I = \frac{(M_I)}{(M_S)}$$

where $M_I$is the ice weight (measured as weight loss after drying (g)) and M_S is dry soil weight (g). Results are expressed as percentages (dimensionless).

Volumetric ice content

Ice volume was measured using a water displacement method. The frozen sample was weighed and lowered into a four-inch diameter PVC tube filled with 1.5 L of water. Water was then extracted from the tube until the initial water level (1.5 L) was achieved. The amount of water displaced was measured using a 250 mL graduated cylinder with a precision of ±2 mL. The sample was then removed from the tube, placed in a clean tin tray, and dried completely in a drying oven at 60°C. The dry sample was then weighed, crushed using a mortar and pestle, vacuum sealed in a clear plastic bag, and labelled according to the borehole and sample increment. The volumes of the vacuum-sealed dry samples were measured using the same methods as the frozen cores, and the volume of the vacuum bags was subtracted from the measurement to obtain a dry sample volume. Assuming the density of ice to be 1.09 cm^3/g, the volumetric ice content was calculated using:

$$IVC_{(\%)} = \left(\frac{W_c \times 1.09}{V_{tot}}\right) x100$$

where W_c is the water mass content and V_{tot} is the total (frozen) core volume. Results are expressed as percentages. For the consolidation test samples, the volume has been measured using Glycol displacement. This allowed the possibility to keep the samples under 0c and avoid the use of vacuumed sealed bag.

Volumetric excess ice content

The volume of excess ice content was calculated using:

$$V_{tot} - V_{sed} = V_{ice}$$

where V_{tot} is the total frozen core volume and V_{sed} is the dry soil volume. The volumetric excess ice content (V_{ice}) is then divided by the total frozen core volume (V_{tot}) and expressed as a percentage (fundamentally meaning cm^3/cm^3). This method is valid for mineral soils only.

Borehole logs

A log for each permafrost borehole was created by assembling laboratory photos of the cores. Borehole logs include maximal depths, grain size ratio and volumetric excess ice content.

Ground temperature

For ground temperature monitoring installations, electrical-grade PVC casings were inserted into the newly-drilled boreholes, and were filled with silicone oil. The holes were backfilled with earth extracted from the borehole and/or filter sand. The boreholes were instrumented with thermistor strings attached to external data loggers (HOBO (UX120-006M) four-channel external or LogR Systems ULogC16-32).

Shallow boreholes (<10 m) were generally instrumented with the HOBO UX120-006 data logger. This stand-alone logger can record data at various intervals and uses a direct USB interface for fast data offload. The logger requires two AAA lithium batteries. The batteries will typically last one year when logging intervals are greater than one minute. To ensure uninterrupted operation, the data loggers are placed in a sealed 15 x 15-cm junction box connected to the borehole casing. The temperature sensors (TMC6-HD to TMC50-HD) can accurately record temperatures ranging from –20°C to +70°C, with interchangeability to a tolerance of ±0.25°C from 0°C to 50°C. They have a resolution of 0.03°C at 20°C.

Deeper borehole (>10 m) are instrumented using the LogR Systems UlogC16-32 series. These are very low-power multi-channel data loggers designed for superior performance and longer deployment. They are encased in a waterproof and rugged plastic casing, support USB-C and SD card download and have an operating environment of −40 to 85°C. They operate using a type C lithium battery, 3.6V 5.8 Ah and internal flash memory. The cables are constructed by the YRC Permafrost and Geoscience Research team using 32 multi-conductors, 22 AWG Stranded tinned copper cables. The YSI 44033 temperature sensors are then soldered on the cable at the desired depth. The thermistors are sealed using a 12 mm heat shrink tubing. The YSI 44033 thermistors have an interchangeability tolerance of ± 0.1°C from 0°C to 70°C.

Permafrost thaw sensitivity mapping

A permafrost thaw sensitivity map for the greater Whitehorse area was developed to indicate the relative likelihood of developing ground surface disturbance (*i.e.,* subsidence or landslides) if permafrost is present and it thaws. It was produced based on a GIS analysis of surficial geology, vegetation, slope orientation, and slope steepness. The mapping and geoprocessing were done using ArcGIS Pro. A screenshot of the permafrost thaw sensitivity webmap (https://yukonu.maps.arcgis.com/apps/MapJournal/index.html?appid=e8c7f5a106aa4567bdf53ee7feed3af4) is shown below in Figure 3.

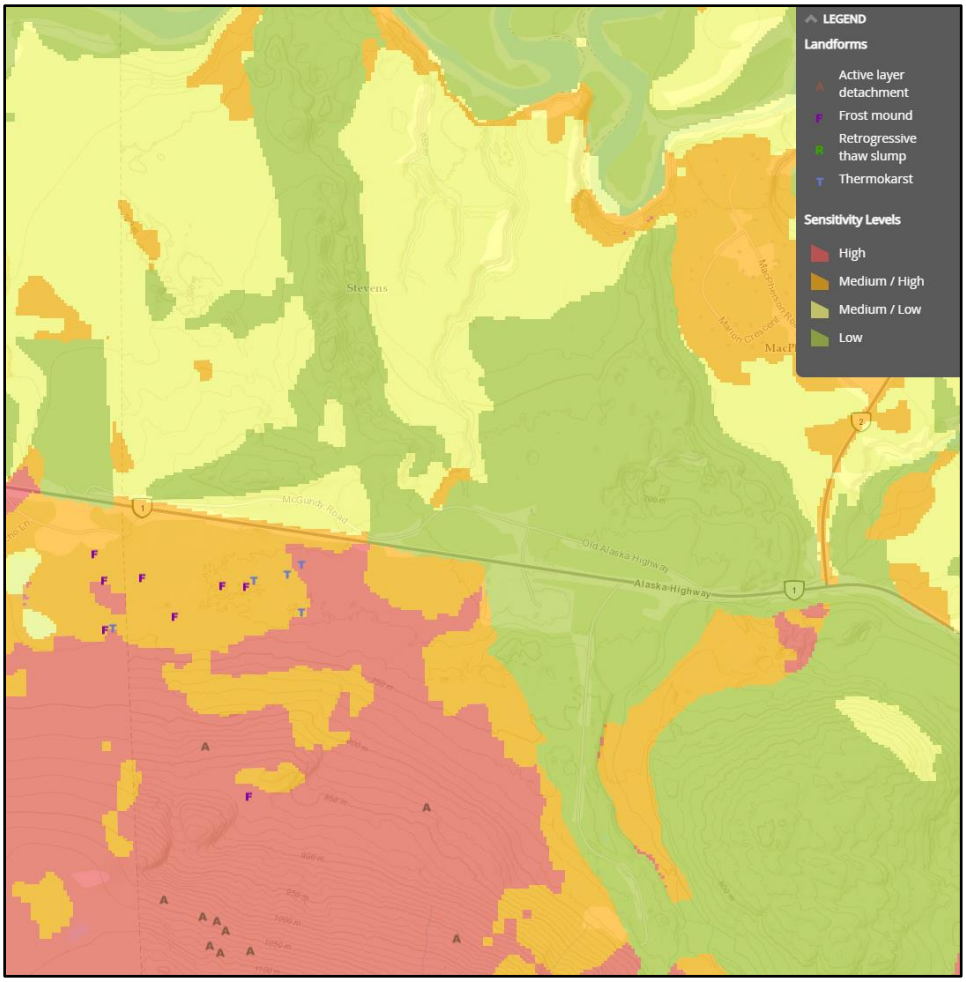

Figure 3. Sample of the permafrost thaw sensitivity webmap for the area near the junction of Alaska Highway and North Klondike Highway.

Limitations

It must be emphasized that permafrost is not necessarily spatially continuous within any particular area shown on the map, and may only occur in small, isolated patches. The map should not be used for site specific planning design or construction, where geotechnical investigations are still essential.

Field observations and photo interpretation

The mapping methodology relies heavily on field observations and photo identification of permafrost landforms. The body of this report details the field investigations conducted at seven sites in the GWA: Cowley Creek, Hamilton Boulevard, Hidden Valley, Ibex Valley, Takhini River Retrogressive Thaw Slump, Old Alaska Highway, and Fish Lake. Field investigations included permafrost core sample collection, borehole instrumentation with ground temperature monitoring, and ERT surveys. These investigations provided information on the characteristics and current condition of permafrost. Other field observation sites confirming the presence of permafrost were provided by Dr. Antoni Lewkowicz (University of Ottawa), Dr. Chris Burn (Carleton University), Highways and Public Works (Yukon Government), YGS, Kryotek, TetraTech EBA, and local citizens (data verified by researchers). Air photo, lidar and satellite imagery interpretation was used to identify landforms related to permafrost. The majority of these landforms are thermokarst ponds and permafrost mounds (palsa and lithalsa), while the rest are permafrost-related landslides (active layer detachments and retrogressive thaw slumps).

Surficial geology

Surficial geology was provided by YGS at four different scales; 1:20 000 for Whitehorse City limits, and 1:50 000, 1:100 000, or 1:250 000 for the rest of the mapping area (Figure 4). New detailed (1:20 000 scale) mapping currently underway at YGS was integrated for targeted areas where permafrost presence was interpreted from air photos and other imagery.

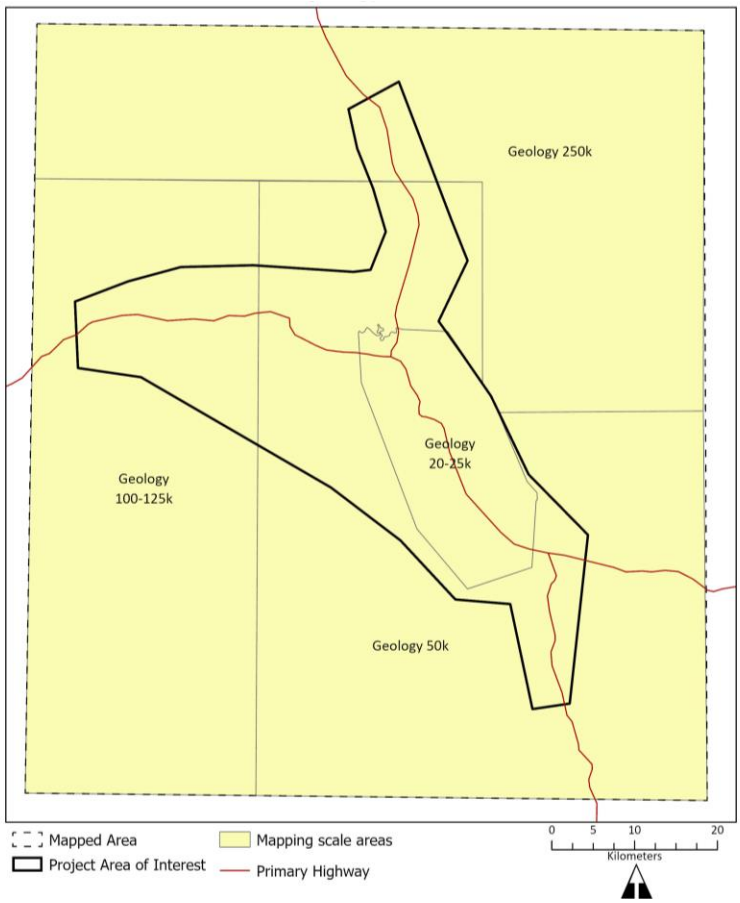

Figure 4. Mapping scale for surficial geology datasets. The "Geology 20-25k" polygon outlines Whitehorse city limits; heavy black line outlines greater Whitehorse area. Red lines indicate highways, with the Alaska Highway running east-west, and the Klondike Highway running north-south.

We first used field observations and air photo interpretations of landforms to determine which types of surficial deposits were most likely associated with permafrost in the greater Whitehorse area. Table 1 shows the geomorphological processes and the material with associated textures identified in this initial overlay analysis. Based on their known affiliation with permafrost from Table 1, the processes and surficial materials present in Table 2 were then queried across the entire mapping area.

Table 1. Surficial materials, geomorphological processes and associated textures which overlapped known permafrost locations identified from field observations and interpretation of landforms from air photos.

Material (A)	Material A texture	Geomorphological Processes
A - Anthropogenic		E – Glacial meltwater channels
C - Colluvium	d – mixed fragments	L – Landslide
F - Fluvial	g – gravel m – mud s – sand	H – Kettled S – Solifluction V – Gully erosion
E - Eolian	s – sand	U – Inundation
L - Lacustrine	c – clay m – mud s – sand	X – Permafrost Xt – Permafrost with thermokarst
M - Morainal	d – mixed fragments s – sand	
O - Organic	e – fibric organic	
R - Bedrock		

Table 2. Surficial materials and geomorphological processes associated with permafrost based on extrapolation of Table 1 criteria to the entire mapping area.

Material (A, B)	Material Texture	Geomorphological Processes
L - Lacustrine	c – clay m – mud s – sand	C – Cryoturbation S – Solifluction X – Permafrost
O - Organic		Xt – Permafrost with thermokarst
		Z – General periglacial processes

An air photo validation was performed at this stage to validate or exclude certain polygons and ensure the best accuracy possible on the final map.

Finally, levels of sensitivity to permafrost thaw were manually attributed to each type of surficial deposit based on local field observations or assumed ice-content if a given material was associated with permafrost. Four surficial geology rankings were assigned: low, medium/low, medium/high and high. Polygons were classified as high sensitivity where they were attributed with solifluction or permafrost processes, or they overlapped with existing permafrost monitoring sites or identified permafrost landforms. Levels of sensitivity for non-uniform surficial deposits (various combinations of material A and material B) were assigned manually as listed in Table 3. Any other combination of surficial deposit present in the dataset and not mentioned in Table 3 was classified as low.

Table 3. Sensitivity to permafrost thaw assigned to surficial materials, based on combinations of Material A and B and the presence of geomorphologic processes.

Process	Material A	Material B	Sensitivity ranking
S – Solifluction	Any	Any	High
X – Permafrost	Any	Any	High
	C – Colluvium	L – Lacustrine	Medium/low
	C – Colluvium	O – Organic	Medium/high
	C – Colluvium 100%	n/a	High
	E – Eolian	L – Lacustrine	Medium/low
	F – Fluvial	L – Lacustrine	Medium/Low
	F – Fluvial	O – Organic	Medium/low
	L – Lacustrine 100%	n/a	Medium/High
	L – Lacustrine	R – Bedrock	Medium/low
	L – Lacustrine +	O – Organic	High
	L – Lacustrine +	M – Morainal	Medium/High
	L – Lacustrine +	F – Fluvial	Medium/High
	L – Lacustrine +	E – Eolian	Medium/High
	L – Lacustrine +	C – Colluvium	Medium/Low
	M – Morainal	O – Organic	Medium/high
	M – Morainal	C – Colluvium	Medium/low
	M – Morainal	L – Lacustrine	Medium/high
	M – Morainal	F – Fluvial	Medium/low
	O – Organic 100%	n/a	High
	O – Organic	F – Fluvial	Medium/high
	O – Organic	L – Lacustrine	High
	O – Organic	M – Morainal	Medium/low
	O – Organic	C – Colluvium	Medium/low

Vegetation

The main vegetation datasets used in this project were provided by Yukon Government at two scales; 1:5000 and 1:40 000 (Figure 5). We used field observations of permafrost and air photo interpretations of permafrost-related landforms (later referred to as observation points) to determine which vegetation types were most likely to indicate the presence of permafrost. Most of the observation points were located in the 1:5000 scale vegetation dataset area and overlapped forested areas (of which white spruce was most often the primary or secondary species), shrub cover of 60% and above, and alpine areas (see Table 4). A few vegetation types classified as urban, burned forest, and non-productive also overlapped the observation points, but in small numbers and were not retained for the analysis as they do not typically indicate the presence of permafrost.

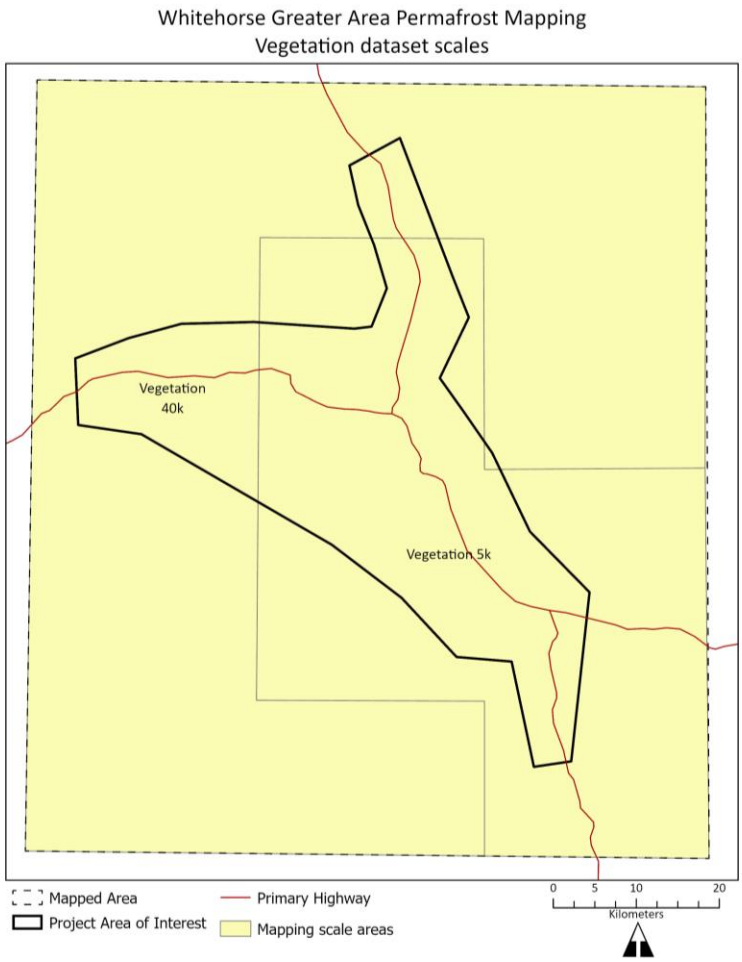

Figure 5. Mapping scale for vegetation datasets. Heavy black line outlines greater Whitehorse area. Red lines indicate highways, with the Alaska Highway running east-west, and the Klondike Highway running north-south.

Table 4. Vegetation types associated with permafrost, as selected by overlay analysis with observation points.

Type of cover	Primary species	Secondary species
Forested	Aspen	Lodgepole pine
		White spruce
	Subalpine fir	White spruce
	Lodgepole pine	White spruce
	White spruce	Subalpine fir
		Lodgepole pine
		Trembling aspen
		N/A (100% white spruce)
Other vegetation	Shrubs	
Alpine		
Urban		
Burned forest		
Non-productive		

The difference in attribute precision between the two vegetation dataset scales was a major challenge. Both scales gave data about primary and secondary tree species but only the 1:5000 scale indicated alpine cover type and shrub cover which were two of the indicators needed to extrapolate the vegetation type selection to the entire mapping area. To compensate, terrain at elevation above 1500 m was used to define alpine areas in the 1:40 000 vegetation dataset area (based on an approximate 1300 m treeline reported for the Wolf Creek area in Lewkowicz and Ednie (2004). For areas of shrub cover over 60%, a 2014 vegetation classification provided by NASA ABoVE was used. The shrub classes were converted to polygons and then integrated into the 1:40 000 scale YG vegetation dataset area. Wetlands, including fens and bogs are known for their strong association with permafrost environments and were therefore also considered good indicators of permafrost presence. Finally, three levels of confidence (low, medium, high) were assigned to each type of vegetation as an indicator of permafrost presence (Table 5).

Table 5. Levels of confidence attributed to each type of vegetation.

Type of cover	Primary species	Secondary species	Confidence level as indicator of permafrost
Forested	Aspen	Lodgepole pine	Low
		White spruce	Low
	Subalpine fir	White spruce	Low
	Lodgepole pine	White spruce	Medium
	White spruce	Subalpine fir	High
		Lodgepole pine	High
		Trembling aspen	Low
		N/A (100% white spruce)	High
Shrubs >60%			High
Alpine			High
Wetland: Fen and bog			High

Slope orientation (aspect)

Slope orientation was calculated using a Digital Elevation Model (DEM) provided by Yukon Government with a spatial resolution of 16 m. Like vegetation, slope orientation was used as an indicator of probability of permafrost presence. Terrain orientation ranges from 0° to 360° and was divided into eight sections depending on their sun exposure. The more sun exposure, the less likely the terrain has of containing permafrost. For example, a north-facing slope is much more likely to have permafrost than a south-facing, and an east-facing slope is considered more likely to have permafrost than a west-facing slope because mornings are cooler. Values from 1 to 10 were assigned to the 8 different slope orientations, where 1 is the least associated with permafrost (Figure 6). A ninth class was added for flat terrain.

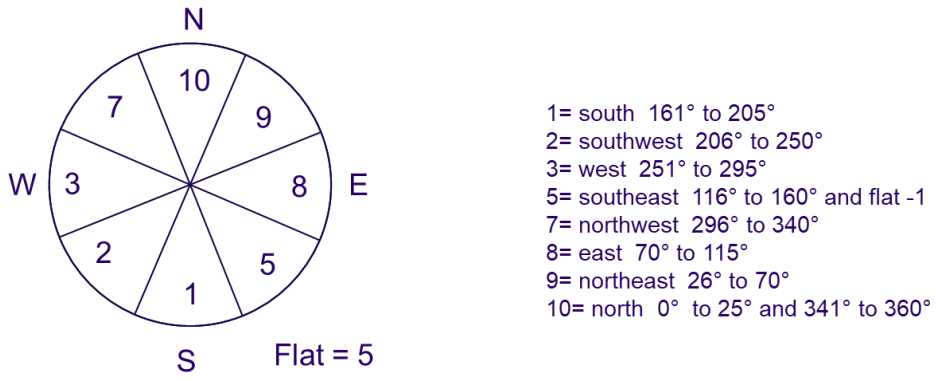

Figure 6. Permafrost probability weights assigned to slope orientation classes, where 10 is most likely associated with permafrost.

Slope steepness

Slope steepness was calculated using a Digital Elevation Model (DEM) provided by Yukon Government with a spatial resolution of 16 m. This was used as a factor to increase the potential of ground disturbances related to permafrost thaw. It was assumed the steeper the slope, the more likely slope movements would occur following permafrost thaw. Values of 1 to 10 were assigned to 5 slope classes as shown in Table 6, where 1 is the least likely to experience disturbances.

Table 6. Weights attributed to slope steepness from Benkert et al. (2016).

Description of Surface	Slope Percentage	Slope Degree	Classified Value
flat to gently undulating	0-5	0-3	1
gentle slope	6-27	4-15	3
moderate slope	28-49	16-26	6
moderately steep slope	50-70	27-35	8
steep slope	>70	>35	10

Mapping model

For ease of processing, the surficial deposits and vegetation datasets were converted from vector to raster format to be compatible with the slope orientation and steepness layers. This was achieved using the *polygon to raster* tool. The outputs were given the same spatial resolution as the slope and were snapped to it to ensure pixel alignment.

The levels of sensitivity given to the surficial deposits and the levels of confidence given to the vegetation types were then normalized into values ranging from 1 to 10 to match the range of values assigned to the two slope layers. The slope orientation and steepness were multiplied to create a single slope layer, therefore producing values from 1 to 100, which were then normalized back to a scale of 1 to 10.

The final cumulative model integrated the three layers: surficial deposit was given a weight of 1, vegetation was given a weight of 0.25, and slope was given a weight of 0.5 (Figure 7). The final sensitivity map includes values ranging from 1 to 17.5 which were divided into four classes using the equal interval method. The class values were then rounded as follows:

- 1 to 5 – low (low chance of ground surface disturbances following permafrost thaw)
- 5 to 9 – low/medium (low to medium chance of ground surface disturbances following permafrost thaw)
- 9 to 13 – medium/high (medium to high chance of experiencing ground surface disturbances following permafrost thaw)
- 13 to 17.5 – high (high chance of experiencing ground surface disturbances following permafrost thaw)

Finally, the final layer was simplified using the *boundary clean* tool, which smoothed the boundaries between zones and eliminated individual pixels isolated in larger zones.

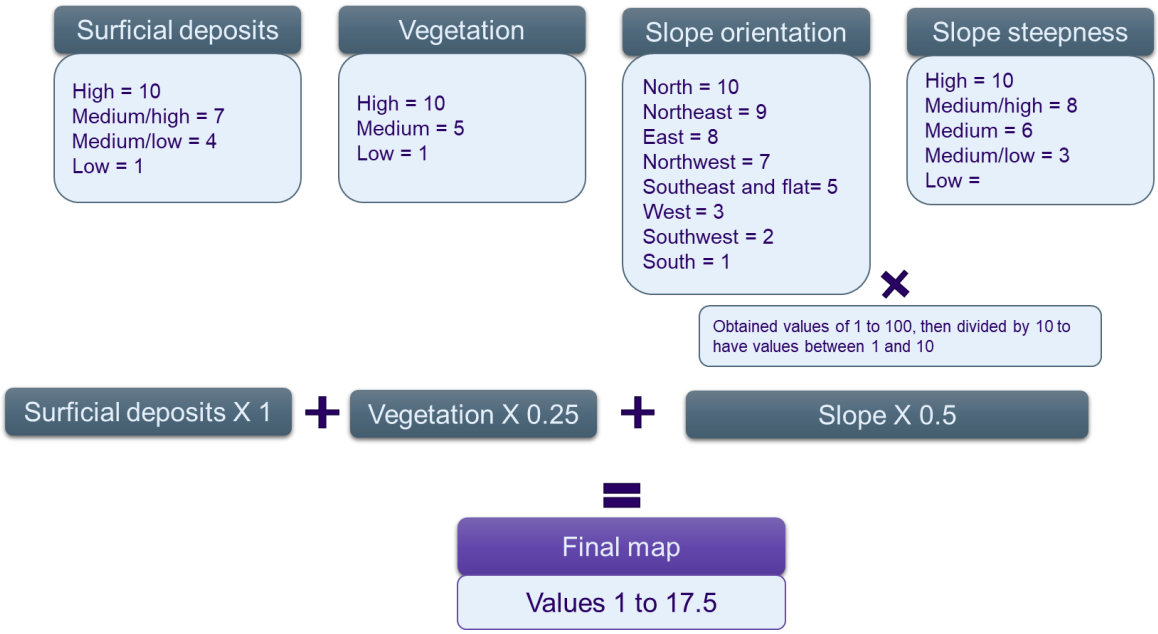

Figure 7. Layer rankings and weights applied to the final permafrost thaw sensitivity model.